

## INFORMATION TO USERS

This manuscript has been reproduced from the microfilm master. UMI films the text directly from the original or copy submitted. Thus, some thesis and dissertation copies are in typewriter face, while others may be from any type of computer printer.

**The quality of this reproduction is dependent upon the quality of the copy submitted.** Broken or indistinct print, colored or poor quality illustrations and photographs, print bleedthrough, substandard margins, and improper alignment can adversely affect reproduction.

In the unlikely event that the author did not send UMI a complete manuscript and there are missing pages, these will be noted. Also, if unauthorized copyright material had to be removed, a note will indicate the deletion.

Oversize materials (e.g., maps, drawings, charts) are reproduced by sectioning the original, beginning at the upper left-hand corner and continuing from left to right in equal sections with small overlaps.

Photographs included in the original manuscript have been reproduced xerographically in this copy. Higher quality 6" x 9" black and white photographic prints are available for any photographs or illustrations appearing in this copy for an additional charge. Contact UMI directly to order.

ProQuest Information and Learning  
300 North Zeeb Road, Ann Arbor, MI 48106-1346 USA  
800-521-0600

UMI<sup>®</sup>



**University of Alberta**

**Experimental and Modelling Study of Reverse  
Flow Catalytic Converters for Natural Gas/Diesel  
Dual Fuel Engine Pollution Control**

by

**Benlin Liu** ©

A thesis submitted to the Faculty of Graduate Studies and Research in partial fulfillment  
of the requirements for the degree of Doctor of Philosophy

Department of Mechanical Engineering

Edmonton, Alberta, CANADA

Fall 2000



National Library  
of Canada

Acquisitions and  
Bibliographic Services

395 Wellington Street  
Ottawa ON K1A 0N4  
Canada

Bibliothèque nationale  
du Canada

Acquisitions et  
services bibliographiques

395, rue Wellington  
Ottawa ON K1A 0N4  
Canada

*Your file Votre référence*

*Our file Notre référence*

The author has granted a non-exclusive licence allowing the National Library of Canada to reproduce, loan, distribute or sell copies of this thesis in microform, paper or electronic formats.

The author retains ownership of the copyright in this thesis. Neither the thesis nor substantial extracts from it may be printed or otherwise reproduced without the author's permission.

L'auteur a accordé une licence non exclusive permettant à la Bibliothèque nationale du Canada de reproduire, prêter, distribuer ou vendre des copies de cette thèse sous la forme de microfiche/film, de reproduction sur papier ou sur format électronique.

L'auteur conserve la propriété du droit d'auteur qui protège cette thèse. Ni la thèse ni des extraits substantiels de celle-ci ne doivent être imprimés ou autrement reproduits sans son autorisation.

0-612-59622-2

**Canada**

**University of Alberta**

**Library Release Form**

**Name of Author:** Benlin Liu

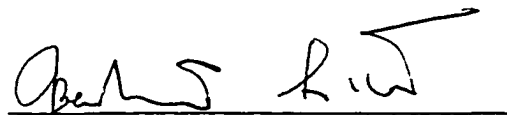
**Title of Thesis:** Experimental and Modelling Study of Reverse Flow Catalytic Converters for Natural Gas/Diesel Dual Fuel Engine Pollution Control

**Degree:** Doctor of Philosophy

**Year this Degree Granted:** 2000

Permission is hereby granted to the University of Alberta Library to reproduce single copies of this thesis and to lend or sell copies for private, scholarly, or scientific research purposes only.

The author reserves all other publication and other rights in association with the copyright in the thesis, and except as hereinbefore provided, neither the thesis nor any substantial portion thereof may be printed or otherwise reproduced in any material form whatever without the author's prior written permission.



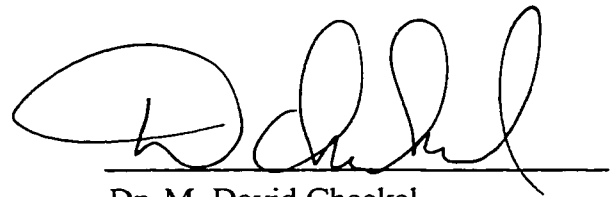
Mr. Benlin Liu  
Department of Mechanical Engineering  
University of Alberta  
Edmonton, Alberta  
CANADA T6G 2G8

**Date:** August 15/2000

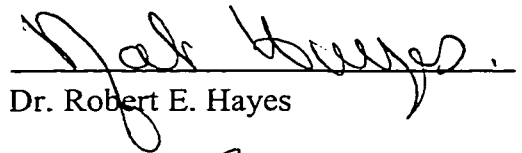
**University of Alberta**

**Faculty of Graduate Studies and Research**

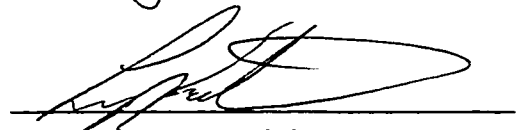
The undersigned certify that they have read, and recommend to the Faculty of Graduate Studies and Research for acceptance, a thesis entitled "Experimental and Modelling Study of Reverse Flow Catalytic Converters for Natural Gas/Diesel Dual Fuel Engine Pollution Control" submitted by Benlin Liu in partial fulfillment of the requirements for the degree of Doctor of Philosophy.



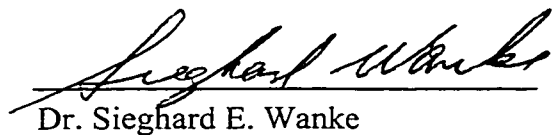
Dr. M. David Checkel



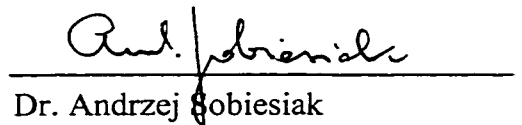
Dr. Robert E. Hayes



Dr. Larry W. Kostiuk



Dr. Sieghard E. Wanke



Dr. Andrzej Sobiesiak

Date: 14 Aug 2000

## ABSTRACT

The desire to reduce urban air pollution and petroleum consumption has renewed interest in the development of natural gas vehicles. The natural gas/diesel dual fuel engine is one of the practical ways to apply natural gas to the conventional diesel engines. Compared to the conventional diesel engines, natural gas/diesel dual fuel engines emit very low NO<sub>x</sub> and carbon soot to the air. However, poor fuel utilization efficiencies and higher emissions of HC and CO may be encountered at light loads. This study focuses on HC and CO control for the natural gas/diesel dual fuel engines at light loads.

A reverse flow catalytic converter has been developed to complement dual fuel engine exhaust characteristics. This study consists of experimental measurement and numerical simulation of reverse flow catalytic converters. It shows that reverse flow can establish a high reactor temperature even when the engine is run with low exhaust temperature level at light loads. The reactor temperature rise from reverse flow could be two or three times higher than the adiabatic temperature rise, which is based on the reactor inlet temperature and concentration. This temperature allows more than 90% of the HC and CO to be converted with a palladium based catalyst. It proved that the reverse flow is an approach superior to the conventional unidirectional flow to deal with natural gas/diesel dual fuel engine pollution at light loads.

During the engine mode transition, reverse flow could have a special “heat trap” effect. Depending on the HC and CO concentration, it can develop reactor temperature, maintain reactor temperature, or slow down reactor temperature drop. Reverse flow could maintain reactor temperature over 800 K and HC conversion about 80% during 6-Mode

test. The reverse flow switch time is evaluated from 5 to 240 second, it shows that the short switch time from 15 to 30 second is good for the engine tested.

A one dimensional single channel model is established to simulate both unidirectional flow and reverse flow reactor performance. The model can simulate the reactor performance with reasonable accuracy. Both CO and methane oxidation over palladium catalyst in an excess oxygen and water are described using apparent first order kinetics. The modified Voltz kinetics is in fact equivalent to first order rate expressions under conditions used in the reactor. The catalyst undergoes an apparent transition at a temperature in the region of 874 K, at which point the apparent activation energy decreased dramatically.

### **Keywords:**

Natural Gas/Diesel Dual Fuel Engine

Reverse Flow Catalytic Converter

Palladium Based Catalyst

Catalytic Combustion

Environment

Experiment

Modelling

Kinetics



*A Proverb is a Short Sentence Based on Long Experience*

*- Miguel de Cervantes*

**- DEDICATION -**

*I dedicate this work to my parents, my wife and my two lovely boys. I thank my parents for their everlasting love and I also thank my wife for her support and patience.*

## ACKNOWLEDGMENTS

I would like to take this opportunity to acknowledge every one who has made the completion of this thesis possible.

Dr. M. David Checkel:

My PhD program supervisor, who gave me a special opportunity to pursue a PhD degree in Canada, directed me for projects unknown, trained me as an engineer, a manager and a scientist, supported my study financially, led me to the path of success.

Dr. Robert E. Hayes:

My PhD program co-supervisor, who led me to catalytic combustion and catalytic reactor modelling.

Dr. Ming Zheng:

AFS (Alternative Fuel Systems Inc.) Senior Engineer, who let me know about the RFC (Reverse Flow Catalytic Converter), watched me carefully in engine tests, and let me know the difference between a scientist and an engineer.

Mr. Wayne Pittman:

For his knowledge in all things electrical, emission test facilities and data acquisition systems.

Mr. Nasser Sallamie:

For his kind support of literature and knowledge of catalytic combustion.

Mr. Oleg Zastavniuk:

For his kind support of engine testing, lab set-up and data analysis.

Mr. Rade Vukadin:

For his contribution of engine lab set-up with new emission test facilities and test set-up of the production version reverse flow system.

Mr. Jason Hawirko:

For his support during my hot summer of engine testing.

Mr. Allan Muir, Mr. Tony van Straten, Mr. Alberta Yuen, Mr. Donald Fuhr:

For their help and support solving all mechanical problems in the engine lab.

Dr. Larry W. Kostiuik, Dr. J Douglas Dale, Dr. David J. Wilson, Mr. Mark Y Ackerman:

The balance of the Combustion and Environmental Group, who provided valuable insights into what I have accomplished.

Helen, Doris, Linda and Gail:

For their assistance of my study

Dr. Ken R. Fyfe, Dr. Warren H. Finlay, Dr. Jeffrey W. Yokota, Dr. Dongqing Li, Dr. Zihui Xia, Dr. Abhijit Bhattacharyya, Dr. Andrew Mioduchowski, Dr. Krishnaswamy Nandakumar:

For their instruction in several technology areas for the achievement in my thesis.

Baljit Dhaliwal, Matt Johnson, Pascal Poudenx, Tim Weis, Glen Thomas, Marlo Reynolds:

My friends in the Combustion and Environmental Group, my mind and body become fresh whenever I am tired and I have a Ping Pong Game with them.

I would also recognize financial support from:

Dr. M. David Checkel, AFS, Department of Mechanical Engineering, CBR Cement Canada Limited, etc. in completing this degree.

## PREFACE

This thesis is concerned with the natural gas/diesel dual fuel engine light load pollution control. Reverse flow techniques is introduced to control dual fuel engine pollution from light loads. The reactor performance with reverse flow operation is evaluated with both experimental and modelling studies.

This thesis is consisted of seven chapters and organized in a “paper-format”, which is specified in the “Thesis Handbook – A Manual of Regulations and Guidelines for Thesis Preparation (October, 1997)” of the Faculty of Graduate Studies and Research. Chapter 1 is a general introduction of the project. Chapter 2 describes the detailed experimental set-up, apparatus used, measurement and correction techniques. Chapter 3 presents the experimental results of reverse flow catalytic converter. Chapter 4 establishes a numerical simulation model for the catalytic converter which is operated in the conventional unidirectional flow manner. Chapter 5 builds up a numerical simulation model for the reverse flow catalytic converter. Chapter 6 makes a more detailed kinetic study of palladium based catalyst for both methane and CO oxidation under reverse flow operations. Chapter 7 summarizes the conclusions of this study and provides some recommendation about future work. A set of Appendices provide more detail information of test and numerical programs.

Chapters 3, 4, 5 and 6 are based on individual papers. The publication details of these papers are given in the footnotes of the respective chapter. The references and nomenclature for each chapter appear at the end of the respective chapter. The references to the literature have been cited in the text by the author name followed by the year

published. The citation format is similar to that used by “The Canadian Journal of Chemical Engineering”.

This work was supported by Alternative Fuel Systems Inc., the Natural Sciences and Engineering Research Council of Canada. It was directed by Dr. M. David Checkel and Dr. Robert E. Hayes. The supports and instructions are highly acknowledged.

# Table of Contents

<b>Chapter 1</b>	<b>Introduction.....</b>	<b>1</b>
1.1	Natural Gas as a Transportation Fuel.....	2
1.2	Diesel Engines Fuelled with Natural Gas.....	6
1.3	Reverse Flow Catalytic Converter.....	11
1.4	Objective.....	17
1.5	Methodology.....	22
1.6	Outline.....	22
1.7	References.....	23
<b>Chapter 2</b>	<b>Experiment Set-up and Measurements.....</b>	<b>28</b>
2.1	Introduction.....	29
2.2	The Natural Gas/Diesel Dual Fuel Engine.....	30
2.3	Layout of Prototype Reverse Flow Catalytic Converters.....	33
2.4	Layout of Production Design Reverse Flow Catalytic Converter.....	40
2.5	Gas Analysis.....	44
2.5.1	Gas Analysis Equipment.....	44
2.5.2	Correction of the Measured Gas Compositions.....	47
2.6	Temperature Measurement and Correction.....	49
2.6.1	Temperature Measurement.....	49
2.6.2	Correction of the Measured Inlet Gas Temperature.....	50
2.7	Test Methods of Catalytic Converters.....	53
2.7.1	Fresh Catalyst Test.....	53
2.7.2	Unidirectional Mode Tests.....	57
2.7.3	Reverse Flow Mode Tests.....	57
2.8	Summary of Experimental Measurement.....	57
2.9	Nomenclature.....	58
2.10	References.....	59

<b>Chapter 3</b>	<b>Experimental Results for Reverse Flow Catalytic Converter.....</b>	<b>60</b>
3.1	Introduction.....	61
3.2	Reverse Flow Catalytic Converter Performance Under Steady Engine Operations.....	65
3.2.1	Comparison of Reactor Performance between Reverse Flow and Unidirectional Flow.....	65
3.2.2	Evaluation of Reverse Flow Switch Time.....	81
3.3	Reverse Flow Catalytic Converter Performance Under Transient Engine Operation.....	90
3.3.1	Introduction of Transient Engine Test with Reverse Flow Catalytic Converters.....	90
3.3.2	Transition from Heavy Load to Light Load.....	94
3.3.3	Transition from Light Load to Idle.....	99
3.3.4	Transition from Light Load to Heavy Load.....	104
3.3.5	Transition from Idle to Light Load.....	109
3.3.6	Summary of Transient Engine Results.....	114
3.4	Reverse Flow Catalytic Converter Performance with Japanese 6-Mode Test.....	115
3.4.1	Introduction of the 6-Mode Test.....	115
3.4.2	Comparison between Unidirectional Flow and Reverse Flow...	117
3.4.3	6-Mode Tests with Variable Reverse Flow Switch Times.....	121
3.4.4	Vary Reverse Flow Switch Time During 6-Mode Test.....	125
3.5	Conclusions.....	131
3.6	Nomenclature.....	133
3.7	References.....	133
<b>Chapter 4</b>	<b>Modelling Study of Unidirectional Flow Catalytic Converter.....</b>	<b>136</b>
4.1	Introduction.....	137
4.2	Experimental Apparatus.....	139
4.3	Mathematical Model.....	143

4.3.1	Assumptions.....	143
4.3.2	Model Equations.....	144
4.4	Physical and Chemical Parameters.....	146
4.4.1	Chemical Kinetics.....	146
4.4.2	Heat and Mass Transfer Coefficients.....	149
4.4.3	Effectiveness Factor.....	150
4.5	Numerical Approach for the Model Solution.....	152
4.6	Model Results and Analysis.....	153
4.6.1	Kinetic and Mass Transfer Control.....	154
4.6.2	Increase in Gas Temperature.....	156
4.6.3	Decrease in Inlet Gas Temperature.....	166
4.7	Conclusions.....	173
4.8	Nomenclature.....	173
4.9	Abbreviations.....	177
4.10	References.....	178
<b>Chapter 5</b>	<b>Modelling Study of Reverse Flow Catalytic Converter.....</b>	<b>183</b>
5.1	Introduction.....	184
5.2	Experimental Apparatus.....	190
5.2.1	Apparatus.....	190
5.2.2	Experimental Results.....	194
5.3	Mathematical Model.....	201
5.3.1	Assumptions.....	201
5.3.2	Model Equations.....	202
5.3.3	Kinetics.....	204
5.3.4	Heat and Mass Transfer Coefficients.....	207
5.3.5	Effectiveness Factor.....	208
5.4	Numerical Approach for the Model Solution Model Results and Analysis.....	211
5.4.1	Model Verification.....	211
5.4.2	Reverse Flow Cycling Time Evaluation.....	217



5.5	Conclusions.....	220
5.6	Nomenclature.....	220
5.7	References.....	223
<b>Chapter 6</b>	<b>Chemical Kinetic Study of Reverse Flow Catalytic Converter .....</b>	<b>226</b>
6.1	Introduction.....	227
6.2	Equipment.....	235
6.3	Experimental Results.....	239
6.4	Mathematical Model.....	247
6.4.1	Assumptions.....	247
6.4.2	Model Equations.....	248
6.4.3	Heat and Mass Transfer Coefficients.....	253
6.4.4	Effectiveness Factor.....	254
6.4.5	Numerical Solution.....	257
6.5	Kinetics.....	257
6.6	Model Results and Analysis.....	264
6.7	Conclusions.....	283
6.8	Nomenclature.....	283
6.9	References.....	286
<b>Chapter 7</b>	<b>Summary and Recommendations .....</b>	<b>291</b>
7.1	Introduction.....	292
7.2	Summary of Studies.....	293
7.3	Recommendations and Future Work.....	297
7.3.1	Control of Reverse Flow Catalytic Converter.....	297
7.3.2	Safety and Durability of Reverse Flow Catalytic Converter.....	299
7.3.3	Optimum Design of Reverse Flow Catalytic Converter.....	300
7.3.4	Modelling of Reverse Flow Catalytic Converter.....	301
7.3.5	Study of Chemical Kinetics of Palladium Based Catalyst.....	302
7.4	References.....	304

<b>Appendix A</b>	Methods to Use Modelling Programs.....	305
<b>Appendix B</b>	Programs for Reverse Flow Operation.....	317
<b>Appendix C</b>	Programs for Data Analysis.....	322

# List of Tables

<b>Chapter 1</b>	<b>Introduction.....</b>	<b>1</b>
Table 1-1	Emission Standards of Gasoline Engines (Breuer et al., 1996).....	4
Table 1-2	Emission Standards of Diesel Engines for Light Duty Vehicle (Zelenka et al., 1996).....	5
Table 1-3	Natural Gas Composition.....	7
Table 1-4	Properties of Diesel and Natural Gas Fuels (Nowak, 1994).....	10
Table 1-5	Comparison of Engine Exhaust Parameters between Dual Fuel Mode and Diesel Only.....	20
<b>Chapter 2</b>	<b>Experiment Set-up and Measurements.....</b>	<b>28</b>
Table 2-1	Engine Specifications.....	30
Table 2-2	Measurement Equipment.....	31
Table 2-3	The Physical Properties of Monolith Catalyst Bricks.....	40
Table 2-4	Emission Measurement Facilities for Prototype Catalytic Converter Test.....	46
Table 2-5	Emission Measurement Facilities for Production Type Catalytic Converter Test.....	46
Table 2-6	Transfer Engine Exhaust from Dry to Wet Basis.....	48
Table 2-7	Comparison of the Measured and Corrected Inlet Gas Temperature.....	53
<b>Chapter 3</b>	<b>Experimental Results for Reverse Flow Catalytic Converter.....</b>	<b>60</b>
Table 3-1	RFO Applications and the Reverse Flow Cycling Time Comparison.....	63
Table 3-2	Engine Exhaust Parameters.....	66

Table 3-3	The Performance of Catalytic Converter Under Three Engine Light Load Operations.....	68
Table 3-4	The Switch Time of Reverse Flow Operations.....	68
Table 3-5	Engine Exhaust Parameters for Case 4.....	79
Table 3-6	Comparison of Reactor Performance for Variable Cycling Time at 2000 rpm,120 Nm.....	84
Table 3-7	Comparison of Reactor Performance for Variable Cycling Time at 2600 rpm,70 Nm.....	87
Table 3-8	Engine Exhaust Parameters.....	91
Table 3-9	Reactor Performance for Three Engine Operations.....	92
Table 3-10	Engine Exhaust Parameters.....	117
Table 3-11	Engine Exhaust Compositions from 6-Mode Test.....	125
Table 3-12	Switch Time in 6-Mode Test.....	126
Table 3-13	Engine Exhaust Compositions of 6-Mode Tests.....	130

#### **Chapter 4 Modelling Study of Unidirectional Flow Catalytic Converter.....136**

Table 4-1	Some References to Monolith Modelling and Experimental Investigations.....	138
Table 4-2	The Main Physical Parameters of the Converter.....	140
Table 4-3	Analytic Equipment for Measurement of Engine Exhaust Composition.....	140
Table 4-4	Engine Exhaust Parameters for Two Steady Engine Operation Modes.....	157
Table 4-5	Steady State Model and Experiment Results.....	157
Table 4-6	Engine Exhaust Parameters for Two Steady Engine Operation Modes.....	166
Table 4-7	Steady Model and Experiment Results.....	169

<b>Chapter 5</b>	<b>Modelling Study of Reverse Flow Catalytic Converter .....</b>	<b>183</b>
Table 5-1	The Main Physical Parameters of the Converter.....	192
Table 5-2	Experiment with Variable Cycling Time.....	196
Table 5-3	Engine Exhaust Parameters for 1500 rpm, 80 Nm.....	211
Table 5-4	Simulation with Variable Cycling Time.....	217
<b>Chapter 6</b>	<b>Chemical Kinetic Study of Reverse Flow Catalytic Converter.....</b>	<b>226</b>
Table 6-1	Physical Parameters of the Converter.....	236
Table 6-2	Exhaust Gas Properties for the Three Cases Studied.....	239
Table 6-3	Reverse Flow Cycling Time.....	241
Table 6-4	Activation Energy and Transition Temperature for Methane Oxidation over Palladium Based Catalyst.....	263
Table 6-5	Steady State Results for the Unidirectional Flow Converter at Low Temperature.....	266
Table 6-6	Best Fit Kinetic Parameters for Reverse Flow Operation.....	271
Table 6-7	Average Values of Kinetic Parameters for the Three Cases Studied.....	272

# List of Figures

<b>Chapter 1</b>	<b>Introduction.....</b>	<b>1</b>
Figure 1-1	Reverse Flow Operation.....	13
Figure 1-2	“heat trap” Effect of Reverse Flow.....	14
Figure 1-3	Heat Transfer Between Fluid Phase and Solid Phase.....	15
Figure 1-4	Diagram of Natural Gas and Diesel Injection in Dual Fuel Engine.....	18
Figure 1-5	The Dual Fuel Engine Exhaust Characteristics.....	21
<b>Chapter 2</b>	<b>Experiment Set-up and Measurements.....</b>	<b>28</b>
Figure 2-1	Experiment Set-up of Prototype Reverse Flow Design.....	34
Figure 2-2	Overview of the Test Set-up for the Prototype Design of Reverse Flow System.....	36
Figure 2-3	Catalytic Converters Tested for the Prototype Design.....	39
Figure 2-4	Experiment Set-up of Production Type Reverse Flow Design.....	41
Figure 2-5	Overview of the Test Set-up for the Production Type Design of Reverse Flow System.....	43
Figure 2-6	The Exhaust Gas Sampling System.....	45
Figure 2-7	Heat Transfer Phenomena Around Thermocouple.....	50
Figure 2-8	The Fresh Catalyst Test for the Prototype Catalyst Shown in Figure 2-3 b).....	55
Figure 2-9	The Fresh Catalyst Test for the Production Type Catalyst.....	56
<b>Chapter 3</b>	<b>Experimental Results for Reverse Flow Catalytic Converter.....</b>	<b>60</b>
Figure 3-1	Steady Reactor Temperature Profiles for Unidirectional Flow Operations.....	67

Figure 3-2	Reactor Temperature Development by Reverse Flow Operation.....	70
Figure 3-3	HC and CO Conversion Resulted from Reverse Flow Operation.....	71
Figure 3-4	Temperature Profiles Along the Catalytic Converter.....	74
Figure 3-5	Comparison of Temperature Rise.....	75
Figure 3-6	Comparison of Reverse Flow and Unidirectional Flow Operation.....	76
Figure 3-7	Comparison of Reactor Temperature between Reverse Flow and Unidirectional Flow Operation.....	80
Figure 3-8	Reactor Temperature Profiles Resulted from Variable Reverse Flow Switch Times.....	83
Figure 3-9	Reactor Temperature Profiles Resulted from Variable Reverse Flow Switch Times.....	86
Figure 3-10	Steady Reactor Temperature Profiles.....	93
Figure 3-11	Comparison of Reactor Temperature with Engine Operation Transition from Heavy Load to Light Load.....	96
Figure 3-12	Comparison of Reactor Temperature Profiles.....	97
Figure 3-13	Comparison of HC and CO Conversion with Engine Transition from Heavy Load to Light Load.....	98
Figure 3-14	Comparison of Reactor Temperature Drop with Engine Operation Transition from Light Load to Idle.....	101
Figure 3-15	Comparison of Reactor Temperature Profiles.....	102
Figure 3-16	Comparison of HC and CO Conversion with Engine Operation Transition from Light Load to Idle.....	103
Figure 3-17	Comparison of Reactor Temperature Development with Operation Transition from Light Load to Heavy Load.....	106
Figure 3-18	Comparison of Reactor Temperature Profiles.....	107
Figure 3-19	Comparison of HC and CO Conversion with Engine Transition from Light Load to Heavy Load.....	108

Figure 3-20	Comparison of Reactor Temperature Development with Engine Operation Transition from Idle to Light Load.....	111
Figure 3-21	Comparison of Reactor Temperature Profiles.....	112
Figure 3-22	Comparison of HC and CO Conversion with Engine Operation Transition from Idle to Light Load.....	113
Figure 3-23	Japanese 6-Mode Test.....	116
Figure 3-24	Comparison of Reactor Temperature Variation in 6-Mode Test.....	119
Figure 3-25	Comparison of HC and CO Conversion.....	120
Figure 3-26	Comparison of Reactor Temperature.....	123
Figure 3-27	Comparison of HC and CO Conversion.....	124
Figure 3-28	Comparison of Reactor Temperature.....	128
Figure 3-29	Comparison of HC and CO Conversion.....	129

**Chapter 4 Modelling Study of Unidirectional Flow Catalytic Converter.....136**

Figure 4-1	Experimental Equipment Showing the Segmented Monolith Reactor.....	141
Figure 4-2	Example Solution of the Predicted Fluid and Solid Axial Concentration Profiles. (a) Methane and (b) Carbon monoxide. The Concentration on the Solid Surface is Between 80 and 90% of the Fluid Phase Concentration, Indicating that the Reactor is Predominantly Controlled by the Kinetics.....	155
Figure 4-3	The Steady State Converter Temperature Profiles for Two Engine Operations. See Table 4-4 for Details.....	158
Figure 4-4	Inlet Temperature to the Reactor as a Function of Time for the Case of an Increased Engine Outlet Temperature.....	159
Figure 4-5	Reactor Outlet Concentrations of HC and CO as a Function of Time for the Case of an Increase in Engine Exhaust Gas Temperature.....	162



Figure 4-6	Simulated Reactor Temperature Profiles at Various Elapsed Times, for the Case of an Increase in Engine Exhaust Gas Temperature.....	163
Figure 4-7	Comparison of Simulated and Experimental Reactor Temperature Profiles at Various Elapsed Times, for the Case of an Increase in Engine Exhaust Gas Temperature.....	164
Figure 4-8	Final Steady State Simulated Reactor Wall and Bulk Gas Temperature Profiles.....	165
Figure 4-9	The Steady State Converter Temperature Profiles for Two Engine Operations. See Table 4-6 for Details.....	167
Figure 4-10	Inlet Temperature to the Reactor as a Function of Time for the Case of a Decreased Engine Outlet Temperature.....	168
Figure 4-11	Reactor Outlet Concentrations of HC and CO as a Function of Time for the Case of a Decrease in Engine Exhaust Gas Temperature.....	170
Figure 4-12	Simulated Reactor Temperature Profiles at Various Elapsed Times, for the Case of a Decrease in Engine Exhaust Gas Temperature.....	171
Figure 4-13	Comparison of Simulated and Experimental Reactor Temperature Profiles at Various Elapsed Times, for the Case of a Decrease in Engine Exhaust Gas Temperature.....	172
<b>Chapter 5 Modelling Study of Reverse Flow Catalytic Converter.....</b>		<b>183</b>
Figure 5-1	Diagram of Reverse Flow Catalytic Converter.....	186
Figure 5-2	Temperature Development and “heat trap” Effect of Reverse Flow Catalytic Converter During the Flow Switch.....	189
Figure 5-3	Experimental Set-up.....	193
Figure 5-4	Initial Reactor Temperature Profile for Reverse Flow Operation with Variable Cycling Time.....	195

Figure 5-5	The Maximum Reactor Temperature $T_3$ and $T_4$ Varies with Reverse Flow Cycling.....	197
Figure 5-6	HC and CO Conversion Varies with Reverse Flow Cycling.....	198
Figure 5-7	The Middle Reactor Temperature $T_3$ and $T_4$ under Unidirectional Flow.....	199
Figure 5-8	HC and CO Conversion under Unidirectional Flow.....	200
Figure 5-9	The Initial Reactor Temperature Profile for Starting Simulation.....	213
Figure 5-10	The Transient Converter Inlet Temperature for the Reverse Flow Simulation.....	214
Figure 5-11	Comparison of Transient HC and CO Conversion between Experiment and Simulation.....	215
Figure 5-12	Comparison of Transient Reactor Temperature between Experiment and Simulation.....	216
Figure 5-13	Comparison of Transient HC and CO Conversion with Different Cycling Time.....	218
Figure 5-14	Comparison of the Maximum Reactor Temperature $T_3$ and $T_4$ with Different Cycling Time.....	219

## **Chapter 6 Chemical Kinetic Study of Reverse Flow Catalytic Converter.....226**

Figure 6-1	The Reverse Flow Catalytic Converter Concept.....	231
Figure 6-2	The “heat trap” Effect for Reverse Flow Operation.....	232
Figure 6-3	Experimental Set-up.....	238
Figure 6-4	Initial Reactor Temperature Profiles.....	243
Figure 6-5	The Development of the Middle Reactor Temperature $T_3$ and $T_4$ with Reverse Flow Cycling.....	244
Figure 6-6	HC and CO Conversion with Reverse Flow Cycling.....	245
Figure 6-7	Comparison Between the Unidirectional Operation and the Reverse Flow Operation.....	246

Figure 6-8	The Transient Reactor Inlet Temperature During Reverse Flow Cycling.....	267
Figure 6-9	Arrhenius Plot for CH <sub>4</sub> and CO Oxidation.....	268
Figure 6-10	Comparison of Transient HC and CO Conversion Between Experiment and Simulation.....	273
Figure 6-11	Comparison of Middle Reactor Temperature T <sub>3</sub> Between Experiment and Simulation.....	274
Figure 6-12	Comparison of Middle Reactor Temperature T <sub>4</sub> Between Experiment and Simulation.....	275
Figure 6-13	Comparison of Simulated and Experimental Reactor Temperature Profiles at Various Elapsed Times for Case 1.....	276
Figure 6-14	Comparison of Simulated and Experimental Reactor Temperature Profiles at Various Elapsed Times for Case 2.....	277
Figure 6-15	Comparison of Simulated and Experimental Reactor Temperature Profiles at Various Elapsed Times for Case 3.....	278
Figure 6-16	Comparison of Transient HC and CO Conversion Between Experiment and Simulation Using Average Values for the Kinetic Parameters.....	279
Figure 6-17	Comparison of HC and CO Conversion Between the Reverse Flow Operation and the Unidirectional Flow Operation.....	281
Figure 6-18	Comparison of Middle Reactor Temperatures T <sub>3</sub> and T <sub>4</sub> Between the Reverse Flow Operation and the Unidirectional Flow Operation.....	282

# **Chapter 1**

## **Introduction**

*Chapter 1 sets the context for this thesis, provides an introduction to reverse flow catalytic converter for natural gas/diesel dual fuel engines, states the research objectives, and outlines the content of each chapter.*

## 1.1 Natural Gas as a Transportation Fuel

Concern over high levels of pollutants in vehicular exhaust gas emissions and the implementation of strict engine pollution regulations has been a driving force behind research efforts in alternative fuel systems for use in road vehicles. This research is also motivated by the economic and strategic advantages of alternative fuels. Several alternative fuels have been recognized as having a significant potential for producing lower overall pollutant emissions compared to gasoline and diesel fuel (Springer, 1991). Alternative fuels which have been studied for replacing conventional transportation fuels include: Natural Gas, Methanol, Ethanol, Hydrogen, Propane, etc. Natural gas, which is composed predominately of methane, has been identified as a leading candidate for transportation applications among these fuels for several reasons.

The first reason is availability. There are large reserves of natural gas which are found in most parts of the world, including: Europe, Asia, New Zealand, North America and South America. According to Bowen (1982), the total estimated remaining recoverable gas is adequate for almost 200 years. In addition to this, synthetic natural gas can be manufactured from coal and biomass conversion (McElroy, 1982; Antal, 1982).

The second attraction of natural gas is its environmental compatibility. Conventional diesel engines have a significant emission of  $\text{NO}_x$ , HC and particulates. Diesel engines fuelled with natural gas give very low emission of NMHC (Non-Methane Hydro-Carbon),  $\text{SO}_2$ ,  $\text{CO}_2$ ,  $\text{NO}_x$  and particulates compared to the straight diesel fuelling (Wong et al., 1991; Kroff, 1990; Weaver, 1989). For natural gas vehicles, the primary HC (Hydro-Carbon) found in the exhaust is methane. THC (Total Hydro-Carbon) emission from natural gas vehicles are generally higher than conventional fueled vehicles (Fritz

and Egluono, 1992). However, the potential for methane participating in photochemical reactions, which is a primary concern in HC emissions, is small. The essentially inert behavior of methane has led to a relaxation in regulating the THC emissions by CARB (California Air Resource Board) and proposed EPA (Environmental Protection Agency) regulations in favor of considering NMHC emissions. In the work reported by Chrysler, total transient emission levels from a developed CNG (Compressed Natural Gas) van were the lowest for any vehicle certified in California in 1992, and demonstrated the potential for meeting LEV (Low Emission Vehicle) and ULEV (Ultra Low Emission Vehicle) requirements (Geiss et al., 1992). These strict regulations are summarized in Tables 1-1 and 1-2.

From Table 1-1, it is easy to see that the vehicle emission regulations are becoming increasingly strict. The standard TIER 1 is still in effect in USA now. This was modified in 1994 through the introduction of NMHC (Non-Methane Hydro-Carbon), and becomes valid for all vehicles from 1996. TIER 2 emission limits are planned for introduction in the year 2004, in which a 50% reduction of the respective standards will apply. In contrast to the rest of the USA, the State of California mandated four different “clean” classes of vehicles: TLEV (Transitional Low Emission Vehicle), LEV, ULEV and ZEV (Zero Emission Vehicle). A similar but much delayed development can be observed in Europe. The standard at present in effect according to EC (European Community) 93 is EC level II. Further more demanding standards are projected following the year 2000 (Rodt et al., 1995). The proposed Level III falls between the California LEV and ULEV standards. Table 1-2 shows the diesel engine emission standards for

passenger cars and heavy duty vehicles for major industrial countries in Europe, USA, Japan and Korea.

Table 1-1 Emission Standards of Gasoline Engines (Breuer et al., 1996)

REGULATIONS	PLACE	HC	NO <sub>x</sub>	CO
TIER 1	USA	0.25	0.4	3.4
TIER 2		0.125	0.2	1.7
TLEV	California	0.125	0.4	3.4
LEV		0.075	0.2	3.4
ULEV		0.040	0.2	1.7
ZLEV		0	0	0
EC II	Europe	0.5		2.2
EC III		0.05	0.14	1.5

Unit: g/km

HC: NMHC (USA, California), THC (Europe)

TLEV: Transitional Low Emission Vehicle

LEV: Low Emission Vehicle

ULEV: Ultra Low Emission Vehicle

ZLEV: Zero Low Emission Vehicle

EC: European Community

Table 1-2 Emission Standards of Diesel Engines for Light Duty Vehicles  
(Zelenka et al., 1996)

Place	Implementation Date	Soot	CO	HC	NO <sub>x</sub>	Test Cycle
Europe	1996 (EURO II)	0.10 (DI)		0.9 (DI)		MVEG (ECE+ EUDC)
		0.08 (ID)	1.0	0.7(ID)		
	1999 <sup>a</sup> (EURO III)	0.04	0.5	0.5 (0.1+0.4)		
	Ca. 2003 <sup>b</sup> (EURO IV)	0.025	?	0.05+0.14		
USA (49 States) <sup>c</sup>	1996	0.1	4.2	0.31 (NMHC)	1.25	FTP
	1998	-	-	-	-	
	2003	-	-	-	-	
California	1996 <sup>d</sup>	0.08	4.2	0.31 (NMHC)	1.0	
	TLEV	0.08	4.2	0.156	0.6	
	LEV	0.08	4.2	0.09	0.3	
	ULEV	0.04	2.1	0.055	0.3	
Japan	Since 1994	0.2	2.1	0.4	0.5/<1250 kg <sup>e</sup> 0.6/>1250 kg	10.15 Cycle
	2000	0.08	2.1	0.4	0.4	
Korea	1996	0.08	2.11	0.25	0.62	FTP 75
	2000	0.05	2.11	0.25	0.62	

Unit: g/km

a: Standards for EURO III proposed by the German EPA

b: First in-official proposal from Germany

c: 100 kmiles for LDV

d: EPA proposal

e: Inertia test weight



The third attraction of natural gas is that it can be used in conventional diesel and gasoline engines. By making some small modifications, conventional diesel and gasoline engine can use natural gas directly. Finally, natural gas is widely distributed and can be used as a fuel without chemical transformation. This reduces the capital and energy cost of developing an alternative fuel for large scale use.

In summary, natural gas is a very good alternative fuel for the conventional diesel and gasoline engines. It has sufficient proven reserves in the world. Natural gas vehicles exhibit significant potential for the reduction of harmful emissions like: NMHC, SO<sub>2</sub>, CO<sub>2</sub>, NO<sub>x</sub> and particulates. There are problems for natural gas applications such as: on-board storage due to low energy/volume ratio, knock at high loads and high emission of methane and carbon monoxide at light loads. However, these can be overcome by the proper design, fuel management and exhaust treatment techniques. In the following section, a natural gas application - natural gas/diesel dual fuel engines is introduced.

## **1.2 Diesel Engines Fuelled with Natural Gas**

The natural gas/diesel dual fuel engine is based on a conventional diesel engine, which is modified to utilize both natural gas and diesel fuels. In the dual fuel scenario, natural gas is the major fuel and a diesel fuel pilot is used as an ignition source. Methane is the principal component of natural gas. Normally more than 90% of natural gas is methane, as shown in Table 1-3.

Table 1-3 Natural Gas Composition

Composition	Formula	Volume Fraction (%)			
		Reference #1	Reference #2	Reference #3	Reference #4
Methane	CH <sub>4</sub>	94.00	92.07	94.39	91.82
Ethane	C <sub>2</sub> H <sub>6</sub>	3.30	4.66	3.29	2.91
Propane	C <sub>3</sub> H <sub>8</sub>	1.00	1.13	0.57	
Iso-Butane	i-C <sub>4</sub> H <sub>10</sub>	0.15	0.21	0.11	
N-Butane	n-C <sub>4</sub> H <sub>10</sub>	0.20	0.29	0.15	
Iso-Pentane	i-C <sub>5</sub> H <sub>12</sub>	0.02	0.10	0.05	
N-Pentane	n-C <sub>5</sub> H <sub>12</sub>	0.02	0.08	0.06	
Nitrogen	N <sub>2</sub>	1.00	1.02	0.96	4.46
Carbon Dioxide	CO <sub>2</sub>	0.30	0.26	0.28	0.81
Hexane	C <sub>6</sub> + (C <sub>6</sub> H <sub>14</sub> )	0.01	0.17	0.13	
Oxygen	O <sub>2</sub>		0.01	<0.01	
Carbon Monoxide	CO		<0.01	<0.01	
Total		100	100	100	100

Reference #1: Ding and Hill, 1986

Reference #2: Bell, 1993

Reference #3: Wong et al., 1991

Reference #4: Nowak, 1994

Natural gas has an octane number as high as 120 (Nowak, 1994). However, the cetane number of natural gas is extremely low, (less than 6), so natural gas can not practically be ignited by compression ignition. It requires an auxiliary ignition source. Octane number is an indication of the knock resistance ability of fuels. The higher the number, the better the knock resistant ability. Natural gas has a very good anti-knock quality and can be safely used on diesel engines, which have high compression ratios and allow the high fuel combustion efficiency (Karim, 1983).

Gunawan (1992) summarized the three principal methods to use natural gas on diesel engines. They are manifold injection, timed port injection and direct injection. All these methods need an ignition source for natural gas combustion because natural gas has an auto-ignition temperature as high as 650 °C. Nowak (1994) compared the properties of natural gas and diesel fuel, as shown in Table 1-4. Without the ignition source, a compression ratio on the order of 60 would be required for the auto-ignition of natural gas, which is about three times higher than the conventional diesel engine compression ratios. The ignition source for natural gas could be from either a spark plug or a pilot injection of diesel fuel. Because the auto-ignition temperature of diesel fuel ranges from 204 to 260 °C and it is easily ignited, normally a small amount of diesel fuel is injected into the combustion chamber near the end of the compression stroke. The auto-ignition of diesel fuel initiates the combustion of natural gas.

According to Barbour et al. (1986), the fraction of diesel fuel that could be replaced by natural gas ranges from 47% to 85%. The upper limitation is owing to the onset of engine knock at high loads, and the lower limit owing to low combustion efficiency at light loads. The low combustion efficiency could result in significant amounts of HC and CO in the engine exhaust (Karim, 1982, 1983).

Wong et al. (1991) summarized several studies of natural gas/diesel dual fuel engines. Some studies showed that NO<sub>x</sub> emissions from dual fuel engine exhausts were reduced compared the straight diesel fuelling (Acker, 1986; Varde, 1983; Karim, 1982, 1983; Ding and Hill, 1986; Barbour et al., 1986; Midkiff et al., 1989; Douville, 1994). On the other hand, some studies showed that NO<sub>x</sub> emissions from dual fuelling were higher than straight diesel fuelling, especially when the engines with dual fuelling were operated

close to stoichiometric conditions (Bro and Pedersen, 1977; Tesarek, 1983). Nowak (1994) and Wong et al. (1991) showed that NO<sub>x</sub> emissions from dual fueling were almost identical from straight diesel fuelling. These results indicate that NO<sub>x</sub> emission levels depend not only on the fuel type, but also on other operating conditions. The emissions of SO<sub>2</sub>, CO<sub>2</sub> and smoke particulate were greatly reduced by dual fuelling (Tesarek, 1983; Barbour et al., 1986; Boisvert et al., 1988; Wong et al., 1991; Midkiff et al., 1989; Nowak, 1994, Checkel et al., 1998). However, Barbour et al. (1986) also discovered that SOF (Soluble Organic Fractions) had a high ratio among the lower amount of particulates produced by dual fuelling. The other general trend is for the CO and HC emissions. THC and CO emissions of diesels tend to be minimal but those of dual fuel engines can be significant at light loads (Acker, 1986; Tesarek, 1983; Karim, 1982, 1983, 1991; Ding and Hill, 1986; Barbour et al., 1986; Midkiff et al., 1989; Nowak, 1994; Checkel et al., 1998). Most of the HC in the dual fuel engine exhaust is methane which, although chemically resistant and toxicologically inert, is a strong "greenhouse" gas (Lampert et al., 1997; Oh et al., 1991). By mass, methane has 12 to 30 times the greenhouse effect as CO<sub>2</sub> (Deluchi et al.). Although the United States diesel engine emission standard only gives limits for the Non-Methane Hydrocarbon (NMHC) exhaust, in the European Community, Japan and Korea, the Total Hydrocarbon (THC) in the exhaust gas is considered (Zelenka et al., 1996; Lampert et al., 1997), as shown in Table 1-2. It may therefore be necessary to use a catalytic converter in the exhaust system to reduce the HC and CO of dual fuel engines to an acceptable level.

Table 1-4 Properties of Diesel and Natural Gas Fuels (Nowak, 1994)

Properties	Diesel Fuel	Natural Gas
Phase at Ambient Temperature	Liquid	Gas
Molecular Weight	About 226	About 17.2
Composition	Long Chain Hydrocarbon $C_nH_{1.8n}$	92% CH <sub>4</sub> , 3% C <sub>2</sub> H <sub>6</sub> , 4% N <sub>2</sub> , 1% CO <sub>2</sub>
Specific Gravity (@15 deg, 1 bar)	0.845	0.00073
H/C Ratio	1.8	3.9
Stoichiometric A/F Ratio (Mass Basis)	14.5-16.0	15.5
Flammability Limit	0.6-6.5%	5-15%
Auto-ignition Temperature	204-260°C	650°C
Lower Heating Value		
Mass (MJ/kg)	43.17	45.3
Volume (MJ/l)	36.5	6.8 <sup>1</sup>

1: In storage condition 15°C, 20.7 MPa

### **1.3 Reverse Flow Catalytic Converter**

Catalytic converters have been widely used on gasoline engines since about 1979, with the most commonly used catalyst at present being the three way catalyst (TWC), which oxidizes CO and HC, and reduces NO<sub>x</sub> (Shelef and Graham, 1994; Miyoshi et al., 1995). Although perhaps less common, catalytic converters have also been used on diesel engines (Clerc, 1996; Hosoya and Shimoda, 1996; Farrauto and Voss, 1996). Owing to the importance of catalytic converters, it is not surprising to find that many experimental and modelling studies have been reported in the literature, although a large amount of the work has been devoted to catalyst development. See for example the reviews of Leclerc and Schweich (1993). Most attention is currently focused on the TWC gasoline converter, and to a lesser extent oxidizing catalysts for straight diesel applications. Some investigations for methane catalytic oxidation in the natural gas fuelled engines were reported by Summers et al. (1991), Sakai et al. (1991), Oh et al. (1991), Lampert et al. (1997). Bittner and Aboujaoude (1992) investigated the catalytic control of NO<sub>x</sub>, CO and NMHC emissions from stationary diesel and dual fuel engines. However, the performance and operating conditions of a catalytic converter for the natural gas/diesel system have not been widely studied. These systems are significantly different from the TWC system. For example, the TWC on a gasoline engine operates at conditions close to stoichiometric, whilst dual fuel engines typically operate in a lean combustion environment, which results in an excess of oxygen in the exhaust gas. The exhaust gas temperatures are also typically much lower than those observed in gasoline engines, which can lead to lower reaction rates. Furthermore, the principal hydrocarbon in the exhaust of a dual fuel engine is methane, which is the most difficult hydrocarbon to

oxidize.

It is a challenge to develop a catalytic converter for dual fuel engines because of the relative unreactivity of methane. Palladium (Pd) based catalysts are the most commonly used for methane oxidation in catalytic combustion applications. A further difficulty faced in the development of a catalytic converter for methane oxidation in dual fuel engine exhaust is the low exhaust temperature at light engine load. One possible solution for low reactor gas inlet temperature is to use a reversing flow catalytic converter, described in the following.

In the reversing flow reactor, the feed is periodically switched between the two ends of the reactor (Matros and Bunimovich, 1996). The concept of the reverse flow catalytic converter is shown schematically in Figure 1-1. In Figure 1-1(a) the control valves 1 and 4 are opened and the engine exhaust flows to the catalytic converter from left to right. This mode can be called the forward flow. In Figure 1-1(b) the control valves 2 and 3 are opened and the engine exhaust flows to the catalytic converter from right to left. This mode is called the reverse flow. The total cycle duration consists of these two operations, and the term switch time is used to denote the time at which the flow is changed from forward flow to reverse flow. If the forward flow time is the same as the reverse flow, the operation is referred to as symmetric reverse flow operation. If the two flow modes have different times then operating mode is referred to as asymmetric operation. For an exothermic reaction, the reverse flow catalytic converter exhibits what has been referred to as a “heat trap” effect, as shown in Figure 1-2 and explained below.

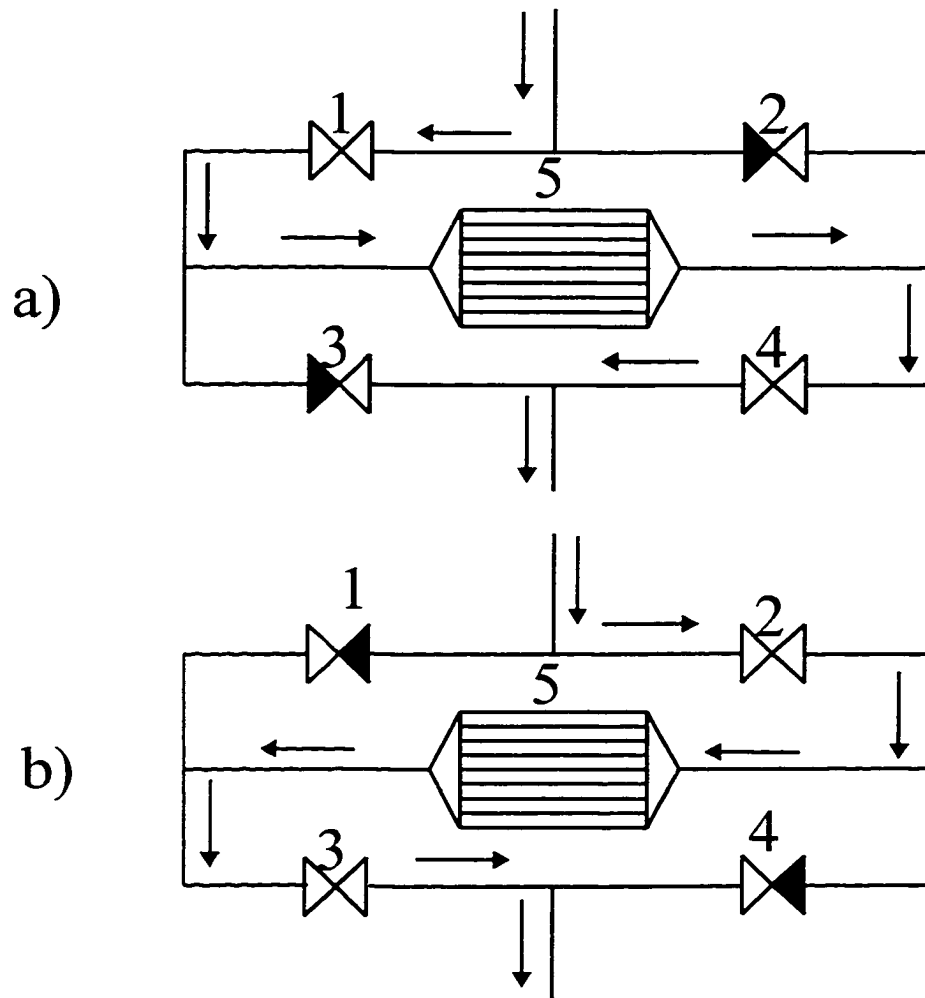


Figure 1-1 Reverse Flow Operation



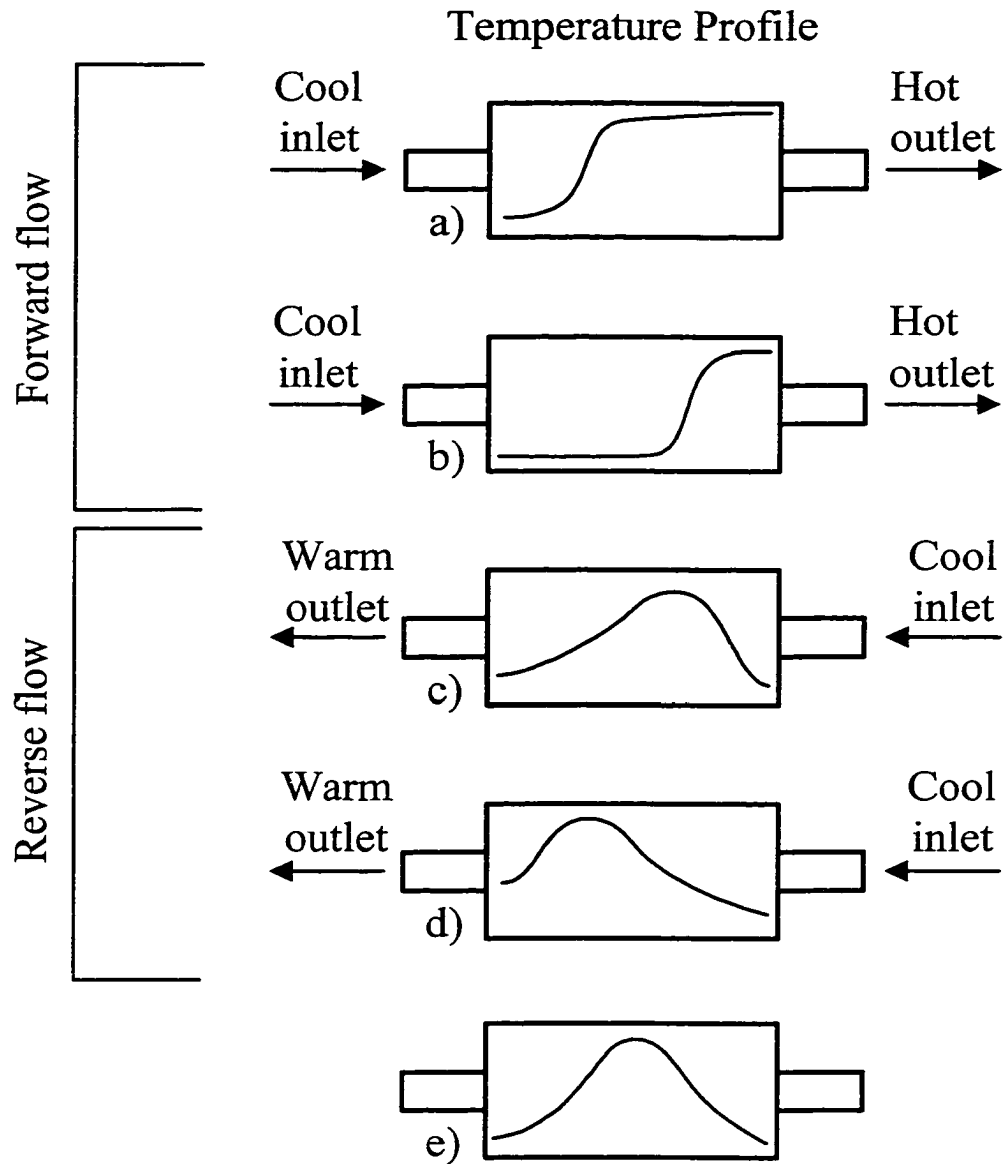


Figure 1-2 “heat trap” Effect of Reverse Flow

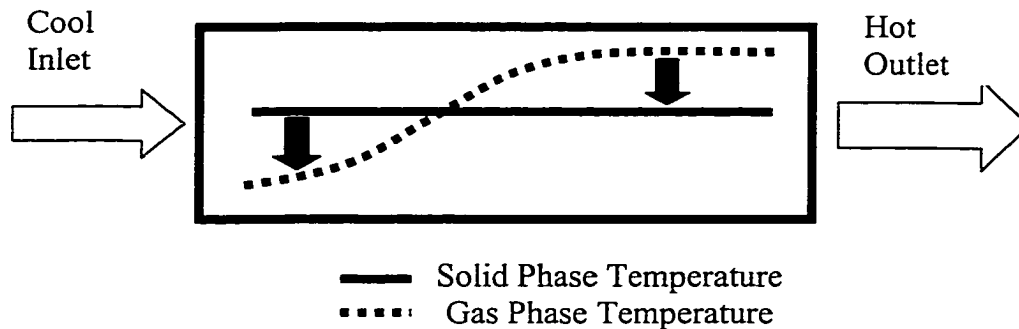


Figure 1-3 Heat Transfer Between Fluid Phase and Solid Phase

In a standard unidirectional flow operation, the converter typically exhibits a temperature profile as shown in Figure 1-2(a). The heat transfer between the fluid phase and solid phase varies as the gas flows through the catalytic converter. In Figure 1-3, the catalytic converter is preheated to a temperature, as shown by the solid line in the center of the reactor. The engine exhaust gas enters the catalytic converter at a lower temperature as represented by the dotted line. In the reactor inlet part, heat is transferred from the solid phase to the cooler gas phase. The gas is gradually heated and the catalytic reaction happens after the gas is heated to a certain temperature. The energy from exothermal reactions is transferred to the reaction products and other fluid gas. This increases the gas temperature higher than the downstream solid phase temperature. At the reactor outlet part, heat transfer is transferred from gas phase to solid phase, as shown in Figure 1-3.

The shape of the curve depends on the operating conditions, especially the inlet gas temperature and composition. If the inlet temperature is lowered, the reaction rate

will fall, and the temperature peak will migrate towards the reactor exit. With continuous unidirectional flow operation, the reaction will effectively be extinguished and the converter will lose most of its effectiveness as the leading edge of the “hot spot” where most reaction occurs migrates out of the reactor. If a temperature pattern shown in Figure 1-2(a) or (b) is established, the reverse flow operation can then be used to take advantage of the high temperatures near the reactor exit. When the feed is switched to the “exit”, the energy stored in the reactor from the previous reaction is then effectively used to preheat the feed. Because this stored energy is added to the feed stream, it is possible to achieve temperatures higher than the gas-phase adiabatic temperature rise (gas phase adiabatic temperature rise calculation is shown in Appendix C), based on the fresh feed inlet temperature.

Provided that the reactor is initially at a sufficiently high temperature and the cycle time is carefully chosen, it is possible to achieve autothermal reactor operation at feed temperatures well below those required for autothermal operation with unidirectional flow operation. In such a case a quasi-steady state operation may be achieved in which the reactor temperature profile has a maximum value near the centre of the reactor, which slowly oscillates as the feed is switched between the two ends of the reactor, as shown in Figures 1-2 (c-e). This temperature effect has been referred to as a heat sink (Matros and Bunimovich, 1996) and also a “heat trap” (Strots et al., 1998). Hanamura et al. (1993) demonstrated a reverse flow operation in which the solid phase temperature rise was as high as 13 times the adiabatic temperature rise. In addition to the experimental study, some modelling studies have been used to investigate the reverse flow thermal effects (Purwono et al.; Guit, 1993; Wallace and Viljoen, 1995; Özgülsen

and Cinar, 1994). Reverse flow reactors have been used industrially for the oxidation of VOC (Volatile Organic Compounds), oxidation of sulphur dioxide (SO<sub>2</sub>), the synthesis of methanol, and other purposes. Typically these applications have very low gas velocity and the reverse flow cycle duration can be as high as 4 hours. Engine exhaust reactors have a much higher gas velocity and consequently a faster switching frequency is expected. The cycling time is the major factor controlling the migration and magnitude of the temperature peak, and as such should be selected with care.

#### **1.4 Objective**

The main objective of this study is to study the use of a reverse flow catalytic converter for reducing the emission levels of HC and CO of natural gas/diesel dual fuel engines at light loads. The engine used for this purpose was a naturally aspirated four cylinders ISUZU 4BE1 engine of 3.6 litre displacement, which had been modified to operate with a dual fuel system. The method to apply natural gas on this diesel engine is timed port injection, as shown in Figure 1-3. Natural gas is injected near the intake port of each cylinder at timed intervals. A small amount of diesel fuel pilot is directly injected to each cylinder. With a proper computer controlled system, both natural gas and diesel fuel are injected according to the engine requirement and proper timing. The auto-ignition of diesel fuel provides the ignition source of natural gas.

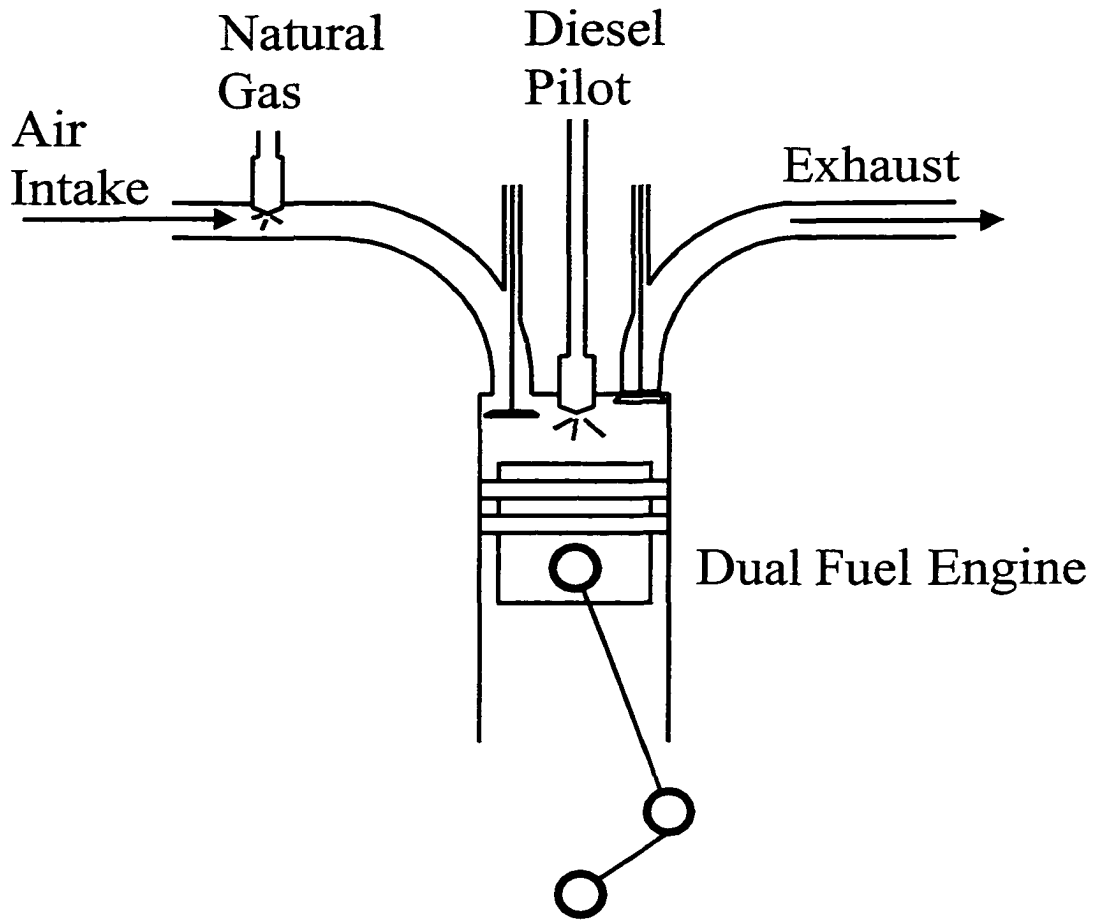


Figure 1-4 Diagram of Natural Gas and Diesel Injection in Dual Fuel Engine

Compared to straight diesel fuelling, this dual fuel engine has a higher exhaust of HC and CO at light loads as in other studies (Acker, 1986; Tesarek, 1983; Karim, 1982, 1983, 1991; Ding and Hill, 1986; Barbour et al., 1986; Midkiff et al., 1989; Nowak, 1994), as shown in Table 1-5. More than 95% of the HC in the dual fuel exhaust mode is methane. As the load of this dual fuel engine changes from high to low, its HC and CO increases, but engine exhaust temperature reduces, as shown in Figure 1-4. Converting the emissions at these light loads with conventional catalytic converters is very difficult because the engine exhaust temperature is too low for effective catalyst operation. This dissertation describes a research program into the use of reverse flow catalytic converters to achieve reactor temperatures high enough to oxidize the HC and CO emissions of dual fuel engines operating at light loads.

Table 1-5 Comparison of Engine Exhaust Parameters between Dual Fuel Mode and Diesel Only

Engine Mode	Speed (rpm)	Torque (NM)	Exhaust Composition (Dry Basis)										Engine Exhaust Temp. (°C)	
			HC (ppm)		CO (ppm)		NO (ppm)		O <sub>2</sub> (%)		CO <sub>2</sub> (%)			
			DFE*	DO <sup>#</sup>	DFE*	DO <sup>#</sup>	DFE*	DO <sup>#</sup>	DFE*	DO <sup>#</sup>	DFE*	DO <sup>#</sup>	DFE*	DO <sup>#</sup>
1	Idle	Idle	304	193	645	302	125	252	18.58	18.50	1.736	1.70	146	99
2	1360	175	1701	285	890	1003	1470	1306	7.532	5.99	7.979	10.78	473	470
3	1360	52	5621	154	1941	356	177	373	16.21	16.81	2.989	2.95	229	174
4	2040	195	1503	178	911	708	1307	1167	6.183	7.07	8.78	10.08	603	560
5	2040	49	4403	170	1751	528	131	287	15.79	16.48	3.364	3.18	271	240
6	2720	116	3737	147	2098	240	429	662	9.75	11.17	6.901	6.67	587	419
Weighted Value over 6 Modes			2520	184	1060	458	396	536	13.62	14.33	4.67	4.85	-	-

Test: Japanese 6 Mode Test

DFE\*: Natural Gas/Diesel Dual Fuel Engine

DO<sup>#</sup>: Diesel Only

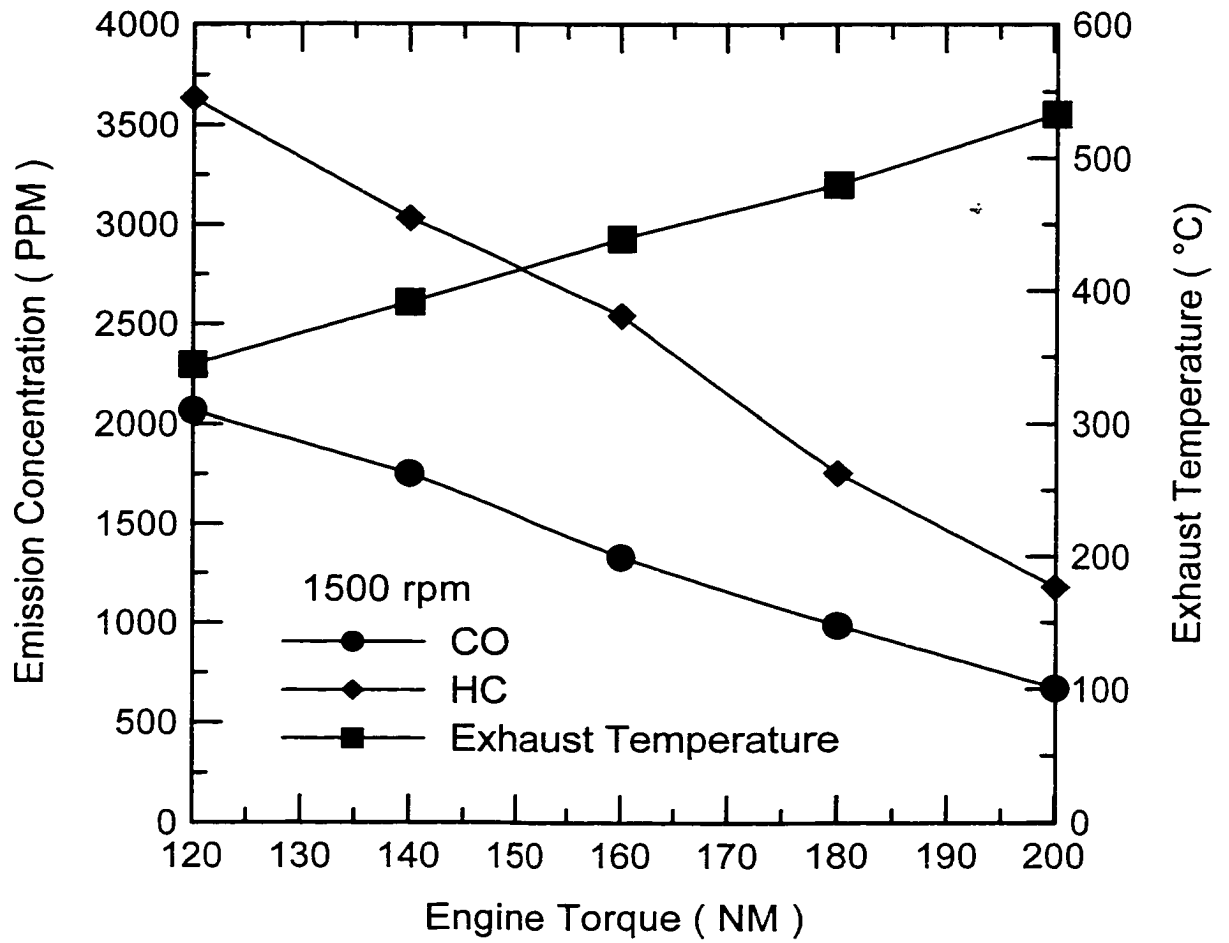


Figure 1-5 The Dual Fuel Engine Exhaust Characteristics



## **1.5 Methodology**

A step-wise approach has been used in this study. First, the reverse flow catalytic converter performance was determined experimentally. Then a numerical simulation model for both unidirectional flow mode and reverse flow mode was established. The model was validated against experiment data. Once the model was proved reasonable, it was used to determine the best operating parameters of reverse flow catalytic converter for variable engine operations. The model was also used to evaluate the reactor designs. The model is a tool for both reactor control and reactor design.

## **1.6 Outline**

This thesis is composed of seven chapters. Chapter 1 is a general introduction of the project. It points out the project problems, challenges and approaches. Chapter 2 describes the detailed experimental set-up, apparatus used, measurement and correction techniques. Chapter 3 presents the experimental results of reverse flow catalytic converter under both steady and transient engine operations. It shows the reverse flow catalytic converter can build-up and maintain a very high reactor temperature even for a dual fuel engine running at light loads with very low exhaust temperatures. This allows for better than 80% HC and CO conversion with a very low reactor inlet temperature. It is proven that reverse flow operation is superior to unidirectional flow at light engine loads.

Chapter 4 establishes a numerical simulation model for the catalytic converter which is operated in the conventional unidirectional flow manner. The kinetic approach used for CO and CH<sub>4</sub> oxidation is the modified version of Voltz kinetics (Voltz et al., 1973). The NO<sub>x</sub> inhibition effect is included. Chapter 5 builds up a numerical simulation

model for the reverse flow catalytic converter. It uses the same kinetic approach as Chapter 4. However, the  $\text{NO}_x$  inhibition effect is eliminated in light of the low  $\text{NO}_x$  concentration in the engine exhaust for light loads. The model includes two kinetic rates for  $\text{CH}_4$  oxidation with low temperature and high temperature regimes. Chapter 6 makes a detailed kinetic study of palladium catalyst for  $\text{CH}_4$  oxidation under reverse flow operations. It shows that CO and  $\text{CH}_4$  catalytic oxidation rate could be derived as first order kinetic processes with respect to the corresponding CO and  $\text{CH}_4$  concentration and that the kinetics for  $\text{CH}_4$  oxidation undergoes a transition with the activation energy dropping as the reactor temperature increases across a threshold temperature. Chapters 3, 4, 5 and 6 are based on individual papers. The publication details of these papers are given in the footnotes of the respective chapter. Chapter 7 summarizes the conclusions of this study and provides some recommendation about future work.

## 1.7 References

- Acker G. H., "A study of the combustion characterization of the dual-fuel engine", Ph. D. Dissertation, The University of Alabama, 1986
- Antal Jr. M. J., "Biomass conversion to methane", Methane – Fuel for the Future, Plenum Press, New York, NY, 1982
- Barbour T. R., M. E. Crouse and S. S. Lestz, "Gaseous fuel utilization in a light-duty diesel engine", SAE 860070, 1986
- Bell S. R., "Natural gas as a transportation fuel", SAE 931829, 1993
- Bittner R. W., F. W. Aboujaoude, "Catalytic control of  $\text{NO}_x$ , CO and NMHC emissions from stationary diesel and dual-fuel engines", J. of Engineering for Gas Turbines and Power, Vol. 114, 597-601, 1992.

- Boisvert J., L. E. Gettel and G. C. Perry, "Particulate emissions of a dual fuel Caterpillar 3208 engine", The Energy –Source Technology Conference and Exhibition, New Orleans, Louisiana, ASME 88-ICE-18, January 10-14, 1988
- Bowen W. J., "Supplies of methane in the united states", Methane – Fuel for the future, Plenum Press, New York, NY, 1982
- Breuer J., P. Hirth, R. Brück and C. Kruse, "Electrically heated catalyst for future USA and European legislation", SAE 960339, 1996
- Bro K. and P. S. Pederson, "Alternative diesel engine fuels: an experimental investigation of methanol, ethanol, methane, and ammonia in a DI diesel engine with pilot injection", SAE 770794, 977
- Checkel M. D., B. Liu, M. Zheng, E. Mirosh, "A Special Catalytic Converter for Dual Fuel Engine Light Load Emissions", 1998 Spring Technical Meeting, Combustion Institute, Canadian Section, 25-27 May, Toronto, Canada, 1998
- Clerc J. C., "Catalytic diesel exhaust aftertreatment", Applied Catalysis B: Environmental 10, 99-115, 1996
- Deluchi M. A., R. A. Johnson and D. Sperling, "Transportation fuels and the greenhouse effect", Transportation Research Record, In Press
- Ding X. and P. G. Hill, "Emissions and fuel economy of a prechamber diesel engine with natural gas dual fuelling", SAE 860069, 1986
- Douville, B., "Performance, emission and combustion characteristics of natural gas fuelling of diesel engines", M.Sc. Thesis, University of British Columbia, Vancouver, BC, 1994.
- Farrauto R. J., K. E. Voss, "Monolithic diesel oxidation catalysts", Applied Catalysis B: Environmental 10, 29-51, 1996
- Fritz S. G. and R. I. Egluono, "Emissions from heavy-duty trucks converted to CNG", ASME paper 92-ICE-10, 1992
- Geiss R. O., W. M. Burkmyre and J. W. Lanigan, "Technical highlights of the Dodge compressed natural gas Ram Van/Wagon", SAE 921151, 1992
- Guit Ir. R. P. M., "The selective catalytic reduction of NO<sub>x</sub> in a reverse flow reactor: quick design procedure", Precision Process Technology, 453-461, 1993 Kluwer

Academic Publishers, 1993

- Gunawan H., "Performance and combustion characteristics of a diesel-pilot gas injection engine", MSc. Thesis, Department of Mechanical Engineering, University of British Columbia, June, 1992
- Hanamura K., R. Echigo and S. A. Zhdanok, " Superadiabatic combustion in a porous medium", *Ind. J. Heat Mass Transfer*, 36, 1993
- Hosoya M. and M. Shimoda, "The application of diesel oxidation catalysis to heavy duty diesel engines in Japan", *Applied Catalysis B: Environmental* 10, 83-97, 1996
- Karim G. A., "Examination of the performance of a dual fuel diesel engine with particulate reference to the presence of some inert diluents in the engine intake charge", SAE 821222, 1982
- Karim, G. A., "Methane and diesel engines", *Methane – Fuel for the Future*, Plenum Press, New York, NY, 1982
- Karim G. A. and I. Wiezba, "Comparative studies of methane and propane as fuels for spark ignition and compression ignition engines", SAE 831196, 1983
- Karim G. A., "The dual fuel engine of the compression ignition type – prospects, problems and solutions – a review", SAE 831073, 1983
- Karim G. A., "An examination of some measurements for improving the performance of gas fuelled diesel engines at light load", SAE 912366, 1991
- Korff P. von M., "Alternative fuels and drive systems for city buses", SAE 905143, 1990
- Lampert J. L., M. S. Kazi and R. J. Farrauto, "Palladium catalyst performance for methane emissions abatement from lean burn natural gas vehicles", *Applied Catalysis B: Environmental* 14, 211-223, 1997
- Leclerc J. P. and D. Schweich, "Modeling catalytic monoliths for automobile emission control", in *Chemical Converter Technology for Environmentally Safe Converters and Products* (Edited by de Lasa, H. I. et al.), 547-576, Kluwer Academic Press, Dordrecht, 1993.
- Matros Yu. Sh. and G. A. Bunimovich, " Reverse-flow operation in fixed bed catalytic reactors", *Catal. Rev.-Sci. Eng.*, 38(1), 1-68, 1996
- McElroy R. O., "Methane from coal conversion", *Methane – Fuel for the Future*, Plenum

Press, New York, NY, 1982

- Midkiff K. C., S. R. Bell, C. B. Ramsey and W. Y. Wong, "Performance and emissions studies of a natural gas fuelled prechamber-type diesel engine", The 9<sup>th</sup> Miami international Congress on Energy and Environment, 1989
- Miyoshi N., S. Matsumoto, K. Katoh, T. Tanaka, J. Harada, N. Takahashi, K. Yokota, M. Sugiura and K. Kasahara, "Development of new concept Three-Way Catalyst for automotive lean-burn engines", SAE 950809, 1995
- Nowak P. P., "Performance and emissions of a dual fuel two stroke bus engine", MSc. Thesis, Department of Mechanical Engineering, University of Alberta, Canada, 1994
- Oh S. H., P. J. Mitchell and R. M. Siewert, "Methane oxidation over alumina-supported noble metal catalysts with and without cerium additives", *J. of Catalysis* **132**, 287-301, 1991
- Özgülsen F. and A. Cinar, "Forced periodic operation of tubular reactors", *Chemical Engineering Science*, Vol. 49, No. 20, pp. 3409-3419, 1994
- Purwono S., Yu. Sh. Matros, R. R. Hudgins and P. L. Silveston, "Modelling of catalytic combustion of low-heating-value gases using non-adiabatic flow reversal", Department of chemical engineering, University of Waterloo.
- Rodt S., A. Friedrich, D. Jost, R. Kolke, W. Rudolf and M. Trappe, "Requirement, technical feasibility and costs of exhaust emission standards for the year 2000 in European Community", Federal Environmental Agency, Berlin, 1995
- Sakai T., B. C. Chol, R. Osuga and Y. Ko, "Purification characteristics of catalytic converters for natural gas fuelled automotive engine", SAE 912599, 1991
- Shelef M. and G. W. Graham, "Why rhodium in automotive three-way catalysts?", *Catal. Rev.-Sci. Eng.*, 36(3), 433-457, 1994
- Springer K. J., "Energy, efficiency, and the environment", the 1991 Soichiro Honda Lecture, ASME publication ICE-Vol. 15, 1991
- Strots V. O., G. A. Bunimovich, Yu. Sh. Matros, M. Zheng and E. A. Mirosh, "Novel catalytic converter for natural gas powered diesel engines", SAE 980194, 1998
- Summers J. C., A. C. Frost, W. B. Williamson and I. M. Freidel, "Control of NO<sub>x</sub>/CO/HC

- emissions from natural gas fuelled stationary engines with three-way catalysts”, 84<sup>th</sup> annual meeting and exhibition, Vancouver, British Columbia, June 16-21, 1991
- Tesarek H., “Investigation concerning the employment possibilities of diesel – gas process for reducing exhaust emissions, especially soot (particulate matters)”, SAE 831197, 1983
- Varde K. S., “Propane fumigation in a direct injection type diesel engine”, SAE 831354, 1983
- Voltz S. E., C. R. Morgan, D. Liederman and S. M. Jacob, “Kinetic study of carbon monoxide and propylene oxidation on platinum catalysts”, Ind. Eng. Chem. Prod. Res. Dev. **12**, 294-301, 1973.
- Wallace K. and H. J. Viljoen, “Modelling of a monolithic catalyst with reciprocating flow”, AIChE Journal, Vol. 41, No. 5, 1229-1234, 1995
- Weaver C. S., “Natural gas vehicles, a review of the State of the art”, Sierra research report No. SR89-04-01, Sierra research, Sacramento, CA., 1989
- Wong W. Y., K. C. Midkiff and S. R. Bell, “Performance and emissions of a natural gas-fuelled, indirect injected diesel engine”, SAE 911766, 1991
- Zelenka P., W. Cartellieri, P. Herzog, " Worldwide diesel emissions standards, Current experience and future needs ", Applied Catalysis B: Environmental **10**, 3-28,1996.

## **Chapter 2**

### **Experiment Set-up and Measurements**

*Chapter 2 gives a detailed description of the experiment set-up and equipment used. It lays out both prototype and production designs of reverse flow catalytic converter, gives the gas and temperature measurement and correction methods and describes the test methods for fresh catalyst, unidirectional flow and reverse flow.*

## **2.1 Introduction**

This chapter gives a description of the experimental equipment used in the investigation of the converter performance for both prototype and production type catalytic converters. The production design reverse flow catalytic converter is a much more compact design than the prototype.

The experimental equipment consisted of three major components: 1). The engine; 2). The catalytic converter; 3). The analytical instrumentation.

The engine used to provide the feed gas to the converter was mounted in a test bed and controlled using a digital dynamometer. It is described in Section 2.2. Two catalytic converters were tested, referred to as the prototype and production version respectively. These are described in Sections 2.3 and 2.4 respectively. The analytical equipment used to determine gas compositions and reactor temperatures is described in Section 2.5.

The measured gas composition in dry basis was transferred to wet basis for the data analysis. The reactor inlet temperature is a critical data input for the simulation of experiments. The measured value is corrected based on heat transfer methods. These techniques are described in Section 2.6.



## 2.2 The Natural Gas/Diesel Dual Fuel Engine

The engine used to provide the feed gas to the converter was a naturally aspirated four cylinder ISUZU 4BE1 engine of 3.6 litre displacement, which had been modified to operate with a dual fuel system. The details of this engine are given in Table 2-1. Engine control and measurement parameters included engine speed, torque, inlet air flow rate, diesel and natural gas flow rate, engine exhaust temperature, inlet gas temperature, cooling water temperature and oil temperature. The equipment used to measure these parameters is summarized in Table 2-2.

Table 2-1 Engine Specifications

Engine Type	ISUZU 4BE1
Number of Cylinders	4
Bore × Stroke	105 mm × 105 mm
Total Displacement	3636 cm <sup>3</sup>
Compression Ratio	17.5
Compression Pressure	3 MPa
Diesel Fuel Injection Type	Direct Injection
Fuel Injection Order	1-3-4-2
Diesel Fuel Injection Time	17 BTDC
Diesel Fuel Injection Nozzle Type	Hole Type, 4 Orifices
Diesel Fuel Injection Pressure	18 MPa
Engine Cooling Type	Water Cooled

Table 2-2 Measurement Equipment

Equipment	Model and Serial	Range	Resolution
Engine Torque	Eddy-Current MidWest	0 to 1000 Nm	1 Nm
Engine Speed	Dynamometer Model 1014A	0 to 10000 rpm	1 rpm
Air Flow Rate	ASME LR Nozzle, W 200L, Validyne Pressure Transducer Model CD75	0 to 1380 Pa	0.5%
Fuel Flow Rate (Diesel Fuel and Natural Gas)	Pacific Scale Model 550	0 to 60 Kg	5 g
Engine Exhaust Temperature	Kromel-Alumel K-Type, 316SS Sheath, A6 18-K-USS-6, by Alltemp Sensors	0 to 1260 °C	2.2 °C
Other Engine Temperatures (Cooling Water, Oil, Intake Air Dry and Wet Bulb, etc.)	Copper-Constantan T-Type, 316SS Sheath, A6 18-T-USS-6, by Alltemp Sensors	-59 to 93 °C	0.9 °C

The engine was installed in an eddy current dynamometer test bed. Engine speed and torque were controlled using a digital dynamometer controller and a digital “throttle” controller. The digital dynamometer controller was set in the RPM (engine speed) mode and the digital “throttle” controller was set in the position mode. For a desired engine operating condition, the engine was first set to the desired engine speed using the dynamometer controller, and then adjusted to give the desired engine torque using the “throttle” controller to control engine fueling.

Air consumption was measured by a 220 litre air drum with two ASME long radius nozzles. The diameters of the nozzles were 73.60 mm and 63.59 mm respectively.

The pressure difference between air drum and ambient pressure was measured by a Validyne type CD75 pressure transducer with a 1380 Pa range. The air consumption was determined directly from the pressure difference according to SAE Recommended Practice J244. The calculation procedures are the same as shown by Nowak (1994).

Both natural gas and diesel fuels were measured by a pair of electronic scales. Their supply tanks were continuously weighed and the consumption rate thereby determined. The engine exhaust temperature was measured using a Chromel-Alumel thermocouple, which was set in a position close to the engine in the engine exhaust tail pipe. The temperatures of engine oil, coolant, air box, intake air dry and wet bulb were measured using copper-constantan thermocouples. The air pressure was obtained by a mercury barometer.

The natural gas used for all tests came from the University of Alberta mains supply provided by Northwestern Utilities Limited. It was compressed from the building pressure to approximately 19 MPa (2760 psi) by a pair of "Fuelmaker" appliances and then stored in steel cylinders. The cylinders were generally refilled when the pressure had dropped to between 1/2 and 1/3 of full pressure to reduce gas supply variations. The composition of the natural gas used for all tested was presented in Table 1-3 in Reference #4 (Nowak, 1994). Both Japanese diesel fuel and Esso summer diesel fuel were used for the test. The Esso summer diesel fuel was grade P-30 and its properties are given in Table 1-4 by Nowak (1994). Compared to Esso diesel fuel, the Japanese diesel had lower sulfur content 0.10% (Esso 0.24%). Its LHV (Lower Heating Value) is 42.96 MJ/kg and density is 0.83 at 15°C. They were close to those from Esso, as shown in Table 1-4.

### **2.3 Layout of prototype reverse flow catalytic converters**

The exhaust system containing the converter is illustrated in Figure 2-1. The gas flow direction to the converter was determined by the position of the control valve. The gas flow direction shown in Figure 2-1 is reverse flow. If the control valve was switched to the other position, the gas flow direction was changed to forward flow. Depending on the operation of the control valve, the catalytic converter could be operated in either unidirectional flow mode or reverse flow mode. The unidirectional flow mode allowed gas flow in either forward flow direction or reverse flow direction continuously. For the reverse flow mode, the flow direction to the reactor was switched frequently. The reverse flow operation could be either symmetric or unsymmetric.

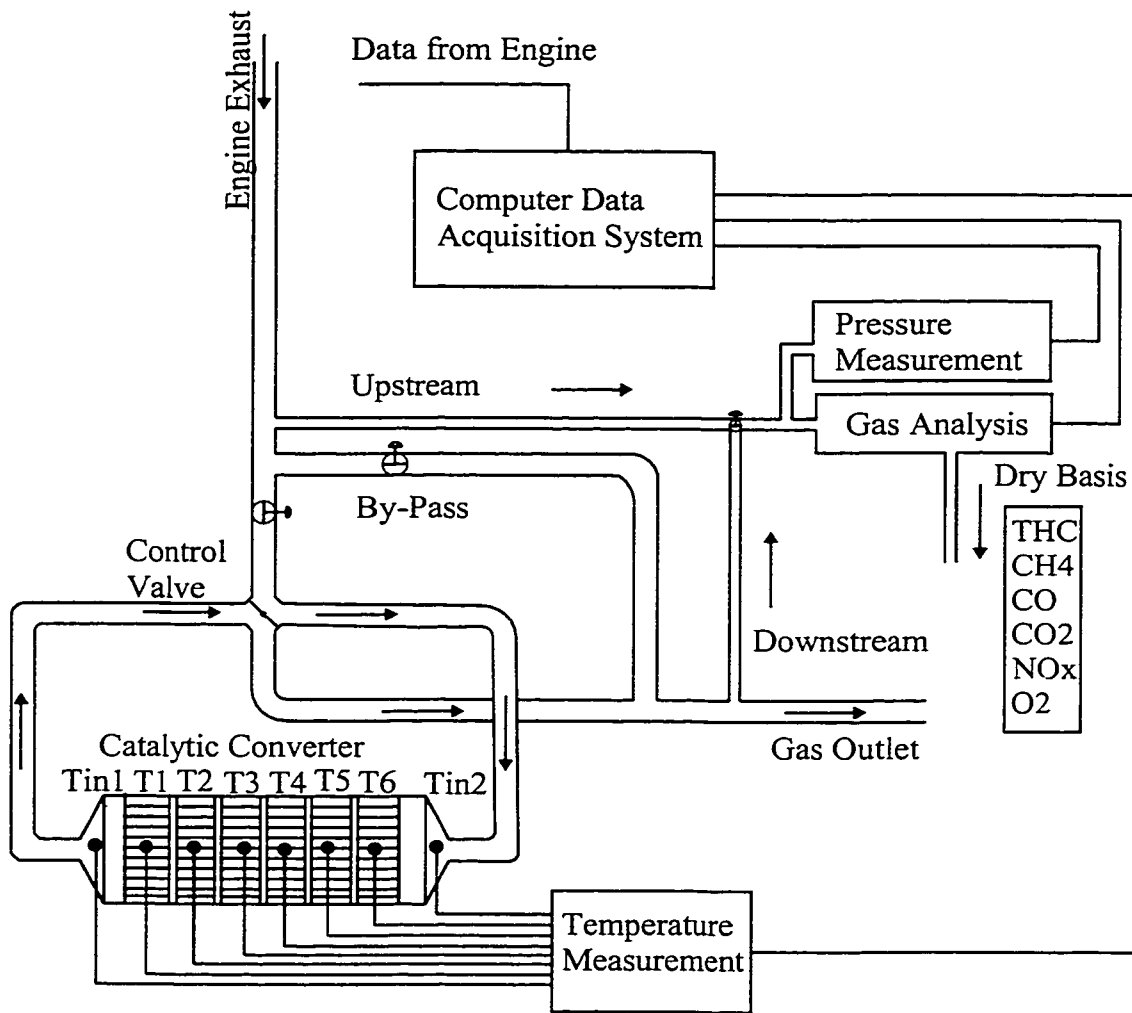


Figure 2-1 Experiment Set-up of Prototype Reverse Flow Design

The composition of the engine exhaust gas was determined before and after the converter using the analytical facilities, which are summarized in Section 2.5. The components measured were O<sub>2</sub>, CO<sub>2</sub>, CO, NO<sub>x</sub> and HC. HC measurement provided both total hydrocarbon (THC) and methane (CH<sub>4</sub>). Normally more than 95% of THC was CH<sub>4</sub>. The instruments were calibrated with standard gases before each test. The data were recorded on a dry basis and were converted to a wet basis for the data analysis.

The catalytic converter consisted of several catalyst bricks in series. The segmented design was used to give the converter multiple entry regions, where the heat and mass transfer coefficients are larger than in the fully developed region. The temperature profile in the catalytic converter was measured by inserting thermocouples ( $T_1$  to  $T_6$ ) into the catalyst segments transversely. The diameter of the thermocouples was 3.18 mm. The response time the thermocouples was 0.3-8.2 second, depended on the probe diameter. The inlet gas temperature was measured by either thermocouple,  $T_{in1}$  or  $T_{in2}$ . For forward flow,  $T_{in1}$  was inlet gas temperature and  $T_{in2}$  was outlet gas temperature. For reverse flow,  $T_{in2}$  was the inlet gas temperature and  $T_{in1}$  was outlet gas temperature. The pressure difference between reactor inlet and outlet was measured by a U-Tube which filled with dyed water. Figure 2-2 shows a schematic of this reverse flow catalyst system. The reverse flow control valve was actuated by compressed air. To prevent heat loss from the system, pipes were wrapped with thermal insulation material.

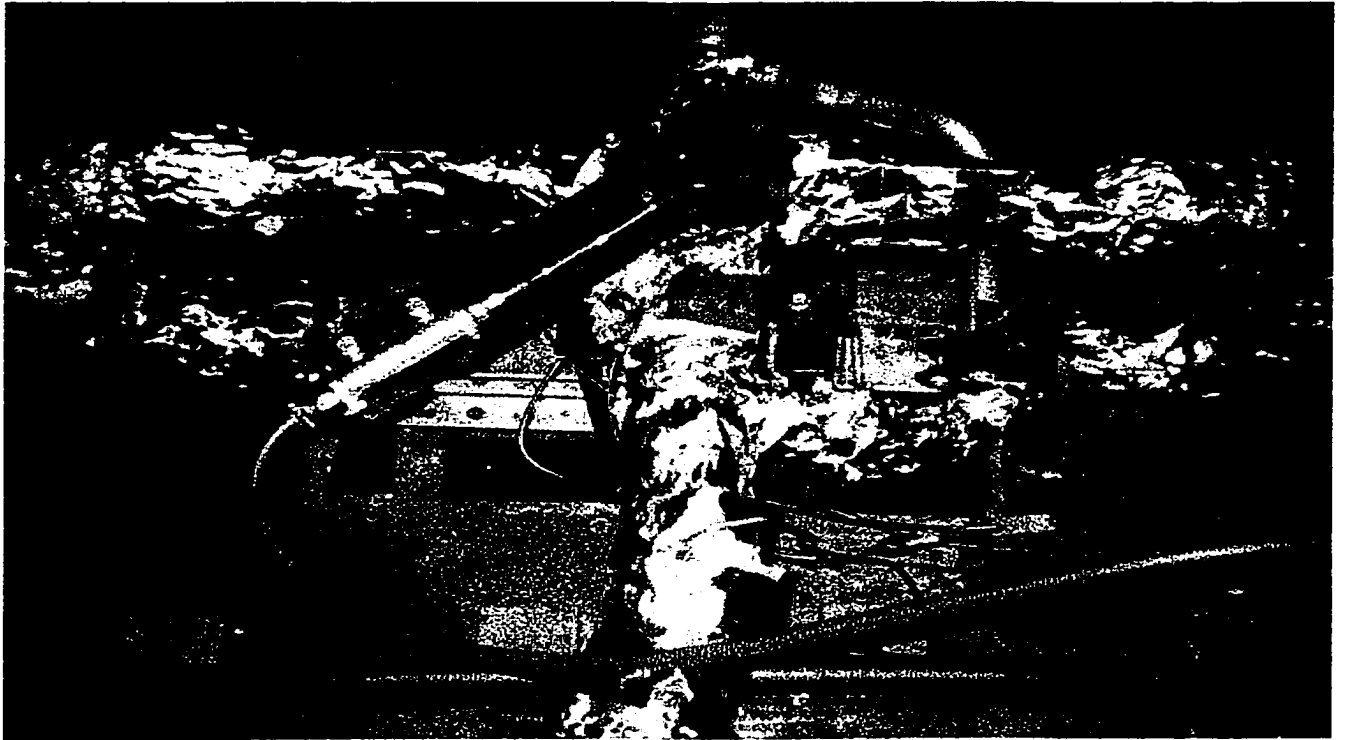


Figure 2-2 Overview of the Test Set-up for the Prototype Design of Reverse Flow System

Several segment designed catalysts were evaluated experimentally. They are shown in Figure 2-3. The catalytic converter in Figure 2-3 a) contained two segments of monolith honeycomb. Each segment had a diameter of 152.4 mm and a length of 152.4 mm. The cell density was 200 cpsi (cells per square inch) or 31 cpsc (cells per square centimeter). Between the segments, there was a 50.8 mm gap. The catalytic segments for converter 2-3 a) were provided by Englehard. All subsequent catalysts were coated by Johnson Matthey.

The converter in Figure 2-3 b) contained four active segments coated with catalyst and one inactive segment coated with carbon absorbent. The inactive segment was placed in the middle of the reactor. Both active and inactive bricks had a ceramic monolith honeycomb support with square channels. The active segments had a surface dimension of width 152.4 mm and height 152.4 mm, and a length 50.8 mm. The inactive segment had the same surface dimension as the active bricks but a length 101.6 mm. The gap between segments was 2 mm. The cell density of active segments was 200 cpsi (31 cpsc). The inactive brick had a cell density of 400 cpsi (62 cpsc). The physical properties of the active monolith segments are given in Table 2-3. This catalytic converter was used to made a basic modelling study for the unidirectional flow catalytic converter, which is described in Chapter 4

The converter shown in Figure 2-3 c) was a modified form of the converter shown in Figure 2-3 b). The design in Figure 2-3 b) had difficulty establishing the proper reactor temperature profile for reverse flow because the inactive brick was set in the middle of the reactor. The segments were rearranged as shown in Figure 2-3 c). The inactive brick was cut into two bricks which were set at each end of the reactor. The four catalyst bricks

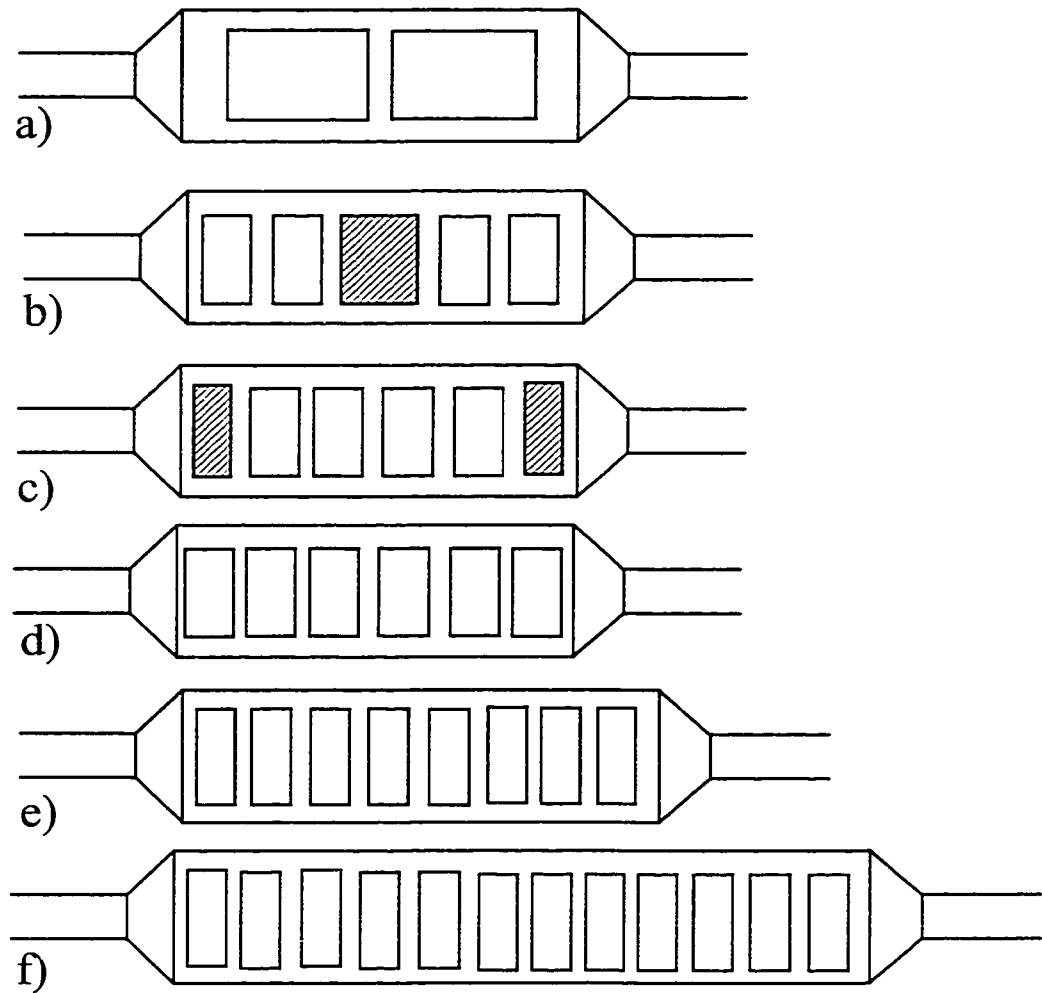


were put in the middle of the reactor. This arrangement could establish a temperature profile which was high in the middle and low in the both ends under reverse flow operation. This catalytic converter was used to make a detailed modelling and catalyst kinetic study of reverse flow catalytic converter, which is given in Chapters 5 and 6. Its catalyst property was the same as shown in Table 2-3.

The converter in Figure 2-3 d) contained six segments with metal substrates. Each segment had a diameter of 150 mm and a length 90 mm. The cell density was 200 cpsi (31 cpsc). The surface shape of each channel was close to trapezoidal. The gap between the segments was 2 mm.

The converter in Figure 2-3 e) contained eight segments. They had a ceramic monolith honeycomb support with square channels. Each segment had a square cross section with surface dimension of 150 mm × 150 mm, and length of 50 mm. The gap between segments was 2 mm. The cell density was 300 cpsi (47 cpsc).

The converter in Figure 2-3 f) contained twelve segments. All segments had a ceramic monolith honeycomb support with square channels. Each segment had the same dimensions as that in Figure 2-3 e). The gap between segments was 2 mm. The cell density was 100 cpsi (16 cpsc).



- a) Englehard 200 cpsi ceramic monolith catalyst, 2 catalyst segments
- b) Johnson-Matthey 200 cpsi ceramic monolith catalyst, 4 catalyst segments, one 400 cpsi inactive segment set in the middle of the reactor
- c) Johnson-Matthey 200 cpsi ceramic monolith catalyst, 4 catalyst segments, two 400 cpsi inactive segments set in the both ends
- d) Johnson-Matthey 200 cpsi metallic monolith catalyst, 6 catalyst segments
- e) Johnson-Matthey 300 cpsi ceramic monolith catalyst, 8 catalyst segments
- f) Johnson-Matthey 100 cpsi ceramic monolith catalyst, 12 catalyst segments

Figure 2-3 Catalytic Converters Tested for the Prototype Design

Table 2-3 The Physical Properties of Monolith Catalyst Bricks

Wall Density $\rho_w$	2500 kg/m <sup>3</sup>
Wall Thermal Conductivity $k_w$	2 W/(m.K)
Wall Heat Capacity $C_{p, w}$	1400 J/(kg. K)
Effective Wall Thickness	0.25 mm
Average Thickness of Washcoat Layer	0.05 mm
Porosity of Washcoat	0.41
Channel Hydraulic Diameter, $D_H$	1.4 mm
Channel Open Frontal Area	1.96 mm <sup>2</sup>
Porosity of Monolith	72%
Size of Catalyst Brick (Length x Width x Height)	50.8mm x 152.4mm x 152.4mm

## 2.4 Layout of production design reverse flow catalytic converter

The production design reverse flow catalytic converter is a much more compact design than the prototype, as shown in Figure 2-4. The converter in this design was made from a cylindrical catalyst-coated substrate provided by Englehard. It had a diameter of 266.7 mm and a length of 152.4 mm. The cell density was 350 cpsi. The catalytic converter was divided into two sections by a gas flow divider on the top of the catalytic substrate. The reverse flow control valve was set on the top of the reactor above the flow divider. By switching the control valve, the exhaust gas flow direction through the reactor could be changed. In Figure 2-4, engine exhaust gas flowed down through the left section and up through the right section. This was the forward flow mode. When the control valve was switched to the other position, the gas flowed down through the right section and up through the left section. This was reverse flow mode.

This design was used to make a detailed experimental investigation of reverse flow catalytic converter. This investigation is described in Chapter 3.

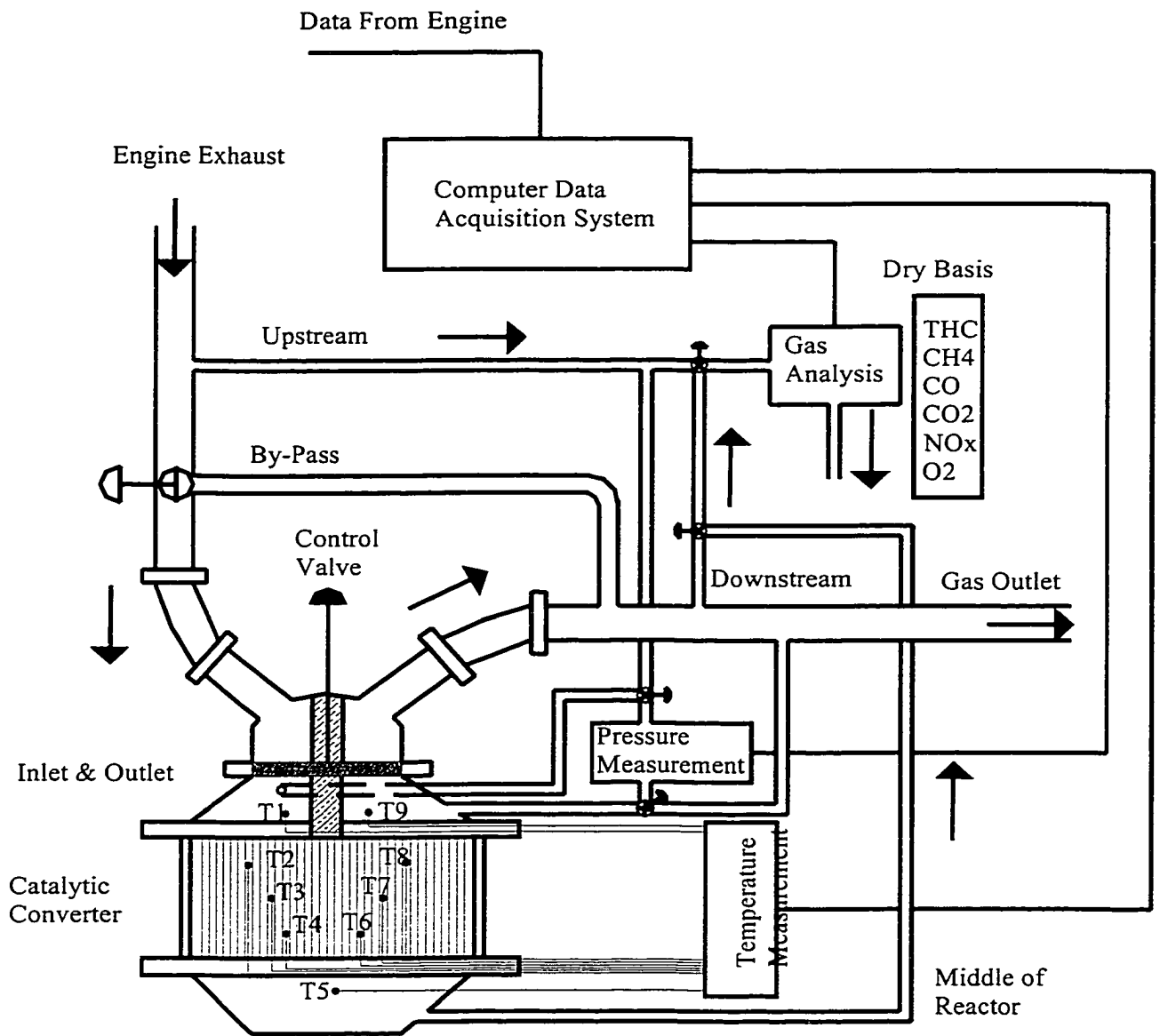


Figure 2-4 Experiment Set-up of Production Type Reverse Flow Design

The gas sampling was the same as in the prototype design. The composition of the engine exhaust gas was determined before and after the converter using the analytical facilities. In some tests, the gas composition in the middle of the reactor was analyzed. The components measured were O<sub>2</sub>, CO<sub>2</sub>, CO, NO<sub>x</sub> and HC. HC measurement provided both total hydrocarbon (THC) and CH<sub>4</sub>. The instruments were calibrated with standard gases before each test. The data were recorded on a dry basis and were converted to a wet basis for the data analysis.

To obtain thermal information from the reactor, several thermocouples were set along the reactor. The temperature profile in the catalytic converter was measured by inserting six thermocouples ( $T_2$  to  $T_4$  and  $T_6$  to  $T_8$ ) into the catalyst channels. The diameter of thermocouples was close to the channel size. The catalyst channel was triangular with an equal side length 2.41 mm. The calculated hydraulic diameter of the cell channel was 1.39 mm. The diameter of thermocouple was 0.81 mm. The channel was enlarged a little bit for insetting the thermocouple to the right position. The channels with thermocouples were blocked in both ends. This avoided gas flow effects on the measured temperature so the measured values were the solid phase temperature. The response time of the thermocouples was about 0.004-3.2 second, depended on the wire size and fluids. The inlet gas temperature was measured by either thermocouple  $T_1$  or  $T_9$ . For forward flow,  $T_1$  was the inlet gas temperature and  $T_9$  was the outlet gas temperature. For reverse flow,  $T_9$  was the inlet gas temperature and  $T_1$  was the outlet gas temperature. Between the left and right section of the reactor, an additional thermocouple  $T_5$  was set in the turning zone at the middle of the reactor. This thermocouple showed the temperature of fluid phase in the middle of the reactor. The pressure drops across the catalyst and across the

whole reactor system were measured by a Validyne pressure transducer. The overview of this system was shown in Figure 2-5.

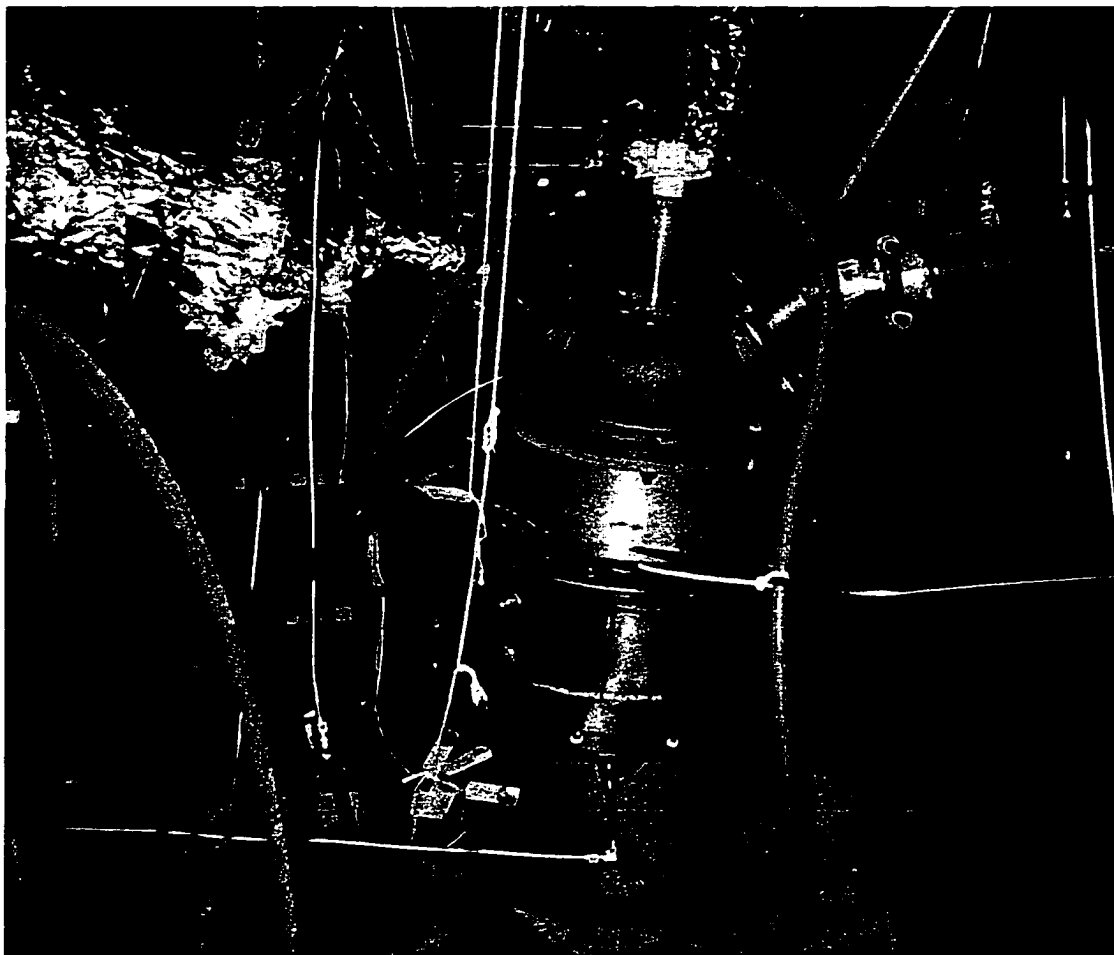


Figure 2-5 Overview of the Test Set-up for the Production Type Design of  
Reverse Flow System

## **2.5 Gas Analysis**

### **2.5.1 Gas Analysis Equipment**

The engine exhaust gas was sampled by a set of analytic instruments after the particulates were filtered and the water was removed. This ensured that the gas to the equipment was clean and dry, which is important because water or particulates could influence the gas measurement and damage the equipment. The sample system is showed in Figure 2-6. The sampling system materials were Teflon and they were made according to SAE standard. The composition of the engine exhaust gas was determined before and after the converter. The components measured were O<sub>2</sub>, CO<sub>2</sub>, CO, NO<sub>x</sub> and HC. HC measurement provided both total hydrocarbon (THC) and CH<sub>4</sub>. The instruments were calibrated with standard gases before each test. The gas measurement facilities were upgraded after the test for the prototype reverse flow system. The details of these facilities were shown in Table 2-4 and Table 2-5. Table 2-4 shows the instruments used for the prototype testing and Table 2-5 those used for the production type testing

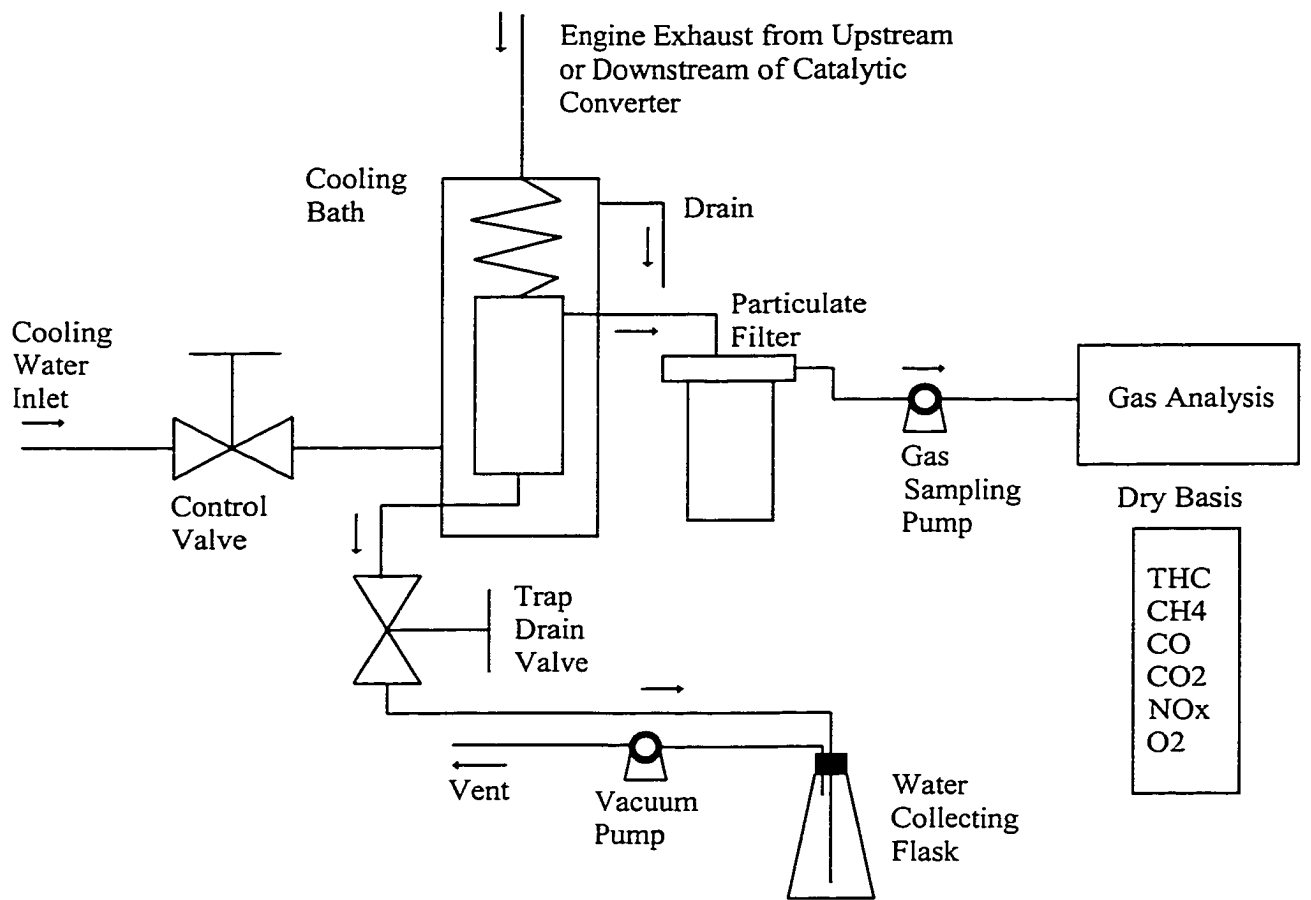


Figure 2-6 The Exhaust Gas Sampling System



Table 2-4 Emission Measurement Facilities for Prototype Catalytic Converter Test

Measured Composition	Model and Serial	Range	Precision	Calibration
THC	Beckman GC 72.5 Dual FID	0-5.0%	5 ppm	0, 102, 580, 1520, 5030, 12400 ppm C
CH <sub>4</sub>	MTI P200 GC	0-1,000,000 ppm	1 to 5 ppm	0, 102, 580, 1520, 5030, 12400 ppm C
CO <sub>2</sub>	Beckman 864 NDIR	0-20%	~0.05%	0%, 4.98%, 10.00%, 15.10%
CO	Beckman 864 NDIR	0-1%	~0.01%	0, 178, 1010, 10000 ppm
O <sub>2</sub>	Taylor Servomex OA.137	0-25%	~0.1%	0%, 21%
NO <sub>x</sub>	Beckman 955 Chemiluminescent	0-0.2%	~1 ppm	0, 1004, 1984 ppm

Table 2-5 Emission Measurement Facilities for Production Type Catalytic Converter Test

Measured Composition	Model and Serial	Range	Precision	Calibration
THC	California Analytical 300M-FID	0-30,000 ppm	0.1 ppm	0, 1000, 2500, 3500, 5000 ppm
CH <sub>4</sub>	California Analytical 300M-HFID	0-30,000 ppm	0.1 ppm	0, 1000, 2500, 3500, 5000 ppm
LCO	California Analytical 300, NDIR	0-1,000 ppm	1% Full Scale	0, 250, 500, 1000 ppm
HCO	California Analytical 300, NDIR	0-25,000 ppm	1% Full Scale	0, 250, 500, 1000, 2500, 3500, 5000 ppm
CO <sub>2</sub>	California Analytical 300, NDIR	0-20%	1%	0%, 1.0%, 2.5%, 3.5%, 5.0%
O <sub>2</sub>	California Analytical 100P, Paramagnetic	0-25%	10 ppm	0%, 4.2%, 10.5%, 16.8%, 21%
NO <sub>x</sub>	California Analytical 300CLD, Chemiluminescence	0-3,000 ppm	3 ppm	0, 400, 1200, 2000, 2800 ppm

## 2.5.2 Correction of the Measured Gas Compositions

The recorded gas compositions were on a dry basis. These compositions were O<sub>2</sub>, CO<sub>2</sub>, CO, NO<sub>x</sub> and HC. They were converted to a wet basis for the actual data analysis. This conversion was done using the relationship of Heywood (1988).

$$Y_i = (1 - Y_{H_2O}) Y_i^* \quad (2.1)$$

$Y_i$  is the mole fraction of species  $i$  in wet basis and  $Y_i^*$  is the mole fraction of species  $i$  in dry basis. For a hydrocarbon C<sub>*n*</sub>H<sub>*m*</sub> the mole fraction of water in the exhaust was calculated using the equation:

$$Y_{H_2O} = \left( \frac{m}{2n} \right) \left( \frac{Y_{CO}^* + Y_{CO_2}^*}{1 + \frac{Y_{CO}^*}{K_1 Y_{CO_2}^*} + \left( \frac{m}{2n} \right) (Y_{CO}^* + Y_{CO_2}^*)} \right) \quad (2.2)$$

The formula C<sub>*n*</sub>H<sub>*m*</sub> represents an averaged composition that depends on the flowrate of each fuel. For diesel fuel, the ratio of  $m$  to  $n$  is between 1.8 and 2. For natural gas, the ratio is about 3.8. The mole flow rates of diesel fuel and natural gas were calculated based on the mass flow rates. The actual ratio of  $m$  to  $n$  depends on fuel mole flow rates. This value ranged from 2.3 to 3.1 for most of engine modes.

$K_1$  is an experimental constant with a value between 3.8 and 3.5 (Douville, 1994). It relates the wet basis concentrations of CO<sub>2</sub>, CO, H<sub>2</sub>O and H<sub>2</sub> in the following way:

$$K_1 = \frac{Y_{CO} Y_{H_2O}}{Y_{CO_2} Y_{H_2}} \quad (2.3)$$

The difference between 3.8 and 3.5 has little effect on the computed magnitude of the mole fraction of water. The average value of 3.65 was used for the calculation. Table 2-6 shows the difference between the dry and wet basis for a Japanese 6 mode test.

Table 2-6 Transfer Engine Exhaust from Dry to Wet Basis

M o d e	Speed (rpm)	Torque (Nm)	Basis	Engine Exhaust Composition						
				HC ppm	CO ppm	NO ppm	O <sub>2</sub> %	CO <sub>2</sub> %	H <sub>2</sub> O %	N <sub>2</sub> %
1	Idle	Idle	Dry	304	645	125	18.58	1.74	-	Bal- ance
			Wet	299	614	123	18.30	1.65	1.51	
2	1360	175	Dry	1701	890	1470	7.53	7.98	-	
			Wet	1476	772	1275	6.53	6.92	13.26	
3	1360	52	Dry	5621	1941	177	16.21	2.99	-	
			Wet	5360	1832	167	15.30	2.82	5.61	
4	2040	195	Dry	1503	911	1307	6.18	8.78	-	
			Wet	1287	780	1119	5.29	7.52	14.39	
5	2040	49	Dry	4403	1751	131	15.79	3.36	-	
			Wet	4129	1642	123	14.81	3.15	6.22	
6	2720	116	Dry	3737	2098	429	9.75	6.90	-	
			Wet	3295	1850	378	8.60	6.09	11.82	

Test: Japanese 6 Mode Test for a Natural Gas/Diesel Dual Fuel Engine

## **2.6 Temperature Measurement and Correction**

### **2.6.1 Temperature Measurement**

The thermocouple arrangement for the reactor temperature profile measurement was different between the production type reverse flow system and the prototype. The thermocouples for the prototype had a diameter 3.18 mm and they were inserted into the catalyst brick transversely. There were some problems with this set up. First, some gas flow channels around thermocouples were damaged because thermocouples were inserted transversely and the diameter of thermocouples was much bigger than the channel size. Second, the temperatures measured have some effect of the gas fluid. The temperature measured was between the solid phase temperature and the gas phase temperature leading to some ambiguity.

The problems mentioned above were avoided in the thermocouple arrangement used for the production type design. The thermocouples for the production type had a very small diameter, (0.81 mm), so they could be inserted axially into a catalyst channel. The channels with thermocouples were enlarged a little bit for inserting the thermocouple to the right position, and were blocked at both ends. This ensured that the measured temperature was solid phase temperature. In addition, the time constant of the fine thermocouples used for the production type was sufficiently short to follow substrate temperature transients accurately.

## 2.6.2 Correction of the Measured Inlet Gas Temperature

Considering that the diameter of the thermocouples of inlet gas temperature measurement for the prototype design was quite big, the measured temperature needed correction to obtain the true value. Figure 2-7 shows the heat transfer phenomena around the thermocouple. Convection occurred between the fluid phase and the surface of the thermocouple. Along the thermocouple, heat was conducted away from the tip. Heat radiation occurred between the thermocouple surface and the surface of catalyst bed.

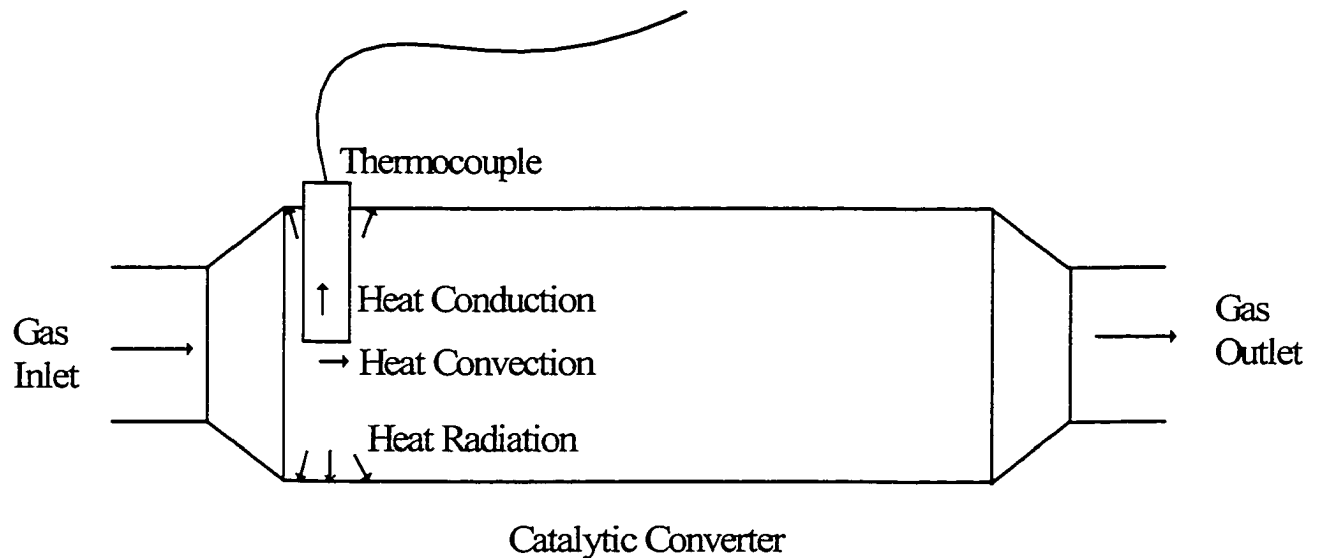


Figure 2-7 Heat Transfer Phenomena Around Thermocouple

An energy balance of the thermocouple tip provides the following equations:

$$[Energy\ In] = [Energy\ Out] \quad (2.4)$$

$$[Energy\ In] = Q_{convection} \quad (2.5)$$

$$[Energy\ Out] = Q_{Conduction} + Q_{Radiation} \quad (2.6)$$

$$Q_{convection} = (T_{Corrected} - T_{Indicated}) h A_1 \quad (2.7)$$

$$Q_{conduction} = (T_{Indicated} - T_{bed}) k A_2 / L \quad (2.8)$$

$$Q_{Radiation} = (T_{Indicated}^4 - T_{bed}^4) \varepsilon \sigma A_1 \quad (2.9)$$

$A_1$  and  $A_2$  is the thermocouple surface area and the cross sectional area respectively. The thermocouple sheath is stainless steel. Its heat conductivity  $k$  is 15 W/(m.K) and emissivity  $\varepsilon$  is 0.3.  $\sigma$  is Stefan-Boltzmann constant,  $5.67 \times 10^{-8}$  W/(m<sup>2</sup>K<sup>4</sup>).

The heat convection coefficient  $h$  was calculated based on the averaged Nusselt number  $Nu$  for the flow across a cylinder. The Reynolds number for flow across a cylinder is (Mills, 1995):

$$Re = VD / \nu \quad (2.10)$$

$V$  is the reactor inlet gas flow velocity and  $\nu$  is its kinematic viscosity. Their values depend on the temperature and composition of the engine exhaust.  $D$  is the thermocouple diameter, 3.18 mm. The calculated Reynolds number for gas flow across the thermocouple for most of engine operations ranges from 200 to 300. The averaged Nusselt number for  $Pr > 0.5$  and  $Re < 10^4$  is given by a correlation suggested by Churchill and Bernstein (1977):

$$Nu = 0.3 + \frac{0.62 Re^{1/2} Pr^{1/3}}{\left[1 + (0.4 / Pr)^{2/3}\right]^{1/4}} \quad (2.11)$$

This condition is valid for most of engine exhaust at the reactor inlet, since most of engine exhaust is air and its Pr number is about 0.7. The heat convection coefficient  $h$  was calculated using:

$$Nu = \frac{hD}{k_f} \quad (2.12)$$

$k_f$  is the heat conductivity of inlet gas.

The value of the measured temperature could be corrected as:

$$T_{corrected} = T_{indicated} + (Q_{Conduction} + Q_{radiation}) / hA_1 \quad (2.13)$$

Some corrected values are shown in Table 2-7. The measured values were lower than the corrected value by a significant amount (16-45 K). However, the relative stability of the correction and the fact that correction trends with speed and load are as expected gives some confidence in the methodology.

Table 2-7 Comparison of the Measured and Corrected Inlet Gas Temperature

Speed (rpm)	Torque (Nm)	Measured Inlet Gas Temperature (K)	Corrected Inlet Gas Temperature (K)	Correction (K)
2600	120	760	796	+36
	130	780	820	+40
	140	800	845	+45
	150	819	860	+41
1500	140	630	646	+16
	160	670	687	+17
	180	700	723	+23
	200	720	747	+27

Correction = Corrected Inlet Gas Temperature - Measured Inlet Gas Temperature

## 2.7 Test Methods of catalytic converters

### 2.7.1 Fresh Catalyst Test

The fresh catalyst has a very high activity for chemical reactions owing to its relatively low activation energy. However, the fresh catalyst loses its activity very quickly. Figure 2-8 shows the fresh catalyst test results from the prototype design shown in Figure 2-3 b) and Figure 2-9 shows the fresh catalyst test results from the production type. Both figures show HC conversion over the catalytic converter against the average reactor temperature. The first tests provided data at the very left side of the figures indicating the high conversion at low temperature. This relationship moved from the left side to the right side as testing progressed indicating that a higher temperature was required for the same conversion. Eventually the catalyst activity stabilized. It took about



ten hours of operation to stabilize the catalyst, as shown in Figure 2-8 and Figure 2-9. The catalyst shown in Figure 2-9 took a little longer to stabilize than that from Figure 2-8. Part of the reason for this was that the catalyst of the production type was heated more gently than the prototype catalyst. Since the test results from the fresh catalyst were not stable, the ultimate data analysis was based only on the aged catalyst values. The aged catalyst has stable performance and provides information relevant to actual applications. However, fresh catalyst testing was performed to stabilize the catalyst and confirm stable operation.

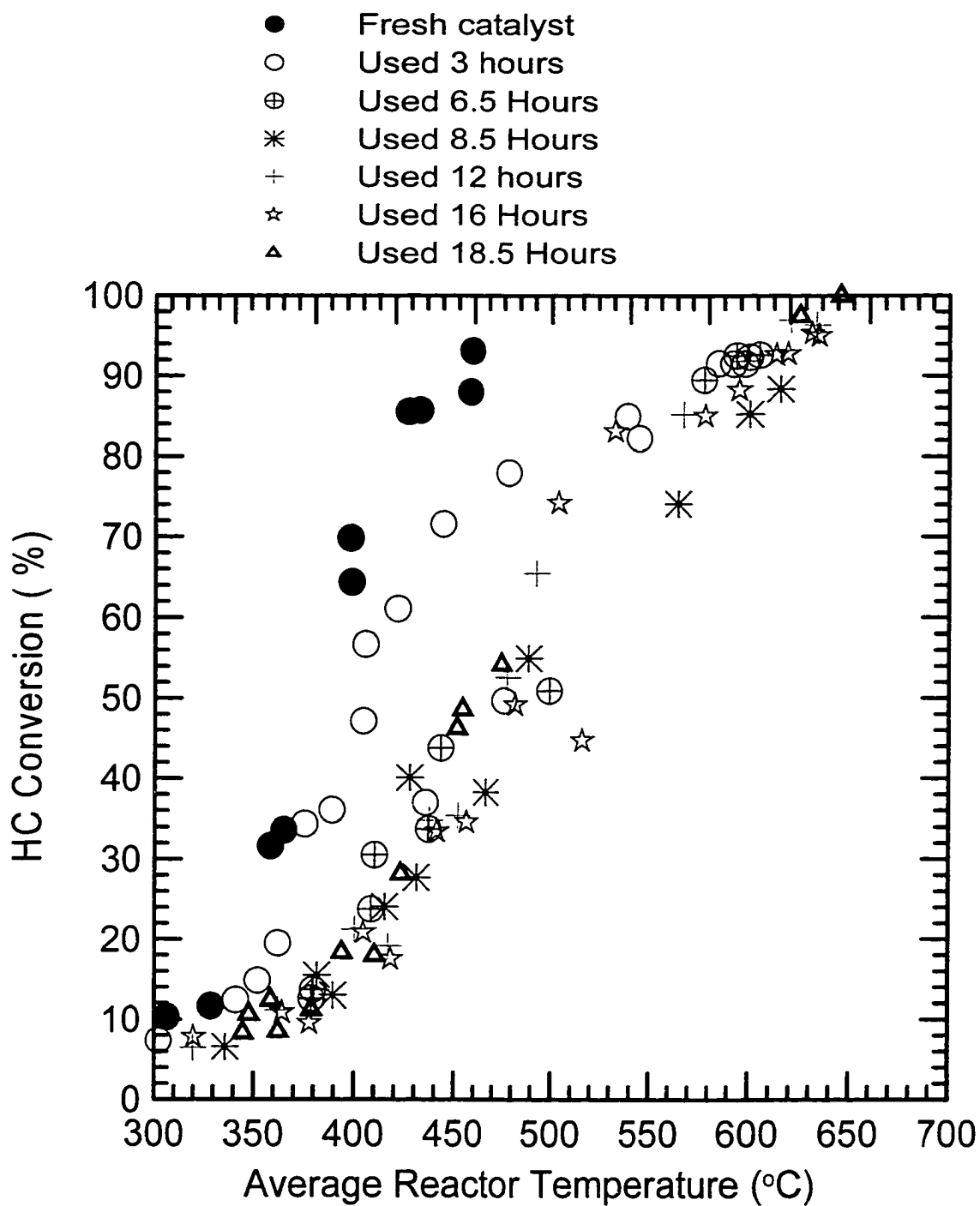


Figure 2-8 The Fresh Catalyst Test for the Prototype Catalyst Shown in Figure 2-3 b)

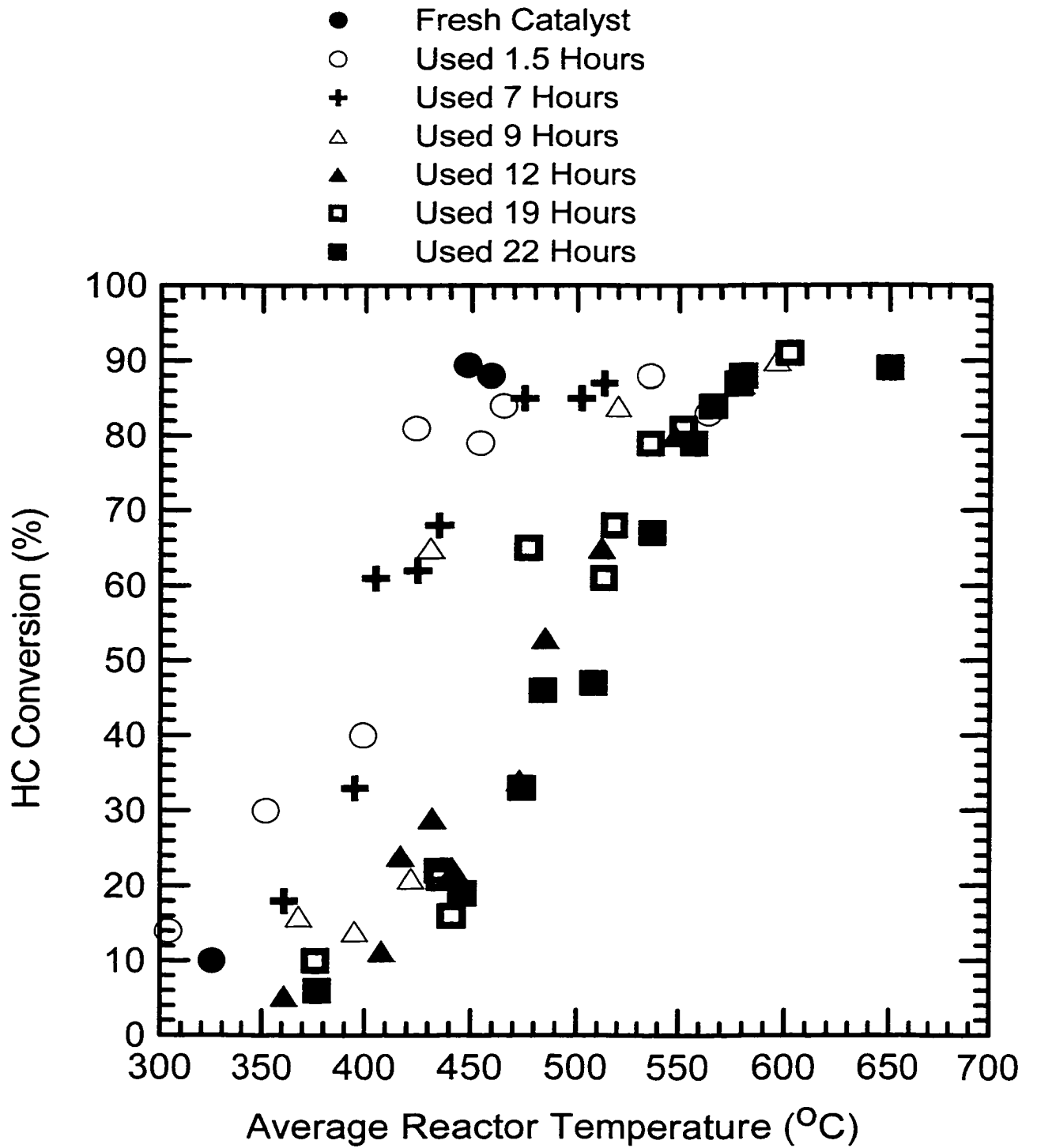


Figure 2-9 The Fresh Catalyst Test for the Production Type Catalyst

### **2.7.2 Unidirectional Mode Tests**

The unidirectional mode is the normal operating mode for conventional catalytic converters. The engine exhaust flows through the catalytic converter in one direction. The reactor temperature increases toward the reactor outlet owing to exothermic reactions. In the reverse flow test setup, unidirectional flow could be achieved by keeping the reverse flow control valve in a fixed position. The exhaust flow through the catalytic converter is fixed continuously in either the forward direction or the reverse direction.

### **2.7.3 Reverse Flow Mode Tests**

For the reverse flow, the flow direction in the catalytic converter is switched from time to time. The forward flow time could be either the same as the reverse flow time or not. If the forward time is the same as the reverse flow time, it is called symmetric reverse flow. If the forward flow time is not the same as the reverse flow time, it is called unsymmetric reverse flow.

## **2.8 Summary of Experimental Measurement**

Engine experiment includes engine control and data acquisition. The engine was controlled with a digital dynamometer. The information for engine control like engine coolant and oil temperature was important during test. There were two major measurements. One was determining gas composition before and after catalytic converter. The other was determining the temperature status of the catalytic converter for certain HC and CO conversion. The test set-up for production type reverse flow design was better than the prototype, especially the set-up of thermocouples. The gas analyzers

for the production type test was new and they gave less trouble during test. The measured gas composition in dry basis was transferred to wet basis for the data analysis. The reactor inlet temperature is a critical data input for the simulation of experiments. The measured value is corrected based on heat transfer methods. The data acquisition system had a good set-up and allow repeat test with the data saved. This had a special advantage for re-acquiring experiment data even after test.

## 2.9 Nomenclature

$A1$ : Thermocouple surface area,  $m^2$

$A2$ : Thermocouple cross sectional area,  $m^2$

$D$ : Diameter of thermocouple, m

$h$ : Heat convection coefficient,  $W/(m^2.K)$

$k$ : Thermal conductivity of thermocouple, 15  $W/(m.K)$  for Stainless Steel

$k_f$ : Thermal conductivity of engine exhaust gas,  $W/(m.K)$

$K_1$ : Experimental constant, 3.65

$L$ : Length of thermocouple inserting into catalyst, m

$Nu$ : Nusselt number, dimensionless

$Pr$ : Prandtl number, dimensionless

$Q_{conduction}$ : Heat conduction along thermocouples, W

$Q_{convection}$ : Heat Convection around thermocouples, W

$Q_{radiation}$ : Heat radiation between the thermocouple and catalyst bed, W

$Re$ : Reynolds number, dimensionless

$T_{corrected}$ : Corrected reactor inlet temperature, K

$T_{indicated}$ : Indicated reactor inlet temperature, K

$V$ : Flow velocity of engine exhaust gas, m/s

$Y_i^*$ : Mole fraction of species i in dry basis

$Y_i$ : Mole fraction of species i in wet basis

$\nu$ : Kinematic viscosity of engine exhaust gas,  $m^2 / s$

$\varepsilon$ : Emissivity of thermocouple, 0.3

$\sigma$ : Stefan-Boltzmann constant,  $5.67 \times 10^{-8} \text{ W}/(\text{m}^2 \cdot \text{K}^4)$

## 2.10 References

Churchill S. W. and M. Bernstein, "A correlating equation for forced convection from gases and liquids to a circular cylinder in crossflow", J. Heat Transfer, 99, 300-306, 1977

Douville, B., "Performance, emission and combustion characteristics of natural gas fuelling of diesel engines", MSc. Thesis, University of British Columbia, Vancouver, BC, 1994.

Heywood J. B., "Internal combustion engine fundamentals", McGraw-Hill Inc., New York, 1988

Mills A. F., "Heat and Mass Transfer", Richard D. Irwin Inc., 1995

Novak P. P., "Performance and Emissions of a Dual Fuel Two Stroke Bus Engine", MSc. Thesis, Department of Mechanical Engineering, University of Alberta, 1994

## **Chapter 3**

# **Experimental Results for Reverse Flow Catalytic Converter**

*Chapter 3 is an experimental study of a reverse flow catalytic converter based on the production type design. It presents the experimental results of reverse flow catalytic converter under both steady and transient engine operations. The reverse flow switch time was evaluated from 5 to 240 seconds. In addition, the reverse flow was evaluated on the transient Japanese 6-Mode tests. It shows the reverse flow catalytic converter can build up and maintain a very high reactor temperature even for a dual fuel engine running at light loads with very low exhaust temperatures. This allows for better than 80% HC and CO conversion with a very low reactor inlet temperature. It is proven that reverse flow operation is superior to unidirectional flow at light engine loads.*

---

Note: This Chapter is planned for submission to “The Canadian Journal of Chemical Engineering” or “Chemical Engineering Science”, 2000

### 3.1 Introduction

RFO (Reverse Flow Operation) has several important advantages. By Boreskov and Matros (1984), it not only reduces energy consumption and enhances selectivity, but also simplifies the reactor construction. Matros and Bunimovich (1996) summarized the advantages as: 1). The possibility of using the fixed catalyst bed as a heat and mass accumulator, and as a regenerative countercurrent heat exchanger which allows autothermal operation of exothermic processes at low and fluctuating inlet conditions of a reactant; 2). Creation of conditions thermodynamically favorable for reversible reactions such as a declining temperature profile for exothermic and increasing profile for endothermic process; 3). Incentive energy trapping that allows efficient recovery of exothermic heat or substantially decreases energy consumption for endothermic processes; 4). The possibility of combining endo- and exothermic reactions in one catalyst bed, which provides energy economy; 5) A smaller reactor size, simplification of the unit flow diagram, and reduction in the average reactor temperature, which provides for a decrease in pressure drop and heat losses. Because RFO has so many advantages on the catalytic combustion, it has been applied in the industries like oxidation of VOC (Volatile Organic Compounds) for purification of industrial exhaust gases, SO<sub>2</sub> oxidation for sulfuric acid production, NO<sub>x</sub> reduction by ammonia, methanol synthesis, hydrocarbons dehydrogenation, CO oxidation, etc. (Guit, 1993; Wallace and Viljoen, 1995; Matros and Bunimovich, 1996).

RFO has also been introduced to control natural gas/diesel dual fuel engine light load emissions of HC and CO (Checkel et al., 1998; Zheng et al., 1998; Strots et al., 1998). These studies show that RFO can build up and maintain a reactor temperature as



high as 670 °C while engine exhaust temperature was only 200 °C. More than 90% methane was converted over the reverse flow catalytic converter. The reactor performance was controlled by the feed reactant concentration and reverse flow switch time. However, for the certain engine operation with the specific engine exhaust compositions, the reverse flow switching time is the key parameter to control the reverse flow reactor performance (Guit, 1993; Wallace and Viljoen 1995; Zheng et al., 1998; Matros and Bunimovich 1996). Matros and Bunimovich (1996) summarized some reverse flow experimental investigations, as shown in Table 3-1. The flow velocity along the catalytic reactor for some industrial applications is as low as 0.03 m/s and the reverse flow cycling time is as high as 240 minutes. However, the flow velocity of dual fuel engine exhaust is about 3-6 m/s and the reverse flow cycling time is as short as 20 second (Zheng, 1998; Checkel et al., 1998).

Table 3-1 RFO Applications and the Reverse Flow Cycling Time Comparison

Applications	References	Catalysts	Linear Gas Flow Velocity (m/s)	Reverse Flow Cycle Duration (min)
SO <sub>2</sub> Oxidation	Boreskov et al. (1982), Matros (1989), Bunimovich et al. (1990), Isozaki et al. (1990), Levina et al. (1990)	Vanadium	0.03-0.6	15-240
VOC Waster Gas Purification	Boreskov et al. (1984), Matros (1989), Matros et al. (1993), Eigenberger and Nieken (1988, 1994), Nieken et al. (1994), Beld et al. (1994), Beld and Westerterp (1993), Sapundzhiev et al. (1988)	Copper Chromate, Palladium, Platinum	0.1-1.7	0.8-200
CH <sub>4</sub> Oxidation	Matros et al. (1988, 1989), Chaouki et al. (1994)	Copper Chromate, Palladium	0.25-0.6	60-200
NO <sub>x</sub> Reduction	Bobrova et al. (1988), Noskov et al. (1993)	Vanadium, Copper-Zinc	0.3-0.7	5-50
Methanol Synthesis	Matros (1989), Neophytides and Froment (1992)	Copper-Zinc	1.3-2.7	1.5-16
Partial Oxidation of CH <sub>4</sub>	Blanks et al. (1990)	Nickel	0.25	120
CO and C <sub>3</sub> H <sub>6</sub> Oxidation	Purwano et al. (1994)	Platinum	—	15-30

The other important factor which affects RFO performance is engine operation. RFO performance varies with engine operation. For some steady engine operations, RFO can build up the reactor temperature automatically, which does not require the pre-heated catalyst bed. However, for some other engine operations, RFO only can build up the reactor temperature for the pre-heated catalyst bed. Under the transient engine operations, RFO could increase reactor temperature and accelerate the reactor temperature development by its “heat trap” effect, but it also has the possibility to slow the reactor temperature development by its “cold trap” effect (Zheng et al., 1998; Strots et al., 1998).

This chapter reports an experimental investigation of reverse flow catalytic converter under both steady and transient engine operations with the experimental set-up of production type reverse flow system, as shown in Figure 2-4 and Figure 2-5. For the steady engine operations, the first objective is trying to find the effects of reverse flow. The second is trying to determine the proper reverse flow switch time. For the transient engine operations, the objective is trying to determine the heat and “cold trap” effect of reverse flow. Finally, the determined approaches are used for Japanese 6-Mode test.

## **3.2 Reverse Flow Catalytic Converter Performance Under Steady Engine Operation**

### **3.2.1 Comparison of Reactor Performance between Reverse Flow and Unidirectional Flow**

This section describes the difference in reactor performance between reverse flow and unidirectional flow observed using steady engine conditions. In these tests the engine speed varied from 1500 to 2600 rpm with a light load. The three cases are summarized in Table 3-2, which gives the engine torque and exhaust gas composition. Engine exhaust temperature was low, ranging from 510 to 699 K and outlet concentrations of CO and HC were relatively high.

The catalytic converter was first operated in the unidirectional flow mode, that is, the exhaust gas flowed in the forward direction only. The reactor temperature profile at steady state is shown in Figure 3-1 for the three cases. Note that T1 corresponds to the inlet gas temperature and T9 the outlet gas temperature. The reactor temperature was observed to increase from the reactor inlet to the outlet. The reactor temperature profiles for engine modes 2000 rpm, 120 Nm and 2600 rpm, 70 Nm were similar, and were much higher than that from engine mode 1500 rpm, 60 Nm. The average reactor temperature, which is the averaged value of T2, T3, T4, T6, T7 and T8, is shown in Table 3-3. Generally, the reactor temperature under these conditions was quite low as a result of the low engine exhaust temperature. The low reactor temperature gave low HC conversion (See Table 3-3), with a maximum HC conversion of 12%. High CO conversion, in excess of 90%, could, however, be achieved.

Table 3-2 Engine Exhaust Parameters

Test Case	Engine Mode		Exhaust Composition						Texh. (K)	Mass Flow Rate (g/s)
	Speed (rpm)	Tor. (Nm)	HC (ppm)	CO (ppm)	NO (ppm)	O <sub>2</sub> (%)	CO <sub>2</sub> (%)	H <sub>2</sub> O (%)		
Case 1	1500	60	5778	1974	171	14.78	3.18	6.31	510	41
Case 2	2000	120	4549	2188	351	10.67	5.20	10.17	699	54
Case 3	2600	70	6982	2222	112	12.89	3.71	7.34	664	70

N<sub>2</sub>: Balance of Exhaust Gas Composition

Texh.: Engine Exhaust Temperature

Tor.: Engine Torque

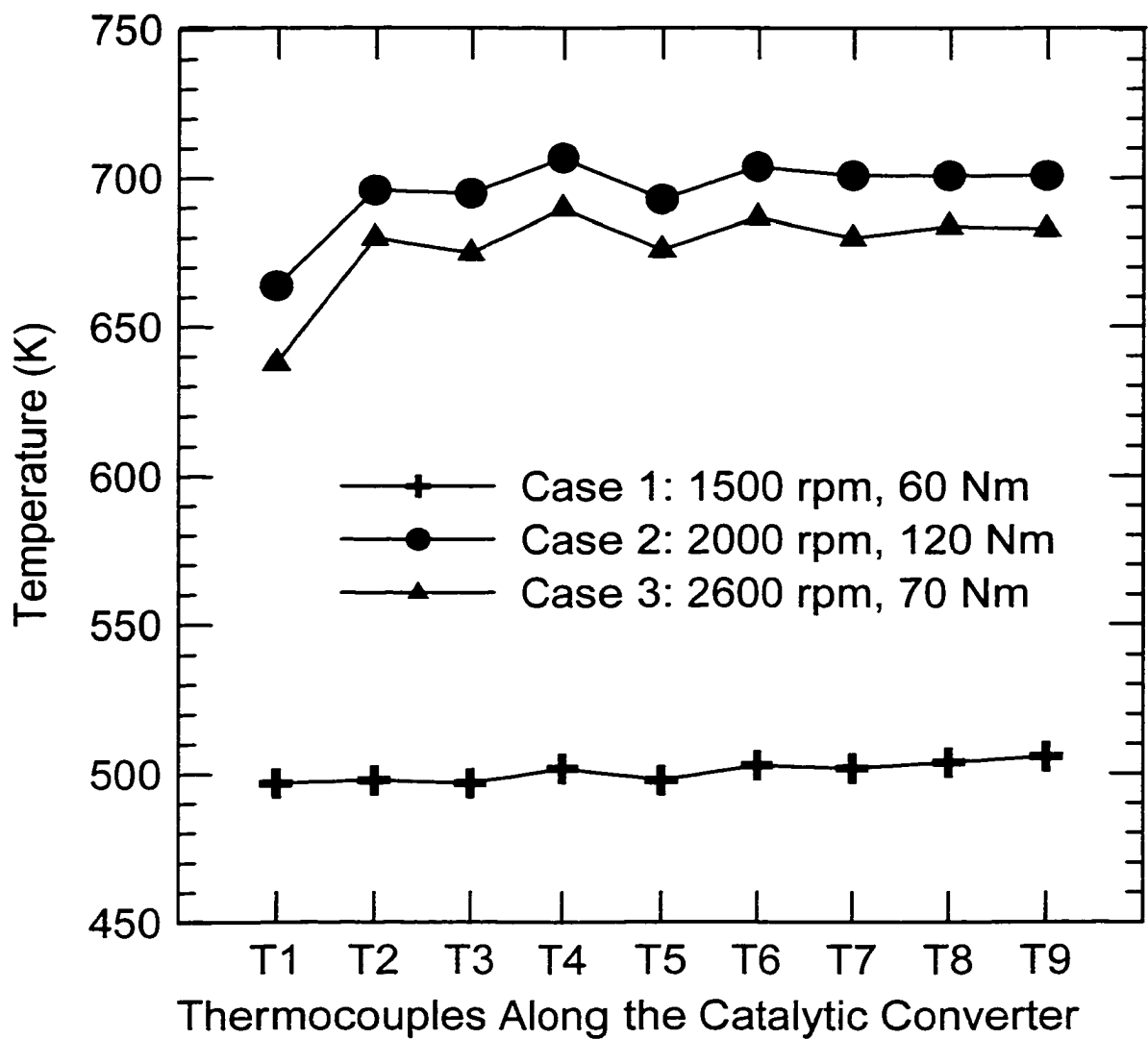


Figure 3-1 Steady Reactor Temperature Profiles for Unidirectional Flow Operations  
 (T1, T5 and T9 are gas-phase temperatures outside the substrate. T2, T3, T4,  
 T6, T7, and T8 are solid phase temperatures, see Figure 2-4)

Table 3-3 The Performance of Catalytic Converter Under Three Engine Light Load Operations

TEST CASE	ENGINE MODE		AVERAGE REACTOR TEMP. (K)	HC CONVERSION (%)	CO CONVERSION (%)
	SPEED (rpm)	TORQUE (Nm)			
Case 1	1500	60	501	3	53
Case 2	2000	120	701	11	93
Case 3	2600	70	683	12	93

After the steady reactor performance was obtained for the unidirectional flow operation, the catalytic converter was operated in the reverse flow mode. The reverse flow operation was symmetric manner, with equal forward and reverse flow times. The switch time for Case 1 was 30 second (cycle duration 60 seconds). The switch time for Case 2 and Case 3 was 15 seconds (cycle duration 30 second). See Table 3-4.

Table 3-4 The Switch Time of Reverse Flow Operations

TEST CASE	ENGINE MODE		FORWARD FLOW TIME (S)	REVERSE FLOW TIME (S)	CYCLE DURATION (S)
	SPEED (rpm)	TORQUE (Nm)			
Case 1	1500	60	30	30	60
Case 2	2000	120	15	15	30
Case 3	2600	70	15	15	30

The development of the reactor temperature under reverse flow operation is shown in Figure 3-2. The temperature shown is the average reactor temperature, which is the average of T2, T3, T4, T6, T7 and T8. T1 and T9 are the gas phase temperature at the entrance/exit of the catalyst and T5 is the gas phase temperature at the catalyst midpoint.

Case 2 and Case 3 had similar development trends. The reactor temperature developed very quickly in the first 15 minutes, then became stable after about 15 minutes. The temperature rise was over 250 K for both Case 2 and Case 3. Compared to Case 2 and Case 3, Case 1 gave only a 60 K temperature rise. This small temperature rise is attributed to the fact that only CO was ignited during the reverse flow switch, as shown in Figure 3-3. CO conversion increased from about 53% to about 80% during reverse flow operation, but HC was not ignited and its conversion remained at zero. For Case 2 and Case 3, HC conversion increased from about 10% to over 85% as the reactor temperature developed. CO oxidation would be essentially complete at the temperatures of Case 2 and Case 3. The limitation to around 90-95% shows the extent of by-pass leakage due to the prototype reverse flow system.



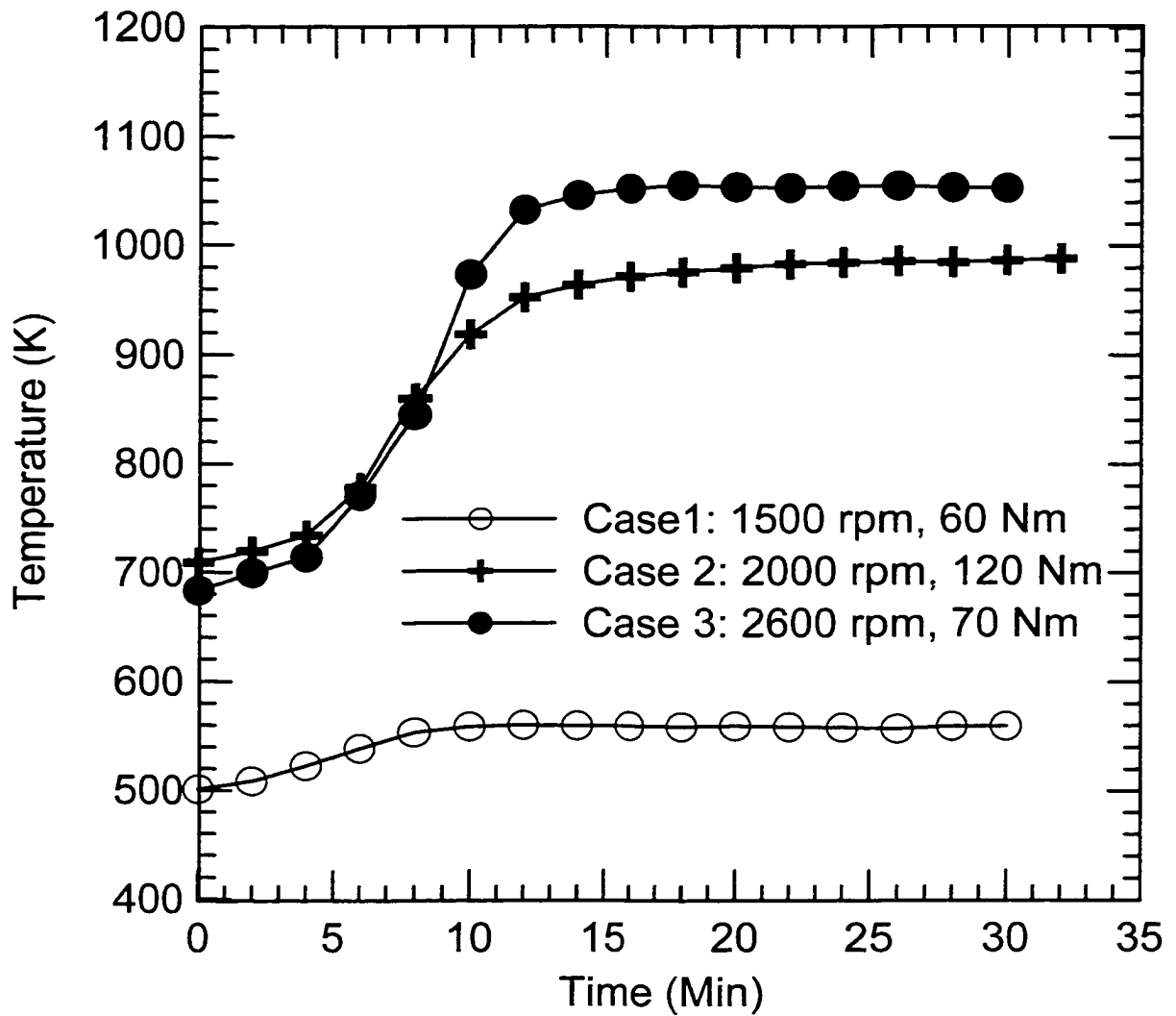


Figure 3-2 Reactor Temperature Development by Reverse Flow Operation

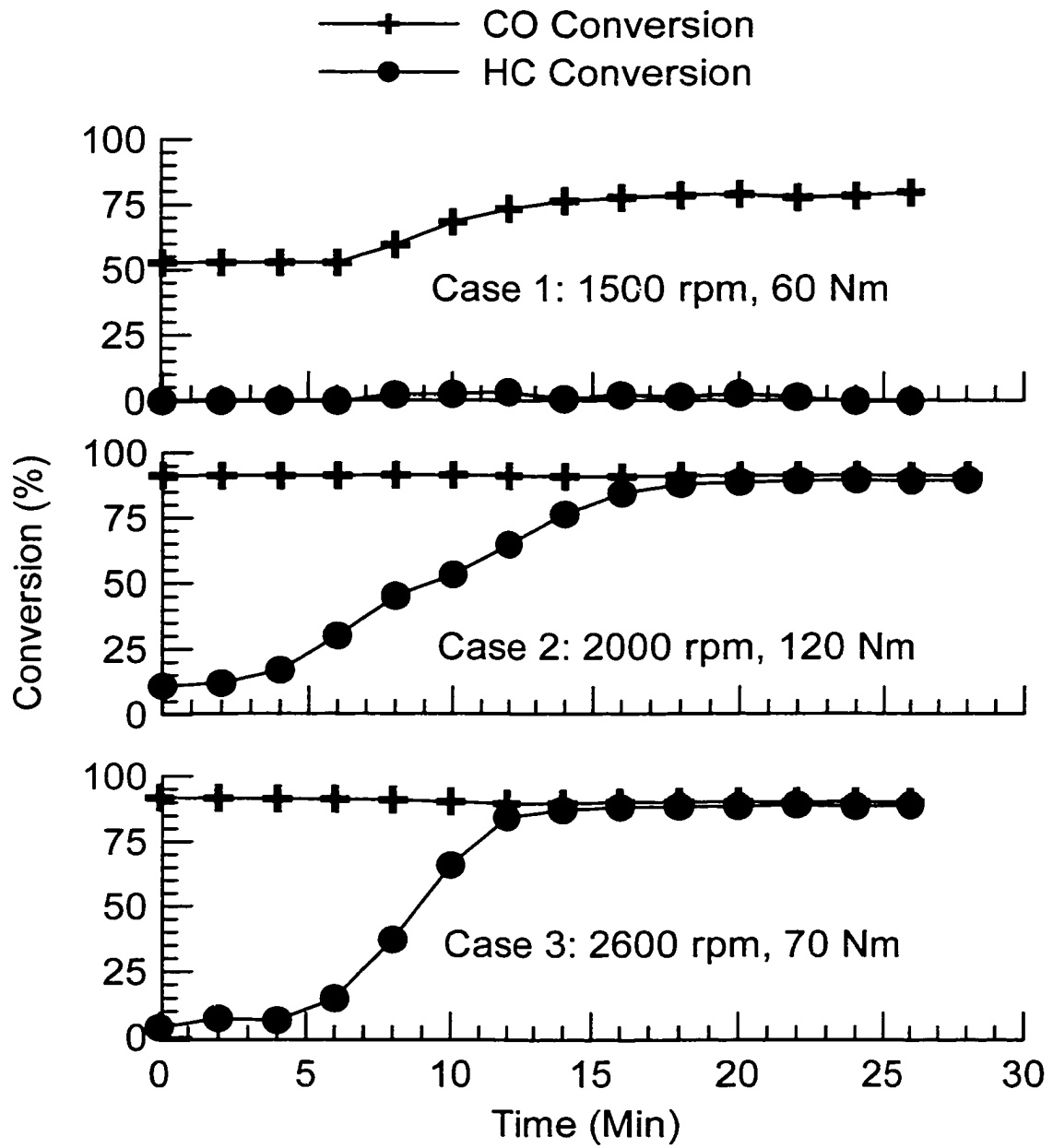


Figure 3-3 HC and CO Conversion Resulted from Reverse Flow Operation

Figure 3-4 compares the steady reactor temperature profiles for the unidirectional flow and the reverse flow operation. Reactor temperature was increased by reverse flow operation with the largest effect being observed for Case 2 and Case 3. Figure 3-5 shows that the adiabatic temperature rises for Case 2 and Case 3 are 130 K and 189 K respectively. During unidirectional flow operation, the observed reactor temperature rises were only 37 K and 52 K. However, during reverse flow operation, their reactor temperature rises were 323 and 421 K. Reverse flow operation gave temperature increases much higher than the adiabatic temperature rise. In these two cases, the actual temperature rises by the reverse flow operations were more than double of their adiabatic temperature rises.

By using reverse flow operation, reactor temperatures could be raised to values well above the gas phase adiabatic temperature rise for the exhaust gas temperature and composition. The gas phase adiabatic temperature rise calculation is shown in Appendix C. The super-adiabatic temperature are accomplished by using heat in the catalyst substrate to preheat the exhaust gas before it reacts. The “heat trap” effect consists of periodically reversing flow direction so that chemical reaction energy is repeatedly deposited near the center of the substrate, raising its temperature well above exhaust gas temperature. (See section 1.3).

Hanamura et al. (1993) designed and operated a porous burner with reverse flow. They were able to raise the solid-phase temperature in the burner to more than 13 times the adiabatic temperature rise. Matros and Bunimovich (1996) reported an experiment of SO<sub>2</sub> catalytic oxidation with reverse flow. The reactor temperature rise was 80°C higher than the adiabatic temperature rise. The temperature rises of Case 2 and Case 3 were less

than that from Hanamura et al. (1993), but higher than that from Matros and Bunimovich (1996). This result is consistent with that from Zheng et al. (1998) for the natural gas/diesel dual fuel engine exhaust.

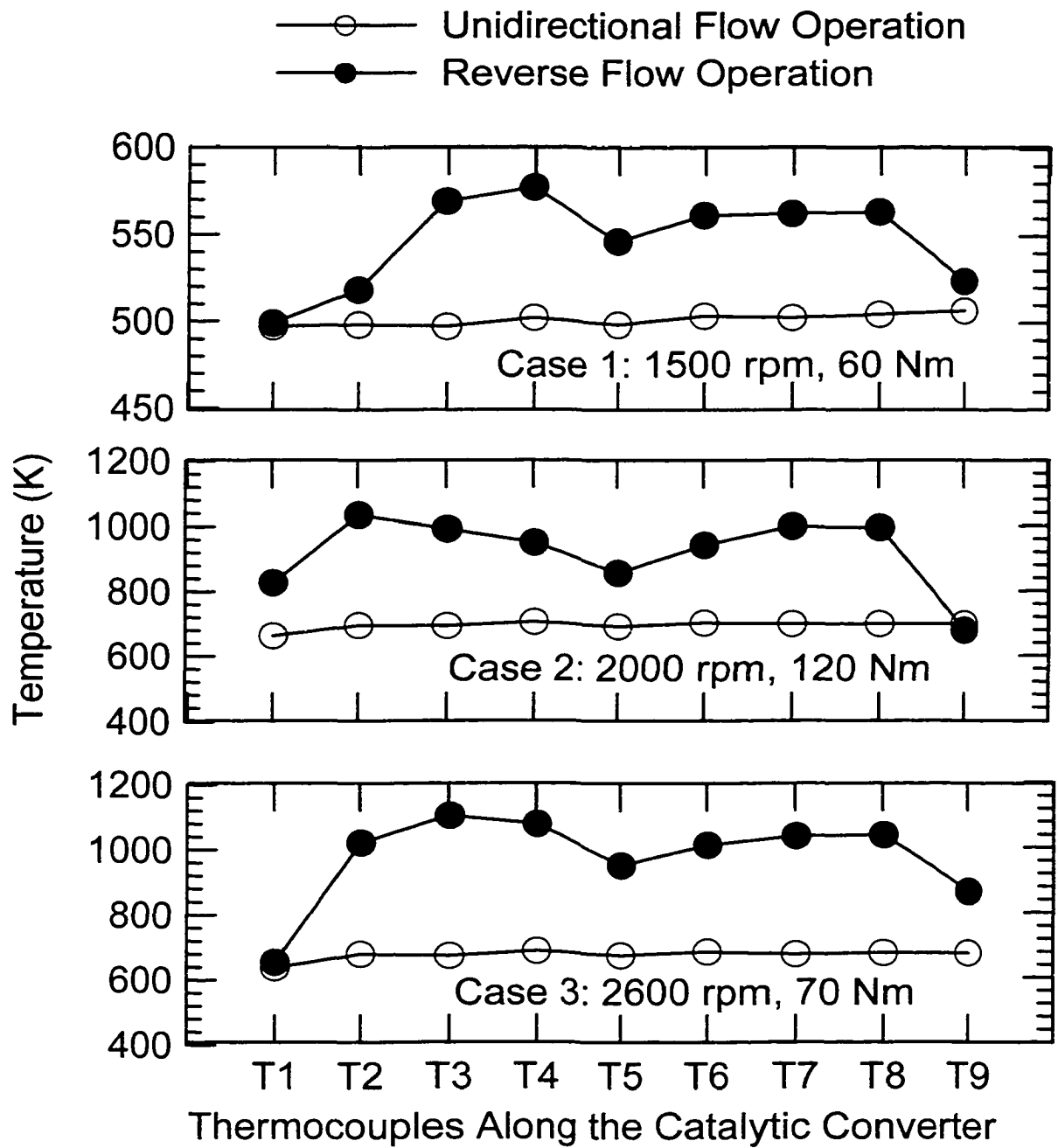


Figure 3-4 Temperature Profiles Along the Catalytic Converter

(T1, T5 and T9 are gas-phase temperatures outside the substrate.

T2, T3, T4, T6, T7, and T8 are solid phase temperatures, see

Figure 2-4)

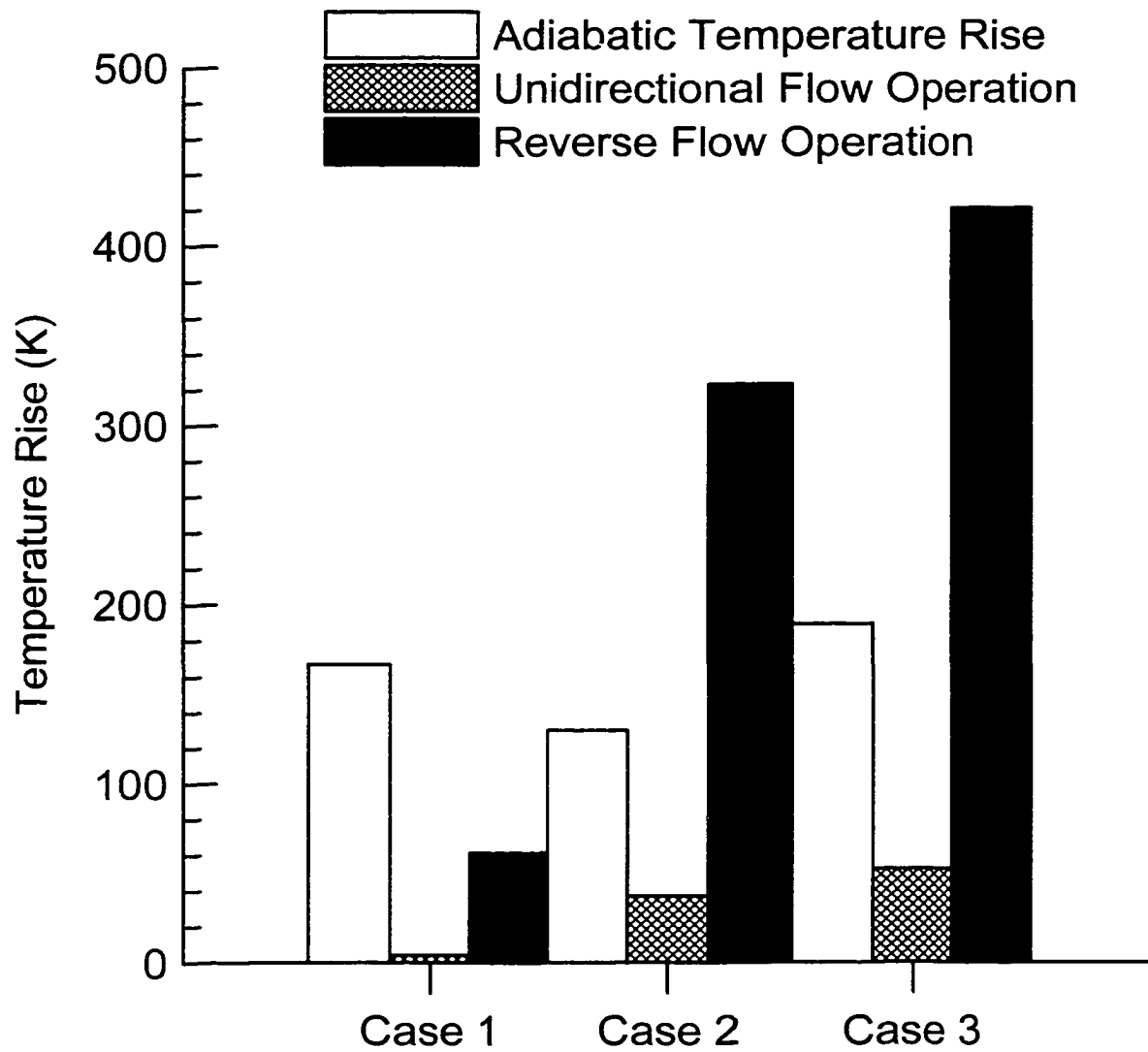


Figure 3-5 Comparison of Temperature Rise

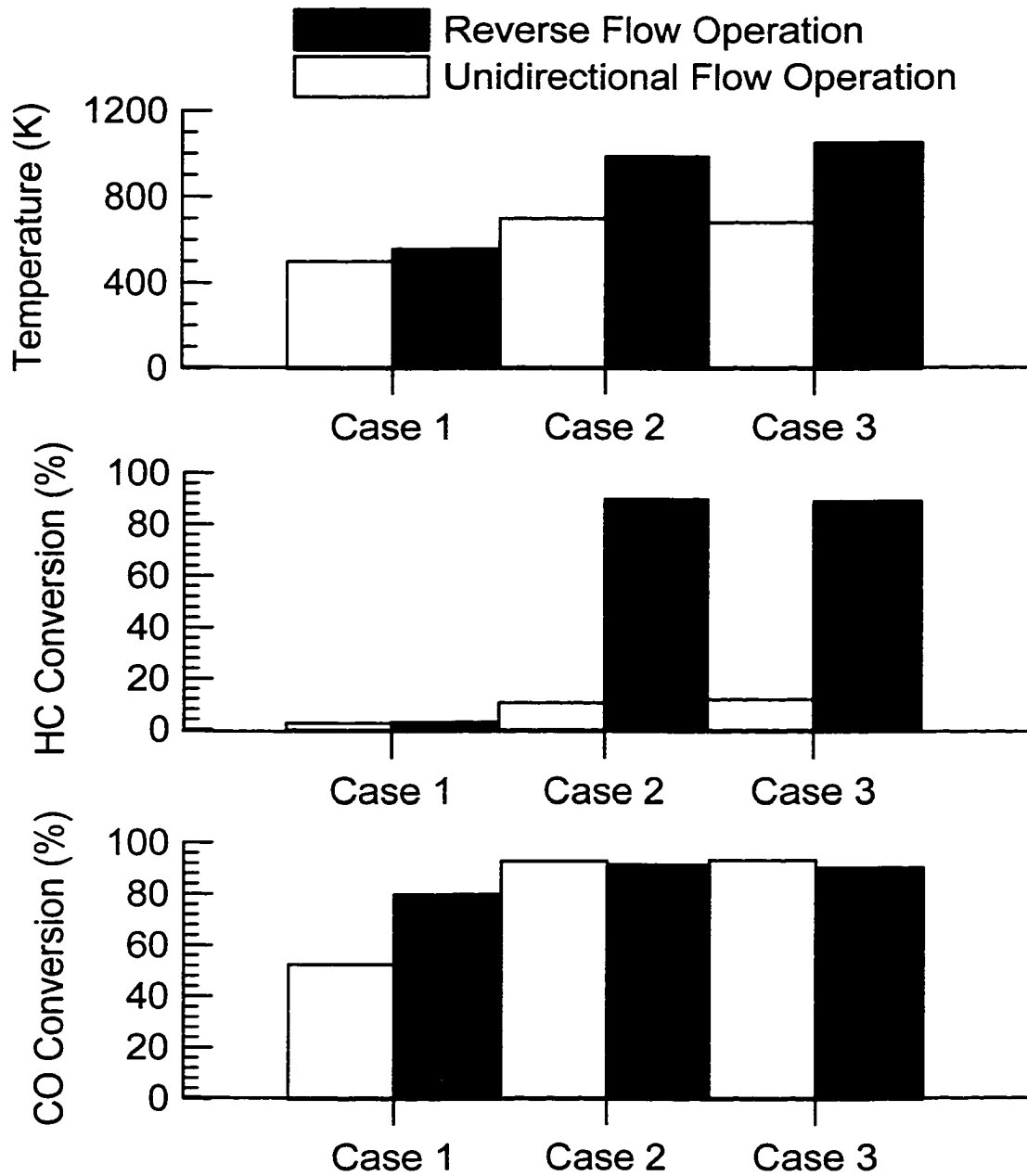


Figure 3-6 Comparison of Reverse Flow and Unidirectional Flow Operation

As shown in Figure 3-6, the average reactor temperature of Case 2 in reverse flow mode rose to 987 K, compared to 701 K for unidirectional flow operation, and HC conversion increased to almost 90% from 10%. Similarly, the reactor temperature of Case 3 rose to 1052 K from 683 K with reverse flow operation. HC conversion increased to almost 90% from 12%. These results show that the reverse flow has an advantage over unidirectional flow operation, and can have a thermal cumulating effect which allows the reactor to have a temperature rise much higher than the adiabatic temperature rise.

Case 1 however did not show a big thermal advantage compared to Case 2 and Case 3 with reverse flow operation, as shown in Figure 3-2 and Figure 3-4. The reactor temperature rise was only 61 K during reverse flow. Although this temperature rise was larger than that from unidirectional flow, (which was only 4 K), it was much lower than the adiabatic temperature rise of 167 K, as shown in Figure 3-5. The reverse flow operation increased CO conversion from 53% to 80%, but methane conversion remained near zero, as with unidirectional flow, as shown in Figure 3-3 and Figure 3-6. In this case, reverse flow could not accumulate enough energy to ignite the methane reaction. It was believed that the reason for the low conversion in Case 1 was the inability of the reactor to achieve the methane ignition temperature, which is about 773 K. Although the temperature increases during reverse flow operation, which caused an increase in CO conversion, the rise was insufficient to cause significant methane oxidation, hence the temperature remained low.

To investigate this effect further, an experiment was performed with a much higher initial reactor temperature. This experiment was denoted Case 4. Engine speed was the same as Case 1, but engine torque was increased from 60 Nm to 190 Nm. The



exhaust gas data are shown in Table 3-5. With steady unidirectional flow operation, the average reactor temperature for this engine mode was 785 K, which was slightly higher than methane light-off temperature. HC conversion was 58% and CO conversion was 93%. After the reactor achieved steady state, the reactor was operated in reverse flow manner with a flow switch time of 15 second (cycle duration 30 second). The reactor temperature for unidirectional and reverse flow modes are compared in Figure 3-7. The averaged reactor temperature of reverse flow was lower than that from unidirectional flow operation. The gas temperature T5 in the middle of the reactor was very low for reverse flow. However, reactor temperatures T2 and T8 were increased by reverse flow. In this case, reactor temperature was reduced by reverse flow operation. Reverse flow was unable to cumulate energy for the methane reaction. Compared with Case 2 and Case 3, the initial reactor temperature was not low. However, its HC and CO inlet concentration was quite low compared to Case 1, Case 2 and Case 3. The inlet HC concentration was only 1276 ppm and CO 776 ppm, as shown in Table 3-5. Reverse flow could not get enough energy for this low inlet reactant concentration. The adiabatic temperature rise for this case was only 37 K. For unidirectional flow, the average reactor temperature was 785 K and the temperature rise was 19 K. For reverse flow, the average reactor temperature was 780 K and the temperature rise was 14 K. Reverse flow did not show any advantage compared unidirectional flow operation for this case. The reason was very low inlet reactant concentration.

Table 3-5 Engine Exhaust Parameters for Case 4

Test Case	Engine Mode		Exhaust Composition						Texh. (K)	Mass Flow Rate (g/s)
	Speed (rpm)	Tor. (Nm)	HC (ppm)	CO (ppm)	NO (ppm)	O <sub>2</sub> (%)	CO <sub>2</sub> (%)	H <sub>2</sub> O (%)		
Case 4	1500	190	1276	776	1550	5.35	7.37	14.10	834	36.84

N<sub>2</sub>: Balanced Exhaust Gas Composition

Texh.: Engine Exhaust Temperature

Tor.: Engine Torque

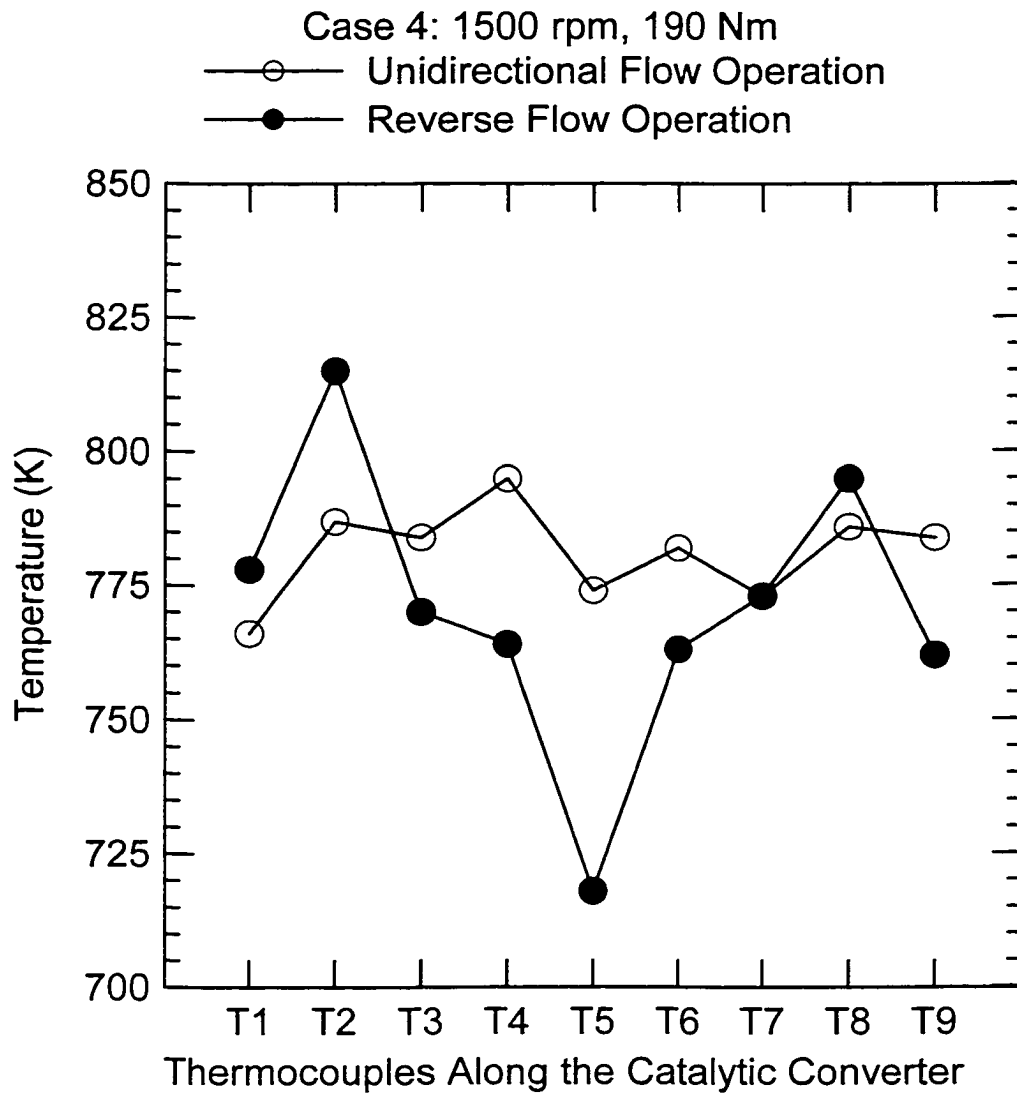


Figure 3-7 Comparison of Reactor Temperature between Reverse Flow and Unidirectional Flow Operation (T1, T5 and T9 are gas-phase temperatures outside the substrate. T2, T3, T4, T6, T7, and T8 are solid phase temperatures, see Figure 2-4)

In conclusion, it has been seen that reverse flow can increase reactor temperature greatly for some steady engine operations, with a reactor temperature rise that can be much higher than the adiabatic temperature rise. However, this effect requires the proper reactor conditions, especially initial reactor temperature profile prior to the start of reverse flow operation, as well as proper reactant concentrations. If either the initial reactor temperature or the inlet reactant concentration is too low, reverse flow can not cumulate enough energy and reverse flow fails to develop reactor temperature and increase methane and CO conversion.

### **3.2.2 Evaluation of Reverse Flow Switch Time**

The reverse flow switch time is a key parameter for controlling the reactor temperature. In this section, the effect of changing the reverse flow switch time is evaluated for two steady engine operations. The two engine operating modes were Case 2 and Case 3 described in Section 3.2.1. All reverse flow operations conducted were symmetric. The switch times investigated were 5, 15, 30, 60, 120 and 240 seconds.

Figure 3-8 and Table 3-6 show comparisons of reactor performance with reverse flow switch times 5, 15, 30, 60, 120 and 240 second for Case 2. Figure 3-8 shows the pseudo-steady state reactor temperature profiles and Table 3-6 shows the HC and CO conversion, plotted against average and the peak reactor temperature. Average reactor temperature is the arithmetic average of T2, T3, T4, T6, T7, and T8. For the switch times of 5, 15 and 30 second, the reactor temperature was quite close to each other, as shown in Figure 3-8. With these fast reverse flow switches, reverse flow established a reactor temperature higher than 950 K, with HC and CO conversions of about 90%, as shown in

Table 3-6. The CO conversion is relatively constant at 90% because the catalyst is well above the threshold temperature for CO oxidation and the inefficiency is probably due to bypass flow. The CO oxidation is close to 100% for the flow going through the catalyst so the percentage unreacted corresponds to flow bypassing the catalyst due to leakage and switching losses in the prototype converter system.

For a switch time of 60 seconds, most of the reactor retained a high temperature status and gave essentially the same HC and CO conversion as the short switch times of 5, 15, and 30 second, as shown in Figure 3-8 and Table 3-6. For the long switch time of 120 second, most of the reactor cooled to a low temperature. Only a very small part of reactor remained in the high temperature status, as shown in Figure 3-8. The average reactor temperature decreased to 801 K and the HC conversion dropped to 66%, as shown Table 3-6. For the very long switch time of 240 second, the entire reactor cooled to a low temperature, as shown in Figure 3-8. The average reactor temperature dropped to 704 K, which was very close to the value of 701 K obtained from unidirectional flow operation. The HC conversion reduced to 15%, which was close to the value of 11% achieved with unidirectional flow operation, shown in Table 3-6. It is easy to see that reverse flow operation behaves like unidirectional flow operation when the switch time is sufficiently long that the “hot spot” leaves the converter.

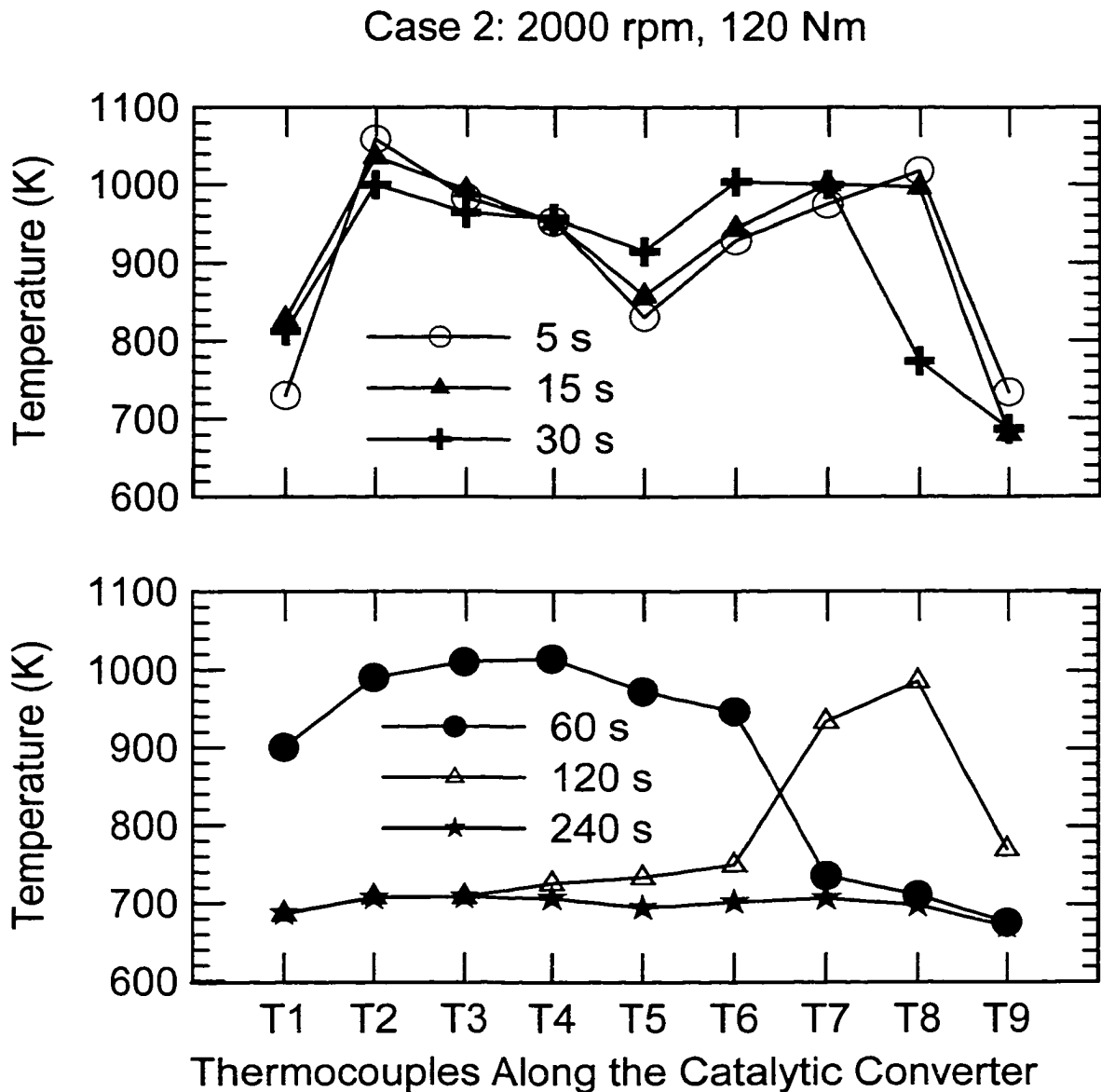


Figure 3-8 Reactor Temperature Profiles Produced by Variable Reverse Flow Switch Times (T1, T5 and T9 are gas-phase temperatures outside the substrate. T2, T3, T4, T6, T7, and T8 are solid phase temperatures, see Figure 2-4)

Table 3-6 Comparison of Reactor Performance for Variable Cycling Time at  
2000 rpm, 120 Nm

Switch Time (S)	Average Reactor Temperature (K)	Peak Reactor Temperature (K)	CO Conversion (%)	HC Conversion (%)
5	986	1059	91	88
15	987	1036	91	90
30	950	1004	91	88
60	901	1014	91	88
120	801	985	92	66
240	704	708	92	15

Essentially, reverse flow loses its “heat trap” effect when the switch time is too long. For this engine operation, the observed critical switch time for the reactor heat extinction was about 180 seconds. For smaller switch times, reverse flow could maintain part of reactor in the high temperature region. The shorter the switch time, the wider the high temperature region, which in turn gives higher HC and CO conversion. However, if the switch time is longer than 180 second, most of the stored thermal energy is removed from the reactor. In this case, reverse flow loses its “heat trap” effect and the reactor behaves in the same manner as in unidirectional flow.

Figure 3-9 and Table 3-7 compares reactor performance with reverse flow switch time 5, 15, 30, 60, 120 and 240 second for Case 3. Figure 3-9 shows the pseudo-steady state reactor temperature profiles and Table 3-7 is about the average reactor temperature and HC and CO conversion. A similar observation as for Case 2 was obtained for this higher engine speed.



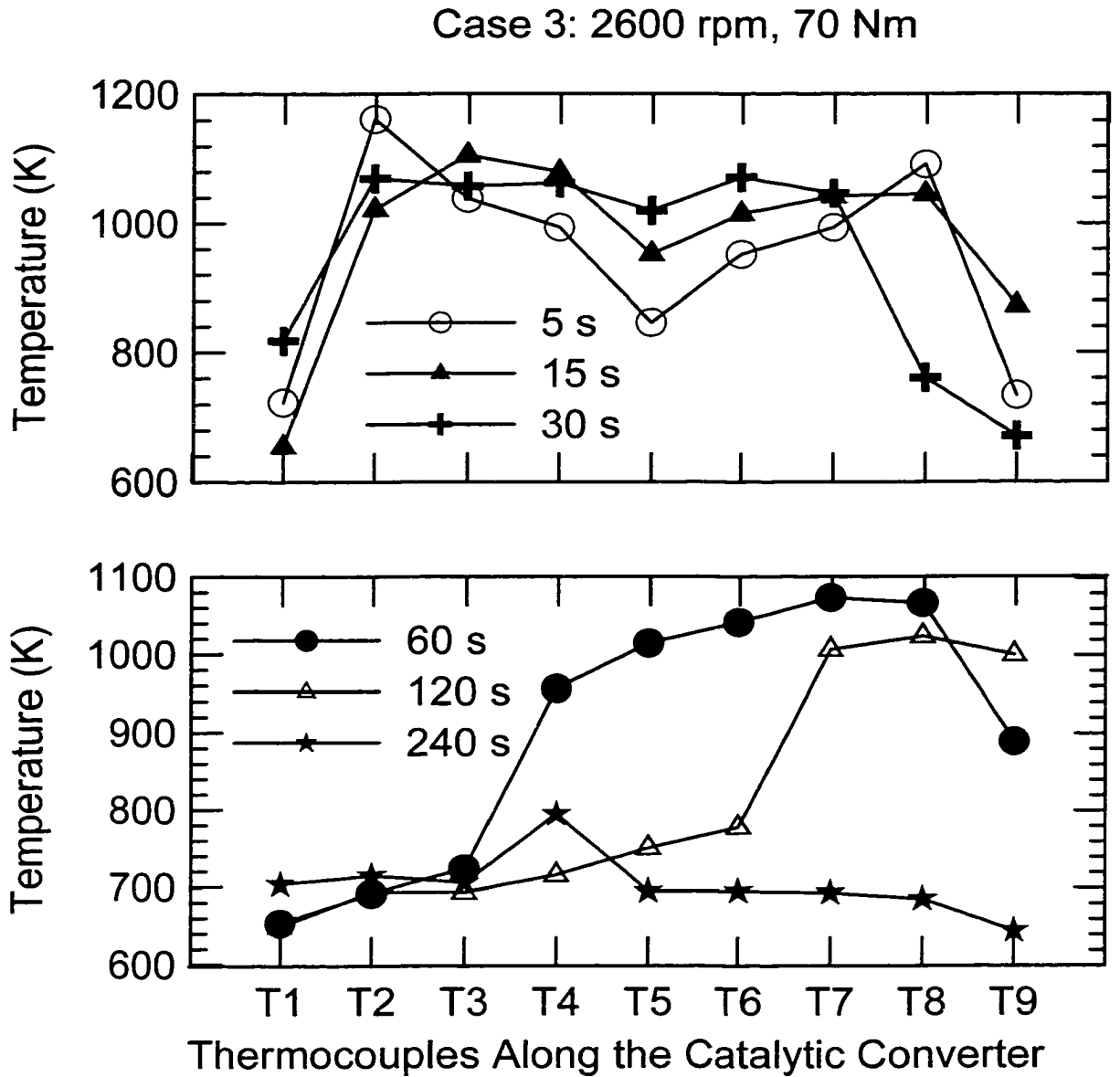


Figure 3-9 Reactor Temperature Profiles Resulted from Variable Reverse Flow

Switch Times (T1, T5 and T9 are gas-phase temperatures outside the substrate. T2, T3, T4, T6, T7, and T8 are solid phase temperatures, see Figure 2-4)

Table 3-7 Comparison of Reactor Performance for Variable Cycling Time at  
2600 rpm, 70 Nm

Switch Time (S)	Average Reactor Temperature (K)	Peak Reactor Temperature (K)	CO Conversion (%)	HC Conversion (%)
5	1039	1162	90	86
15	1052	1106	90	89
30	1012	1072	91	89
60	925	1073	92	91
120	818	1023	93	87
240	714	794	94	21

For the short switch times of 5, 15 and 30 seconds, the average reactor temperature was about 1000 K, with HC conversion close to 90% and CO conversion more than 90%. For a switch time of 60 seconds, the reactor remained mostly in a high temperature region and gave higher HC and CO conversion than the short switch times of 5, 15, and 30 second, as shown in Figure 3-9 and Table 3-7. Although the average reactor temperature fell to 925 K, the maximum reactor temperature rose to 1073 K, which explains the higher HC and CO conversion than observed with the short switch times of 5, 15 and 30 seconds.

For the switch time of 120 seconds, most part of reactor cooled to a low temperature, with only a small part of the reactor in the high temperature region, as

shown in Figure 3-9. The average reactor temperature decreased to 818 K, but HC conversion was maintained with a high value 87%, as shown Table 3-7.

For the very long switch time of 240 seconds, the whole reactor cooled to a low temperature, as shown in Figure 3-9. The average reactor temperature dropped to 714 K, which was close to the value of 683 K observed for unidirectional flow operation. HC conversion was reduced to 21%, close to the value of 12% obtained with unidirectional flow operation, as shown in Table 3-7. Again, it is easy to see that reverse flow operation is just like the unidirectional flow operation for such a long switch time.

These results at 2600 rpm showed the same trend of CO conversion as the 2000 rpm case. The CO conversion was always greater than 90% and increased as the switching became less frequent. Again, this is attributed to essentially 100% conversion of the exhaust flowing through the catalyst and a decrease in bypass flow with longer switch times.

Even though engine speed was higher in Case 3 than Case 2, the observed critical switch time for Case 3 for the reactor heat extinction was still about 180 second. In order to maintain the reverse flow special “heat trap” effect, the reverse flow switch time should be less than 180 second. A switch time of 60 seconds was able to keep most of the reactor in a high temperature region and gave high HC and CO conversion, however steep temperature gradients were observed in the reactor. Reactor structure thus experienced a large thermal stress from this steep temperature gradient. This could be avoided by choosing short switch time like 15 or 30 second, which gave a much flat reactor temperature profile.

In conclusion, the reverse flow with short switch time like 5, 15 and 30 second can build up a very high reactor temperature and give very high HC and CO conversion. The reverse flow with medium switch time 60 second could maintain most of the reactor in the high temperature region and give high HC and CO conversion, however, it produces steep temperature gradient along the reactor and results in the big thermal stress, which can reduce the lifetime of the reactor. The reverse flow with a switch time of 120 seconds still kept a small part of reactor in the high temperature region, however the HC conversion drops significantly in some engine operations. The reverse flow with a switch time of 240 seconds works like unidirectional flow operation. Reverse flow loses its special “heat trap” effect for such long switch time.

For the cases studied, the observed critical switch time for the reactor heat extinction was about 180 second. In order to maintain the reverse flow special “heat trap” effect, the reverse flow switch time should be less than 180 second. To maintain the best HC and CO conversion and reduce the thermal stress along the reactor, the switch time should be as short as possible. However, for the same reactor performance, in order to reduce the flow switches and extend the life time and durability of reverse flow control facilities, the switch time should be chosen as long as possible. Considering these competing principles, the switch time between 15 second and 30 second will be good for this reverse flow catalytic converter.

### **3.3 Reverse Flow Catalytic Converter Performance Under Transient Engine Operation**

#### **3.3.1 Introduction of Transient Engine Test with Reverse Flow Catalytic Converters**

The objective of this section is to evaluate the reactor heating and cooling process under the transition of engine modes with reverse flow. In the previous section, it was shown that reverse flow could develop reactor temperature and increase HC and CO conversion for some steady engine operations. However, reverse flow could not achieve this objective for some other engine operating conditions. This occurred because either the initial reactor temperature was too low or the inlet reactant concentration was too low. When the engine operates in light load modes, the factor limiting performance is the low inlet gas temperature. Inlet HC and CO concentrations were very high for most dual fuel engine light load modes. To increase reactor temperature and convert HC at light load modes, one good approach is to run the engine first with a relatively heavy load, which has a high exhaust temperature. The catalytic converter is pre-heated during this operation. Then the engine can be changed to the light engine mode with the converter operating with reverse flow. Provided that the catalyst bed was preheated to a sufficiently high level, reverse flow enabled the development of a high reactor temperature even though the inlet gas temperature was low. High CO and HC conversion can then be achieved, which releases sufficient energy to maintain a high reactor temperature even with low inlet gas temperature. A temperature higher than the adiabatic rise is observed.

The following sections report the results observed with engine transitions among varying loads: heavy, light and idle.

The engine operating conditions and resulting exhaust gas temperature and composition are summarized in Table 3-8. Mode 1 (2000 rpm, 170 Nm) corresponds to heavy load, Mode 2 (2000 rpm, 50 Nm) was a light load while Mode 3 corresponded to engine idle. The HC emissions produced in Modes 1 and 2 are mostly methane as the engine is operating in dual fuel mode. The HC emissions in Mode 3 (idle) are all non-methane HC because the engine idles on diesel only.

Table 3-8 Engine Exhaust Parameters

Mode	Engine		Exhaust Composition						T <sub>exh.</sub> (K)	Mass Flow Rate (g/s)
	Speed (rpm)	Tor. (Nm)	HC (ppm)	CO (ppm)	NO (ppm)	O <sub>2</sub> (%)	CO <sub>2</sub> (%)	H <sub>2</sub> O (%)		
Mode 1	2000	170	1734	955	784	7.09	6.63	12.72	833	51
Mode 2	2000	50	5364	1681	105	15.00	3.04	6.01	527	53
Mode 3	Idle	Idle	363	409	190	17.69	1.83	3.54	388	21

N<sub>2</sub>: Balance of Exhaust Gas Composition

T<sub>exh.</sub>: Engine Exhaust Temperature

Tor.: Engine Torque

When the catalytic converter was operated in the unidirectional flow manner, under steady state, the results shown in Figure 3-10 were obtained. For these tests, engine exhaust gas flowed through the catalytic converter in the forward direction. T<sub>1</sub> was the inlet gas temperature and T<sub>9</sub> was the outlet gas temperature. Table 3-9 gives the reactor performance with these three engine modes. Compared to Mode 2 and Mode 3, Mode 1 resulted in a higher reactor temperature. The average reactor temperature of Mode 1 was

827 K, which gave about 77% HC conversion. The average reactor temperature for Mode 2 was only 522 K. For this low reactor temperature, the HC conversion was almost zero. Mode 3 had a very low reactor temperature, however its HC conversion was about 78%. This was because the engine idles on diesel only so the most of the HC in the exhaust gas for this engine mode was not methane. The CO conversion was about 90% for these three engine modes.

Table 3-9 Reactor Performance for Three Engine Operations

Mode	Engine		Average Reactor Temp. (K)	CO Conversion (%)	HC Conversion (%)	Adiabatic Temp. Rise (K)
	Speed (rpm)	Torque (Nm)				
Mode 1	2000	170	827	90	77	49
Mode 2	2000	50	522	89	5	152
Mode 3	Idle	Idle	449	87	78	14

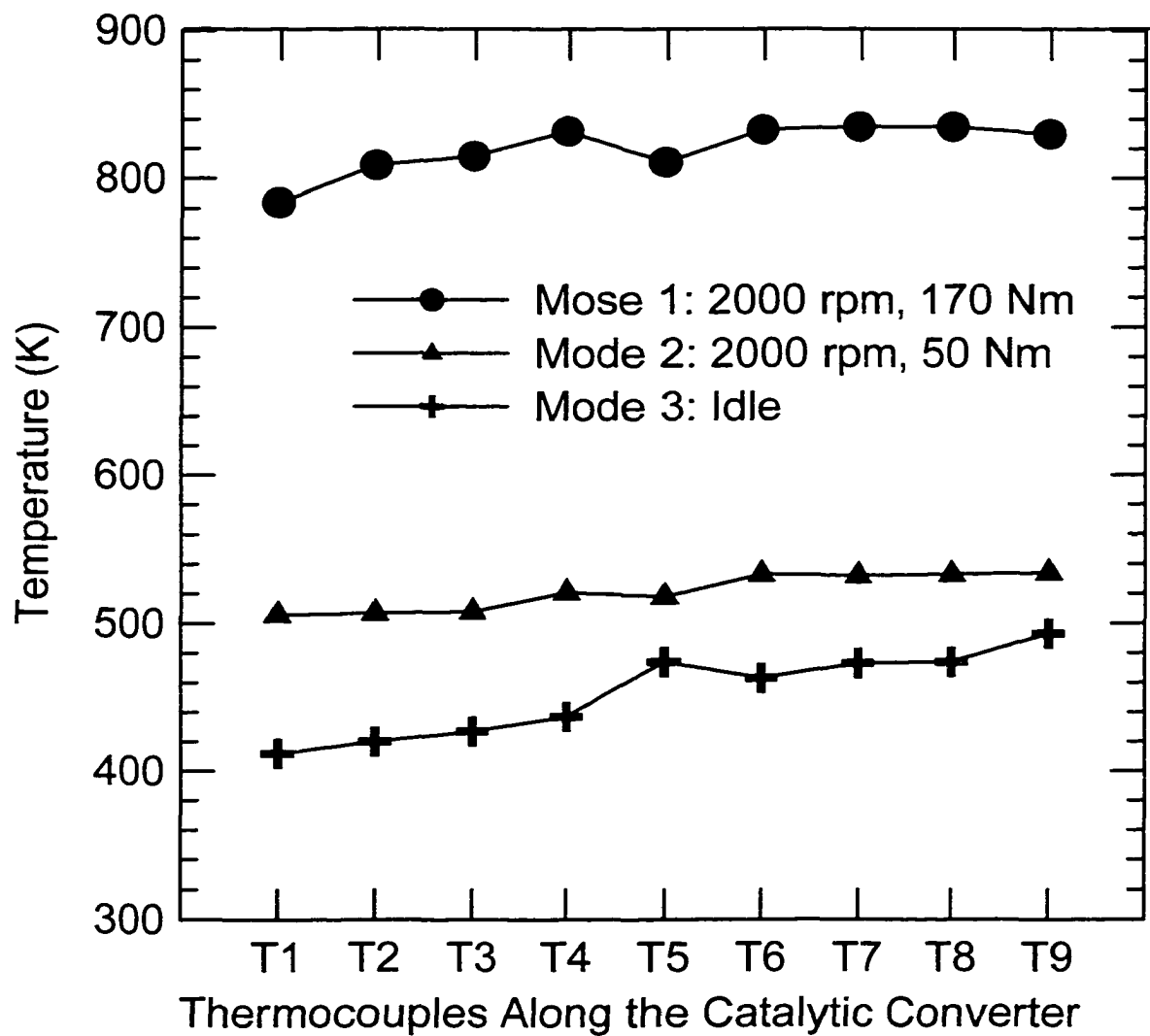


Figure 3-10 Steady Reactor Temperature Profiles (T1, T5 and T9 are gas-phase temperatures outside the substrate. T2, T3, T4, T6, T7, and T8 are solid phase temperatures, see Figure 2-4)



### 3.3.2 Transition from Heavy Load to Light Load

The first engine transition studied was from heavy load (Mode 1) to light load (Mode 2). The objective of this operation was to see how the reactor temperature changes with reverse flow operation. These results were compared with those from unidirectional flow operation. The engine was first operated in Mode 1 with the catalytic converter in unidirectional flow until steady reactor performance was observed. At this point, the average temperature of the catalytic converter was about 820 K.

After steady reactor operation was observed, the engine was changed to Mode 2. At the same time, the catalytic converter was set to operate in the reverse flow manner. A symmetric reverse flow operation with a switch time of 15 seconds was used. For comparison purpose, the same experiment was repeated, however the reactor was allowed to continue with unidirectional flow operation after the change from Mode 1 to Mode 2. The variation in reactor temperature with time during this engine transition is shown in Figure 3-11. With reverse flow, the average reactor temperature increased to about 1000 K, however, with unidirectional flow the reactor temperature dropped to about 540 K, a difference of almost 500 K. The calculated adiabatic temperature rise for Mode 2 was only 152 K. The actual temperature rise during reverse flow was thus about 3 times the adiabatic temperature rise. This effect was bigger than that observed previously with reverse flow under steady engine operations. Under the steady engine operations, the temperature rise by reverse flow was about 2 times higher than the unidirectional flow operation, as shown in Figure 3-5. Figure 3-12 shows the reactor temperature profiles for

these operations. It is the pseudo-steady state reactor temperature for reverse flow and the steady reactor temperature for unidirectional flow. Figure 3-13 compares the HC and CO conversion for this engine transition. With reverse flow, the HC conversion increased to about 88% for Mode 2. However, without reverse flow, HC conversion dropped to almost zero. The advantage of reverse flow when switching engine operation from heavy to light load is obvious.

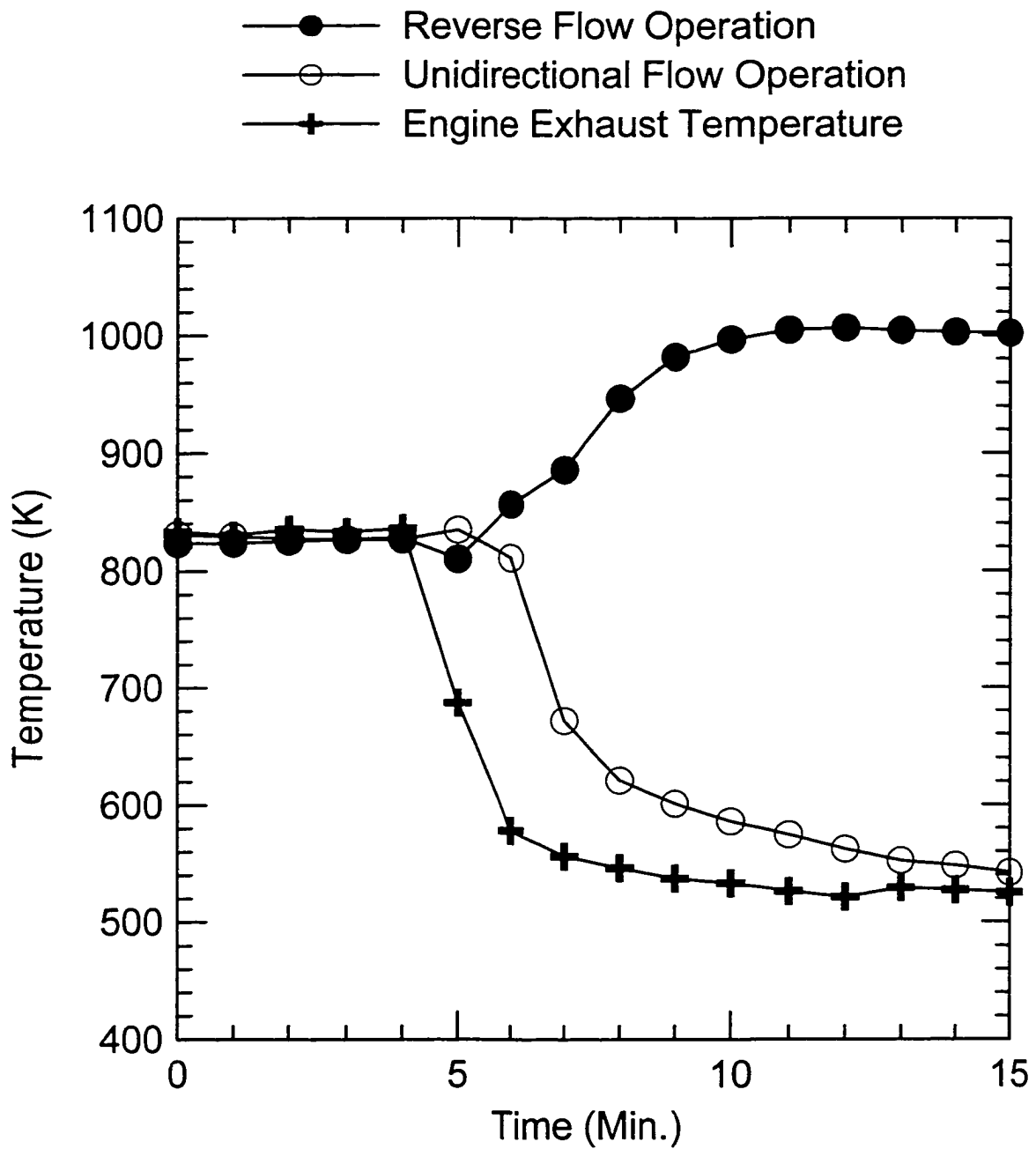


Figure 3-11 Comparison of Reactor Temperature with Engine Operation  
Transition from Heavy Load to Light Load at four minutes

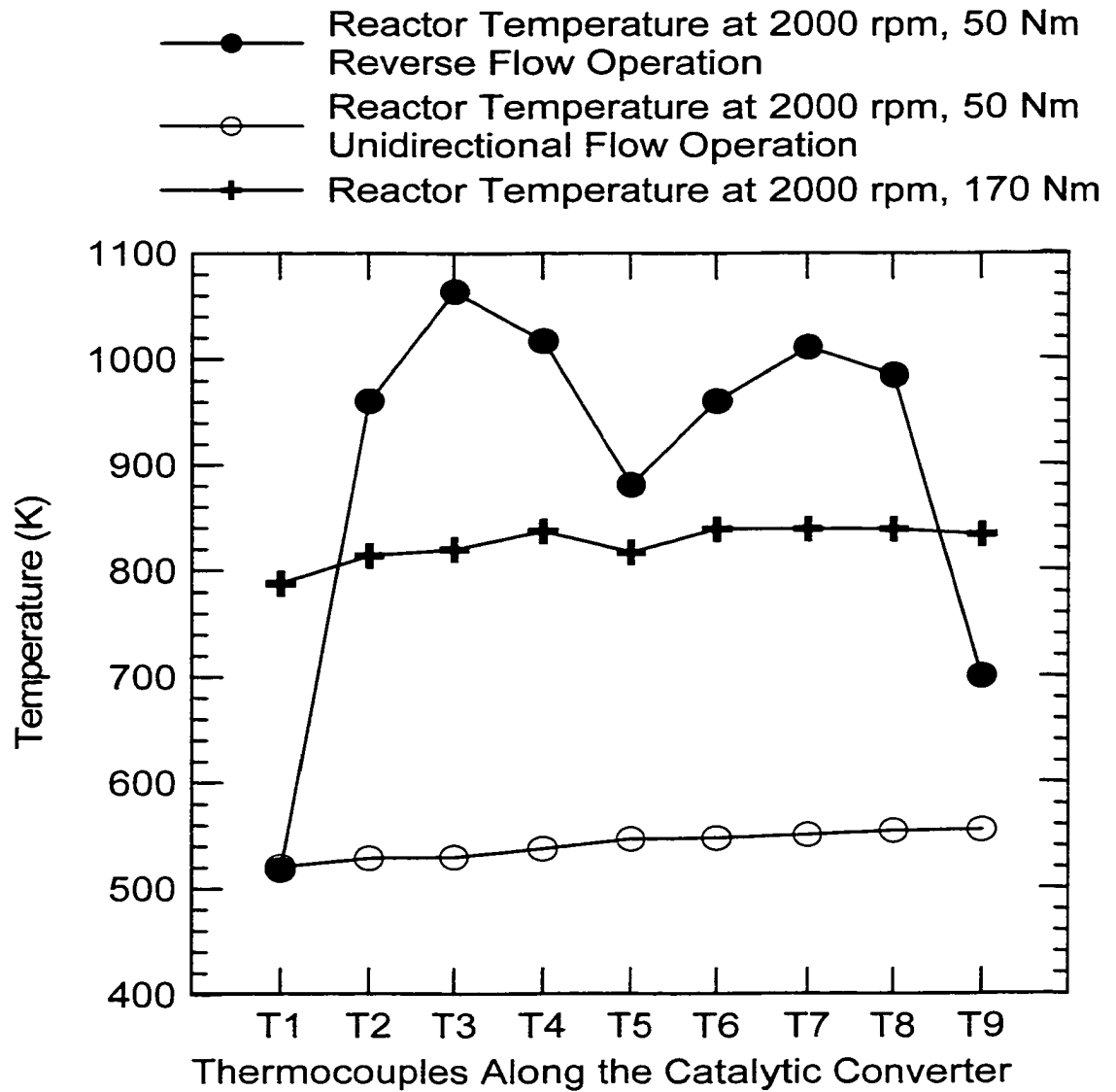


Figure 3-12 Comparison of Reactor Temperature Profiles (T1, T5 and T9 are gas-phase temperatures outside the substrate. T2, T3, T4, T6, T7, and T8 are solid phase temperatures, see Figure 2-4)

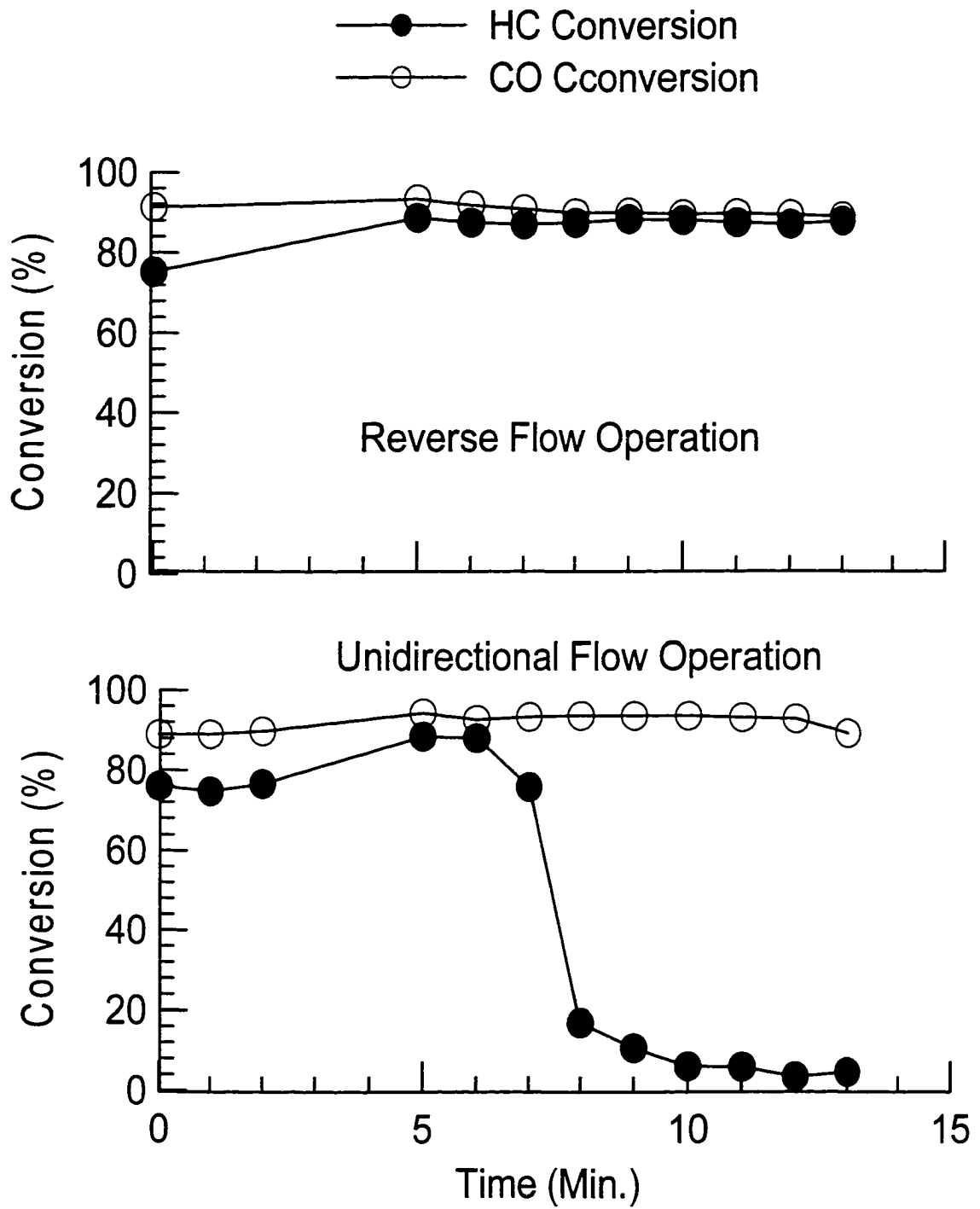


Figure 3-13 Comparison of HC and CO Conversion with Engine Operation  
Transition from Heavy Load to Light Load

### 3.3.3 Transition from Light Load to Idle

The second engine transition studied was from light load (Mode 2) to idle (Mode 3). Because both engine exhaust temperature, HC and CO concentration were very low in Mode 3, the reactor temperature decreased with time. However, the rate of temperature decrease was slow if the catalytic converter was operated in reverse flow manner. The objective of this experiment was to compare the rate of temperature decrease with reverse flow operation to that obtained with unidirectional flow. The initial reactor temperature used corresponded to the pseudo steady state profile that resulted from the transition from engine Mode 1 to Mode 2, with the converter operated in a reverse flow manner. In other words, this transition from Mode 2 to Mode 3 was made following the transition described in Section 3.3.2. The average initial reactor temperature was thus about 1000 K.

After the engine was changed to Mode 3, the catalytic converter was operated in symmetric reverse flow with a switch time of 15 seconds. A further test was performed using the same initial condition, but with the converter operated with unidirectional flow. The reactor temperature changed with time during this engine operation transition is shown in Figure 3-14. With reverse flow, the reactor temperature dropped slowly, however, for unidirectional flow, the reactor temperature dropped much more rapidly. The reactor temperature profiles at 12 minutes after engine transition are shown in Figure 3-15. Because most of the HC was not methane in Mode 3, both HC and CO conversion remained at a high value for the time tested, as shown in Figure 3-16. However, it is an advantage to maintain a high reactor temperature for as long as possible, to improve

performance in subsequent transitions. For example, if the transition was made from Mode 1 to Mode 2, in which significant quantities of methane are present in the exhaust, it is desirable to have a high reactor temperature to ensure light-off. See, for example, Section 3.3.2.

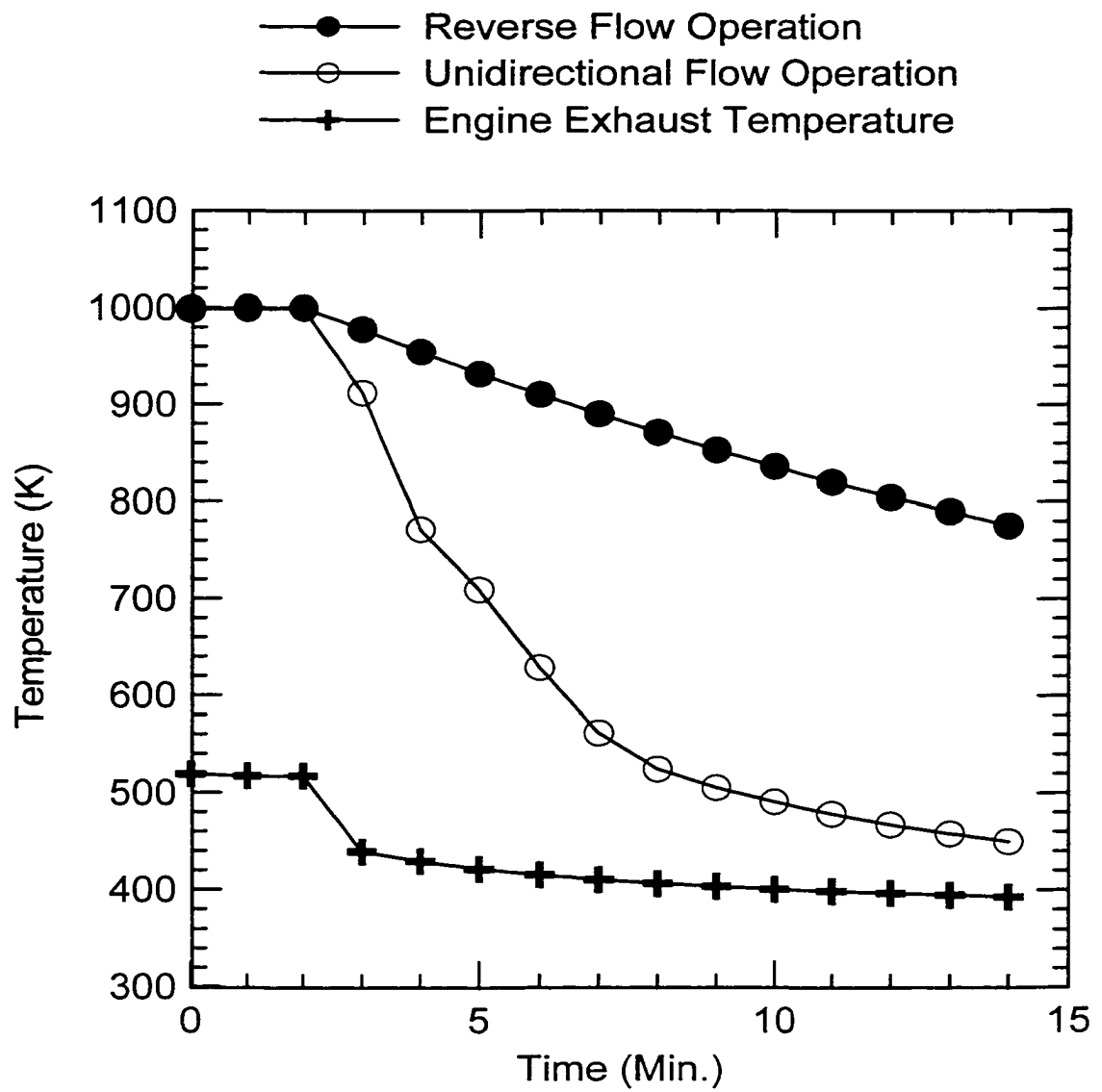


Figure 3-14 Comparison of Reactor Temperature Drop with Engine Operation  
Transition from Light Load to Idle



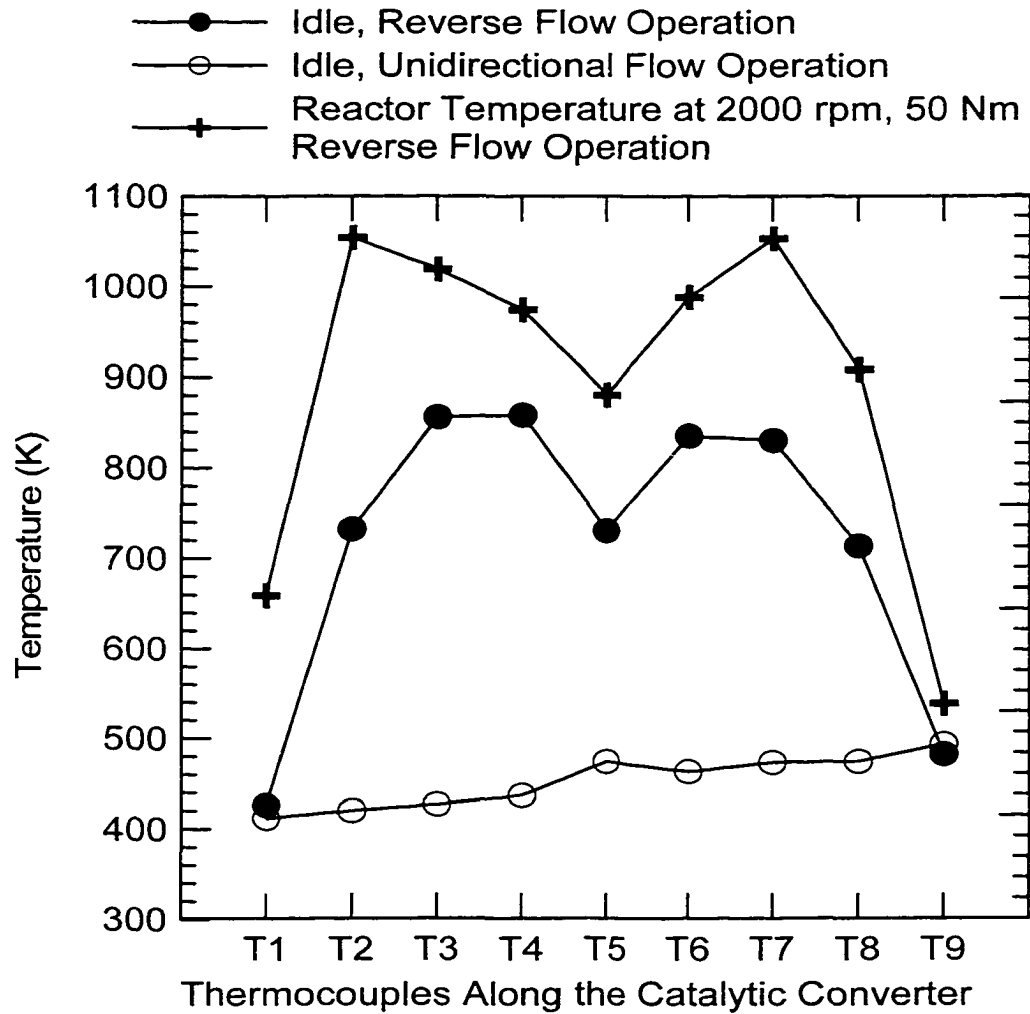


Figure 3-15 Comparison of Reactor Temperature Profiles (T1, T5 and T9 are gas-phase temperatures outside the substrate. T2, T3, T4, T6, T7, and T8 are solid phase temperatures, see Figure 2-4)

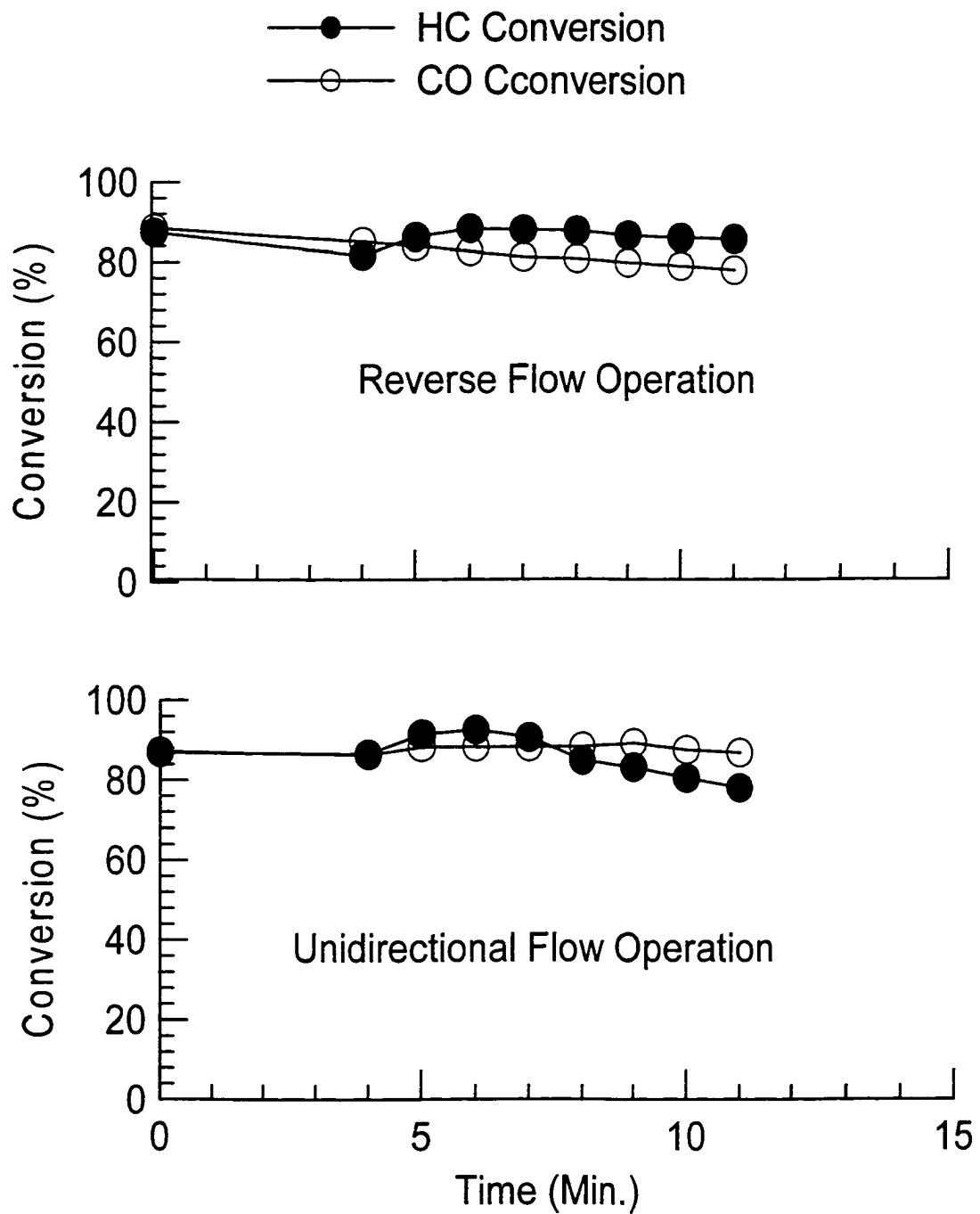


Figure 3-16 Comparison of HC and CO Conversion with Engine Operation  
 Transition from Light Load to Idle

### 3.3.4 Transition from Light Load to Heavy Load

The third engine transition was from light load (Mode 2) to heavy load (Mode 1). The objective of this operation was to see how the reactor temperature developed with the reverse flow operation. For this heating process, reverse flow could potentially hinder the reactor temperature development because of its “cold trap” effect. Reverse flow was compared to unidirectional flow operation. The engine was first operated in Mode 2 with the catalytic converter operating in unidirectional flow until steady reactor performance was obtained. The steady average reactor temperature was about 520 K for engine Mode 2. This reactor temperature was the initial condition.

After steady state was obtained, the engine was changed to Mode 1. The catalytic converter was operated with symmetric reverse flow and a switch time of 15 seconds. Alternatively, the reactor was operated with unidirectional flow after the engine transition. The reactor temperature changed with time as shown in Figure 3-17. With reverse flow, the reactor temperature developed slowly, taking about 22 minutes for the reactor temperature to increase to 800 K. With unidirectional flow, the reactor temperature increased quickly, only 10 minutes for the reactor temperature to rise to 800 K. However, in the later stage, reactor temperature shows further development with reverse flow operation. Figure 3-18 shows the reactor temperature profiles for these operations. The pseudo-steady state reactor temperature for reverse flow and the steady reactor temperature for unidirectional flow are both illustrated. Figure 3-19 compares the HC and CO conversion for this engine transition. With reverse flow, HC conversion increased slowly, but for unidirectional flow the HC conversion increased quickly. This

experiment shows the disadvantage of reverse flow when switching engine operation from light to heavy load. Reverse flow slowed down reactor temperature development, which illustrates the “cold trap” effect of reverse flow.

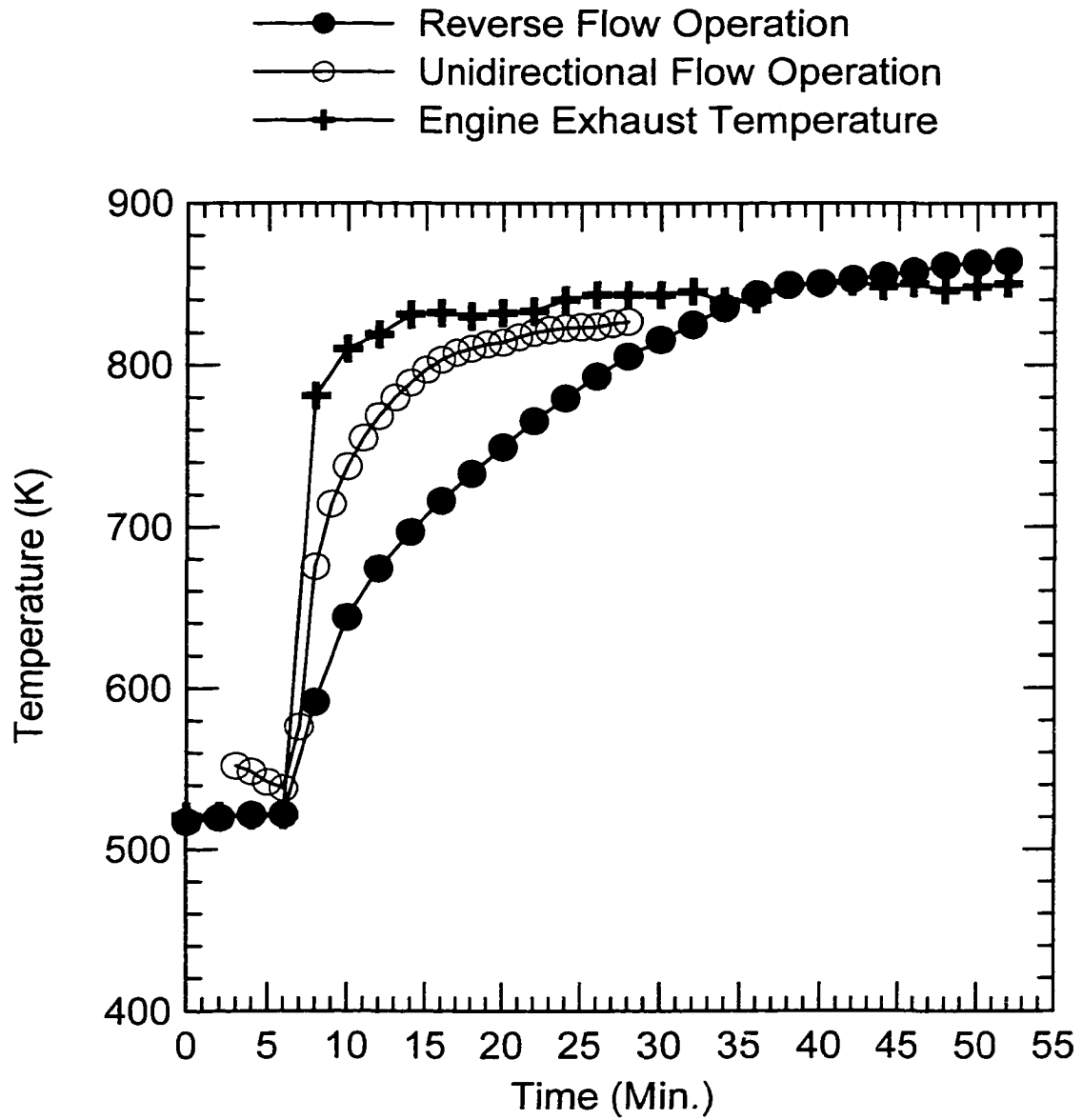


Figure 3-17 Comparison of Reactor Temperature Development with Engine Operation Transition from Light Load to Heavy Load

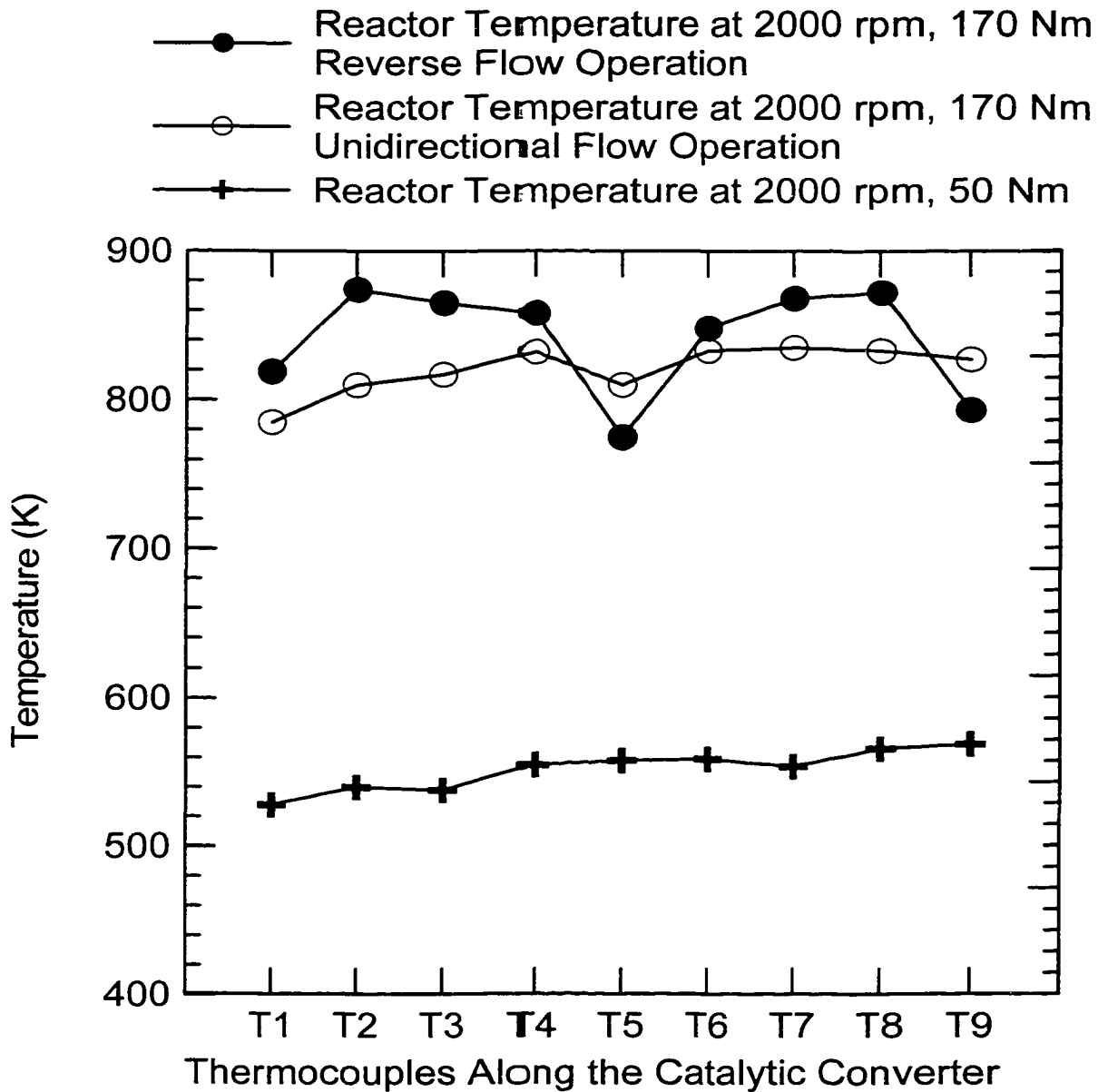


Figure 3-18 Comparison of Reactor Temperature Profiles (T1, T5 and T9 are gas-phase temperatures outside the substrate. T2, T3, T4, T6, T7, and T8 are solid phase temperatures, see Figure 2-4)

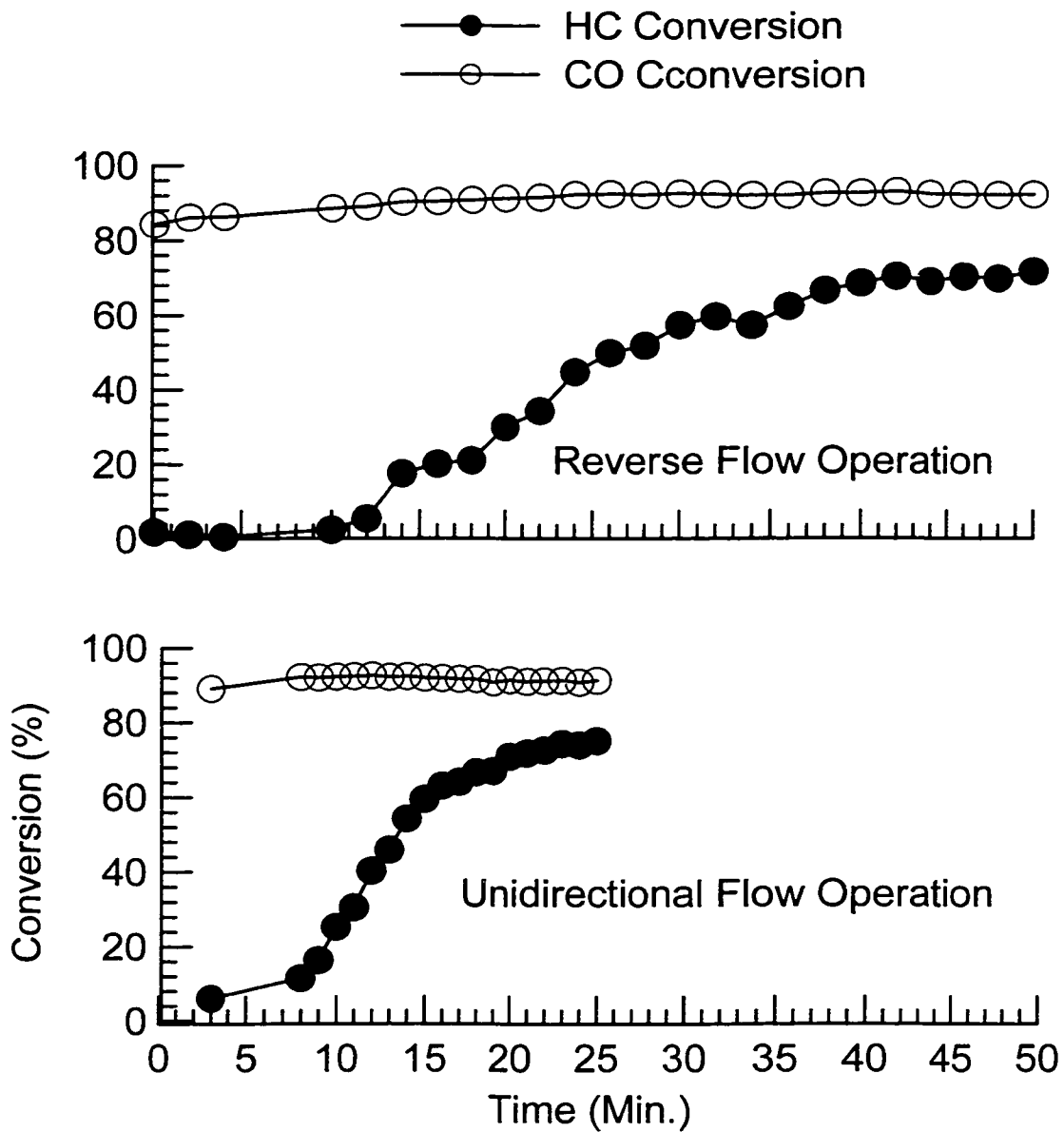


Figure 3-19 Comparison of HC and CO Conversion with Engine Operation  
Transition from Light Load to Heavy Load

### 3.3.5 Transition from Idle to Light Load

The fourth engine transition was from idle (Mode 3) to light load (Mode 2). Similarly to the transition described in Section 3.3.4, this transition results in a heating process which could be hindered by the “cold trap” effect observed in reverse flow. The initial reactor condition was obtained by operating the engine in Mode 3 (idle) with the converter operating with unidirectional flow. The engine mode was then changed from Mode 3 to Mode 2 and the converter operated in either symmetric reverse flow with a switch time of 15 seconds or with unidirectional flow.

The reactor temperature changed with time during this engine transition are shown in Figure 3-20. With reverse flow, the reactor temperature developed more slowly than with unidirectional flow at the early stage of engine mode transition, even though its initial reactor temperature was about 50 K higher than with unidirectional flow operation. In the later stage, reverse flow showed more advantage than unidirectional flow. Reverse flow trapped some energy from CO combustion, and the average reactor temperature was about 50 K higher than that from unidirectional flow. Figure 3-21 shows the reactor temperature profiles. The initial reactor temperature from engine idle was quite low with an increase from the reactor inlet to the outlet. After the engine was switched to light load, the reactor temperature profile from reverse flow operation was about 50 K above that from unidirectional flow. Figure 3-22 compares the HC and CO conversion for this engine transition. CO conversion increased with time in both cases. However, HC conversion was about zero even with reverse flow, because reactor temperature was too



low to ignite methane. Reverse flow could not accumulate sufficient energy from CO combustion to initiate methane combustion.

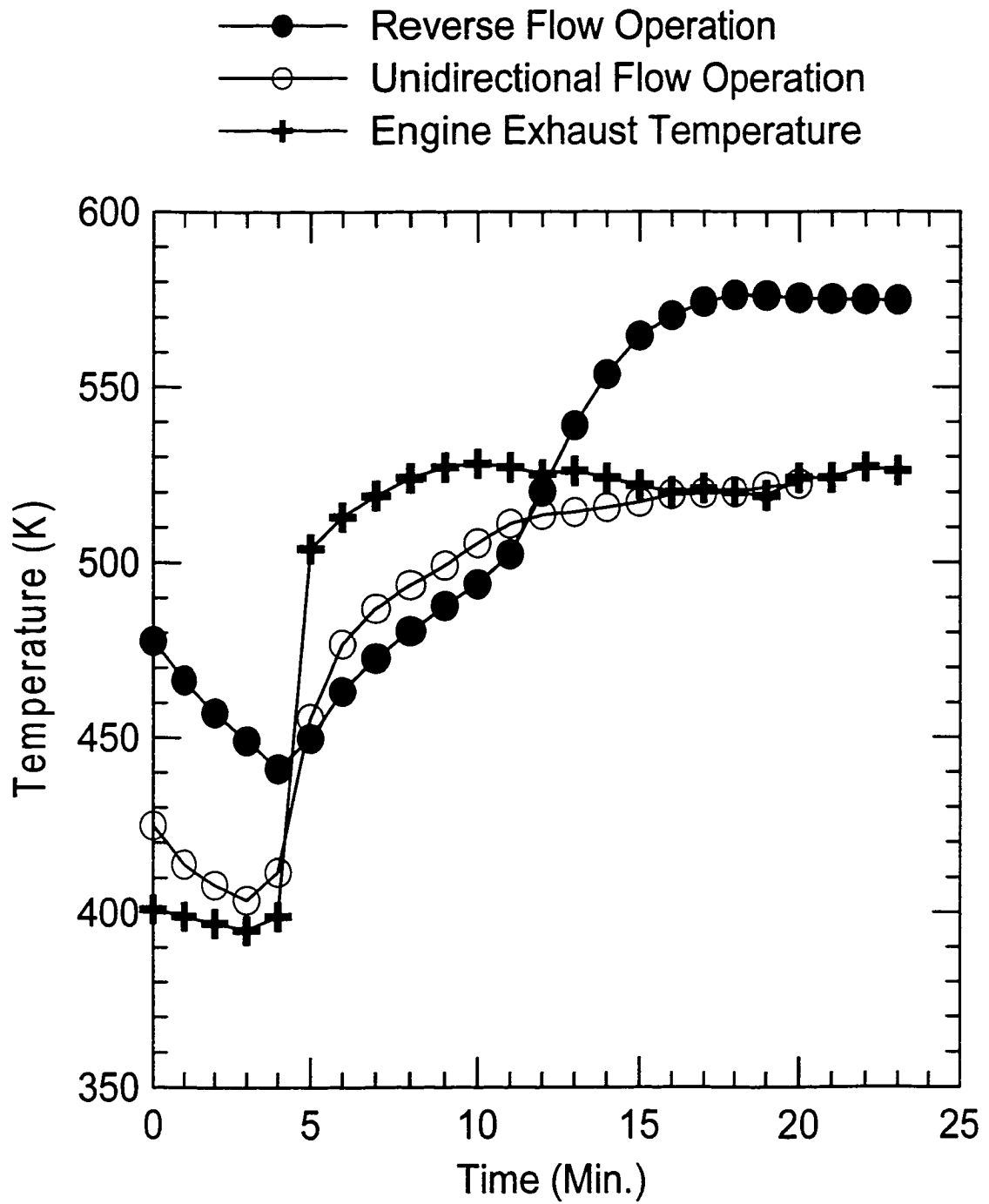


Figure 3-20 Comparison of Reactor Temperature Development with Engine Operation Transition from Idle to Light Load

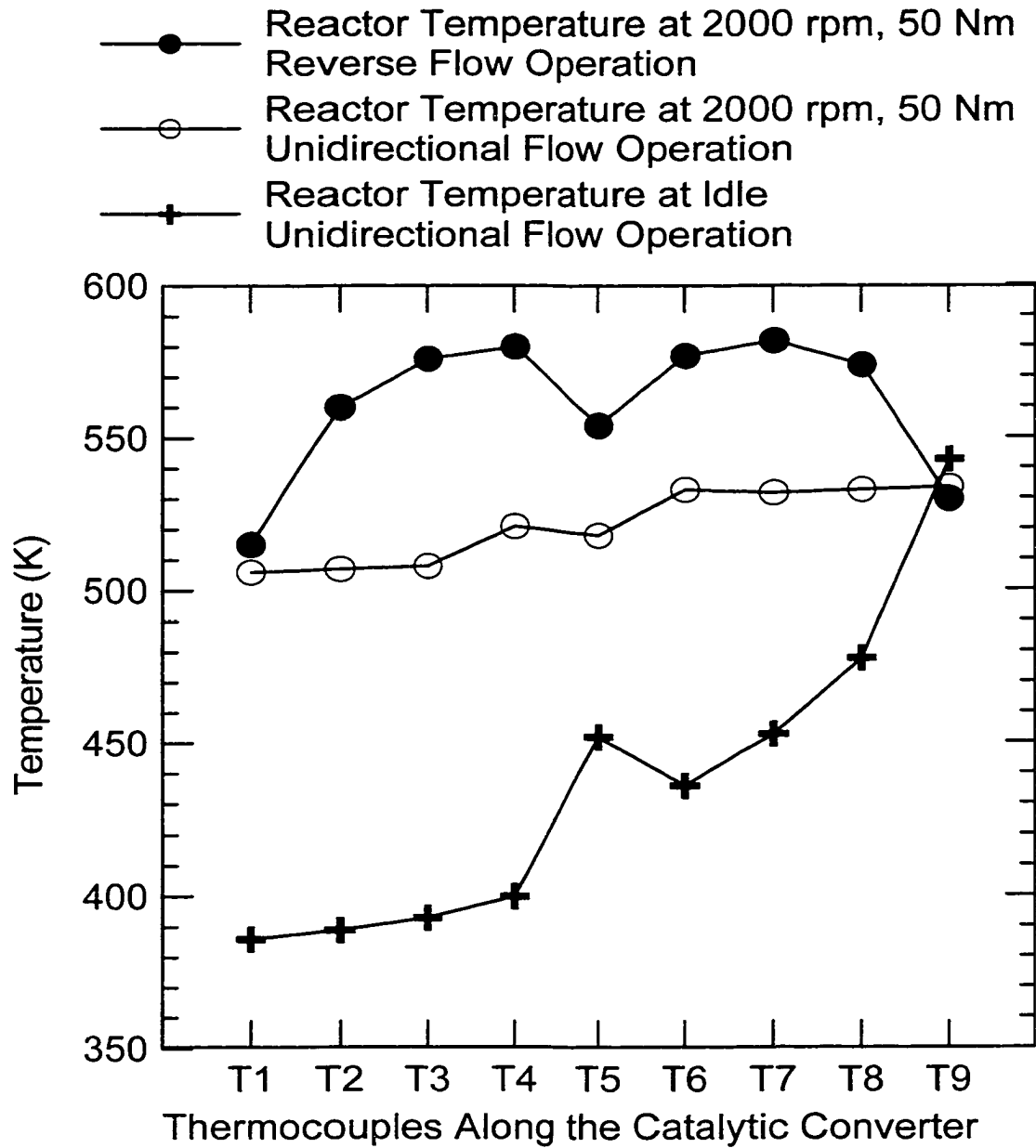


Figure 3-21 Comparison of Reactor Temperature Profiles (T1, T5 and T9 are gas-phase temperatures outside the substrate. T2, T3, T4, T6, T7, and T8 are solid phase temperatures, see Figure 2-4)

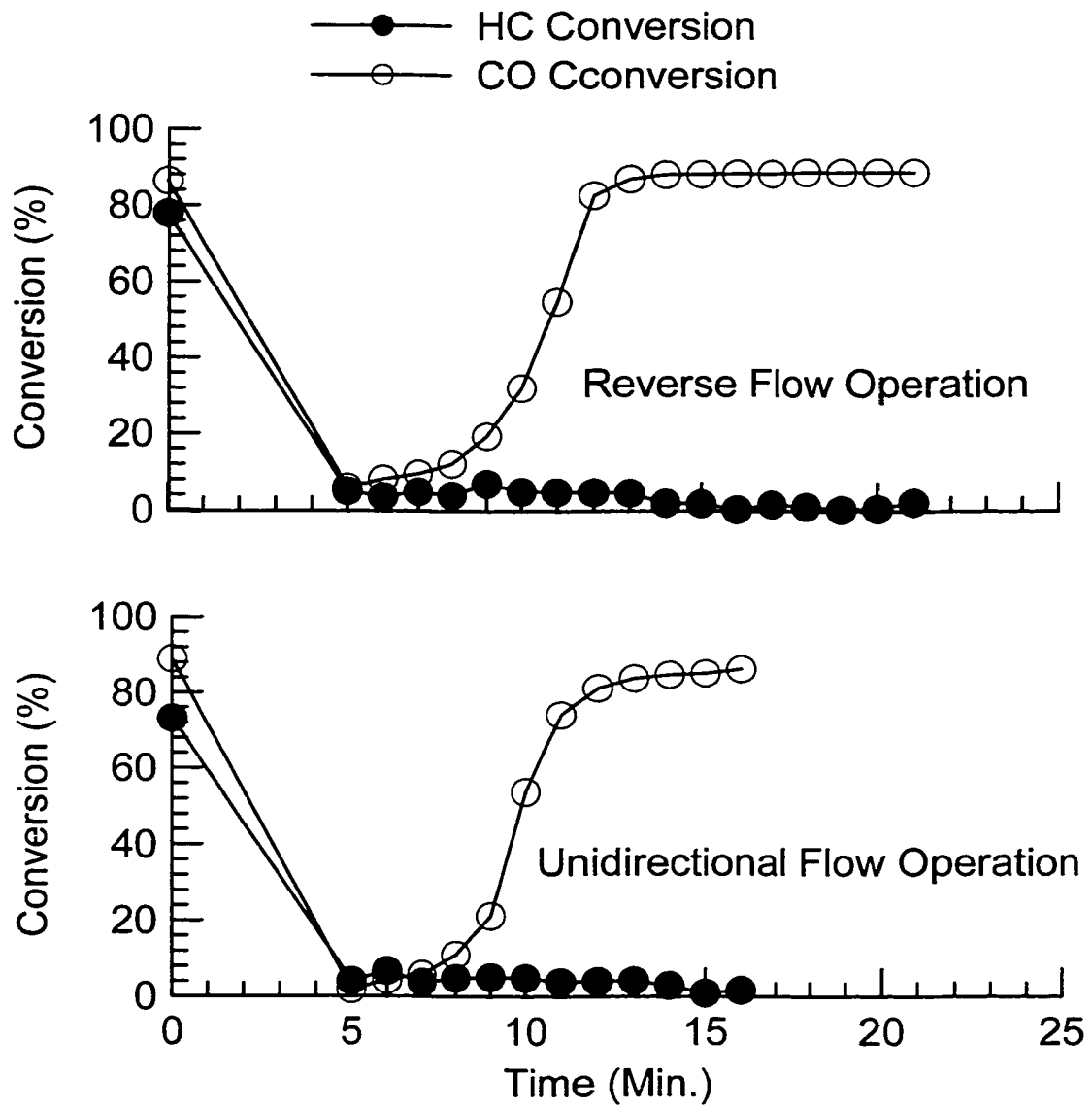


Figure 3-22 Comparison of HC and CO Conversion with Engine Operation Transition from Idle to Light Load

### **3.3.6 Summary of Transition Engine Results**

In conclusion, reverse flow either gave a “heat trap” or a “cold trap” effect during the engine mode transition. When initial reactor temperature was high and engine was switched to a mode with low exhaust temperature, reverse flow has a “heat trap” effect. Depending on the HC and CO concentration, reverse flow could develop reactor temperature, maintain reactor temperature, or slow down reactor temperature drop. When initial reactor temperature was low and engine was switched to engine mode with high exhaust temperature, reverse flow has a “cold trap” effect. It slows down reactor temperature development with engine exhaust temperature in the early stage of transition. However, in the later stage, reverse flow shows the advantage to develop reactor temperature. The control strategy of reverse flow operation is to use its “heat trap” effect and avoid its “cold trap” effect. When initial reactor temperature is high and engine is changed to engine mode with low exhaust temperature, reverse flow should start for developing reactor temperature, maintaining reactor temperature, or slowing down reactor temperature drop. When initial reactor temperature is low and engine was changed to engine mode with high exhaust temperature, reverse flow should be stopped to avoid slowing down reactor temperature development with engine exhaust temperature in the early stage of engine operation transition (about 10 minutes). However, in the later stage (after 10 minutes), reverse flow could start to develop reactor temperature further.

## **3.4 Reverse Flow Reactor Performance with Japanese 6-Mode Test**

### **3.4.1 Introduction of the 6-Mode Test**

The Japanese 6-Mode test is an official standard procedure for a diesel engine. The emission data from this test are intended to provide a standard evaluation over a typical range of operating conditions. The engine operation modes cover a wide engine variety of operations, such as engine idle, light and heavy load, as shown in Figure 3-23. The test consists of operating the engine sequentially in modes 1 through 6 with approximately 3 minutes of operation in each mode and a two minute transition period between modes. The weighting factors are used for calculating composite results from the individual modes and emphasize the operating conditions which are important in normal use. For this test, the engine was first warmed up at for least 20 minutes with Mode 5 before testing in Modes 1 through 6. The measured data were taken continuously including the transition periods. The results of each mode were multiplied by the appropriate weighting factor and summed to give the value from the 6-Mode test.

The engine exhaust properties for the 6 modes of operation are given in Table 3-10. HC concentration ranged from 201 to 5243 ppm and CO from 120 to 1974 ppm. The weighted HC value for these 6 modes was 2282 ppm and CO 956 ppm. Engine exhaust temperature varied from 418 to 873 K and the total mass flow rate from 22.72 to 70.66 g/s.

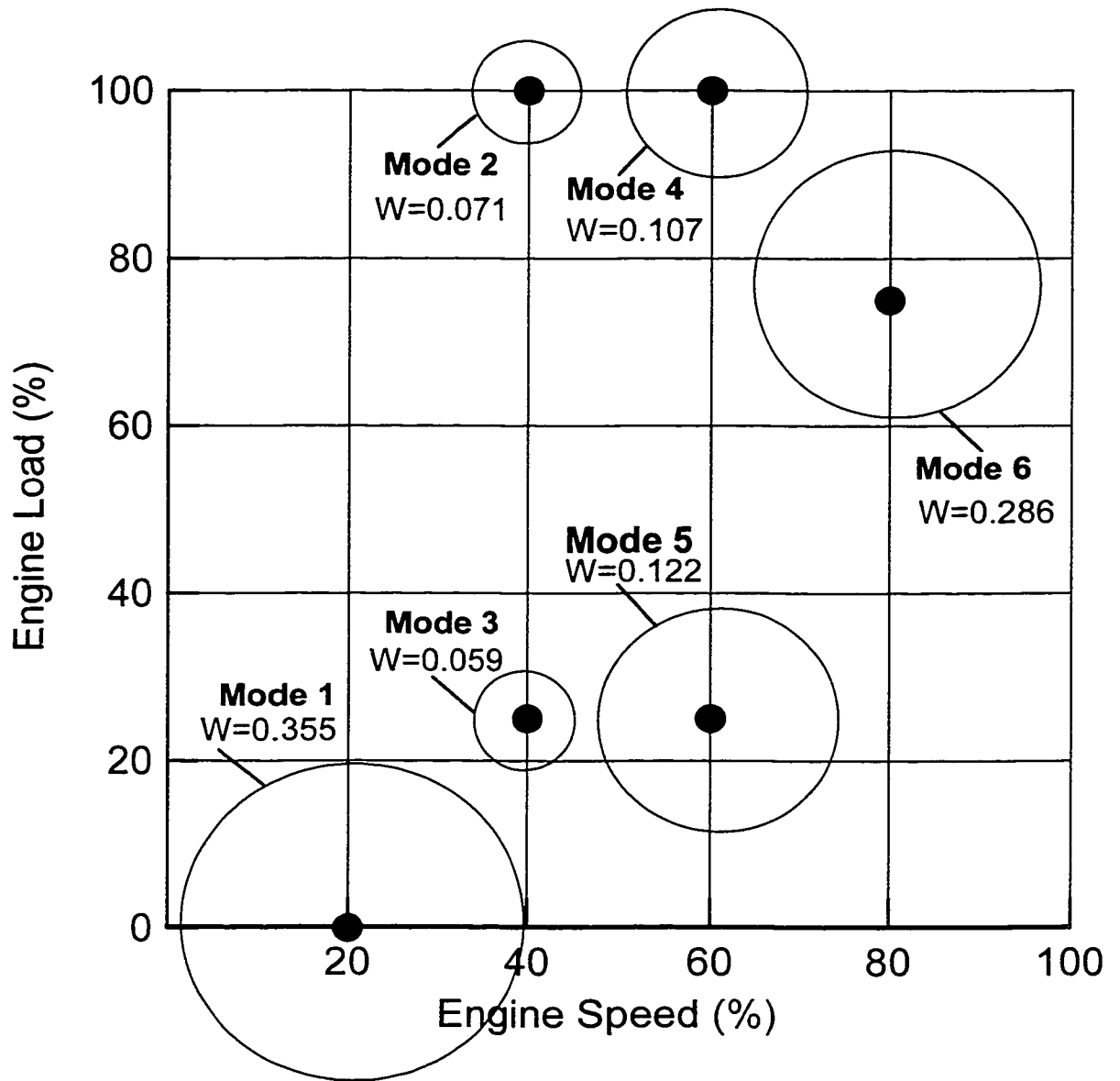


Figure 3-23 Japanese 6-Mode Test (The engine speeds and loads are non-dimensionalized as a fraction of rated torque and rated operating speeds)

Table 3-10 Engine Exhaust Parameters

Engine Mode	Speed (rpm)	Tor. (Nm)	Exhaust Composition						Texh. (K)	Mass Flow Rate (g/s)
			HC (ppm)	CO (ppm)	NO (ppm)	O <sub>2</sub> (%)	CO <sub>2</sub> (%)	H <sub>2</sub> O (%)		
1	Idle	Idle	201	120	183	17.73	1.79	3.41	418	22.72
2	1360	176	1523	726	1277	7.08	6.78	12.98	748	33.39
3	1360	52	5243	1676	169	15.25	2.88	5.69	499	36.43
4	2040	180	1251	699	1122	5.64	7.47	14.29	873	51.53
5	2040	49	4982	1732	112	14.80	3.17	6.25	538	54.73
6	2720	116	3677	1974	338	9.10	5.97	11.62	838	70.66

N<sub>2</sub>: Balance of Exhaust Gas Composition

Texh.: Engine Exhaust Temperature

Tor.: Engine Torque

### 3.4.2 Comparison between Unidirectional Flow and Reverse Flow

In this section, the difference in reactor performance between the reverse flow and unidirectional flow was evaluated with 6-Mode tests. For the first 6-Mode test, engine was warmed up in Mode 5 until the converter temperature approximately 500 K. and the catalytic converter was operated in the unidirectional flow manner. In the second 6-Mode test, the catalytic converter was operated with reverse flow using a switch time of 15 seconds and a total cycle time of 30 seconds. To establish a good reactor temperature before this 6-Mode test, the engine was first run in Mode 4 which produces exhaust temperature as high as 873 K. Then the engine was changed to Mode 5 and the catalytic



converter was operated in reverse flow manner which resulted in a stabilized converter temperature of approximate 960 K.

The reactor performance for these two 6-Mode tests is compared in Figure 3-24 and Figure 3-25. Figure 3-24 compares average reactor temperature and Figure 3-25 compares HC and CO conversion. For the reverse flow operation, reactor temperature was maintained over 800 K during the entire 6-Mode test. The HC conversion was around 80% and most of CO conversion was above 80%. The weighted HC exhaust was 329 ppm and CO 127 ppm.

For the unidirectional flow operation, reactor temperature varied with engine exhaust temperature during 6-Mode test and remained below 800 K. The highest HC conversion was only about 60%, but in some cases, HC conversion was near zero. CO conversion was over 80% most of the time. The weighted HC in the exhaust was 1560 ppm and CO 87 ppm. This test shows that using reverse flow operation is a good approach to maintain reactor temperature and activity for methane oxidation during 6-Mode tests. (Note that previous testing such as shown in Figure 3-11 indicates that even if the unidirectional flow catalyst could be preheated to 960 K, its temperature could have fallen to approximately exhaust temperature during the first idle period).

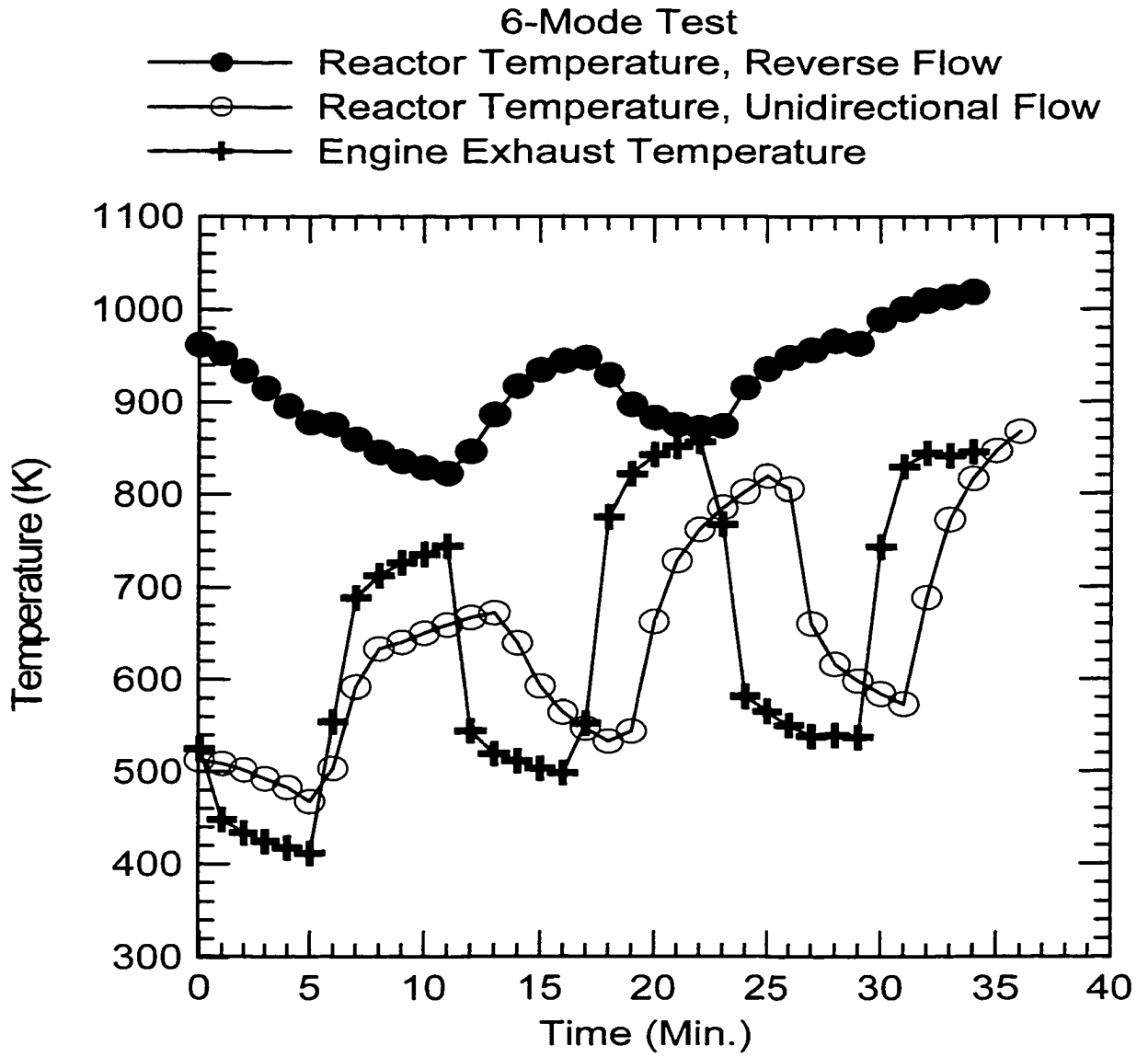


Figure 3-24 Comparison of Reactor Temperature Variation in 6-Mode Test

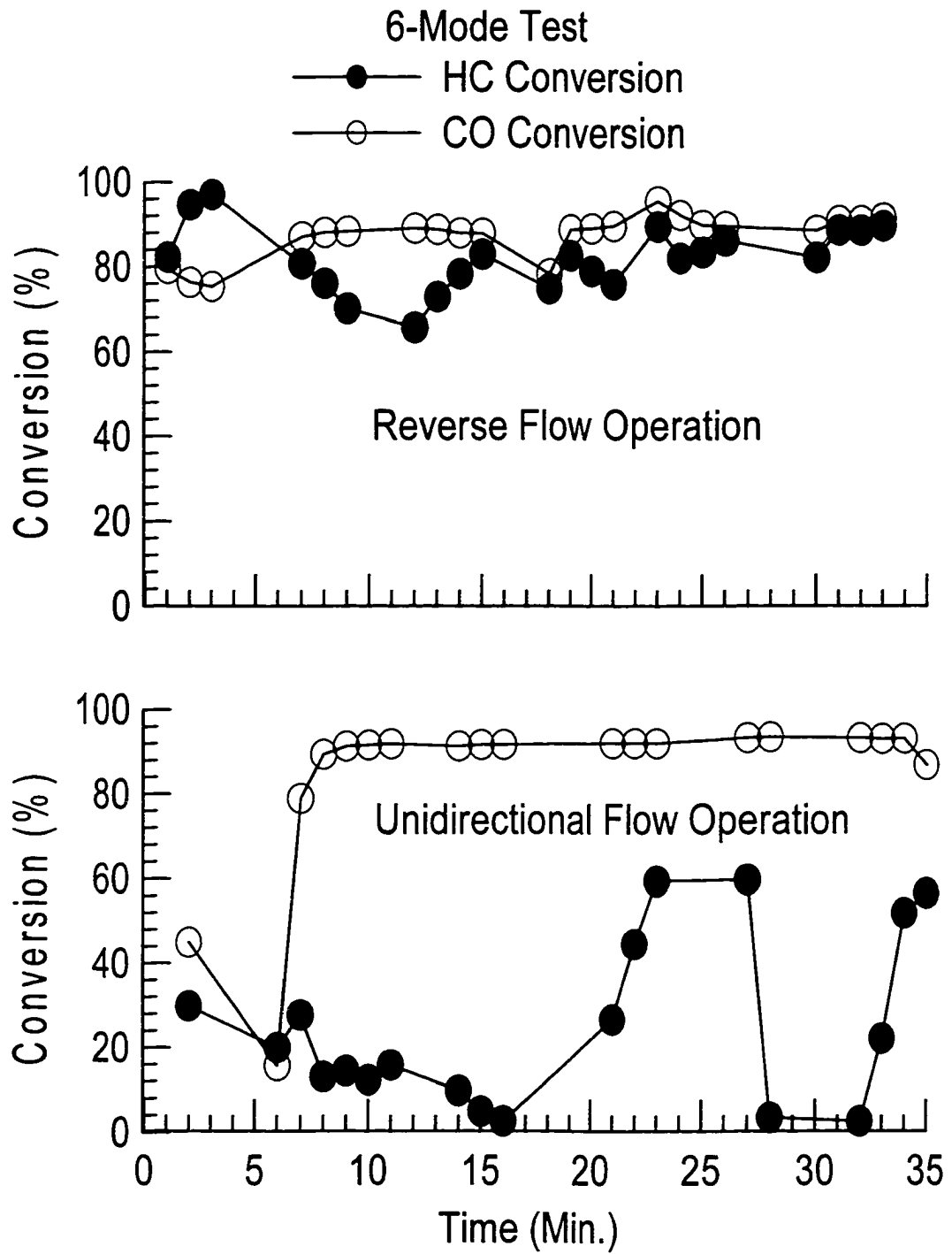


Figure 3-25 Comparison of HC and CO Conversion

### 3.4.3 6-Mode Tests with Variable Reverse Flow Switch Times

In this section, the reactor performance with three reverse flow switch times was evaluated with three 6-Mode tests. In each 6-Mode test, the flow switch time was kept the same. The switch times used were 5, 15 and 30 seconds. They were symmetric reverse flow operation and the corresponding cycle times were 10, 30 and 60 seconds. The engine reactor warm-up procedures in each case was the same as described in Section 3.4.2 for the reverse flow case. That is, the engine was run in Mode 4, followed by Mode 5, with reverse flow operation until pseudo steady state was obtained in the reactor.

The reactor performances for these three 6-Mode tests are compared in Figure 3-26 and Figure 3-27. Figure 3-26 compares average reactor temperature and Figure 3-27 compares HC and CO conversion. For these reverse flow operations, reactor temperature was maintained over 800 K during 6-Mode tests. They did not show too much difference for maintaining reactor temperature with switch times of 5, 15 and 30 seconds, as shown in Figure 3-26. Reactor temperature with a switch time of 15 seconds was very close to that with a 5 second switch time. For a switch time of 30 seconds, reactor temperature was about 40 K lower than those with a switch time of 5 and 15 seconds. CO conversion remained at about 90% for these three 6-Mode test. However, some difference for HC conversion was observed, as shown in Figure 3-27. For switch time 5 seconds, HC conversion was over 80% for most of engine modes. Only a few data points fell below 80% in Mode 2, but these points were still higher than 70%. For a switch time 15 seconds, HC conversion was around 80% during 6-Mode test. It was below 80% in some parts of Mode 2, Mode 3 and Mode 4, but most of the HC conversion was higher than

70%. For a switch time of 30 seconds, most of the HC conversion varied between 70% and 80%. It had a few data points fell between 60% and 70% in some parts of Mode 2 and Mode 3. Table 3-11 shows the weighted HC and CO concentration from 6-Mode tests. The weighted CO exhaust was about 120 ppm for these three 6-Mode tests. For the short switch time 5 seconds, the weighted HC exhaust was 274 ppm. It rose to 329 ppm for switch time 15 seconds. For the long switch time 30 seconds, it increased to 424 ppm. These results showed that HC conversion could be maintained a high value during 6-Mode test with the short switch time. Since the general reactor performance was close for switch time 5 seconds and 15 seconds, it was recommend 15 seconds should be used for 6-Mode test.

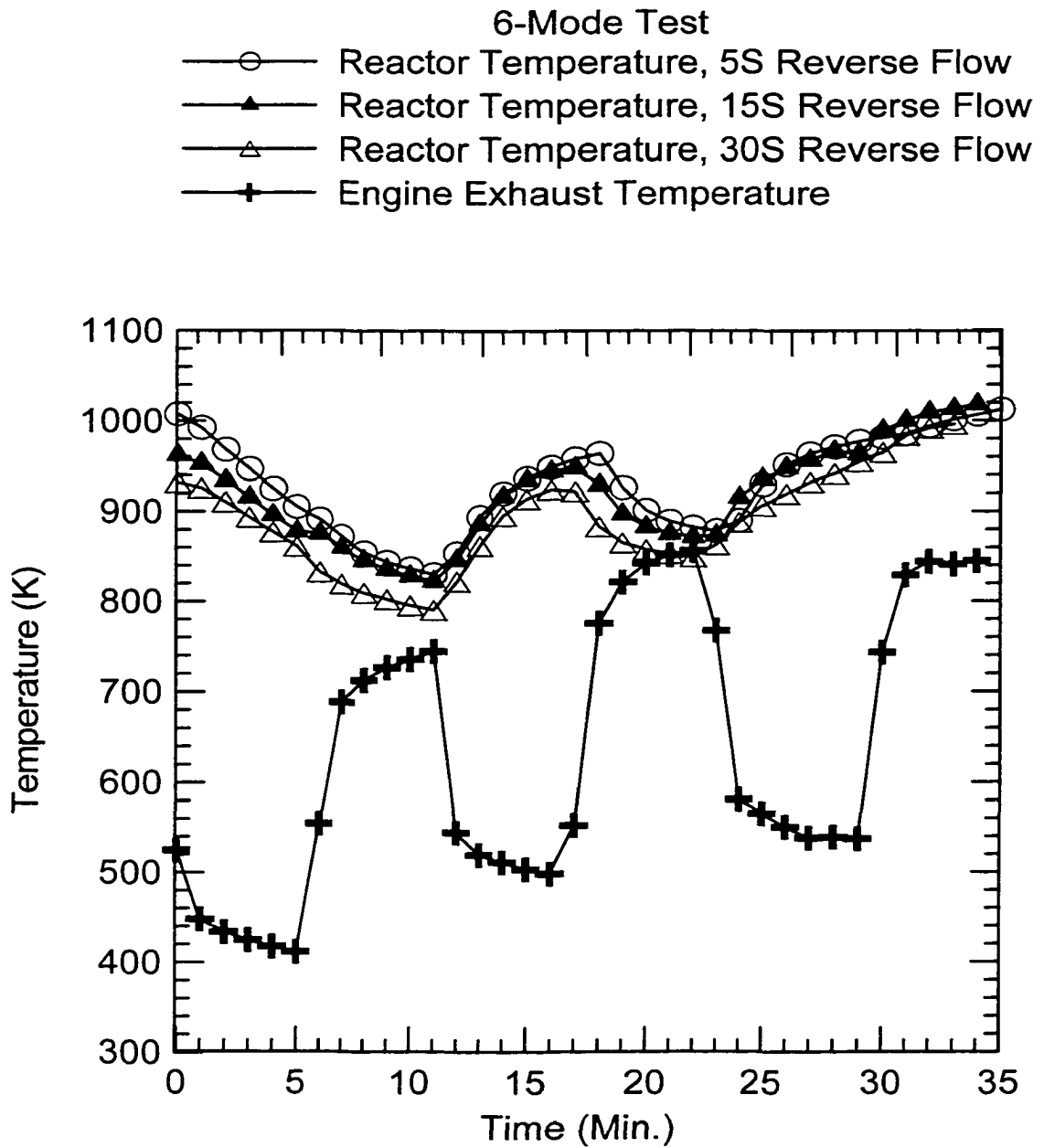


Figure 3-26 Comparison of Reactor Temperature

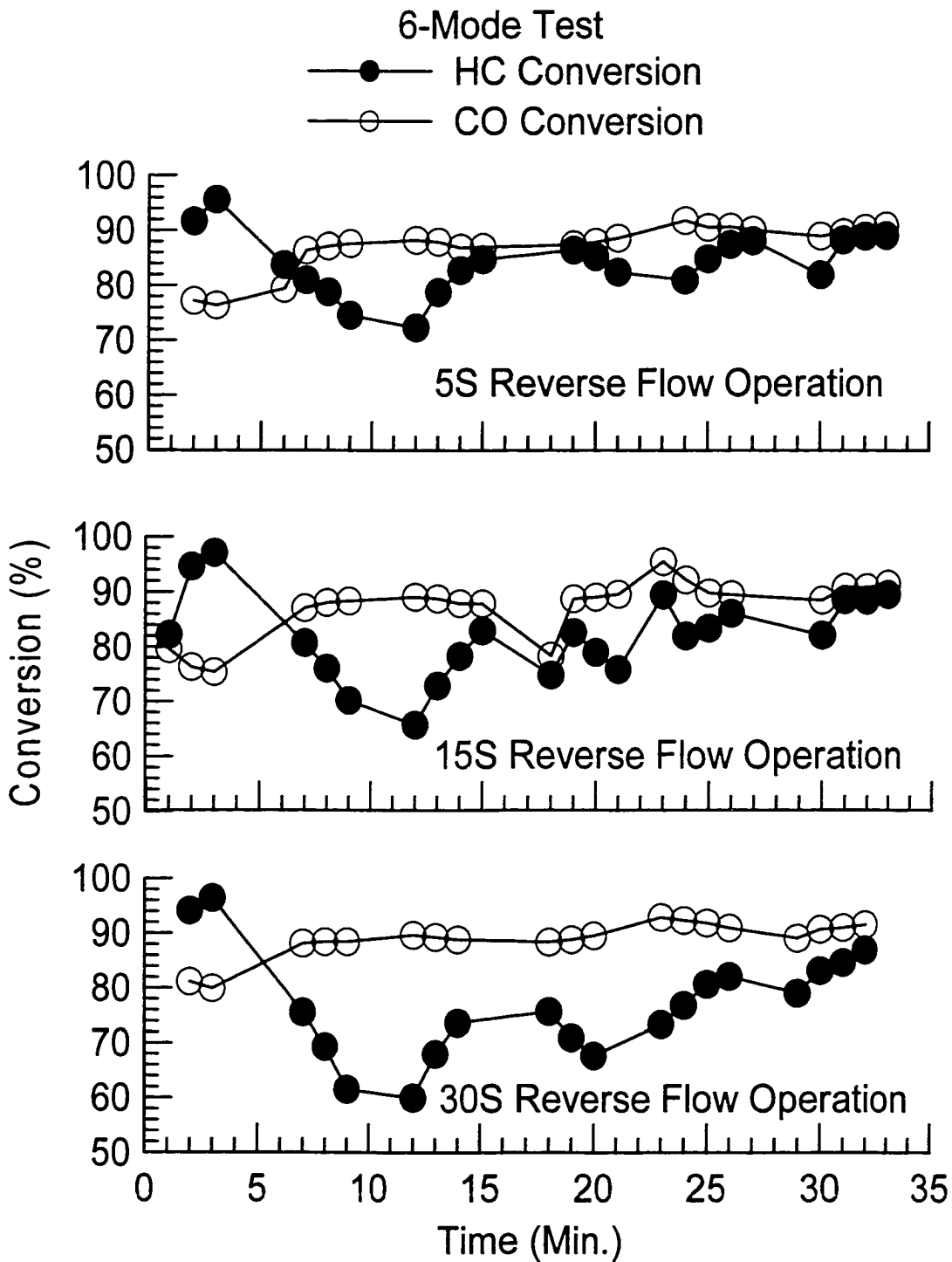


Figure 3-27 Comparison of HC and CO Conversion

Table 3-11 Engine Exhaust Compositions from 6-Mode Test

REACTOR OPERATION	EXHAUST COMPOSITION		
	HC (ppm)	CO (ppm)	NO (ppm)
Downstream, 5s Reverse Flow	274	126	381
Downstream, 15s Reverse Flow	329	127	390
Downstream, 30s Reverse Flow	424	115	376

### 3.4.4 Vary Reverse Flow Switch Time During 6-Mode Test

In this section, the reactor performance with varied reverse flow switch time during 6-Mode test was evaluated. The different switch times were used for each engine Mode, as shown in Table 3-12. In the first approach, the reverse flow switch times were 5, 15, 30, 5, 30, 15, corresponding to each engine mode. In the second approach, the reverse flow switch times used were 5, 5, 15, 5, 15, 15 corresponding to each engine mode. The engine was warmed up in the same way as for the 6-Mode tests with reverse flow described in the previous sections.



Table 3-12 Switch Time in 6-Mode Test

Engine Mode	Speed (rpm)	Torque (Nm)	Reverse Flow Switch Time	
			Approach 1	Approach 2
1	Idle	Idle	5	5
2	1360	176	15	5
3	1360	52	30	15
4	2040	180	5	5
5	2040	49	30	15
6	2720	116	15	15

The reactor performance for each of the two 6-Mode tests were compared with that from the 6-Mode test with constant switch time 15 seconds, as shown in Figure 3-28 and Figure 3-29. Figure 3-28 compares the average reactor temperature and Figure 3-29 compares HC and CO conversion. Compared with reverse flow with constant switch time, the reactor temperature did not show big difference for reverse flows with varied switch time during 6-Mode test. The two approaches with varied switch time even showed some disadvantage in Mode 5. For Approach 1, the HC conversion ranged between 60% and 90%, as shown in Figure 3-29. For Approach 2, most of the HC conversion ranged between 60% and 80%. However, neither approach showed a big advantage compared with constant switch time of 15 seconds. It had a HC conversion

around 80%. Table 3-13 shows the weighted HC and CO concentration from these 6-Mode tests. Their weighted CO exhaust was about 120 ppm. For the first approach, the weighted HC exhaust was 460 ppm. The second approach had a value 383 ppm. They were higher than that using constant switch time 15 seconds, which had a value of 329 ppm. These results showed that two approaches varying reverse flow switch time during 6-Mode test did not have a big advantage for maintaining reactor temperature and HC conversion. They increased the complexity of reverse flow operation and this was not recommended.

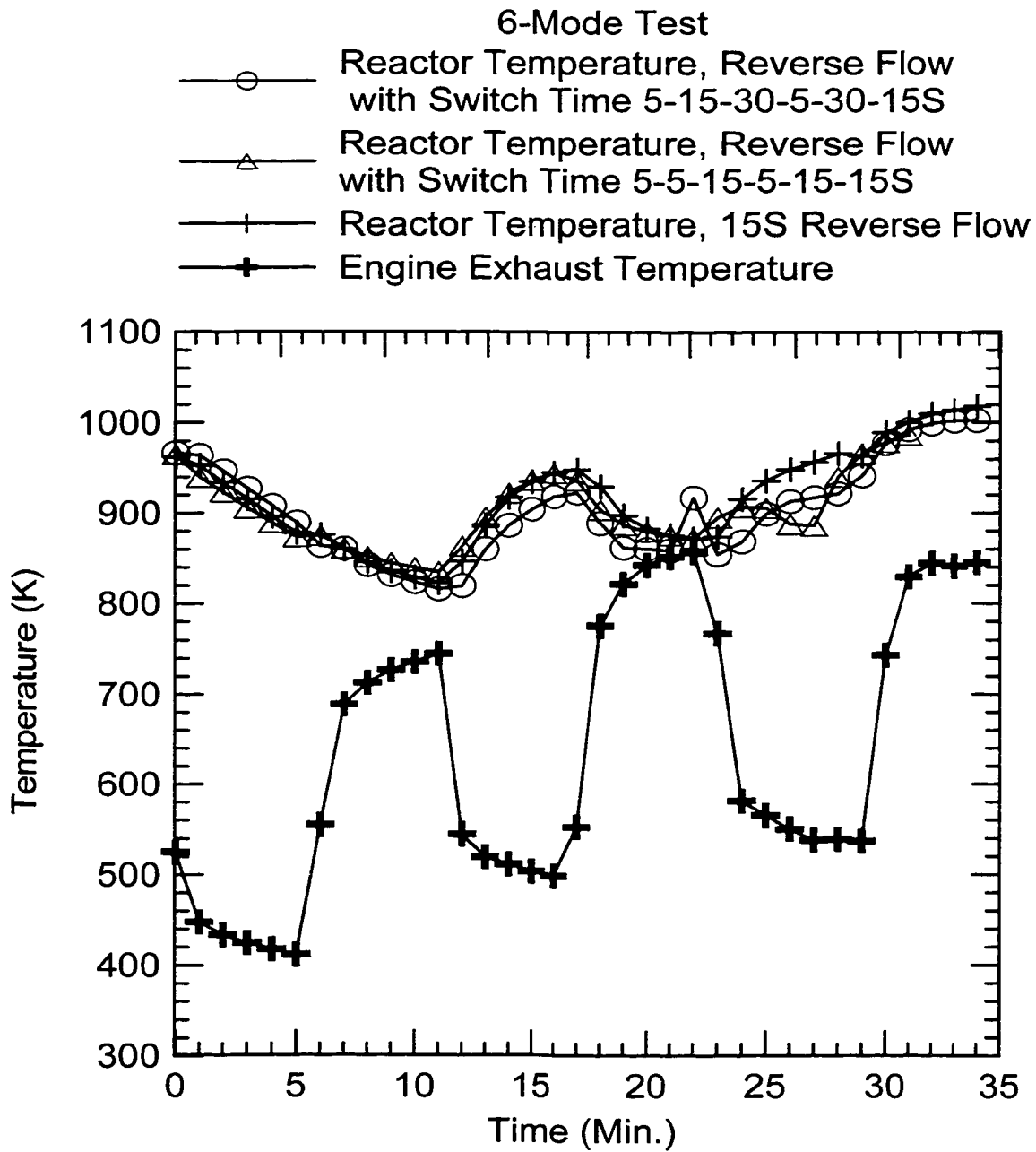


Figure 3-28 Comparison of Reactor Temperature

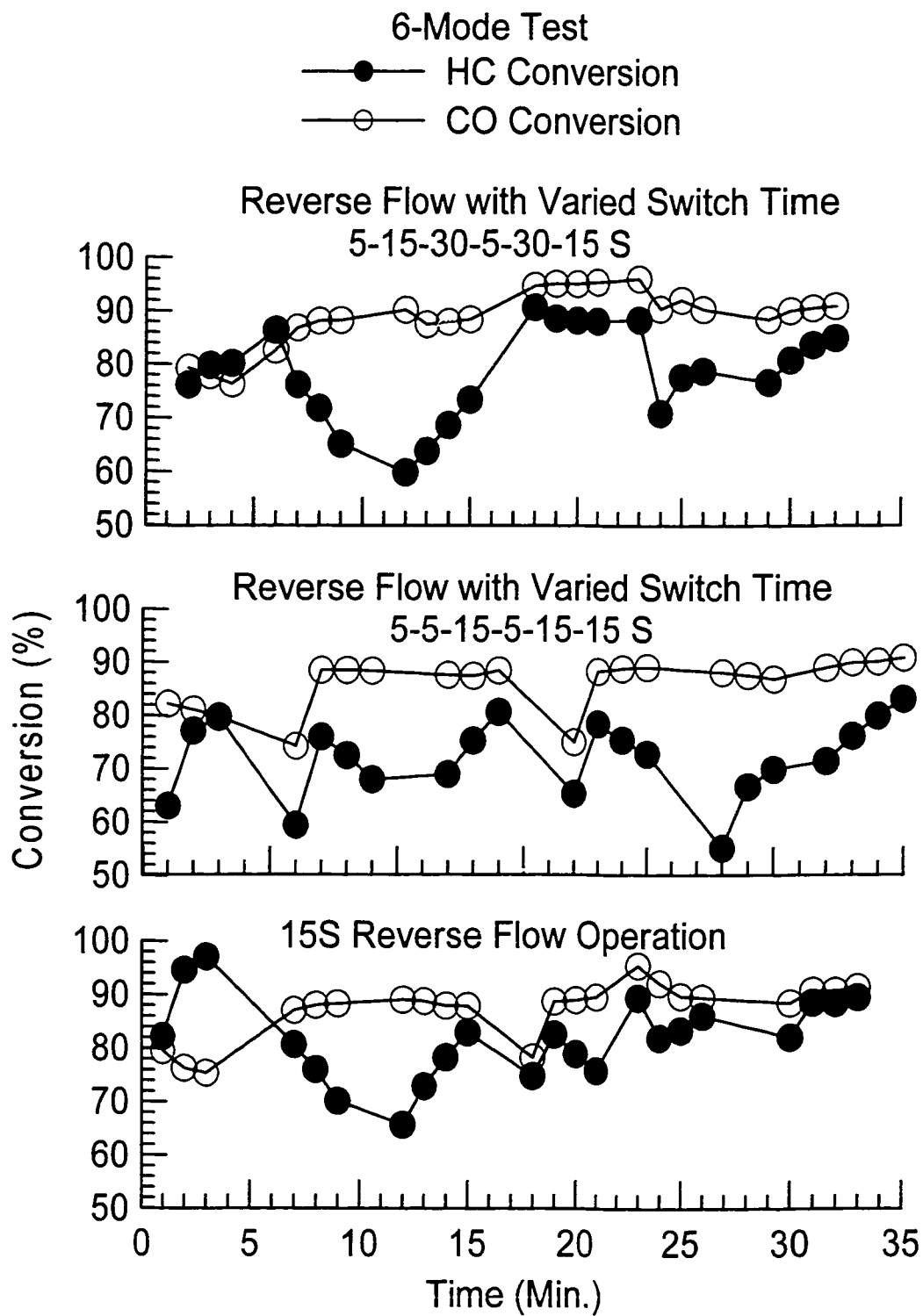


Figure 3-29 Comparison of HC and CO Conversion

Table 3-13 Engine Exhaust Compositions of 6-Mode Tests

REACTOR OPERATION	EXHAUST COMPOSITION		
	HC (ppm)	CO (ppm)	NO (ppm)
Downstream, 15S Reverse Flow	329	127	390
Downstream, 5-15-30-5-30-15S Reverse Flow	460	131	383
Downstream, 5-5-15-5-15-15S Reverse Flow	383	114	398

In conclusion, reverse flow was a good strategy for 6-Mode test, showing some advantage over unidirectional flow. Reverse flow could maintain reactor temperature over 800 K and HC conversion around 80%. For switch time 5, 15 and 30 seconds, the reactor performance was close and it was recommended to use 15 seconds. The two approaches with varied switch time did not show an advantage compared to constant switch time of 15 seconds. To make a simple but effective reverse flow control, it was not recommended to vary switch time during 6-Mode test.

### 3.5 Conclusions

Based on these studies, the following conclusions were drawn:

1. Reverse flow could develop reactor temperature and increase HC and CO conversion greatly under some engine light load operations. The reactor temperature rise by reverse flow could be about two times higher than the adiabatic temperature rise. However, this depends on the proper engine exhaust and reactor temperature status. In some engine light loads, reverse flow fails to develop reactor temperature and increase HC and CO conversion. This failure occurs because either reactor temperature is too low or HC and CO concentrations in engine exhaust too low.
2. Reverse flow switch time was evaluated from 5 to 240 seconds. It was shown that short switch time was better than long switch time. To reduce reverse flow operations and the thermal stress resulted from reverse flow switch for the similar reactor performance, switch times of the order of 15 and 30 seconds was recommended.
3. During the engine mode transition, reverse flow performed either a “heat trap” or a “cold trap” effect. When initial reactor temperature was high and the engine was switched to an engine mode with low exhaust temperature, reverse flow has a “heat trap” effect. Depending on the HC and CO concentration, reverse flow could develop reactor temperature, maintain reactor temperature, or slow down reactor temperature drop. When initial reactor temperature was low and engine was switched to engine mode with high exhaust temperature, reverse flow has a “cold trap” effect. It slows down reactor temperature development with engine exhaust temperature in the early

stage of transition. However, in the later stage, reverse flow shows the advantage to develop reactor temperature. The control strategy of reverse flow operation is to use its “heat trap” effect and avoid its “cold trap” effect. When initial reactor temperature was high and engine was changed to engine mode with low exhaust temperature, reverse flow should start for developing reactor temperature, maintaining reactor temperature, or slowing down reactor temperature drop. When initial reactor temperature was low and engine was changed to engine mode with high exhaust temperature, reverse flow should be stopped to avoid slowing down reactor temperature development with engine exhaust temperature in the early stage of engine operation transition (about 10 minutes). However, in the later stage (after 10 minutes), reverse flow could start to develop reactor temperature further.

4. Reverse flow was good strategy for Japanese 6-Mode test. It showed a bigger advantage than unidirectional flow. Reverse flow could maintain reactor temperature over 800 K and HC conversion about 80% during 6-Mode test. The switch time 15 seconds was recommended for reverse flow switch during 6-Mode test.

### 3.6 Nomenclature

$$\chi_{HC} : \text{HC conversion over the catalytic converter: } \chi_{HC} = \frac{[HC]_{in} - [HC]_{out}}{[HC]_{in}} \times 100\%$$

$$\chi_{CO} : \text{CO conversion over the catalytic converter: } \chi_{CO} = \frac{[CO]_{in} - [CO]_{out}}{[CO]_{in}} \times 100\%$$

$[HC]_{in}$  : Reactor inlet HC concentration, ppm

$[HC]_{out}$  : Reactor outlet HC concentration, ppm

$[CO]_{in}$  : Reactor inlet CO concentration, ppm

$[CO]_{out}$  : Reactor outlet CO concentration, ppm

### 3.7 References

Beld L. van de, R. A. Borman, O. R. Derkx, B. A. A. van Woezik, and K. R. Westerterp, Ind. Eng. Chem. Res., 33, 2946, 1994

Beld L. van den and K. R. Westerterp, "Purification of waster air in a reverse flow reactor", in Preprint Volume of First Topical Conference on Industrial Chemical Engineering Technology, (J. B. Cropley, Coord.), St. Louis Annual Meeting of AIChE, 1993

Blanks R. F., T. S. Wittrig and D. A. Petterson, Chem. Eng. Sci., 45, 2407, 1990

Bobrova, E. M. Slavinskaya, A. S. Noskov and Yu. Sh. Matros, React. Kinet. Catal. Lett., 37, 267, 1988

Boreskov G. K., G. A. Bunimovich, Y. S. Matros and A. A. Ivanov, Kinet. Catal., 23, 402, 1982

Boreskov G. K. and Y. S. Matros, "Fixed catalyst bed reactors operated in steady and



- unsteady-state conditions”, in *Recent Advances in the Engineering of Chemically Reacting Systems* (Edited by L. K. Doraiswamy), pp. 142-155. Wiley, New Delhi, India, 1984
- Bunivovich G. A., V. O. Strots and O. V. Goldman, “Theory and industrial application of SO<sub>2</sub> oxidation reverse-process for sulfur acid production”, in *Unsteady State Processes in Catalysis* (Yu. Sh. Matros, ed.), VPS BV, Utrecht, 1990
- Checkel M. D., B. Liu, M. Zheng, E. Mirosh, “A Special Catalytic Converter for Dual Fuel Engine Light Load Emissions”, 1998 Spring Technical Meeting, Combustion Institute, Canadian Section, 25-27 May, Toronto, Canada.
- Eigenberger G. and U. Nieken, *Chem. Eng. Sci.*, 43, 2109, 1988
- Eigenberger G. and U. Nieken, *Int. Chem. Eng.*, 34, 4, 1994
- Chaouki J., G. Gui, C. Sapundzhiev, D. Kusohorsky and D. Klvana, *Ind. Eng. Chem. Res.*, 33, 2957, 1994
- Guit Ir. R. P. M., “The selective catalytic reduction of NO<sub>x</sub> in a reverse flow reactor: a quick design procedure”, *Precision Process Technology*, 453-461, 1993
- Hanamura K., R. Echigo and S. A. Zhdanok, " Superadiabatic combustion in a porous medium", *Ind. J. Heat Mass Transfer*, 36, 1993
- Isozaki C., T. Katagiri, Y. Nakamura, S. Hirabayashi, S. Yabe and T. Yamaki, “Demonstration of DC/DA sulphur acid plant based on unsteady-state process”, in *Unsteady State Processes in Catalysis* (Yu. Sh. Matros, ed.), VPS BV, Utrecht, 1990
- Levina L. M., V. O. Strots, S. A. Popov and Yu. Sh. Matros, *React. Kinet. Catal. Lett.*, 42, 73, 1990
- Matros Yu. Sh. and G. A. Bunimovich, " Reverse-flow operation in fixed bed catalytic reactors", *Catal. Rev.-Sci. Eng.*, 38(1), 1-68, 1996
- Matros Yu. Sh., A. S. Noskov and V. A. Chumachenko, *Chem. Eng. Processing*, 32, 89, 1993
- Matros Yu. Sh., “Catalytic processes under unsteady state conditions”, Elsevier, Amsterdam, 1989
- Matros Yu. Sh., A. G. Ivanov and L. L. Gogin, *Teoreticheskie Osnovy Khimicheskoi Tekhnologii* [Theoretical Fundamentals Chemical Engineering], 22, 481, 1988
- Neophytides and G. F. Froment, *Ind. Eng. Chem. Res.*, 31, 1583, 1992

- Nieken U., G. Kolios and G. Eigenberger, *Catal. Today*, 20, 335, 1994
- Noskov A. S., L. M. Bobrova and Yu. Sh. Matros, *Catal. Today*, 17, 293, 1993
- Purwano S., H. Budman, R. R. Silveston and Yu. Sh. Matros, *Chem. Eng. Sci.*, 49, 5437, 1994
- Sapundzhiev Ch., G. A. Bunimovich, V. I. Drobishevich, G. Grozev, L. V. Yausheva, Yu. Sh. Matros and D. Elenkov, *Teoreticheskie Osnovy Khimicheskoi Tekhnologii [Theoretical Fundamentals Chemical Engineering]*, 22(3), 349-355, 1988
- Sapundzhiev Ch., G. A. Bunimovich, V. I. Drobishevich, G. Grozev, L. V. Yausheva, Yu. Sh. Matros and D. Elenkov, "Teoreticheskie osnovy khimicheskoi tekhnologii [Theoretical fundamentals chemical engineering]", 22(3), 349-355, 1988
- Strots V. O., G. A. Bunimovich, Yu. Sh. Matros, M. Zheng and E. A. Mirosh, "Novel catalytic converter for natural gas powered diesel engines", SAE 980194, 1998.
- Wallace K. and H. J. Viljoen, "Modelling of a monolithic catalyst with reciprocating flow", *AICHE Journal*, Vol. 41, No. 5, 1229-1234, 1995
- Zheng M., E. A. Mirosh, Yu. Sh. Matros, G. A. Bunimovich, V. O. Strots, N. Sallamie, M. D. Checkel and H. Windawi, "Novel catalytic converter for natural gas powered diesel engines to meet stringent exhaust emission regulations", *International Conference and Exhibition for Natural Gas Vehicles, NGV-98: Becoming a Global Reality*, Cologne, Germany, May 26-28, 1998

## Chapter 4

# Modelling Study of Unidirectional Flow Catalytic Converter

*Chapter 4 is an experimental and modelling study based on the prototype reverse flow design shown in Figure 2-3 b). It establishes a numerical simulation model for the catalytic converter which is operated in the conventional unidirectional flow manner. The model is one dimensional single channel model, which uses locally correct values for the heat and mass transfer coefficients and incorporates washcoat diffusion. The catalytic kinetic approach used is the modified Voltz kinetics. It includes the NO<sub>x</sub> inhibition effect. The activation energy found for methane and CO catalytic reaction is 132.1 and 55 kJ/mol respectively. This model is able to predict the transient operation of the converter to a level sufficient to identify the important trends of reactor response, including the reactor thermal response, as well as HC and CO conversion. It provides an acceptable model for the engine operated in the low temperature region. This is a basic modelling exercise. The developed model is used to simulate the reverse flow catalytic converter in Chapters 5 and 6.*

---

Note: This chapter has been accepted for publication by “The Canadian Journal of Chemical Engineering”. It will appear in the issue of June 2000. Co-authors: M. David Checkel, Robert E. Hayes, Ming Zheng and Edward Mirosh.

## 4.1 Introduction

As a result of concern over exhaust gas emission from mobile sources much research is currently being directed towards alternative fuel systems for use in road vehicles. One such alternative is the natural gas/diesel dual fuel engine, which offers an alternative to the standard diesel fuel compression ignition engine. In the dual fuel configuration, the primary fuel is natural gas, replacing as much as 90% of the diesel fuel, with a small amount of diesel fuel required to ensure effective ignition. The main constituent of natural gas is methane, which has a high combustion efficiency. Compared to a conventional diesel engine, dual fuel engines offer the promise of lower  $\text{NO}_x$  emissions and fewer particulates. At moderate engine loads, however, a lower fuel combustion efficiency has been observed, which results in significant amounts of hydrocarbon (HC) and carbon monoxide (CO) being present in the exhaust gas (Karim, 1991; Checkel et al., 1998). It is therefore necessary to use a catalytic converter in the exhaust system to reduce these emissions to an acceptable level.

Catalytic converters have been widely used on gasoline engines since 1976, with the most commonly used catalyst at present being the three way catalyst (TWC), which oxidizes CO and HC, and reduces  $\text{NO}_x$ . Many experimental and modelling studies have been reported for automotive catalytic converters, some of which are summarized in Table 4-1. The performance and operating conditions of a catalytic converter for the natural gas/diesel system have not been widely studied. Compared with a gasoline engine running at conditions close to stoichiometric, dual fuel engines provide higher exhaust gas oxygen levels and lower exhaust gas temperatures. The high oxygen concentrations, in excess of 4% and up to 10% or more, are a consequence of lean combustion and the

high compression ratios used in the engine. This chapter reports on the development and implementation of a numerical model for a dual fuel engine catalytic converter. The model is validated against experimental results for both transient and steady state operation.

Table 4-1 Some References to Monolith Modelling and Experimental Investigations.

---

**Lumped, 1-D, 2-D and 3-D Model:**

Siemund et al. (1996); Kuo et al. (1971); Heck et al. (1976); Young et al. (1976 a, b); Oh et al. (1982, 1983, 1985 Part 1, 2, 3); Pattas et al. (1994); Chen et al. (1988, 1989); Zygourakis (1989); Hayes et al. (1992); Psyllos et al. (1992); Bennett et al. (1992); Barresi et al. (1993)

---

**Kinetic Parameter Evaluation:**

Voltz et al. (1973); Montreuil et al. (1992); Subramanian and Varma (1992)

---

**Modelling of Heat and Mass Transfer:**

Heck et al. (1974); Votruba et al. (1975); Bennett et al. (1991, 1992); Ullah et al. (1992); Hawthorn (1974); Heck et al. (1976); Ryan et al. (1991); Hayes and Kolaczkowski (1994); Young and Finlayson (1976 a, b); Lee and Aris (1977); Ryan et al. (1991); Mondt (1987)

---

**Modelling of Internal Diffusion:**

Zygourakis and Aris (1983); Leclerc and Schweich (1993); Leung et al. (1996)

---

**Various Experimental Evaluations:**

Morgan et al. (1973); Howitt and Sekella (1974); Wendland et al. (1986); Germidis et al. (1993); Leclerc et al. (1994); Hertz (1987); Lee and Aris (1977)

---

## 4.2 Experimental Apparatus

Experimental engine emissions were obtained using a naturally aspirated four cylinder ISUZU 4BE1 engine of  $3.6 \times 10^{-3} \text{ m}^3$  (3.6 litres) displacement, modified to operate with a dual fuel system. The engine was installed in a test bed equipped with a catalytic converter. Engine speed and torque were controlled using a digital dynamometer controller and a digital throttle controller. The digital dynamometer controller was set in the RPM (engine speed) mode and the digital throttle controller was set in the position mode. For a desired engine operating condition, the engine was first set to the desired engine speed using the dynamometer controller, and then adjusted to give the desired engine torque using the throttle controller.

The catalytic converter used a ceramic (cordierite) monolith honeycomb support with square channels. The converter contained five square segments of monolith honeycomb measuring 0.1524 m on each side, each separated by a gap of 2 mm. The central segment was inactive, that is, it did not contain a catalyst washcoat. The catalytically active segments were 0.0508 m in length whilst the inactive segment was 0.106 m in length. The segmented design was used to give multiple entry regions in the converter, where the heat and mass transfer coefficients are larger than in the fully developed region. The physical properties of the monolith segments are given in Table 4-2. The washcoated monolith segments were supplied by Johnson-Matthey. The exhaust system containing the converter is illustrated in Figure 4-1, which also shows the analytic instrumentation.

Table 4-2 The Main Physical Parameters of the Converter

Wall Density $\rho_w$	2300 kg/m <sup>3</sup>
Wall Thermal Conductivity $k_w$	2 W/(m.K)
Wall Heat Capacity $C_{pw}$	1005 J/(kg.K)
Effective Wall Thickness	0.25 mm
Average Thickness of Washcoat Layer	0.05 mm
Porosity of Washcoat	0.41
Channel Hydraulic Diameter, $D_H$	1.4 mm
Open Frontal Area	1.96 mm <sup>2</sup>
Porosity of Monolith	72%
Size of Each Brick (Width × Height × Length)	152.4mm × 152.4mm × 50.8 mm

Table 4-3 Analytic Equipment for Measurement of Engine Exhaust Composition.

Component	Instrument	Range	Resolution
O <sub>2</sub>	Taylor Servomex OA.137	0-25%	~0.1%
CO <sub>2</sub>	Beckman 864 NDIR	0-20%	~0.05%
CO	Beckman 864 NDIR	0-1%	~0.01%
Total HC	Beckman GC 72.5 FID	0-1.2%	5 ppm
NO <sub>x</sub>	Beckman 955 Chemiluminescent	0-0.2%	1 ppm

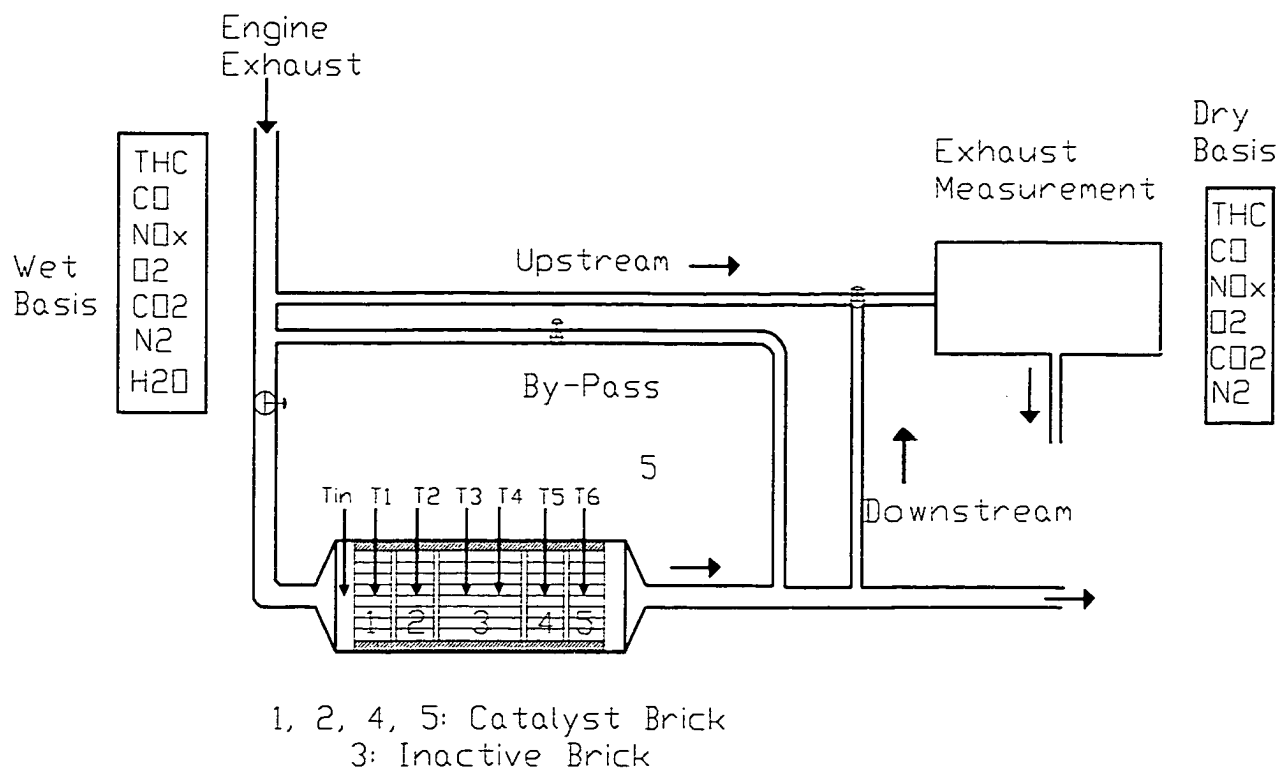


Figure 4-1 Experimental equipment showing the segmented monolith reactor.



The composition of the engine exhaust gas was determined before and after the converter using the analytical facilities summarized in Table 4-3. The components measured were O<sub>2</sub>, CO<sub>2</sub>, CO, NO<sub>x</sub> and the total hydrocarbon content. The instruments were calibrated with standard gases before each test. The measured values were recorded on a dry basis, and conversion to a wet basis was done using the relationship of Heywood (1988).

$$Y_i = (1 - Y_{\text{H}_2\text{O}}) Y_i^* \quad (4.1)$$

For a hydrocarbon C<sub>n</sub>H<sub>m</sub> the mole fraction of water in the exhaust was calculated using:

$$Y_{\text{H}_2\text{O}} = \left( \frac{m}{2n} \right) \left( \frac{Y_{\text{CO}}^* + Y_{\text{CO}_2}^*}{1 + \frac{Y_{\text{CO}}^*}{K_1 Y_{\text{CO}_2}^*} + \left( \frac{m}{2n} \right) (Y_{\text{CO}}^* + Y_{\text{CO}_2}^*)} \right) \quad (4.2)$$

As two fuels were present (natural gas and diesel fuel), the formula C<sub>n</sub>H<sub>m</sub> represents an averaged composition that depends on the flowrate of each fuel. K<sub>1</sub> is an experimental constant with a value between 3.8 and 3.5 (Douville, 1994).

The temperature profile in the catalytic converter was measured by inserting thermocouples into the catalyst segments. A single thermocouple was installed in the centre of each active segment, whilst two thermocouples were used in the inactive segment.

## 4.3 Mathematical Model

### 4.3.1 Assumptions

The simulation of a catalytic converter can be performed using models of varying complexity (Hayes and Kolaczkowski, 1997). In this study a one dimensional single channel model was selected. The single channel model assumes that all of the channels in the reactor experience the same operating conditions. As noted in Hayes and Kolaczkowski (1997), for small channels under the operating conditions found in this converter, the 1D model provides a very close agreement to the 2D model, and offers a greatly reduced computational time compared to 2D or 3D models. The 1D model ignores radial temperature and concentration gradients and accounts for the discontinuity at the wall with heat and mass transfer coefficients. Some other major assumptions made are listed below:

- The gas is assumed to be a variable density ideal gas, that is, volume changes owing to temperature changes are included.
- The pressure in the reactor is constant, that is, the pressure drop is zero and pressure fluctuations resulting from flow pulsation are ignored.
- In the transient model, the gas phase is in a pseudo-steady state with the wall.
- Accumulation of mass in the washcoat is ignored.
- Washcoat diffusion is included. The washcoat is modelled as a 1D isothermal flat plate. This assumption is discussed in more detail shortly.
- The mole average velocity is taken to be equal to the mass average velocity. This assumption is reasonable because the reactants are present in low concentration and the mass transport by advection dominates the mass transport by diffusion.

- The start of each segment corresponds to the beginning of a new development length for the fluid phase. The solid phase is continuous across the segments. This assumption is expanded in the section on model equations.

### 4.3.2 Model Equations

The one-dimensional dispersion model equations which accounts for the axial mixing are based on those given in Hayes and Kolaczowski (1997). Two reacting species were assumed, CO and CH<sub>4</sub>. The mole balance equations for the fluid phase are then written as:

$$\frac{d}{dz} \left( (D_l)_{CH_4} C_b \frac{dY_{CH_4,b}}{dz} \right) - \frac{d(C_b v_m Y_{CH_4,b})}{dz} - (-R_{CH_4})_H - \frac{4}{D_H} k_{m,CH_4} C_b (Y_{CH_4,b} - Y_{CH_4,S}) = 0 \quad (4.3)$$

$$\frac{d}{dz} \left( (D_l)_{CO} C_b \frac{dY_{CO,b}}{dz} \right) - \frac{d(C_b v_m Y_{CO,b})}{dz} - (-R_{CO})_H - \frac{4}{D_H} k_{m,CO} C_b (Y_{CO,b} - Y_{CO,S}) = 0 \quad (4.4)$$

The bulk fluid energy balance equation is:

$$\frac{d}{dz} \left( \alpha_l \frac{dT_b}{dz} \right) - v_m \frac{dT_b}{dz} - \sum_{i=1}^n \left[ \frac{(\Delta H_R)_i}{\rho C_p} (-R_i)_H \right] + \frac{4}{D_H} \frac{h}{\rho C_p} (T_S - T_b) = 0 \quad (4.5)$$

These equations are valid for the steady state and transient converter operation with the assumption of pseudo steady state (Hayes et al., 1992, Lee and Aris, 1977). The boundary conditions employed for Equations (4.3), (4.4) and (4.5) were:

$$\text{at } z = 0: \quad Y_{\text{CH}_4} = (Y_{\text{CH}_4})_0; \quad Y_{\text{CO}} = (Y_{\text{CO}})_0; \quad T_b = T_{b0}$$

$$\text{at } z = L \quad \frac{dY_{\text{CH}_4,b}}{dz} = 0; \quad \frac{dY_{\text{CO},b}}{dz} = 0; \quad \frac{dT_b}{dz} = 0$$

Although diffusive boundary conditions (Danckwerts conditions) are more appropriate at the reactor inlet for the dispersed plug flow equation, their use does not lead to a significantly better solution when the advection dominates the flow (Hayes and Kolaczowski, 1997). When laminar flow is modelled using a one dimensional model, the effective dispersion coefficients which account for the axial mixing are (Hayes and Kolaczowski, 1997):  $D_I = D_{AB} + \frac{v_m^2 R^2}{48 D_{AB}}$  and  $\alpha_I = \alpha + \frac{v_m^2 R^2}{48 \alpha}$ . The effective dispersion coefficients  $D_I$  and  $\alpha_I$  combine laminar diffusion, (first term), and the distribution effect of the laminar flow profile, (second term).

The mole balance equations for the solid phase are:

$$k_{m,\text{CH}_4} C_b (Y_{\text{CH}_4,b} - Y_{\text{CH}_4,S}) = \eta_{\text{CH}_4} (-R_{\text{CH}_4})_S \quad (4.6)$$

$$k_{m,\text{CO}} C_b (Y_{\text{CO},b} - Y_{\text{CO},S}) = \eta_{\text{CO}} (-R_{\text{CO}})_S \quad (4.7)$$

The energy balance equation for the solid phase is:

$$\frac{\partial}{\partial z} \left( k_w \delta_w \frac{\partial T_S}{\partial z} \right) - h(T_S - T_b) - \sum_{i=1}^n [\eta_i (\Delta H_R)_i (-R_i)_S] = \delta_w \rho_w C_{pw} \frac{\partial T_S}{\partial t} \quad (4.8)$$

The boundary and initial conditions for Equation (4.8) are:

$$\text{at } z=0 \text{ and at } z=L, \quad \frac{dT_s}{dz} = 0; \quad \text{at } t=0, \quad T_s = T_{s0}$$

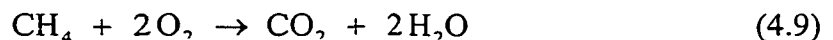
Note that the assumption that  $\frac{dT_s}{dz} = 0$  at  $z=0$  and  $z=L$  works for catalysts where the exothermic reaction occurs predominately near the center of the converter. It would be less valid for catalysts where the hot spot is at the end of the catalyst. The alternative is to use Danckwerts boundary conditions (Hayes and Kolaczkowski, 1997) which allow diffusion to continue beyond the ends, but this was not required for this situation where the temperature peaks near the center of the reactor.

The boundary conditions were applied at the entrance and exit to the reactor only. For the sake of computation, the gap was ignored and the reactor was assumed to be continuous. Therefore axial dispersion was assumed to occur across segment boundaries, as well as axial heat conduction in the solid phase. This latter assumption is not expected to cause significant error, because the conduction in the substrate is relatively low.

## 4.4 Physical and Chemical Parameters

### 4.4.1 Chemical Kinetics

The main hydrocarbon in the exhaust of a dual fuel engine is methane which, together with carbon monoxide, comprise the primary pollutants in the exhaust gas. In this model two reactions were considered, namely the oxidation of  $\text{CH}_4$  and  $\text{CO}$ , which can be represented by the following overall reactions:



These reactions are both highly exothermic. The enthalpies of reaction in kJ/mol can be written as the following functions of temperature:

$$(\Delta H_R^\circ)_{\text{CH}_4} = -806.9 + 1.586 \times 10^{-2} T - 8.485 \times 10^{-6} T^2 - 3.963 \times 10^{-9} T^3 + 2.16 \times 10^{-12} T^4 \quad (4.11)$$

$$(\Delta H_R^\circ)_{\text{CO}} = -279.6 - 1.861 \times 10^{-4} T + 2.52 \times 10^{-5} T^2 - 1.2247 \times 10^{-8} T^3 + 2.255 \times 10^{-12} T^4 \quad (4.12)$$

Equation (4.11) is derived by Hayes and Kolaczkowski (1997). Equation (4.12) is derived based on the same principles.

The kinetics of the reactions involved in automotive catalytic converters have been widely studied for gasoline engines, although most modelling studies use modified versions of the expressions proposed by Voltz et al. (1973); see, for example, Oh and Cavendish (1982), and Siemund et al. (1996). The expressions of Voltz et al. (1973) are of the LHHW type, and consider the oxidation of CO and HC in the presence of  $\text{NO}_x$ . Hydrocarbons are subdivided into "slow" and "fast" burning HC. Considering  $\text{CH}_4$  to be a "slow burning" HC, the Voltz et al. (1973) equations adapted for this work have the following form:

$$(-R_{\text{CH}_4})_S = k_{\text{CH}_4} \frac{Y_{\text{CH}_4,S} Y_{\text{O}_2,S}}{R(\theta)} \quad (4.13)$$

$$(-R_{\text{CO}})_S = k_{\text{CO}} \frac{Y_{\text{CO},S} Y_{\text{O}_2,S}}{R(\theta)} \quad (4.14)$$

$$R(\theta) = T_S [1 + k_{a1} Y_{\text{CO},S}]^2 [1 + k_{a4} Y_{\text{NO},S}^m] \quad (4.15)$$

$$k_{\text{CH}_4} = A_1 \exp\left(\frac{-E_1}{R_g T}\right) \quad (4.16)$$

$$k_{\text{CO}} = A_2 \exp\left(\frac{-E_2}{R_g T}\right) \quad (4.17)$$

$$k_{a1} = A_3 \exp\left(\frac{-E_3}{R_g T}\right) \quad (4.18)$$

$$k_{a4} = A_4 \exp\left(\frac{-E_4}{R_g T}\right) \quad (4.19)$$

The kinetic constants in the rate equations are unique to each catalyst formulation. Typically, the values are adjusted for each catalyst used so as to give a good agreement between experimental and predicted values over a wide range of operating conditions. The following values gave a good agreement for the converter studied in this investigation:

$$A_1 = 4.456 \times 10^{17} \frac{\text{mol} \cdot \text{K}}{\text{m}^2 \text{s}} \quad E_1 = 1.321 \times 10^5 \frac{\text{J}}{\text{mol}}$$

$$A_2 = 9.28 \times 10^{13} \frac{\text{mol} \cdot \text{K}}{\text{m}^2 \text{s}} \quad E_2 = 5.5 \times 10^4 \frac{\text{J}}{\text{mol}}$$

$$A_3 = 65.5 \quad E_3 = 7990 \frac{\text{J}}{\text{mol}}$$

$$A_4 = 4.79 \times 10^5 \quad E_4 = -3733 \frac{\text{J}}{\text{mol}}$$

$$m = 0.2$$

The homogeneous reaction of CO was included in the model. The rate expressions for homogeneous CO oxidation proposed by Dryer (1972) was used:

$$(-R_{\text{CO}})_H = 1.26 \times 10^{10} \exp\left(-\frac{20131}{T_b}\right) C_{\text{CO},b} C_{\text{O}_2,b}^{0.25} C_{\text{H}_2\text{O},b}^{0.5} \quad (4.20)$$

The homogeneous reaction of methane was ignored in the model since its reaction is negligible at the catalytic converter.

#### 4.4.2 Heat and Mass Transfer Coefficients

The one-dimensional model requires values for the local heat and mass transfer coefficients. These values were obtained from the Nusselt and Sherwood numbers, and included the entry length effects. The entry length is important because of the segmented design used in the converter. In this investigation, it was assumed that the channels could be approximated as cylindrical ducts for the purposes of calculating heat and mass transfer coefficients. Although the channels of the ceramic substrate are square, the application of the washcoat tends to round the corners, so a round channel is a better approximation than a square one (Hayes and Kolaczkowski, 1994). Correlations for  $Nu$  have been proposed for the two common wall boundary conditions, constant wall temperature and constant wall heat flux. For constant wall temperature, Tronconi and Forzatti (1992) developed a  $Nu$  correlation for simultaneously developing thermal and hydrodynamic boundary layers for a gas with a Prandtl number of 0.7:

$$Nu_T = 3.657 + 8.827 \left(\frac{1000}{Gz}\right)^{-0.524} \exp\left(-\frac{48.2}{Gz}\right) \quad (4.21)$$



The correlation for simultaneously developing flow at a Prandtl number of 0.7 with constant wall flux is given by Hayes and Kolaczowski (1997):

$$Nu_H = 4.364 + 13.18 \left( \frac{1000}{Gz} \right)^{-0.524} \exp \left( -\frac{60.2}{Gz} \right) \quad (4.22)$$

Following Groppi et al. (1995), the local  $Nu$  value in a system with chemical reaction at the wall was approximated by interpolating between  $Nu_T$  and  $Nu_H$  using the interpolation formula of Brauer and Fetting (1966):

$$\frac{Nu - Nu_H}{Nu_T - Nu_H} = \frac{Da \ Nu}{(Da + Nu) Nu_T} \quad (4.23)$$

The Graetz number,  $Gz$ , and the Damköhler number,  $Da$ , are defined for an arbitrary reaction of component A by:

$$Gz = \frac{D_T}{z} Re Pr \quad (4.24)$$

$$Da = \frac{\eta(-R_A)_S D_H}{4 C_{A,S} D_{AB}} \quad (4.25)$$

The Sherwood number was obtained by substituting the Schmidt number,  $Sc$ , for the Prandtl number in the equation for Graetz number, that is, Equation (4.24). Further discussion of  $Nu$  and  $Sh$  in a single channel monolith can be found in Hayes and Kolaczowski (1999).

#### 4.4.3 Effectiveness Factor

The kinetic expressions give values for the intrinsic reaction rate, that is, the rate in the absence of internal heat and mass transfer limitation. It has been shown (Hayes and Kolaczowski, 1994; Leung et al., 1996) that diffusion in the washcoat can be significant

at typical reactor operating conditions, and must be included in the reactor model. The effectiveness factor can be used to quantify the effect of the diffusion in the catalyst, and is defined for reactant A as:

$$\eta = \frac{\text{Average rate for the catalyst washcoat}}{\text{Rate at the surface conditions}} = \frac{(-R_A)_{\text{Average}}}{(-R_A)_S} \quad (4.26)$$

Both methane and carbon monoxide react in the washcoat. Because of the low reactant concentration and the thickness of the washcoat it is valid to assume that the washcoat is isothermal (Leung et al., 1996). The effectiveness factor for each reaction must be determined numerically, because of the non-linear kinetic model. The washcoat geometry for the square channel typically consists of a fillet type structure, with the washcoat thicker in the corners than the mid-side. This structure would require a minimum of a 2D model to simulate exactly. A 1D approximation can be made by approximating the washcoat as a flat plate with the same characteristic length as the non-uniform washcoat. Although this approximation introduces a small error (see Leung, et al. (1996) for details), it results in a substantial saving in execution time. Furthermore, the exact geometry, porosity and tortuosity factor in the washcoat were not known, and therefore the added rigor of the 2D washcoat model was not considered to be justified. Errors associated with modelling the washcoat will be reflected in the values of the rate constants. The mole balance equations for the two reacting species in a one dimensional washcoat are:

$$(D_{\text{eff}})_{\text{CH}_4} C \frac{dY_{\text{CH}_4}^2}{dx^2} - \frac{(-R_{\text{CH}_4})}{L} = 0 \quad (4.27)$$

$$(D_{\text{eff}})_{\text{CO}} C \frac{dY_{\text{CO}}^2}{dx^2} - \frac{(-R_{\text{CO}})}{L} = 0 \quad (4.28)$$

The boundary condition for Equations (4.27) and (4.28) are:

$$\text{at } x = 0, \quad \frac{dY_{\text{CO}}}{dx} = 0 \quad \text{and} \quad \frac{dY_{\text{CH}_4}}{dx} = 0$$

$$\text{at } x = L \text{ (washcoat surface)} \quad Y_{\text{CO}} = Y_{\text{CO},S} \quad \text{and} \quad Y_{\text{CH}_4} = Y_{\text{CH}_4,S}$$

$(D_{\text{eff}})_{\text{CH}_4}$  and  $(D_{\text{eff}})_{\text{CO}}$  are the effective diffusivities of methane and carbon monoxide in the washcoat based on the entire cross sectional area of the catalyst, both catalyst and pores, and include terms for the catalyst porosity and tortuosity. The diffusion in the pores of a typical monolith reactor washcoat is dominated by Knudsen diffusion, and therefore the effective diffusion coefficient can be written as:

$$D_{\text{eff}} = \frac{\varepsilon}{\tau} 97 a \left( \frac{T}{M} \right)^{0.5} \quad (4.29)$$

The tortuosity factor for the washcoat was taken as 8.0, the washcoat porosity was 0.41 and the mean pore diameter 10 nanometres (Li, 1996). The washcoat analyzed by Li (1996) was similar to the one used in this study, and was also supplied by Johnson-Matthey, and therefore it was felt that these values were reasonable assumptions.

#### 4.5 Numerical Approach for the Model Solution

Equations (4.3)-(4.8), (4.27) and (4.28) are a set of eight coupled nonlinear equations. The differential equations were solved using the Galerkin finite element method with quadratic shape functions. The discretization of the time differential in the transient solid phase energy balance [Equation (4.8)] was done using a fully implicit Gear scheme. The non-linear algebraic equations [Equations (4.6) and (4.7)] were expressed in the weak form to aid convergence. The systems of non-linear equations

arising from the discretization were solved using a quasi-Newton method with under-relaxation for the solid phase energy balance equation. Further information on the finite element modelling of monolith reactor channels can be found in Hayes et al. (1992) and Hayes and Kolaczkowski (1997). In all of the simulations reported the reactor was discretized using 120 quadratic finite elements. The washcoat thickness was discretized with 10 quadratic finite elements. The step size in all cases was 1 second. Refining the discretization gave no noticeable improvement in the solution.

#### **4.6 Model Results and Analysis**

This section presents some experimental data and simulation studies obtained from the transient operation of the catalytic converter following a step change in engine operation. During the transients the engine was operating at steady state, and thus the composition of the exhaust gas was constant. The procedure followed was first to achieve a steady state operation for both the engine and converter. The engine speed or load was then changed to a new, predetermined value. The inlet and outlet composition of the exhaust gas, the inlet gas temperature, and the temperature profile in the reactor were monitored as a function of time until new steady state values were reached. The transients reported in the following sections occur after the engine has achieved steady state, thus the inlet composition of the exhaust gas was constant during the converter transient. It should be noted that changes in engine speed or load resulted in changes in the exhaust gas temperature, composition and/or flowrate. Generally speaking, an increase in exhaust temperature or a decrease in flowrate should lead to an increase in conversion of HC and CO, everything else being equal. An increase in HC or CO

emissions can result in either a higher or lower conversion, depending on the magnitude of the exotherm and its relationship to the other operating parameters. In the following two sections, changes that resulted in increased and decreased exhaust gas temperature are presented and discussed.

#### **4.6.1 Kinetic and Mass Transfer Control**

Prior to presenting results, it is relevant to demonstrate that the reactor was operating in the region of kinetic control. Monolith type reactors operating in the laminar flow regime are always influenced to some extent by mass and heat transfer from the bulk fluid, the effect of which can be to raise or lower the global reaction rate. Under extreme cases it is possible for the wall concentration to approach zero, at which point the kinetics are no longer important as the rate is governed solely by the rate of mass transfer. For the simulations reported in this paper, it was observed that the difference in concentration between the bulk gas and the wall was of the order of 5%, which indicates that the reactor performance was governed predominantly by the kinetics. A plot of the wall and bulk fluid concentration for the two main reactants for typical operating conditions is shown in Figure 4-2(a) and 2(b) respectively. Note the sudden changes in wall concentration at the beginning of each new segment. This change results from the increase in mass transfer coefficient as the a new development length is started.

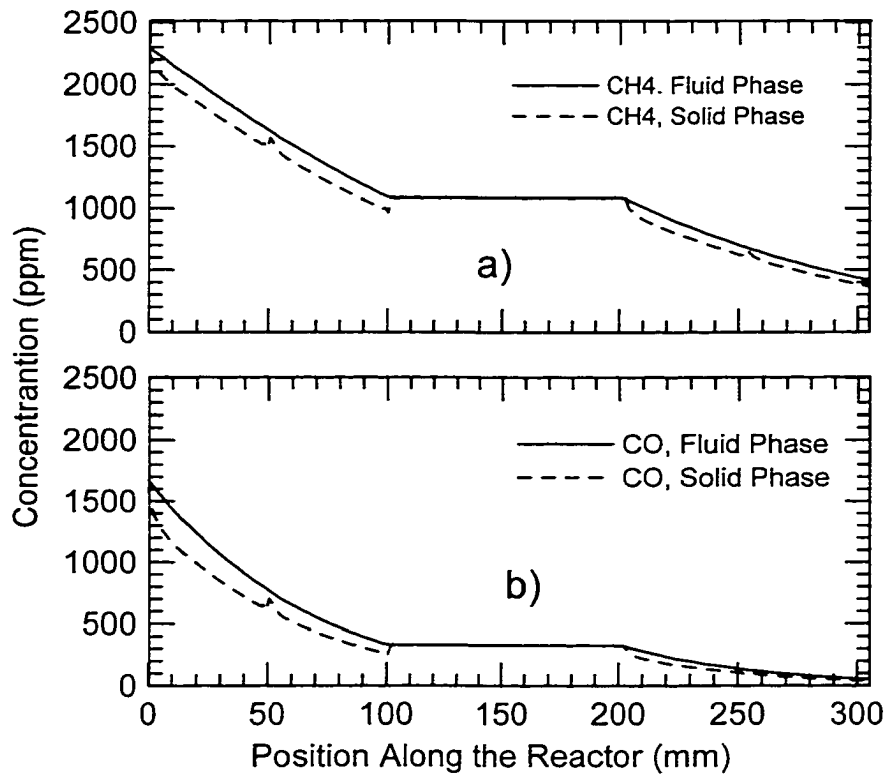


Figure 4-2 Example solution of the predicted fluid and solid axial concentration profiles. (a) Methane and (b) Carbon monoxide. The concentration on the solid surface is between 80 and 90% of the fluid phase concentration, indicating that the reactor is predominantly controlled by the kinetics.

## 4.6.2 Increase in Gas Temperature

This section describes reactor operation following a change in engine operation that gave an increase in exhaust gas temperature. The engine was initially run at a speed of 1500 RPM with a load of 140 NM (22 kW) until overall steady state was achieved. The engine speed was then increased to 2600 RPM while the load was held constant at 140 NM (38 kW). The steady state conditions corresponding to these two modes of operation are given in Table 4-4, and the reactor temperature profiles are shown in Figure 4-3. Note that the change in engine speed results in approximately 200 K increase in exhaust gas temperature, about a 20% increase in CO concentration, a 5% decrease in HC concentration, and a 66% increase in total mass flowrate. The change in exhaust state was not instantaneous when engine operation changed. Rather it required between 30 and 120 seconds before the exhaust gas composition was observed to be constant. The transient simulation is based on a start time after the engine exhaust composition was constant. Although the temperature of the exhaust gas was also constant at the engine outlet at this time, the reactor inlet temperature takes much longer to achieve steady state owing to the thermal mass of the ductwork between the engine and the converter. The reactor inlet temperature was thus observed to change over the time period of interest. The inlet reactor temperature as a function of time is shown in Figure 4-4 for the time period covered by the simulation.

The predicted outlet temperature and conversions for the steady state simulations at these two engine conditions are given in Table 4-5. From these data it is seen that the agreement between experiment and prediction is reasonable, especially considering the assumptions made in developing the model.

Table 4-4 Engine exhaust parameters for two steady engine operation modes.

Engine mode		Exhaust gas composition						T <sub>in</sub>	Mass Flow Rate
Speed (rpm)	Torque (Nm)	HC (ppm)	CO (ppm)	NO (ppm)	O <sub>2</sub> (%)	CO <sub>2</sub> (%)	H <sub>2</sub> O (%)	(K)	g/s
1500	140	2421	1291	731	9.01	5.63	10.87	646	43.90
2600	140	2293	1674	273	7.61	6.26	12.11	845	72.72

N<sub>2</sub>: Balance of Exhaust Gas Composition

T<sub>in</sub>: Reactor Inlet Gas Temperature

Table 4-5 Steady state model and experiment results.

	Simulation	Experimental	Relative error (%)
X <sub>HC</sub> (%)	86	85	0.9
X <sub>CO</sub> (%)	96	97	-0.8
T <sub>6</sub> (K)	905	903	0.2



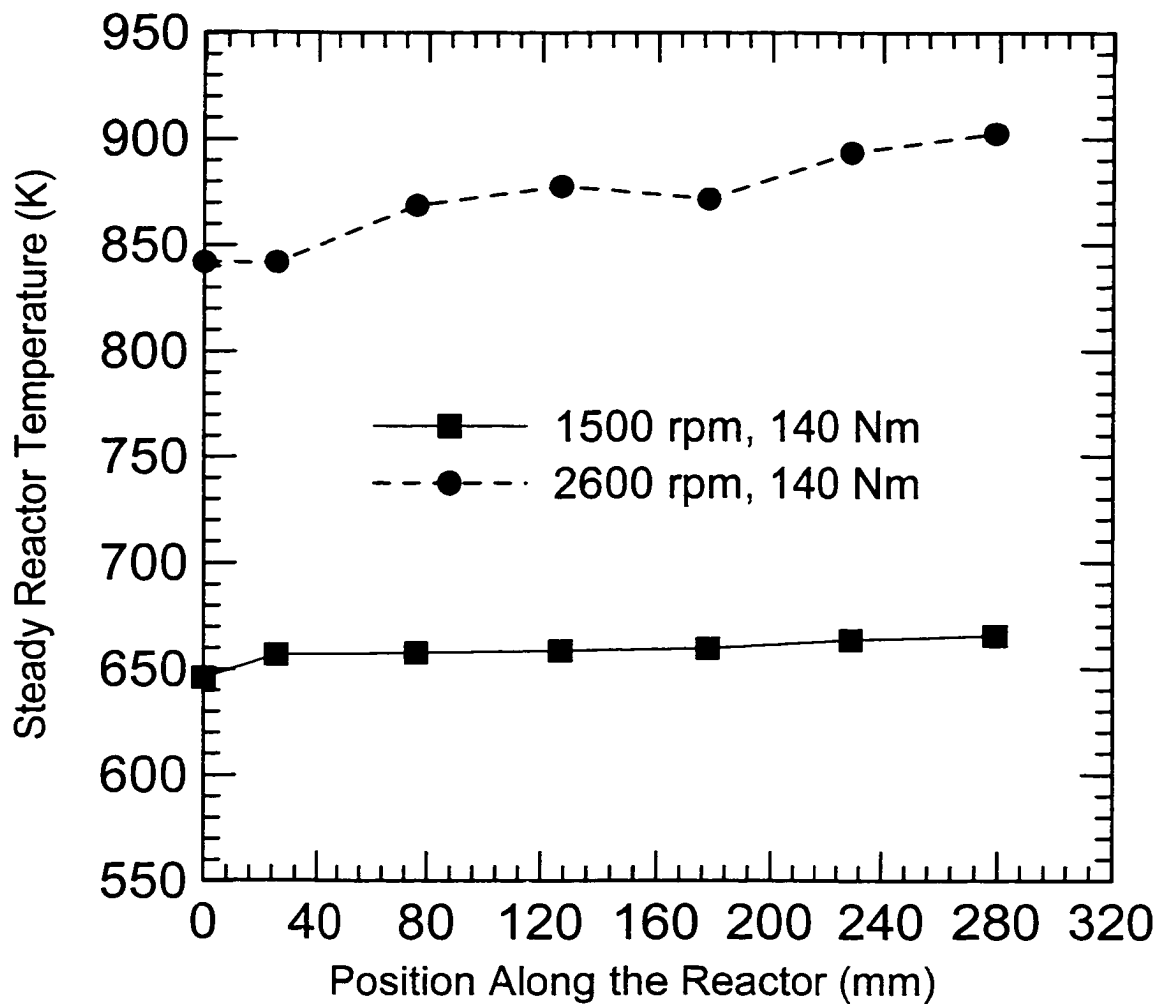


Figure 4-3 The steady state converter temperature profiles for two engine operations.

See Table 4-4 for details.

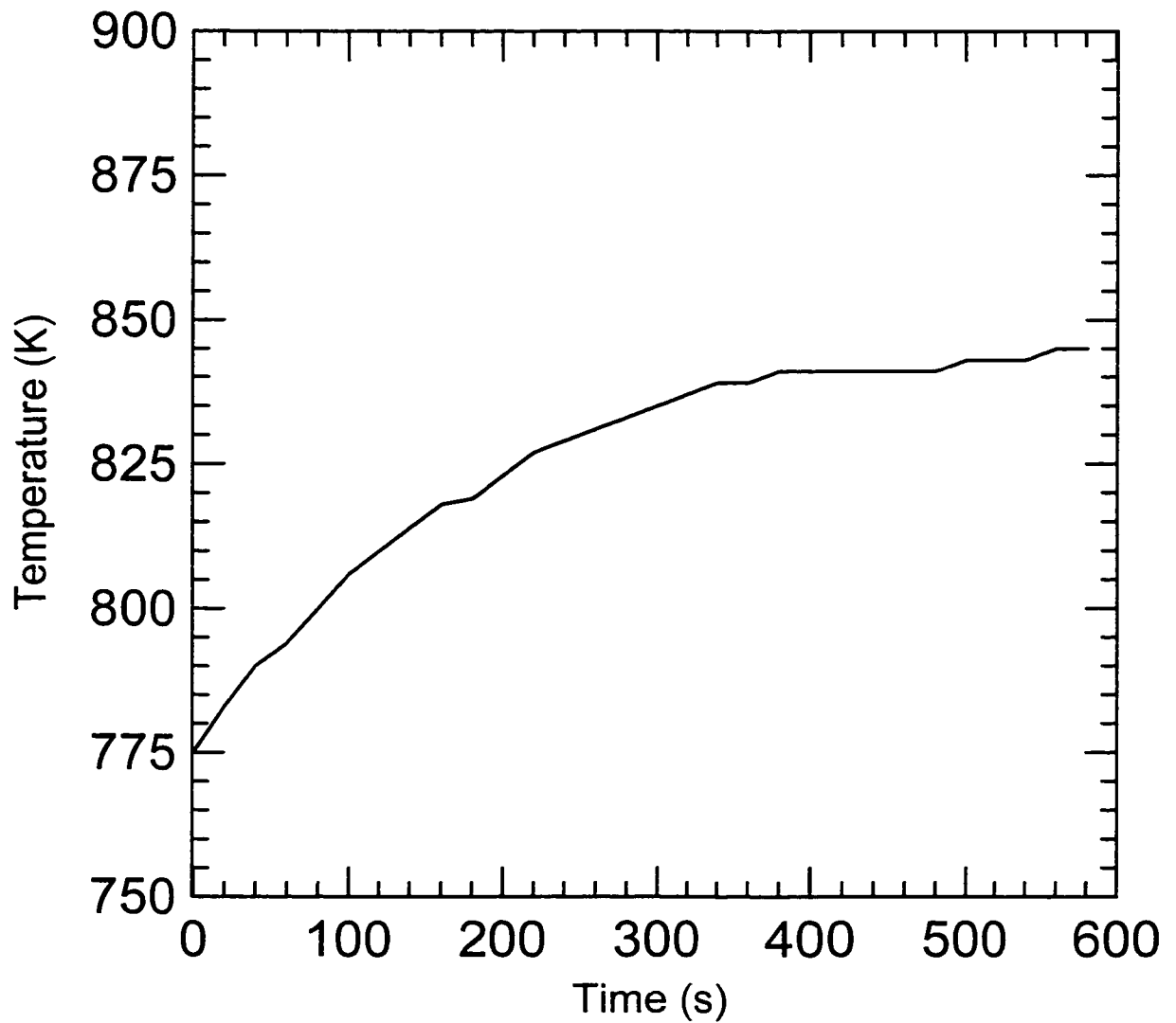


Figure 4-4 Inlet temperature to the reactor as a function of time for the case of an increased engine outlet temperature.

The transient simulations required an initial condition to be given. As the change in engine operation occurred over a finite period of time, and not instantaneously, the initial condition is not the steady state corresponding to the first engine condition. Therefore, the initial condition used in the model was the experimentally measured reactor temperature profile at the time denoted zero. The inlet temperature boundary condition was the experimentally measured inlet gas temperature, which changed as a function of time.

The concentrations of HC and CO at the reactor exit are plotted as a function of time for both experimental and simulated values in Figure 4-5. It is seen that the composition of the reactor effect is reasonably well approximated by the model, with the HC concentration being underestimated by a maximum of 10% in early stages of the transient.

The final steady state values obtained from the simulations and experiments are given in Table 4-5. It is seen that good agreement is achieved between the two, with errors of less than 1% for all quantities.

The development of the reactor temperature profile as a function of time is shown in Figure 4-6 and Figure 4-7. Figure 4-6 shows a series of simulated temperature profiles, whilst Figure 4-7 shows a comparison of three of these profiles to experimental values. The shape of the developing temperature profiles is typical of transient converter operation in which the inlet gas temperature is increased, and the temperature of the reactor inlet is higher than the ignition temperature. The temperature rises at the front of the reactor as the exothermic reaction heats the gas. Downstream the thermal mass of the reactor acts as a heat sink, as the reaction rate is not sufficiently fast to overcome the

thermal inertia of the system. See, for example, Hayes et al. (1996). At steady state, the reaction exhibits a steady increase in temperature from inlet to the outlet. Note that the central section of the reactor, which at steady state shows a flat temperature profile, corresponds to a catalytically inactive monolith segment.

Figure 4-8 shows the steady state simulated temperature profiles for the reactor wall and the bulk gas. The difference in temperature between the gas and the wall is seen to be about 5 K.

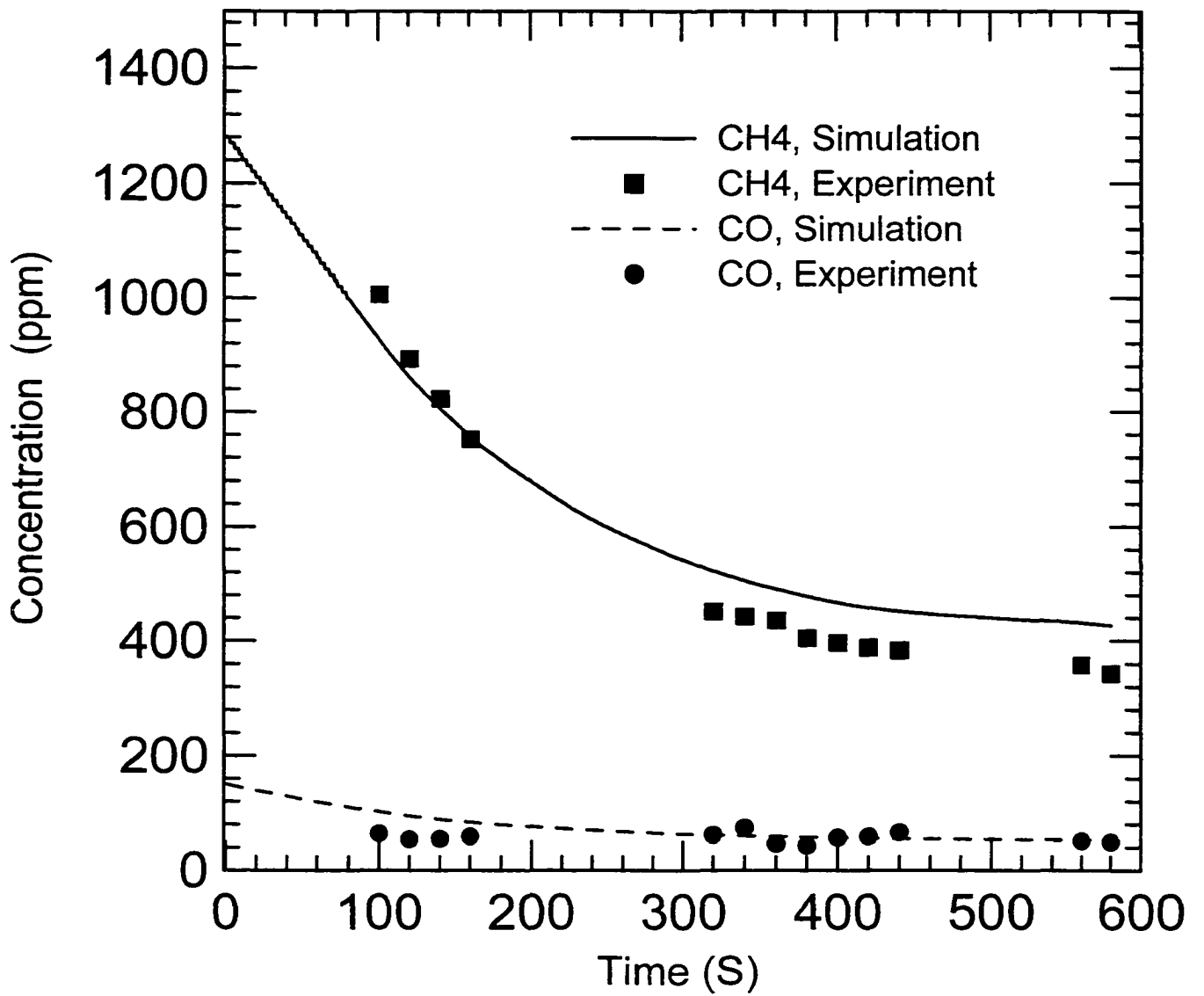


Figure 4-5 Reactor outlet concentrations of HC and CO as a function of time for the case of an increase in engine exhaust gas temperature.

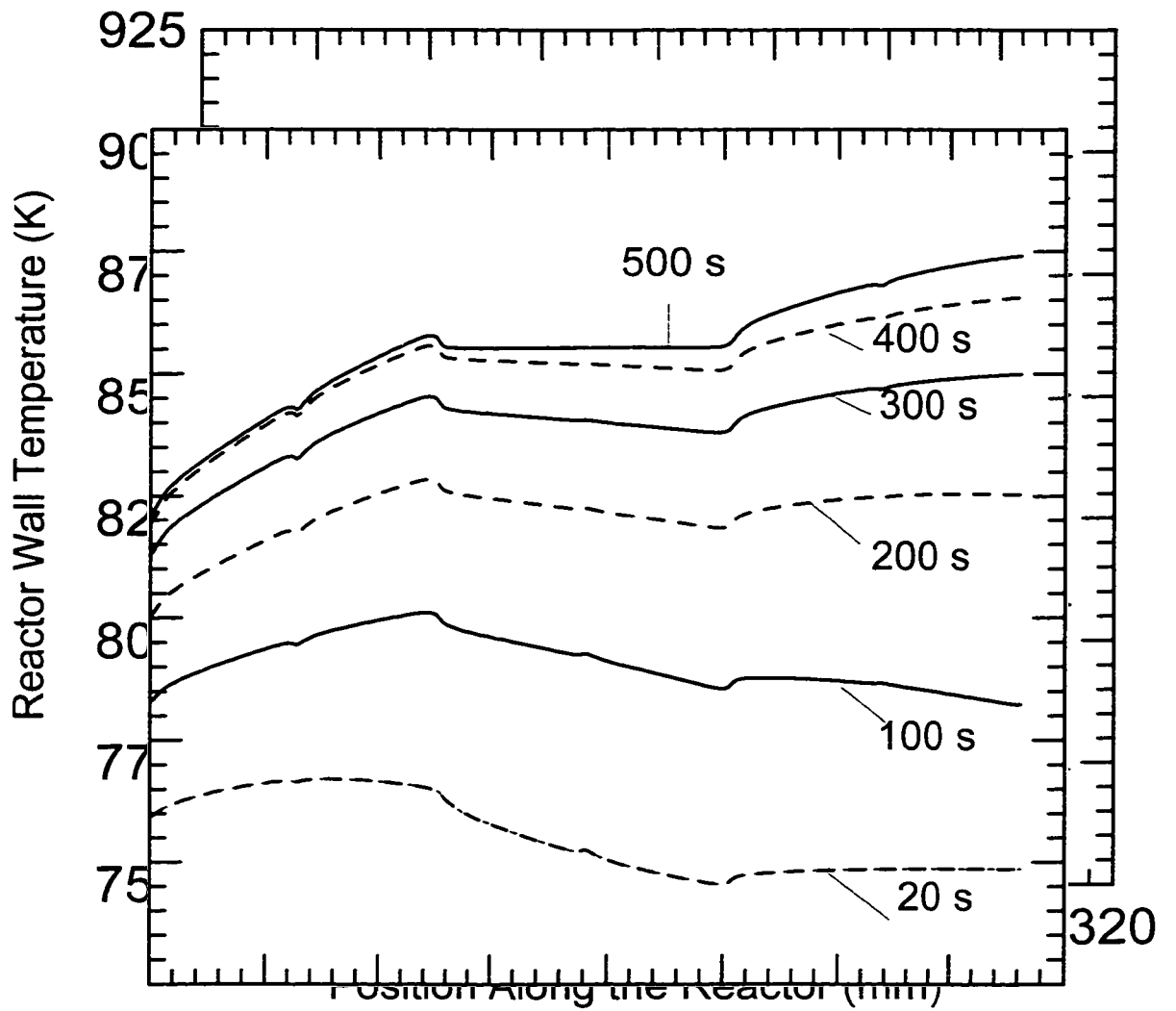


Figure 4-6 Simulated reactor temperature profiles at various elapsed times, for the case of an increase in engine exhaust gas temperature.

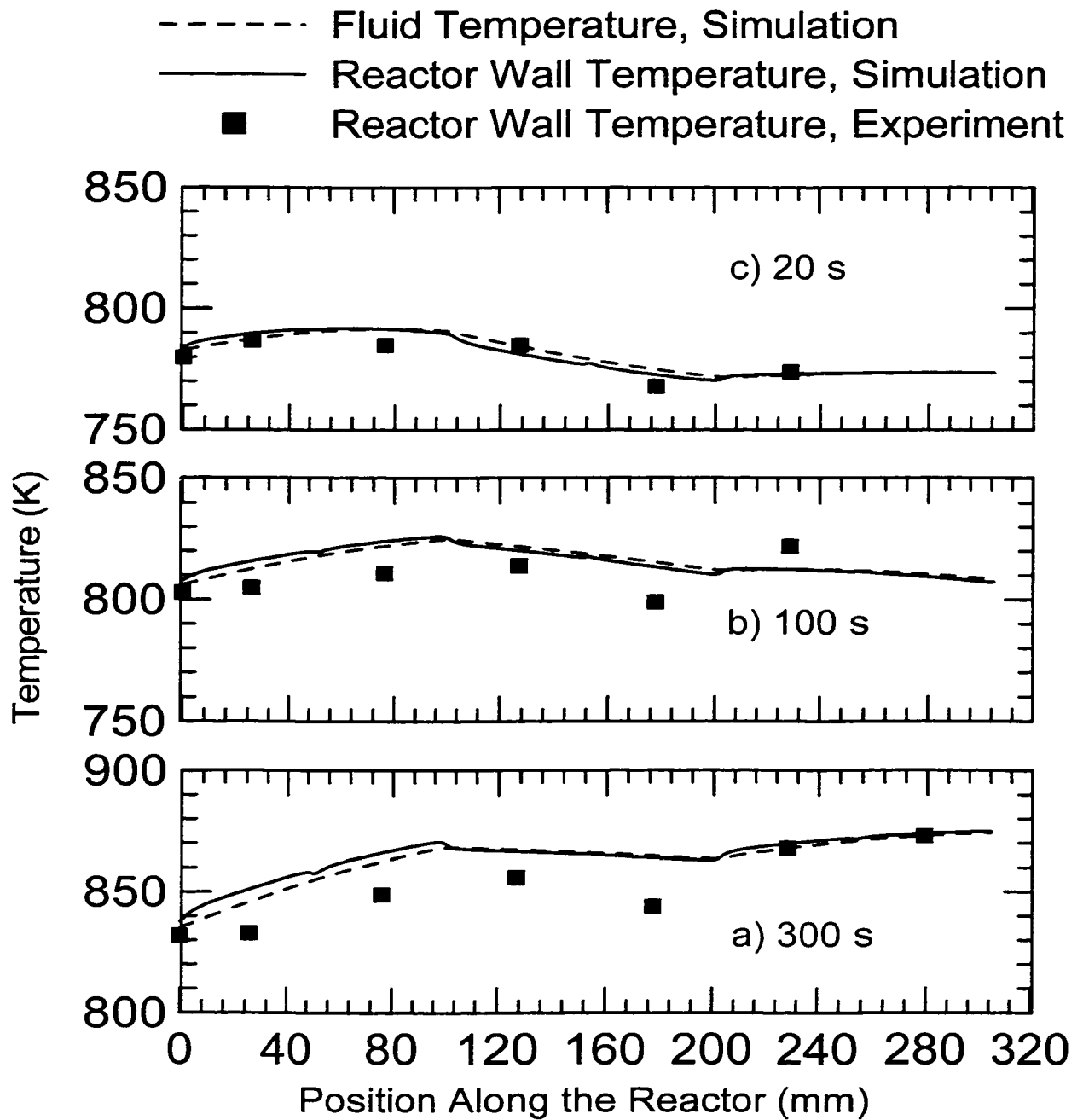


Figure 4-7 Comparison of simulated and experimental reactor temperature profiles at various elapsed times, for the case of an increase in engine exhaust gas temperature.

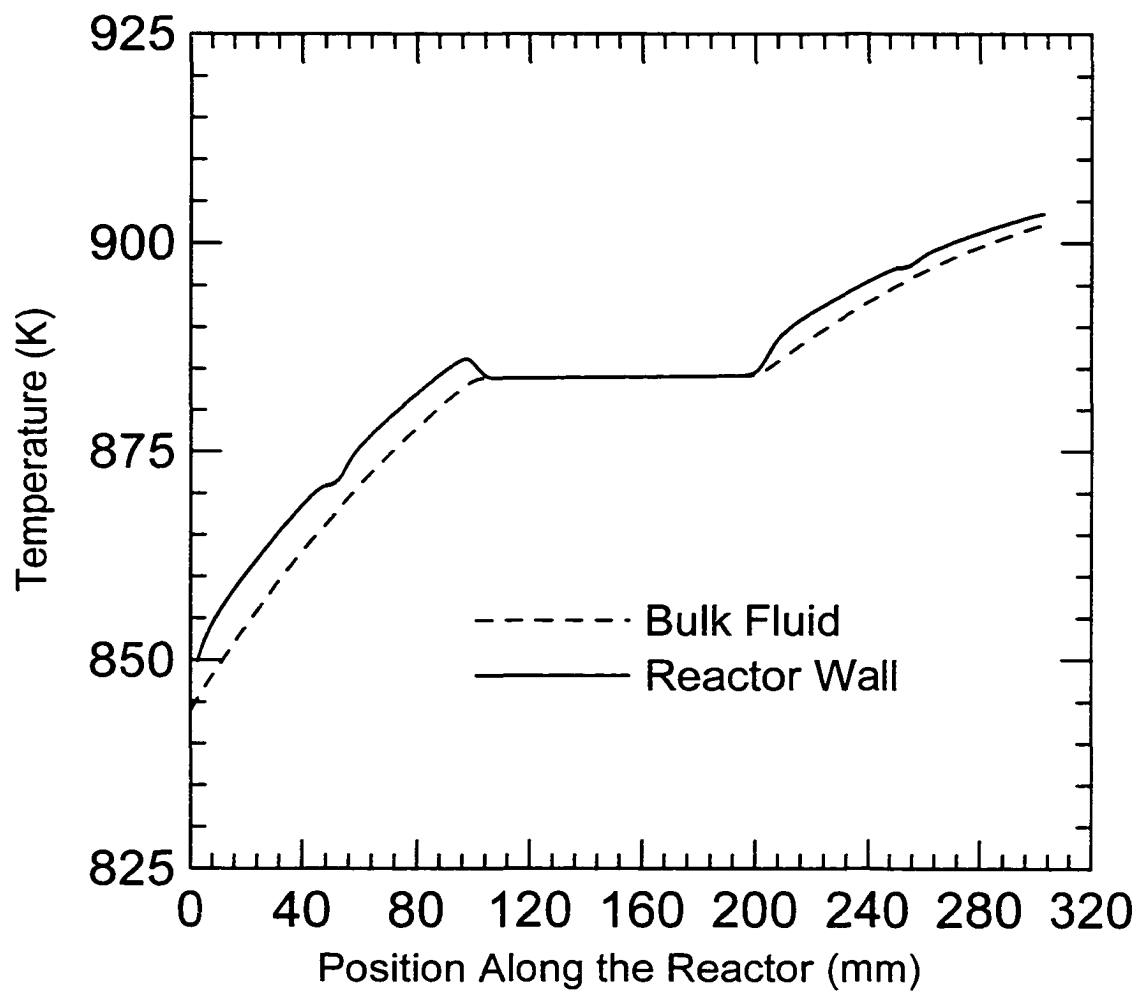


Figure 4-8 Final steady state simulated reactor wall and bulk gas temperature profiles.



### 4.6.3 Decrease in Inlet Gas Temperature

This section describes a change in engine operation that gave a decrease in the inlet gas temperature to the converter. The engine was initially run at 1500 rpm and 200 Nm (31 kW). After steady state was achieved, the engine load was reduced to 180 Nm whilst the engine speed was unchanged ( engine power of 28 kW). Table 4-6 gives the engine exhaust parameters for these two steady states, whilst the temperature profile are given in Figure 4-9. The transient inlet gas temperature observed during the period of simulation is shown in Figure 4-10.

Table 4-6 Engine exhaust parameters for two steady engine operation modes

Engine mode		Exhaust Gas Composition						T <sub>in</sub>	Mass Flow Rate
Speed (rpm)	Torque (Nm)	HC (ppm)	CO (ppm)	NO (ppm)	O <sub>2</sub> (%)	CO <sub>2</sub> (%)	H <sub>2</sub> O (%)	(K)	g/s
1500	200	879	492	1518	5.55	7.52	14.36	747	44.56
1500	180	1334	785	1214	7.03	6.81	13.05	723	43.35

N<sub>2</sub>: Balance of Exhaust Gas Composition

T<sub>in</sub>: Reactor Inlet Gas Temperature

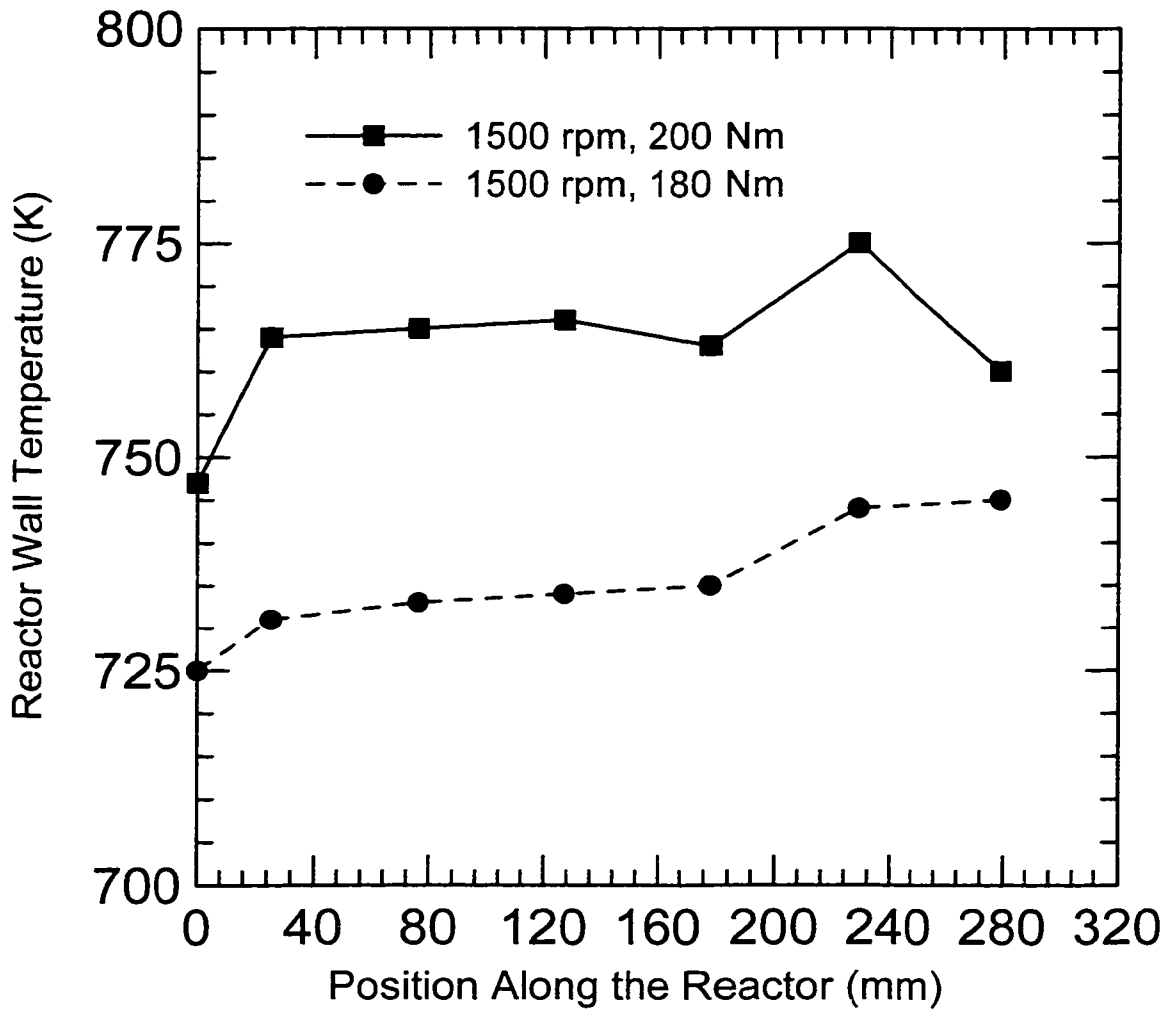


Figure 4-9 The steady state converter temperature profiles for two engine operations.

See Table 4-6 for details.

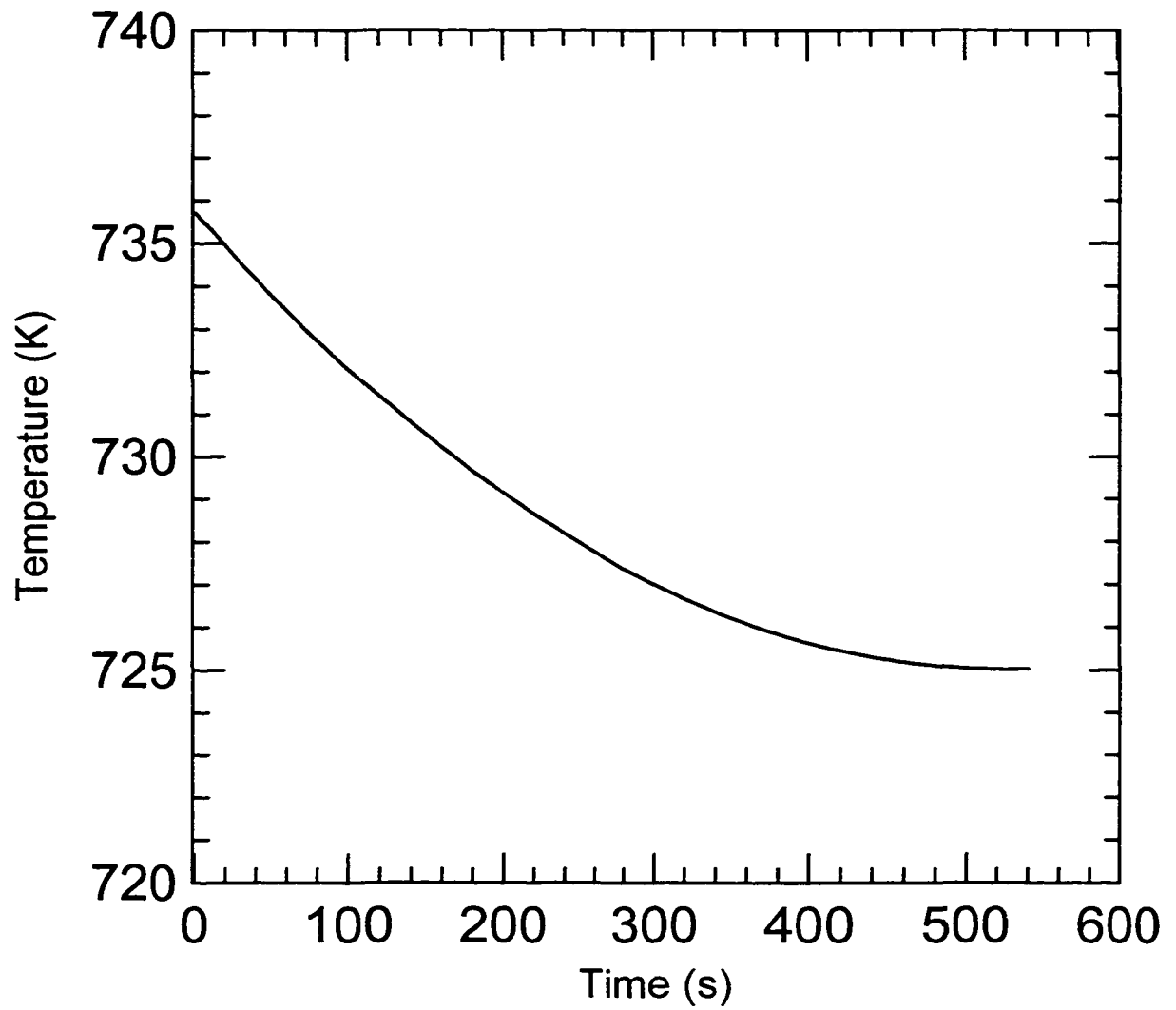


Figure 4-10 Inlet temperature to the reactor as a function of time for the case of a decreased engine outlet temperature.

The initial and boundary conditions used in the simulation followed the same pattern as described in the previous section. The experimental reactor temperature profile was imposed at time zero, and the transient reactor inlet gas temperature was imposed at the reactor inlet. The reactor inlet gas composition was constant during the simulation.

The experimental and simulated reactor exit composition as a function of time is shown in Figure 4-11. It is seen that the HC emissions increase as the reactor temperature falls. The experimental values for HC concentration are consistently about 10% lower than the predicted values. The final steady state values for simulation and experiment are shown in Table 4-7.

Table 4-7 Steady Model and Experiment Results

	Simulations	Experimental	Relative Error (%)
$X_{\text{HC}}$ (%)	34	37	-7.9
$X_{\text{CO}}$ (%)	95	93	2.4
$T_6$ (K)	744	745	-0.13

The temperature profile as a function of time obtained from the simulation are illustrated in Figure 4-12. It is seen that the reactor temperature declines with time. Two factors are at work in this method of operation. The lower inlet gas temperature tends to decrease the reactor temperature, whilst the increased HC and CO emissions (see Table 4-6) from the engine can increase the temperature, provided that the catalyst is sufficiently active to achieve ignition. In the operating scenario studied, this was not the case, and the reactor temperature fell, giving an increase in the HC and CO emissions in the reactor effluent. The agreement between the experimental and simulated temperature

profile is shown in Figure 4-13, where it is seen that a close match was obtained.

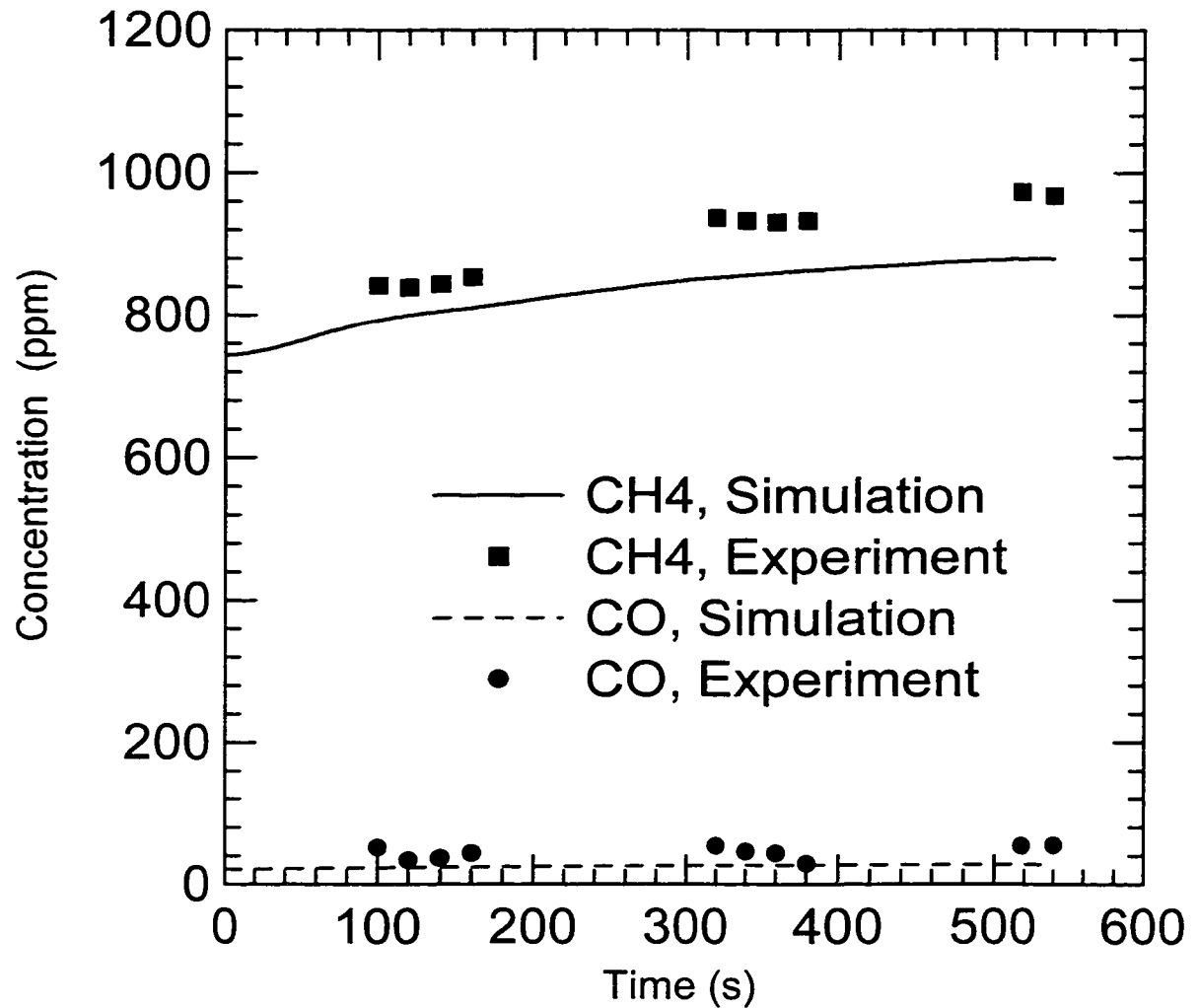


Figure 4-11 Reactor outlet concentrations of HC and CO as a function of time for the case of a decrease in engine exhaust gas temperature.

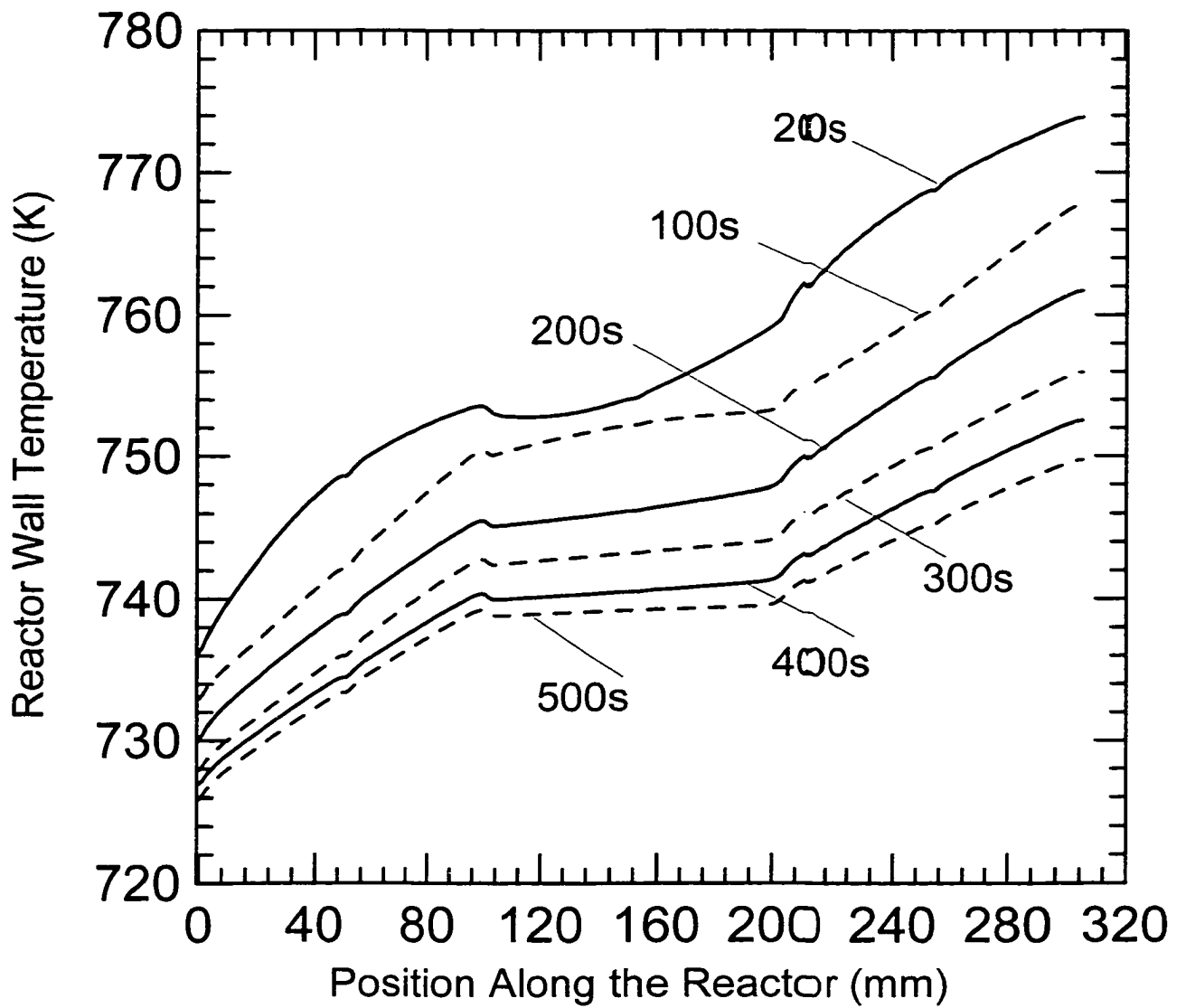


Figure 4-12 Simulated reactor temperature profiles at various elapsed times, for the case of a decrease in engine exhaust gas temperature.

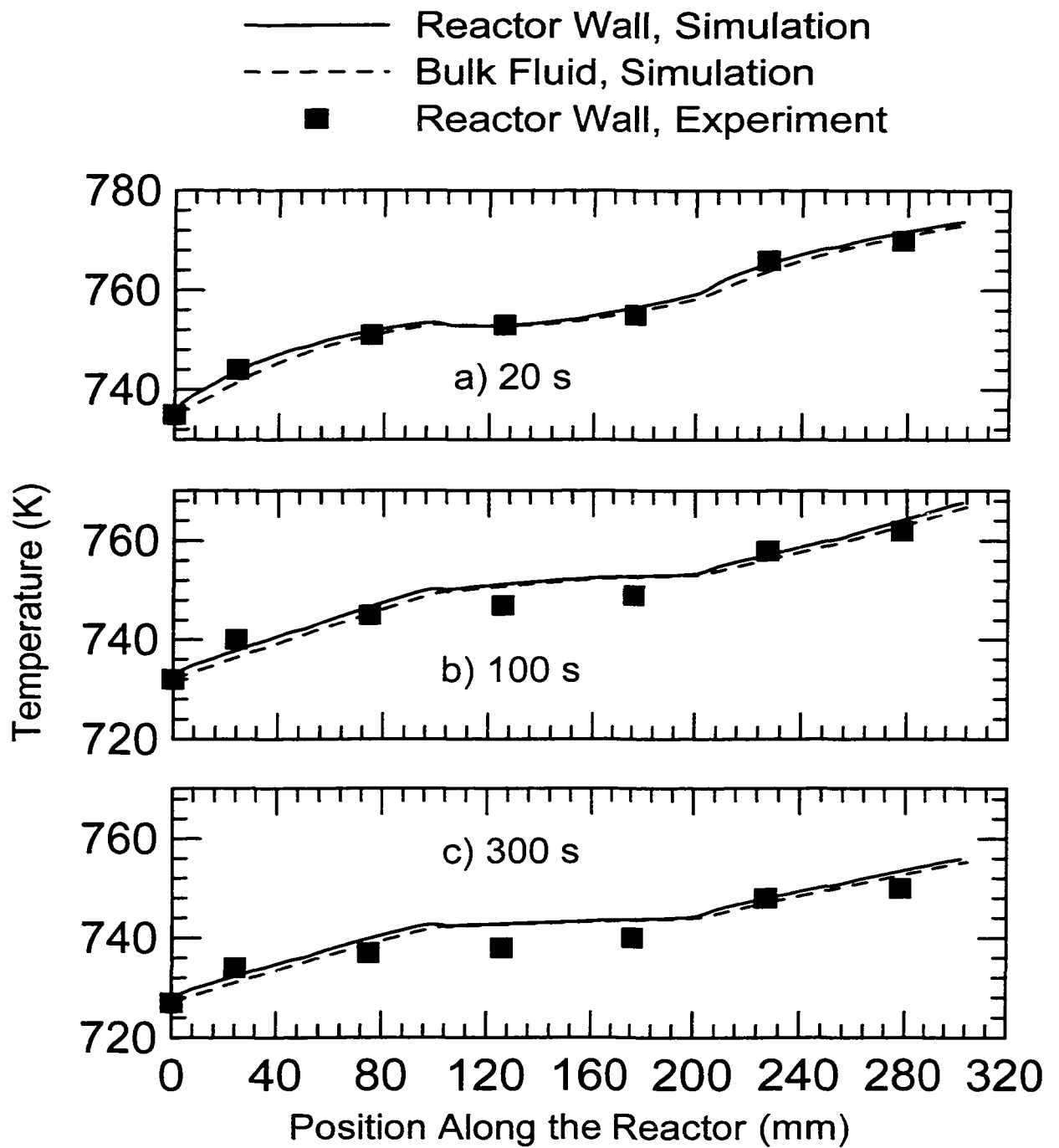


Figure 4-13 Comparison of simulated and experimental reactor temperature profiles at various elapsed times, for the case of a decrease in engine exhaust gas temperature.

## 4.7 Conclusions

Based on the study of the transient reactor operation for the dual fuel engine, the following conclusions may be drawn.

1. The 1D model using locally correct values for the heat and mass transfer coefficients and incorporating washcoat diffusion provides an acceptable model for this dual fuel engine converter combination.
2. The modified Voltz kinetics are able to predict the transient operation of the converter to a level sufficient to identify the important trends in reactor response for the dual fuel engine converter for HC and CO conversion.

## 4.8 Nomenclature

$A_1$ : Pre-exponent factor for CH<sub>4</sub> kinetics, mol · K/(m<sup>2</sup>s)

$A_2$ : Pre-exponent factor for CO kinetics, mol · K/(m<sup>2</sup>s)

$A_3$ : Pre-exponent factor for CO inhibition

$A_4$ : Pre-exponent factor for NO inhibition

$A_c$ : Cross-sectional area of channel, m<sup>2</sup>

$A_w$ : Wall cross-sectional area, m<sup>2</sup>

$a$ : Mean pore radius of washcoat, m

$[CO]_{in}$ : Reactor inlet CO concentration, ppm

$[CO]_{out}$ : Reactor outlet CO concentration, ppm

$C_b$ : Total molar concentration, mol/m<sup>3</sup>

$C_i$ : Concentration for species  $i$  in the bulk, mol/m<sup>3</sup>



- $(C_i)_S$ : Concentration for species  $i$  in the surface of washcoat, mol/m<sup>3</sup>
- $C_p$ : Constant pressure heat capacity, J/(kg · K)
- $C_{pW}$ : Constant pressure heat capacity of the wall, J/(kg · K)
- $Da$ : Dämkholer number,  $\frac{\eta(-R_A)_S D_H}{4 C_{A,S} D_{AB}}$ , dimensionless
- $D_{AB}$ : Binary diffusion coefficient, m<sup>2</sup>/s
- $(D_{eff})_i$ : Effective diffusivity in washcoat, m<sup>2</sup>/s
- $D_H$ : Hydraulic diameter,  $\frac{4A_c}{W_p}$ , m
- $(D_I)_i$ : Dispersion coefficient for species  $i$ , m<sup>2</sup>/s
- $D_T$ : Channel diameter, m
- $E_1$ : Activation energy for CH<sub>4</sub> kinetics, J/mol
- $E_2$ : Activation energy for CO kinetics, J/mol
- $E_3$ : Activation energy for CO inhibition, J/mol
- $E_4$ : Activation energy for CH<sub>4</sub> kinetics, J/mol
- $Gz$ : Graetz number,  $\frac{D_T}{z} Re Pr$ , dimensionless
- $h$ : Heat transfer coefficient, W/(m<sup>2</sup>K)
- $[HC]_{in}$ : Reactor inlet HC concentration, ppm
- $[HC]_{out}$ : Reactor outlet HC concentration, ppm
- $(\Delta H_R)_i$ : Heat of species  $i$  reaction, J/mol
- $k_f$ : Thermal conductivity of fluid, W/(m · K)
- $k_{m,i}$ : Mass transfer coefficient for species  $i$ , m / s
- $k_w$ : Thermal conductivity of converter wall, W/(m · K)

- $L$ : Effective washcoat thickness, m
- $M$ : Molar mass of a substance, g/mol
- $m$ : The power for NO inhibition in the catalytic kinetic equation
- $Nu$ : Nusselt number,  $\frac{h D_H}{k_f}$ , dimensionless
- $Nu_H$ : Nusselt number with constant heat surface flux boundary condition,  $\frac{h D_H}{k_f}$ , dimensionless
- $Nu_T$ : Nusselt number with constant wall temperature boundary condition,  $\frac{h D_H}{k_f}$ , dimensionless
- $Pr$ : Prandtl number,  $\frac{C_p \mu}{k_f}$ , dimensionless
- $R_g$ : Gas constant, 8.314 J/(mol · K)
- $R$ : Radius of Channel, m
- $Re$ : Reynolds number,  $\frac{v_m \rho D_H}{\mu}$ , dimensionless
- $(-R_i)$ : Reaction rate of species  $i$ , mol/(m<sup>2</sup>s)
- $(-R_i)_{\text{Average}}$ : Average reaction rate of species  $i$  at the washcoat, mol/(m<sup>2</sup>s)
- $(-R_i)_H$ : Rate of species  $i$  homogeneous reaction, mol/(m<sup>3</sup>s)
- $(-R_i)_S$ : Reaction Rate of species  $i$  at the external surface of washcoat, mol/(m<sup>2</sup>s)
- $Sc$ : Schmidt number,  $\frac{\mu}{\rho D_{AB}}$ , dimensionless
- $Sh$ : Sherwood number,  $\frac{k_m D_H}{D_{AB}}$ , dimensionless
- $T_b$ : Bulk mean temperature, K
- $T_S$ : Washcoat surface temperature, K

- $v_m$ : Mean axial mass average velocity, m/s  
 $W_p$ : Wetted wall perimeter, m  
 $Y_i$ : Mole fraction of species  $i$  in wet basis  
 $Y_i^*$ : Mole fraction of species  $i$  in dry basis  
 $Y_{i,b}$ : Molar fraction of species  $i$  in bulk flow  
 $(Y_{i,b})_o$ : Molar fraction of species  $i$  at the inlet of converter  
 $Y_{i,s}$ : Molar fraction of species  $i$  in washcoat

### Greek Symbols

- $\alpha$ : Thermal diffusivity,  $m^2/s$   
 $\alpha_t$ : Thermal dispersion coefficient,  $m^2/s$   
 $\rho$ : Gas mass density,  $kg/m^3$   
 $\rho_w$ : Wall density,  $kg/m^3$   
 $\eta_i$ : Effectiveness factor for species  $i$   
 $\delta_w$ : Converter effective wall thickness, m  
 $\varepsilon$ : Porosity of washcoat  
 $\tau$ : Tortuosity factor of washcoat

$\chi_{HC}$ : HC conversion over the catalytic converter:  $\chi_{HC} = \frac{[HC]_{in} - [HC]_{out}}{[HC]_{in}} \times 100\%$

$\chi_{CO}$ : CO conversion over the catalytic converter:  $\chi_{CO} = \frac{[CO]_{in} - [CO]_{out}}{[CO]_{in}} \times 100\%$

## **4.9 Abbreviations**

1D One dimensional

2D Two dimensional

NDIR Non-dispersive infra-red

FID Flame ionization detector

HC Hydrocarbons

LHHW Langmuir Hinshelwood Hougan Watson

ppm Parts per million

rpm Revolutions per minute

TWC Three-way-catalyst

## 4.10 References

- Barresi A. A., I. Mazzarino, M. Vanni and G. Baldi, "Catalytic afterburners with not fully developed flow: modelling and experimental performances", *Chem. Eng. J.* **52**, 79-88, 1993.
- Bennett C. J., R. E. Hayes, S. T. Kolaczkowski and W. J. Thomas, "An experimental and theoretical study of catalytic monolith to control automobile exhaust emissions", *Proc. Roy Soc. Lond.* **A439**, 465-483, 1992.
- Bennett C. J., S. T. Kolaczkowski and W. J. Thomas, "Determination of heterogeneous reaction kinetics and reaction rates under mass transfer controlled conditions for a monolith converter", *Trans. I. Chem. Eng.* **B69**, 209-220, 1991.
- Brauer H. W. and F. Fetting, "Stofftransport bei wandreaktion im einlaufgebeit eines strömungsrohres", *Chem. ing. Technol* **38**, 30-35, 1966.
- Checkel M. D., B. Liu, M. Zheng, E. Mirosh, "A Special Catalytic Converter for Dual Fuel Engine Light Load Emissions", Spring Technical Meeting for the Combustion Institute, Canadian Section, 25-27 May, University of Toronto, Toronto, Ontario, Canada, 1998.
- Chen D. S. K. and C. E. Cole, "Numerical simulation and experiment verification of conversion and thermal response for a Pt/Rh metal monolithic converter", SAE 890798, 1989
- Chen D. S. K., S. H. Oh, E. J. Bissett and D. L. Van Ostrom, "A three-dimensional model for the analysis of transient thermal and conversion characteristics of monolithic catalytic converters", SAE 880282, 1988.
- Douville, B., "Performance, emission and combustion characteristics of natural gas fuelling of diesel engines", M.Sc. Thesis, University of British Columbia, Vancouver, BC, 1994.
- Dryer F. L., "High temperature oxidation of carbon monoxide and methane in a turbulent flow converter", Ph. D. Thesis, Department of mechanical and aerospace engineering, Princeton University, Princeton, New Jersey, 1972.
- Germidis A., F. Castagna and J. Banaigs, "Thermal measurement inside a three-way

- catalytic converter on engine bench”, SAE 930624, 1993.
- Groppi G., A. Betolli, E. Tronconi and P. Forzati, “A comparison of lumped and distributed models of monolith catalytic combustors”, *Chem. Eng. Sci.* **50**, 2705-2715, 1995.
- Hawthorn R. D., “Afterburner catalyst effects of heat and mass transfer between gas and catalyst surface”, *AIChE Symp. Ser.* **137**, 428-438, 1974.
- Hayes R. E., S. T. Kolaczkowski and W. J. Thomas, “Finite-element model for a catalytic monolith converter”, *Comput. Chem. Eng.* **16**, 645-657, 1992.
- Hayes R. E. and S. T. Kolaczkowski, “Mass and heat transfer effects in catalytic monolith reactor”, *Chem. Eng. Sci.*, **49** 3587-3599, 1994.
- Hayes R. E., S. T. Kolaczkowski, W.J. Thomas and J. Titiloye, “Transient experiments and modeling of the catalytic combustion of methane in a monolith reactor”, *Ind. Eng. Chem. Res.*, **35** 406-414, 1996.
- Hayes R. E. and S. T. Kolaczkowski, “Introduction to catalytic combustion”, Gordon and Breach Science Publishers, Reading, UK, 1997.
- Hayes R. E. and S. T. Kolaczkowski, “A study of Nusselt and Sherwood numbers in a monolith reactor”, *Catalysis Today*, **47** 295-303, 1999.
- Heck R. H., J. Wei and R. J. Katzer, “Mathematical modeling of monolithic catalysts”, *AIChE J.* **22**, 477-484, 1976.
- Heck R. H., J. Wei and R. J. Katzer, “The transient response of a monolithic catalyst support”, *Int. Adv. Chem. Ser.* **133**, 34-45, 1974.
- Hertz R. K., “Dynamic behavior of automotive three-way emission control systems”, In *Catalysis and Automotive Pollution Control* (Edited by A. Crucq and A. Frennet), 427-444, Elsevier, Amsterdam, 1987.
- Heywood J. B., “Internal combustion engine fundamentals”, McGraw-Hill Inc., New York, 1988
- Howitt J. S. and T. C. Sekella, “Flow effects in monolithic honeycomb automotive catalytic converters”, SAE 740244, 1974.
- Karim, G. A., “An examination of Some Measures for Improving the Performance of Gas

- Fueled Diesel Engines at Light Load”, SAE 912366, 1991.
- Kuo J. C. W., C. R. Morgen and H. G. Lassen, “Mathematical modeling of CO and HC catalytic converter systems”, SAE Trans. 80, SAE710289, 1971.
- Leclerc J. P. and D. Schweich, “Modeling catalytic monoliths for automobile emission control”, in *Chemical Converter Technology for Environmentally Safe Converters and Products* (Edited by H. I. de Lasa, G. Dogu, A. Ravella.), Proceedings of NATO-ASI, Vol. 225, 547-576, Kluwer Academic Press, Dordrecht, 1993.
- Leclerc J. P., D. Schweich, S. Siemund and J. Villermaux, “An experimental study of flow and transient thermal response in a race-track monolith catalytic converter”, *Revue Inst. Fran. du Pétrol.* **49**, 681-691, 1994.
- Lee S. and R. Aris, “On the effects of radiative heat transfer in monoliths”, *Chem. Eng. Sci.* **32**, 827-837, 1977.
- Leung D., R. E. Hayes and S. T. Kolaczowski, “Diffusion limitation effects in the washcoat of a catalytic monolith reactor”, *Can. J. Chem. Eng.* **74**, 94-103, 1996.
- Li, P.K.C, “Catalytic combustion of methane in monoliths”, Ph.D. Thesis, University of Bath, Bath, UK, 1996.
- Mondt J. R., “Adapting the heat and mass transfer analogy to model performance of automotive catalytic converters”, *J. Engng. G. T. P.* 109, 200-206, 1987.
- Montreuil C. N., S. C. Williams and A. A. Adamczyk, “Modeling current generation catalytic converters: laboratory experiments and kinetic parameter optimization-steady state kinetics”, SAE 920096, 1992.
- Morgan C. R., D. W. Carlson and S. E. Voltz, “Thermal response and emission breakthrough of platinum monolithic catalytic converters”, SAE730569, 1973.
- Oh S. H. and J. C. Cavendish, “Transients of monolithic catalytic converters: response to step changes in feed stream temperature as related to controlling automobile emissions”, *Ind. Engng. Chem. Prod. Res. Dev.* **21**, 29-37, 1982.
- Oh S. H. and J. C. Cavendish, “Design aspects of poison resistant automobile monolithic catalysts”, *Ind. Engng. Chem. Prod. Res. Dev.* **22**, 509-518, 1983.

- Oh S. H. and J. C. Cavendish, "Mathematical modeling of a catalytic converter lightoff, Part I, II and III", *AIChE J.* **31**, 935-949, 1985.
- Pattas K. N., A. M. Stamatelos, P. K. Pistikopoulos, G. C. Koltsakis and P. A. Konstandinidis, "Transient modeling of 3-way catalytic converters", SAE 940934, 1994.
- Psylos A. and Philippopoulos C., "Modelling of monolithic catalytic converters used in automotive pollution control", *Appl. Math. Simulation* **16**, 484-490, 1992.
- Ryan M. J., E. R. Becker and K. Zygourakis, "Light-off performance of catalytic converters: the effect of heat/mass transfer characteristics", SAE 910610, 1991.
- Siemund S., J. P. Leclerc, D. Schweich, M. Prigent and F. Castagna, "Three-Way monolithic converter: simulations versus experiments", *Chem. Eng. Sci.* **51**, 3709-3720, 1996.
- Subramanian B. and A. Varma, "Reaction kinetics on a commercial three-way catalyst: the CO-NO-O<sub>2</sub>-H<sub>2</sub>O system", *Ind. Eng. Chem. Prod. Res. Dev.* **24**, 512-516, 1992.
- Tronconi E. and P. Forzatti, "Adequacy of lumped parameter models for SCR converters with monolith structure", *AIChE J.* **38**, 201-210, 1992.
- Ullah U., S. P. Waldram, C. J. Bennett and T. Truex, "Monolithic converters: mass transfer measurements under converter conditions", *Chem. Eng. Sci.* **47**, 2413-2418, 1992.
- Voltz S. E., C. R. Morgan, D. Liederman and S. M. Jacob, "Kinetic study of carbon monoxide and propylene oxidation on platinum catalysts", *Ind. Eng. Chem. Prod. Res. Dev.* **12**, 294-301, 1973.
- Votruba J., J. Sinkule, V. Hlaváček and J. Skrivánek, "Heat and mass transfer in monolith honeycomb catalysts", *Chem. Eng. Sci.* **30**, 117-123, 1975.
- Wendland D. W. and W. R. Matthes, "Visualization of automotive catalytic converter internal flow", SAE 861554, 1986.
- Young L. C. and B. A. Finlayson, "Mathematical models of the monolith catalytic converter: Part I. Development of model and application of orthogonal collocation", *AIChE J.* **22**, 331-343, 1976a.



- Young L. C. and B. A. Finlayson, "Mathematical models of the monolith catalytic converter: Part II. Application to automobile exhausts", *AIChE J.* **22**, 343-353, 1976b.
- Zygourakis K., "Transient operation of monolith catalytic converters: a two dimensional converter model and the effects of radially nonuniform flow distributions", *Chem. Eng. Sci.* **44**, 2075-2086, 1989.
- Zygourakis K., and R. Aris, "Multiple oxidation reactions and diffusion in the catalytic layer of monolith converters", *Chem. Eng. Sci.* **38**, 733-744, 1983.

## Chapter 5

# Modelling Study of Reverse Flow Catalytic Converter

*Chapter 5 builds up a numerical simulation model for the reverse flow catalytic converter. It is an experimental and modelling study based on the prototype reverse flow design shown in Figure 2-3 c). The catalyst is the same as that in Chapter 4, but two inactive bricks are set at each end of the reactor. The model established is a one dimensional single channel model, which uses locally correct values for the heat and mass transfer coefficients and incorporates washcoat diffusion. The model boundary condition changes with the flow direction switch. In general, the model uses the same kinetic approach as Chapter 4. However, the explicit NO<sub>x</sub> inhibition effect was removed as its essentially fixed effect could be incorporated into the apparent rate constant. The activation energy of methane catalytic reaction was found to vary with reactor temperature region for Palladium based catalyst. The kinetic data found in the low temperature are close to those found in Chapter 4. Based on the proven model, Chapter 5 evaluates the proper reverse flow switch time of reverse flow operation.*

---

Note: This chapter has been published in “SAE (Society of Automotive Engineers) 2000 Annual Congress, Michigan, USA, March 6-9, 2000”, SAE 2000-01-0213, Co-authors: M. D. Checkel, R. E. Hayes, M. Zheng and E. Mirosh. It is advised that some content of Section 5.1 and Section 5.2 may repeat material in the previous Chapters.

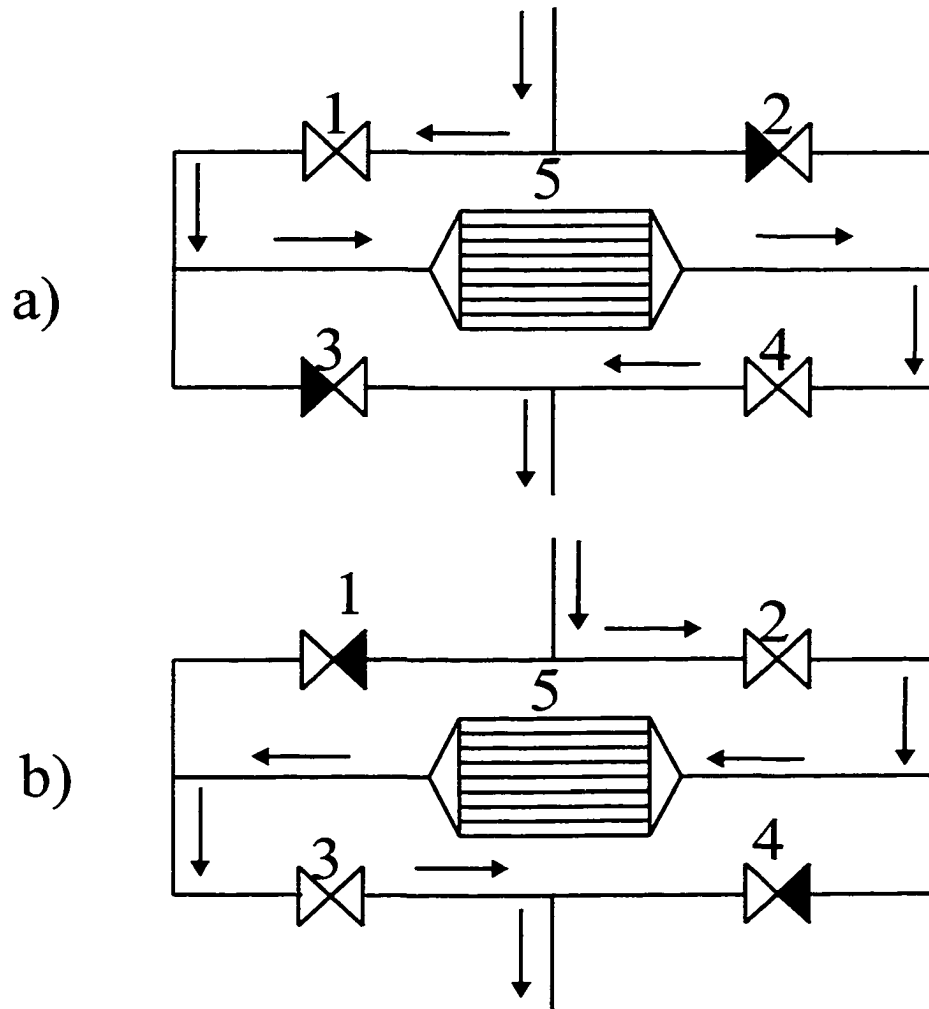
## 5.1 Introduction

Natural gas, which is predominately methane, has been considered a viable fuel for internal combustion engines as an alternative to gasoline or diesel fuel. Methane offers useful physical-chemical properties such as wide flammability range, the capability of forming homogeneous air-fuel mixtures, low photochemical reactivity, and low global toxicity of the exhaust gases compared to that from diesel engines (Gambino et al., 1993). Furthermore, its low C/H ratio permits carbon dioxide emissions to be reduced for a given engine efficiency (Corbo et al., 1995). One option is to convert existing diesel engines to run on a mixture of natural gas and diesel. In this dual fuel scenario, natural gas is the primary fuel and a diesel pilot is used as the ignition source. Dual fuel engines can maintain the high efficiency of conventional diesel engines while reducing nitric oxides ( $\text{NO}_x$ ) and particulates (Mtui, 1996). However, for light load engine operation, dual fuel engines may give a low combustion efficiency resulting in significant hydrocarbon (HC) and carbon monoxide (CO) levels in the engine exhaust (Checkel et al., 1998). Most of the HC in the dual fuel engine exhaust is methane which, although chemically resistant and toxicologically inert, is a strong "greenhouse" gas. By mass, methane has 12 to 30 times the greenhouse effect as  $\text{CO}_2$  (Deluchi et al.). Although the United States diesel engine emission standard only gives limits for the Non-Methane Hydrocarbon (NMHC) exhaust, in the European Community, Japan and Korea, the Total Hydrocarbon (THC) in the exhaust gas is considered (Zelenka et al., 1996). It is therefore necessary to use a catalytic converter in the exhaust system to reduce the HC and CO to an acceptable level.

It is a challenge to develop a catalytic converter for dual fuel engines because of

the relative unreactivity of methane. Palladium (Pd) based catalysts are the most commonly used for methane oxidation in catalytic combustion applications. A further difficulty faced in the development of a catalytic converter for methane oxidation in dual fuel engine exhaust is the low exhaust temperature at engine light load. One possible solution to low reactor gas inlet temperature is to use a reversing flow catalyst, described in the following paragraphs.

In the reversing flow reactor, the feed is periodically switched between the two ends of the reactor (Matros and Bunimovich, 1996). The concept of the reverse flow catalytic converter is shown schematically in Figure 5-1. In Figure 5-1(a) the control valves 1 and 4 are opened and the engine exhaust flows to the catalytic converter from left to right. This mode can be called the forward flow. In Figure 5-1(b) the control valves 2 and 3 are opened and the engine exhaust flows to the catalytic converter from right to left. This mode is called the reverse flow. The total cycle duration consists of these two operations, and the term switch time is used to denote the time at which the flow is changed from forward flow to reverse flow. If the forward flow time is the same as the reverse flow, the operation is referred to as symmetric reverse flow operation. If the two flow modes have different times then operating mode is referred to as unsymmetric operation.



1, 2, 3, 4: Control Valve  
 5: Catalytic Converter

Figure 5-1 Diagram of reverse flow catalytic converter.

For an exothermic reaction, the reverse flow catalytic converter exhibits what has been referred to as a “heat trap” effect, as shown in Figure 5-2. In a standard unidirectional flow operation, the converter typically exhibits a temperature profile as shown in Figure 5-2(a). The shape of the curve depends on the operating conditions, especially the inlet gas temperature. If the inlet temperature is lowered, the reaction rate will fall, and the temperature peak will migrate towards the reactor exit. At sufficiently low temperature, the reaction will effectively be extinguished and the converter will lose most of its effectiveness as the leading edge of the “hot spot” where most reaction occurs migrates out of the reactor. If a temperature pattern shown in Figure 5-2(a) or (b) is established, the reverse flow operation can then be used to take advantage of the high temperatures near the reactor exit. When the feed is switched to the “exit”, the energy stored in the reactor from the previous reaction is then effectively used to preheat the feed. Because this stored energy is added to the feed stream, it is possible to achieve temperatures higher than the adiabatic temperature rise, based on the fresh feed inlet temperature. Provided that the reactor is initially at a sufficiently high temperature and the cycle time is carefully chosen, it is possible to achieve autothermal reactor operation at feed temperatures well below those required for autothermal operation with unidirectional flow operation. In such a case a quasi-steady state operation may be achieved in which the reactor temperature profile has a maximum value near the centre of the reactor, which slowly oscillates as the feed is switched between the two ends of the reactor, as shown in Figure 5-2 (c-e). This temperature effect has been referred to as a heat sink (Matros and Bunimovich, 1996) and also a “heat trap” (Strots et al., 1998). Hanamura et al. (1993) demonstrated a reverse flow operation in which the solid phase

temperature rise was as high as 13 times the adiabatic temperature rise. Reverse flow reactors have been used industrially for the oxidation of VOC (Volatile Organic Compounds), oxidation of sulphur dioxide ( $\text{SO}_2$ ), the synthesis of methanol, and others. Typically these applications have very low gas velocity and the reverse flow cycle duration can be as high as 4 hours. Engine exhaust reactors have a much higher gas velocity and consequently a faster switching frequency is expected. The cycling time is the major factor controlling the migration and magnitude of the temperature peak, and as such should be selected with care.

This chapter describes the use of a reversing flow catalytic converter with a Pd catalyst to control the emissions from a diesel/natural gas dual fuel engine. A numerical model for the converter is developed and validated against the experimental results. The reverse flow cycling time is examined using both modelling and experiments.

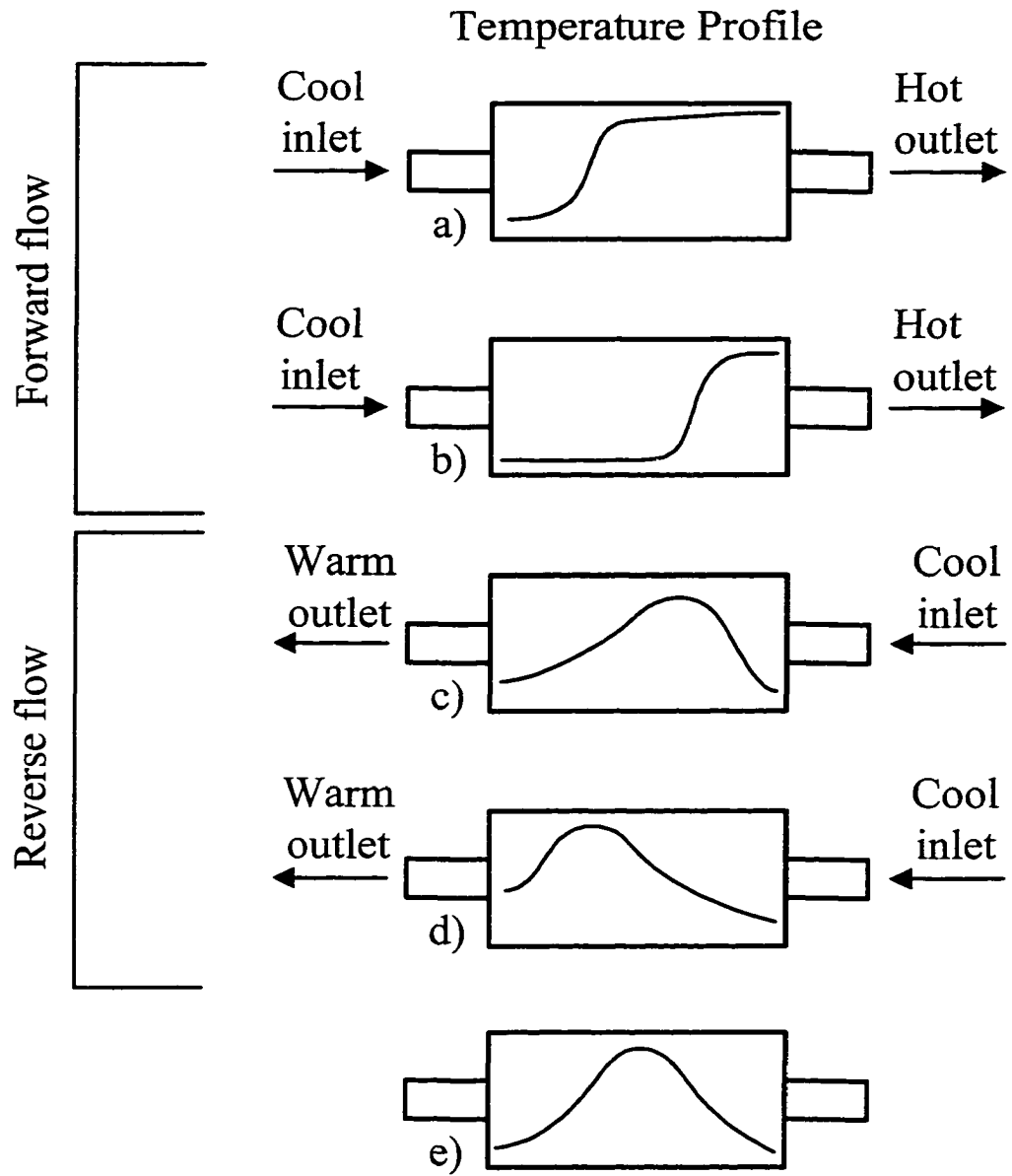


Figure 5-2 Temperature development and "heat trap" effect of reverse flow catalytic converter during the flow switch.



## 5.2 Experimental

### 5.2.1 Apparatus

Experimental engine emission data were obtained using a naturally aspirated four cylinder ISUZU 4BE1 engine of  $3.6 \times 10^{-3} \text{ m}^3$  displacement, modified to operate with a dual fuel system. The engine was installed in an eddy current dynamometer test bed equipped with a reversing flow catalytic converter. Engine speed and torque were controlled using a digital dynamometer controller and a digital throttle controller. The digital dynamometer controller was set in the RPM (engine speed) mode and the digital throttle controller was set in the position mode. For a desired engine operating condition, the engine was first set to the desired engine speed using the dynamometer controller, and then adjusted to give the desired engine torque using the “throttle” controller to control engine fueling .

The catalytic converter used a ceramic monolith honeycomb support with square channels. The converter contained six segments of monolith honeycomb in series, each measuring  $0.152 \text{ m} \times 0.152 \text{ m}$  and separated by a 2 mm gap. An inactive segment was placed at each end of the reactor. Both active and inactive segments were 0.0508 m in length. The segmented design was used to give multiple entry regions in the converter, where the heat and mass transfer coefficients are larger than in the fully developed region. The physical properties of the monolith segments are given in Table 5-1. The washcoated monolith segments were provided by Johnson-Matthey. The exhaust system containing the converter is illustrated in Figure 5-3. The gas flow direction to the converter is determined by the position of the control valve. The gas flow direction shown in Figure 5-3 is reverse flow. When the control valve is switched to the other

position, the gas flow direction will be changed to forward flow. The composition of the engine exhaust gas was determined before and after the converter using the analytical facilities which are summarized by (Liu et al., 1999). The components measured were O<sub>2</sub>, CO<sub>2</sub>, CO, NO<sub>x</sub> and HC. HC measurement provided both total hydrocarbon (THC) and CH<sub>4</sub>. The instruments were calibrated with standard gases before each test. The data were recorded on a dry basis and were converted to a wet basis using the relationship of Heywood (1988).

$$Y_i = (1 - Y_{H_2O}) Y_i^* \quad (5.1)$$

For a hydrocarbon C<sub>n</sub>H<sub>m</sub> the mole fraction of water in the exhaust was calculated using the equation:

$$Y_{H_2O} = \left( \frac{m}{2n} \right) \left( \frac{Y_{CO}^* + Y_{CO_2}^*}{1 + \frac{Y_{CO}^*}{K_1 Y_{CO_2}^*} + \left( \frac{m}{2n} \right) (Y_{CO}^* + Y_{CO_2}^*)} \right) \quad (5.2)$$

The formula C<sub>n</sub>H<sub>m</sub> represents an averaged composition that depends on the flowrate of each fuel. K<sub>1</sub> is an experimental constant with a value between 3.8 and 3.5 (Douville, 1994).

The temperature profile in the catalytic converter was measured by inserting thermocouples (T<sub>1</sub> to T<sub>6</sub>) into the catalyst segments. A single thermocouple was installed in the centre of each segment. The inlet gas temperature was measured by thermocouple, either T<sub>in1</sub> or T<sub>in2</sub>. For forward flow, T<sub>in1</sub> is inlet gas temperature and T<sub>in2</sub> is outlet gas temperature. For reverse flow, T<sub>in2</sub> is the inlet gas temperature and T<sub>in1</sub> is the outlet gas temperature.

Table 5-1 The Main Physical Parameters of the Converter

Wall Density $\rho_w$	2500 kg/m <sup>3</sup>
Wall Thermal Conductivity $k_w$	2 W/(m.K)
Wall Heat Capacity $C_{p,w}$	1400 J/(kg. K)
Effective Wall Thickness	0.25 mm
Average Thickness of Washcoat Layer	0.05 mm
Porosity of Washcoat	0.41
Channel Hydraulic Diameter, $D_H$	1.4 mm
Channel Open Frontal Area	1.96 mm <sup>2</sup>
Porosity of Monolith	72%
Size of Each Brick (Length x Width xHeight)	50.8mm x152.4mm x 152.4mm

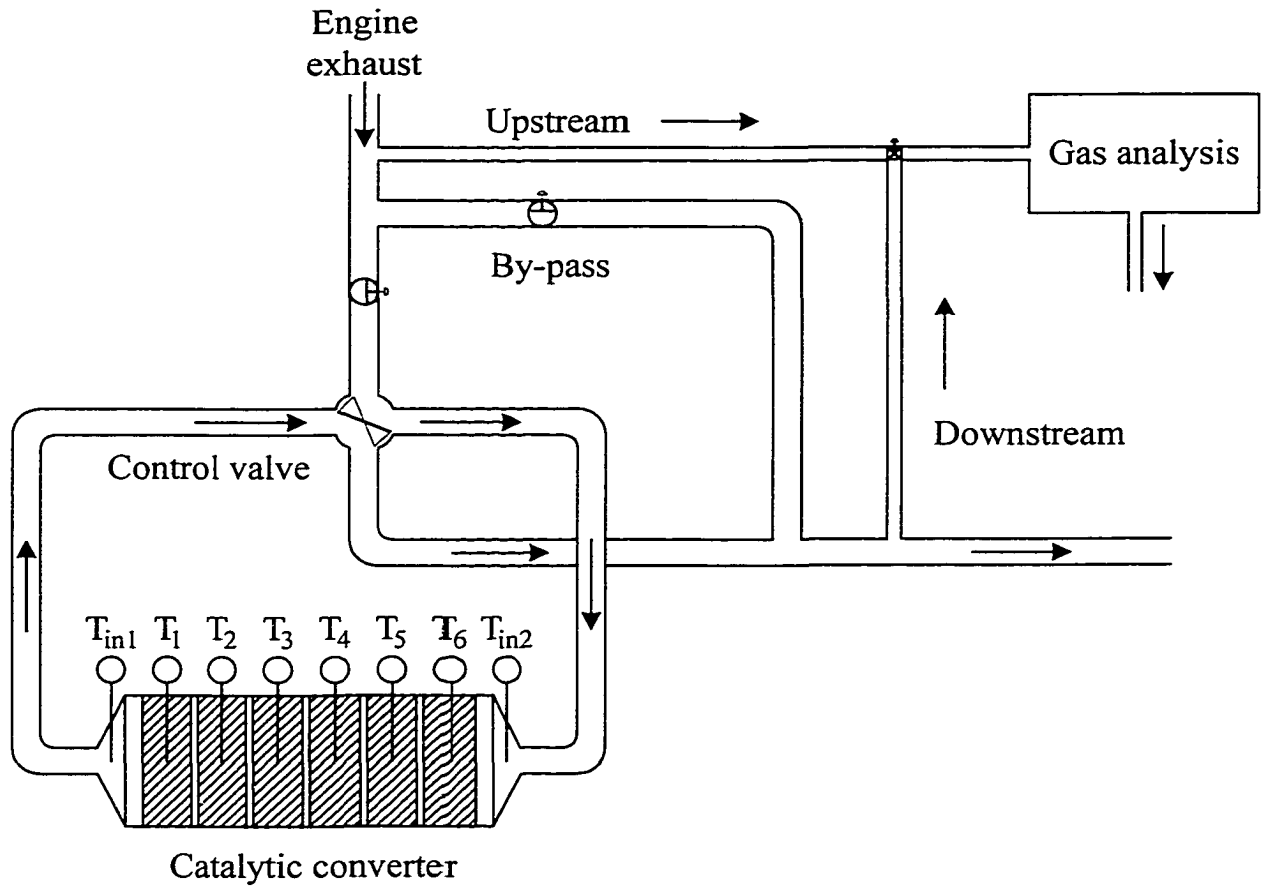


Figure 5-3 Experimental set-up

### 5.2.2 Experimental Results

In this section some experimental data of reverse flow operation with variable cycle time are presented. For the experiment described in the following, the catalytic converter was initially heated by running the engine at a relative heavy load which provided a high exhaust temperature, which was sufficient to achieve a large degree of conversion. The flow direction in the catalytic converter was manually controlled to establish a temperature profile with a temperature peak in the middle of the reactor, as shown in Figure 5-4. Once this point was reached, the reverse flow operation was started and the engine operating conditions were changed to a light load of 1500 RPM and 80 N·m (12 kW). This new engine mode had an exhaust temperature as low as 257°C, which was lower than the autothermal temperature of the catalyst. The HC and CO concentrations in this low-load exhaust were higher than in the previous heavy load mode.

The complete reverse flow operation consisted of 37 cycles ranging in duration from 30 seconds to 75 seconds. Both symmetric and unsymmetric cycles were used: Table 5-2 gives the details for the 37 cycles.

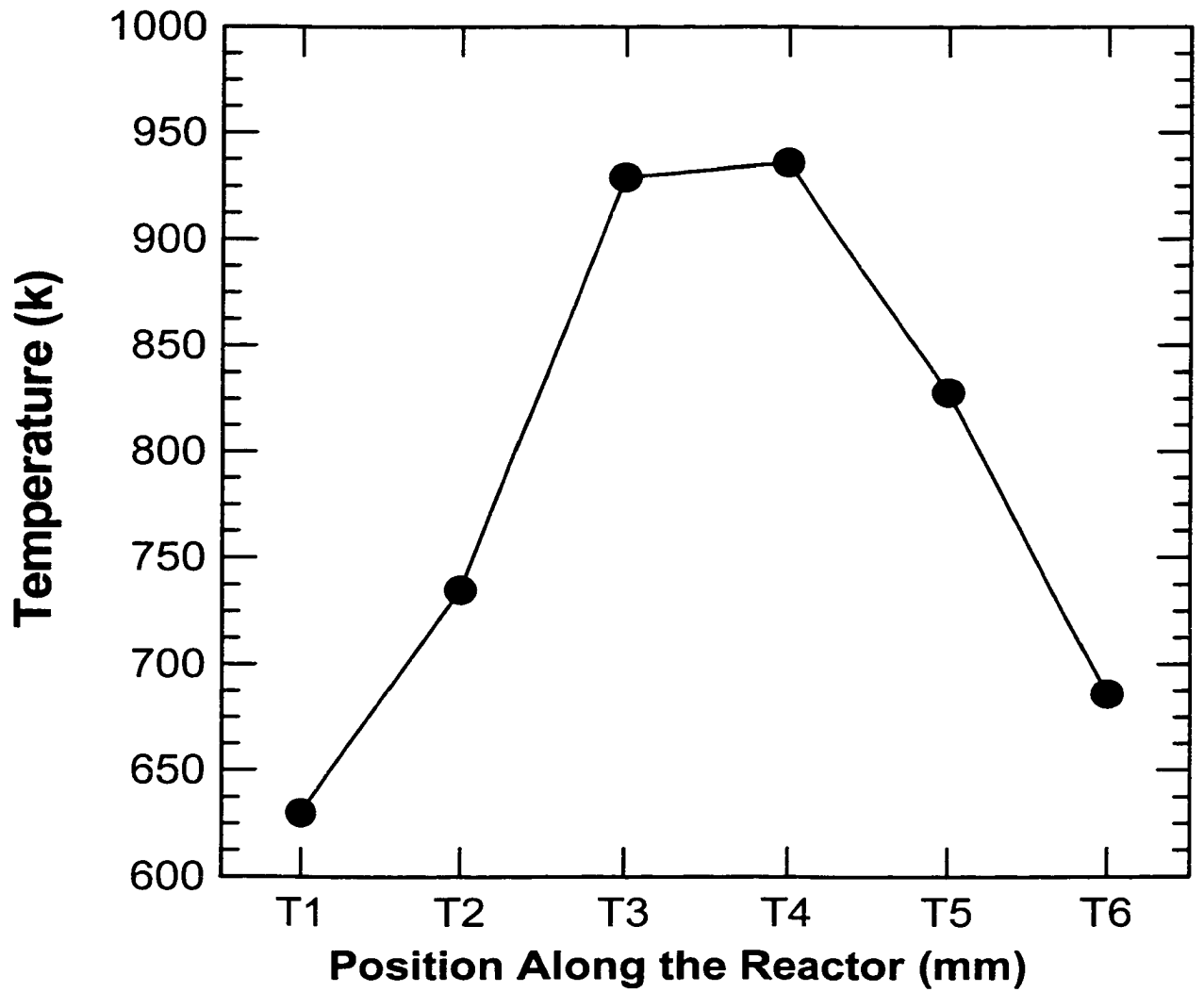


Figure 5-4 Initial reactor temperature profile for reverse flow operation with variable cycling time

Table 5-2 Experiment with Variable Cycling Time

Cycle Number	Forward Flow Time (s)	Reverse Flow Time (s)	Cycle Duration (s)
1	25	20	45
2	25	20	45
3	20	20	40
4	35	35	70
5	25	15	40
6	20	20	40
7	25	25	50
8	25	10	35
9	20	20	40
10	25	15	40
11	20	20	40
12	25	20	45
13	20	15	35
14	25	20	45
15	25	20	45
16	15	20	35
17	20	15	35
18	15	15	30
19	20	10	30
20	15	15	30
21	20	15	35
22	15	20	35
23	40	35	75
24	35	35	70
25	35	30	65
26	30	35	65
27	35	30	65
28	40	30	70
29	35	30	65
30	30	30	60
31	35	30	65
32	35	35	70
33	35	30	65
34	35	30	65
35	40	30	70
36	35	30	65
37	35	30	65

Figure 5-5 shows the middle reactor temperatures corresponding to thermocouples  $T_3$  and  $T_4$  as a function of time. Up to 885 seconds, the total cycle duration was short (around 40 seconds) and the reactor temperature exhibited a general upward trend. At cycle number 23 (from 885 to 960 second) the cycle time was increased to a forward flow time of 40 seconds and reverse flow time of 35 seconds for total cycle duration of 75 seconds. This longer cycling caused a downward trend in the reactor temperature. In spite of the downward trend, the reactor was maintained at a sufficiently high temperature to achieve high methane conversion (about 85%) and carbon monoxide conversion (about 93% ) for more than half a hour, as shown in Figure 5-6.

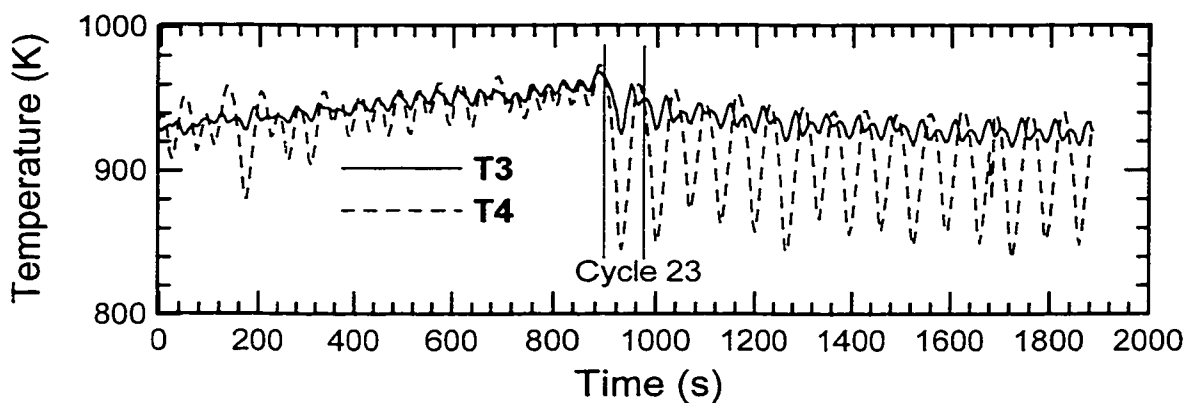


Figure 5-5 The maximum reactor temperature  $T_3$  and  $T_4$  varies with reverse flow cycling.



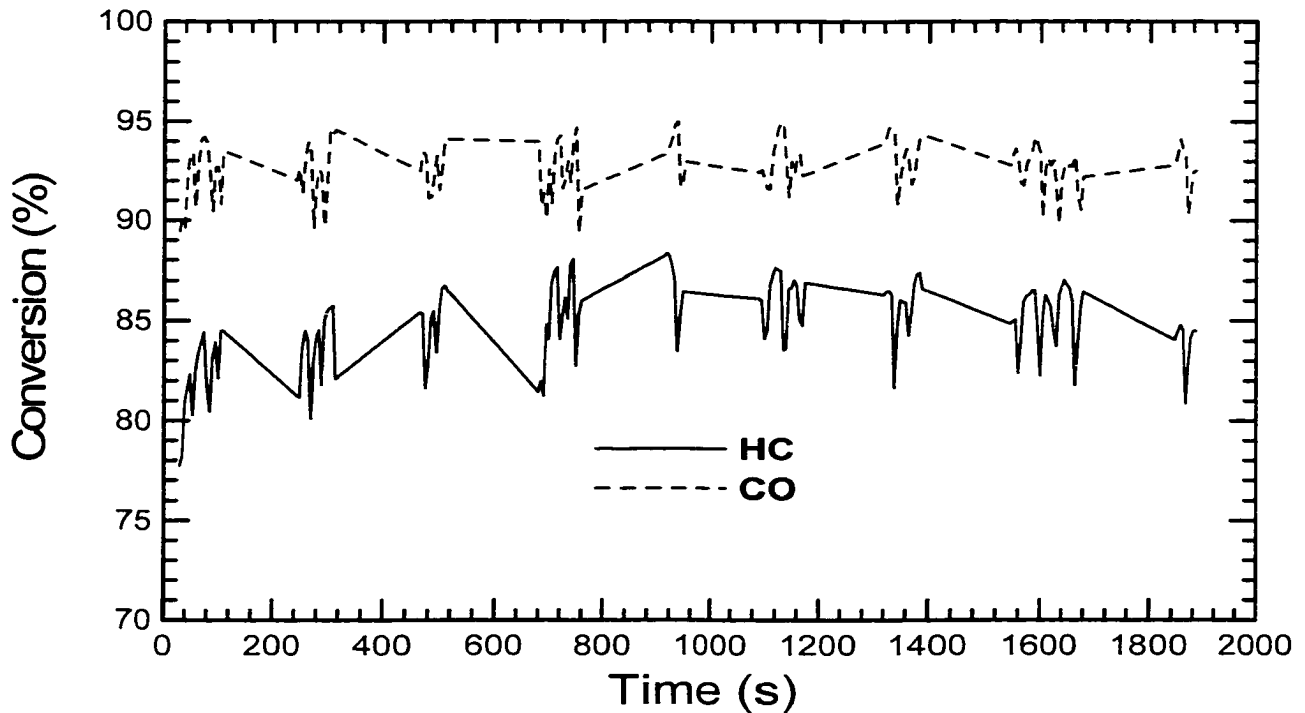


Figure 5-6 HC and CO Conversion varies with reverse flow cycling

However, for the same engine operation, if the engine exhaust flowed to the catalytic converter unidirectionally, the reactor temperature was very low, as shown in Figure 5-7. The middle reactor temperature  $T_3$  and  $T_4$  declined with time with the engine exhaust gas temperature dropping because the engine was run slightly high load before it was switched to 1500 RPM, 80N.m. This low reactor temperature gave very low HC conversion (about 10%), as shown in Figure 5-8, although the CO conversion was maintained higher than 90%. This results shows that the reverse flow operation is superior to unidirectional flow at such a light engine load.

In the following section, a reverse flow model is first established and evaluated by the experimental data. Then it is used to evaluate reactor performance with different cycling time.

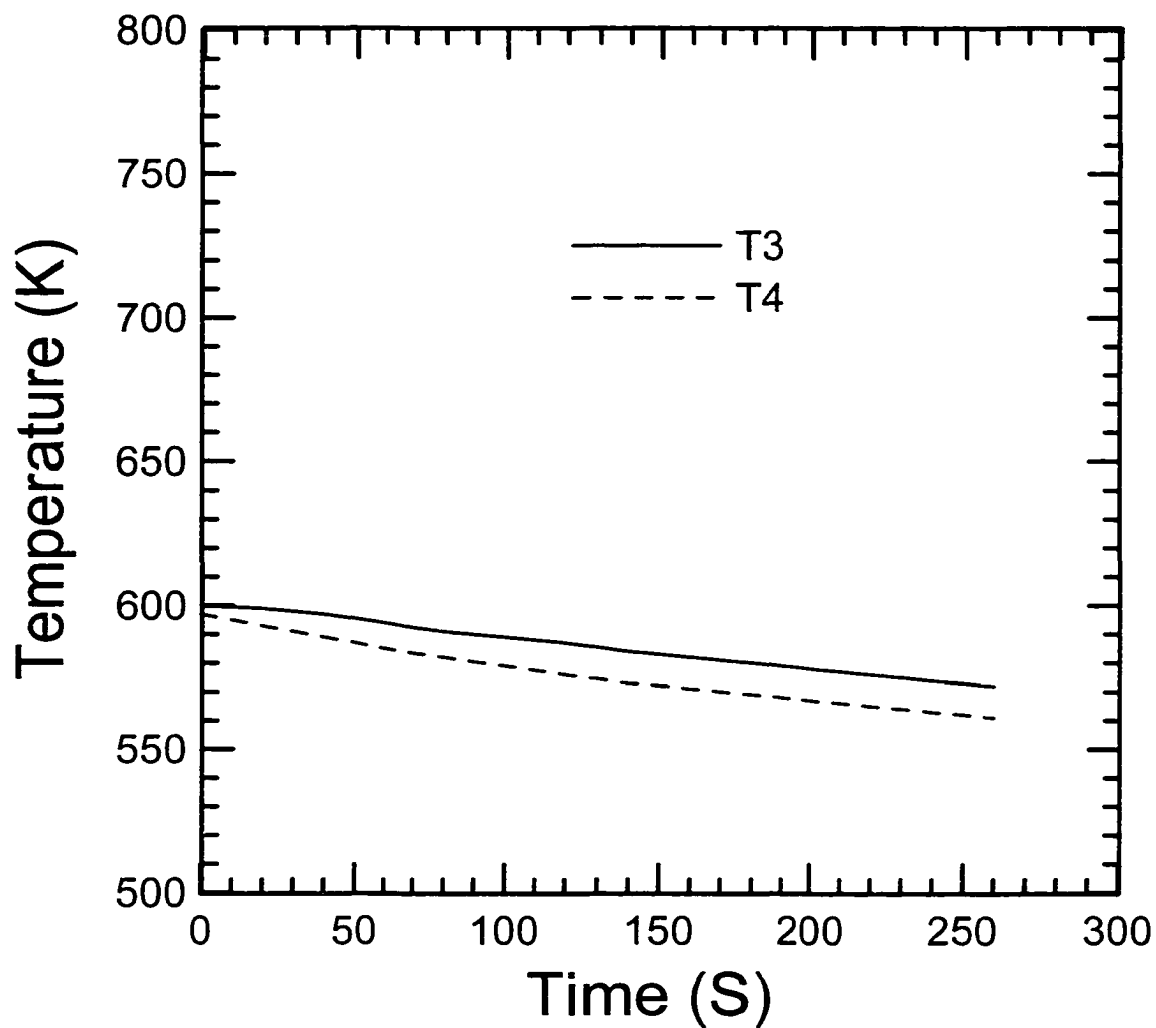


Figure 5-7 The middle reactor temperature  $T_3$  and  $T_4$  under unidirectional flow.

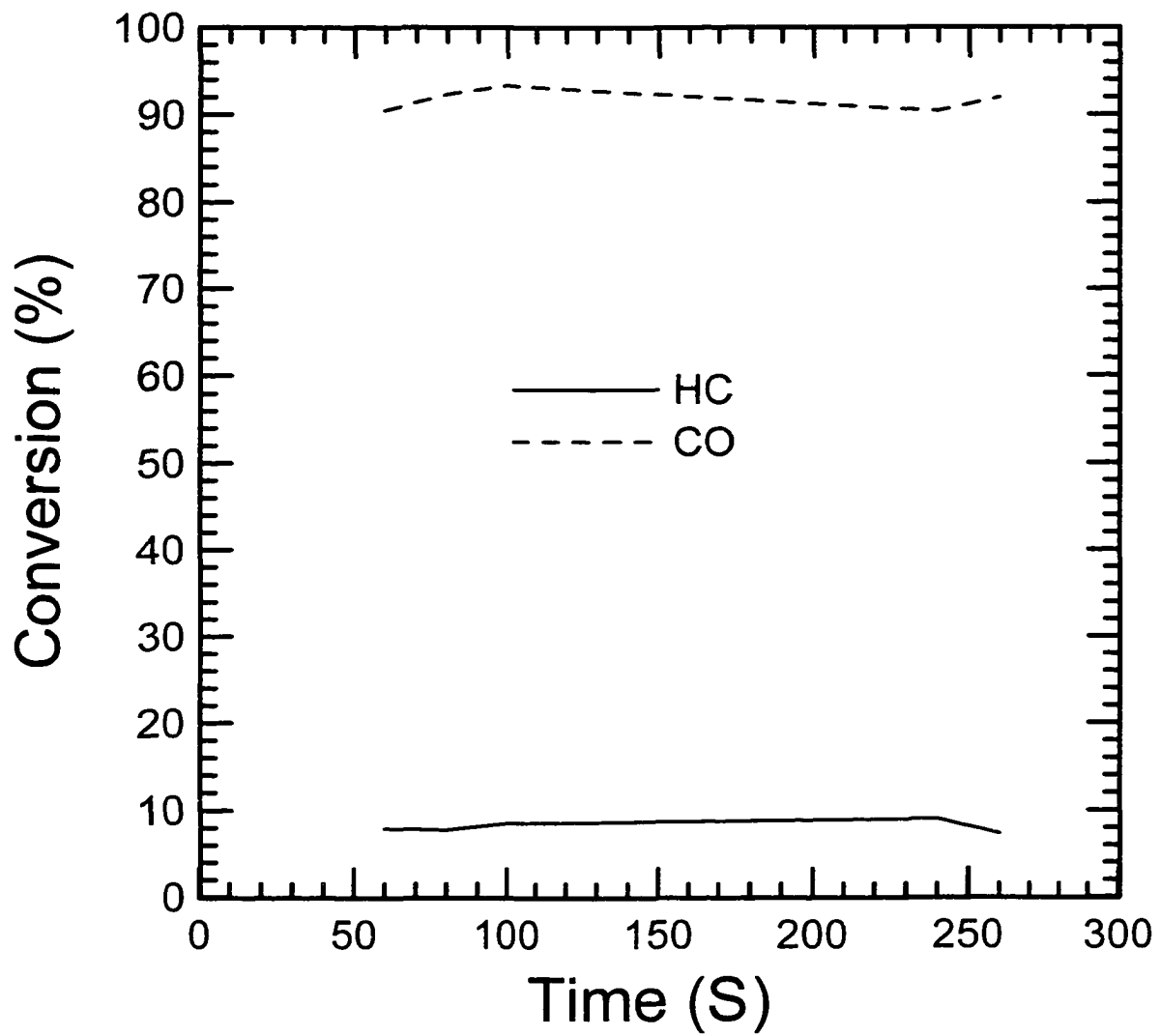


Figure 5-8 HC and CO conversion under unidirectional flow.

## **5.3 Mathematical Model**

### **5.3.1 Assumptions**

The monolith reactor was simulated using a one dimensional, single channel model, which assumes that all of the channels in the reactor experience similar operating conditions. As noted in Hayes and Kolaczowski (1997), for small channels under the operating conditions found in this converter, the 1D model provides a very close agreement to the 2D model, and offers a greatly reduced computational time. The 1D model ignores radial temperature and concentration gradients, and assumes that all of the channels in the reactor experience the same operating conditions. Other major assumptions are listed below:

- The gas is assumed to be a variable density ideal gas.
- The transition of concentration during the instant of the flow switch is ignored.
- The pressure in the reactor is constant, that is, the pressure drop is zero and pressure fluctuations resulting from flow pulsation are ignored.
- In the transient model, the gas phase is in a pseudo-steady state with the wall. This assumption is valid because of the widely differently time scales governing the transient terms in the solid and gaseous phases.
- Accumulation of mass in the washcoat is ignored.
- Washcoat diffusion is included.
- The mole average velocity is taken to be equal to the mass average velocity.

### 5.3.2 Model Equations

The one-dimensional model equations given in the following are based on those given in Hayes and Kolaczowski (1997). Two reacting species were modelled, CO and CH<sub>4</sub>. The mole balance equations for the fluid phase are:

$$\frac{d}{dz} \left( (D_l)_{\text{CH}_4} C_b \frac{dY_{\text{CH}_4,b}}{dz} \right) - \frac{d(C_b v_m Y_{\text{CH}_4,b})}{dz} - (-R_{\text{CH}_4})_H - \frac{4}{D_H} k_{m,\text{CH}_4} C_b (Y_{\text{CH}_4,b} - Y_{\text{CH}_4,s}) = 0 \quad (5.3)$$

$$\frac{d}{dz} \left( (D_l)_{\text{CO}} C_b \frac{dY_{\text{CO},b}}{dz} \right) - \frac{d(C_b v_m Y_{\text{CO},b})}{dz} - (-R_{\text{CO}})_H - \frac{4}{D_H} k_{m,\text{CO}} C_b (Y_{\text{CO},b} - Y_{\text{CO},s}) = 0 \quad (5.4)$$

The bulk fluid energy balance equation is:

$$\frac{d}{dz} \left( \alpha_l \frac{dT_b}{dz} \right) - v_m \frac{dT_b}{dz} - \sum_{i=1}^n \frac{(\Delta H_R)_i}{pc_p} (-R_i)_H + \frac{4}{D_H} \frac{h}{\rho C_p} (T_s - T_b) = 0 \quad (5.5)$$

The boundary conditions for Equations (5.3), (5.4) and (5.5) are:

At the reactor inlet:

$$Y_{\text{CH}_4} = (Y_{\text{CH}_4})_0 \quad Y_{\text{CO}} = (Y_{\text{CO}})_0 \quad T_b = T_{b0}$$

At the reactor outlet:

$$\frac{dY_{\text{CH}_4,b}}{dz} = 0, \quad \frac{dY_{\text{CO},b}}{dz} = 0, \quad \frac{dT_b}{dz} = 0$$

The inlet for forward flow switches to the outlet for reverse flow and vice versa. When laminar flow is modelled using a one dimensional model, the effective dispersion coefficient for the mole and energy balance equations are (Hayes and Kolaczowski, 1997):

$$D_f = D_{AB} + \frac{v_m^2 R^2}{48 D_{AB}} \quad \text{and} \quad \alpha_f = \alpha + \frac{v_m^2 R^2}{48 \alpha} \quad (5.6)$$

The mole balance equations for the solid phase are:

$$k_{m,CH_4} C_b (Y_{CH_4,b} - Y_{CH_4,s}) = \eta_{CH_4} (-R_{CH_4})_s \quad (5.7)$$

$$k_{m,CO} C_b (Y_{CO,b} - Y_{CO,s}) = \eta_{CO} (-R_{CO})_s \quad (5.8)$$

The energy balance equation for the solid phase is:

$$\frac{\partial}{\partial z} \left( k_w \delta_w \frac{\partial T_s}{\partial z} \right) - h(T_s - T_b) - \sum_{i=1}^n \eta_i (\Delta H_R)_i (-R_i)_s = \delta_w \rho_w C_{pw} \frac{\partial T_s}{\partial t} \quad (5.9)$$

The boundary condition for Equation (5.9) are the same for reactor inlet and outlet:

$$\frac{dT_s}{dz} = 0$$

The initial condition is:

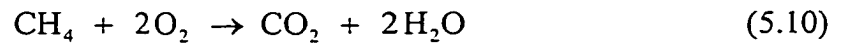
$$t=0: T_s = T_{s0}$$

Note that dependence on time,  $t$ , only appears in equation (5.9), the solid phase energy equation. The time constant for the fluid phase is approximately 1000 times shorter than that of the solid phase so the fluid phase equations are formatted as quasi-steady state and the system responds with time at a rate determined by the solid phase. The assumption of zero temperature gradient at either end of the reactor would appear to limit the general application of this model. However, it has been used by Hayes and Kolaczkowski (1997). In addition, the normal operation of the reverse flow catalytic

converter produces a high temperature peak at the center of the reactor and low gradients at the entrance and exit.

### 5.3.3 Kinetics

The main hydrocarbon in the exhaust of a dual fuel engine is methane which, together with carbon monoxide, comprise the primary pollutants in the exhaust gas. The oxidation of CH<sub>4</sub> and CO can be represented by the following overall reactions:



These reactions are both highly exothermic. The enthalpies of reaction in kJ/mol can be written as the following functions of temperature:

$$(\Delta H_R^\circ)_{\text{CH}_4} = -806.9 + 1.586 \times 10^{-2} T - 8.485 \times 10^{-6} T^2 - 3.963 \times 10^{-9} T^3 + 2.16 \times 10^{-12} T^4 \quad (5.12)$$

$$(\Delta H_R^\circ)_{\text{CO}} = -279.581 - 1.861 \times 10^{-2} T + 2.52 \times 10^{-5} T^2 - 1.2247 \times 10^{-8} T^3 + 2.255 \times 10^{-12} T^4 \quad (5.13)$$

The kinetics of the reactions involved in automotive catalytic converters have been widely studied for gasoline engines, although most modelling studies use modified versions of the expressions proposed by Voltz et al. (1973); see, for example, Oh and Cavendish (1982), and Siemund et al. (1996). The expressions of Voltz et al. (1973) consider the oxidation of CO and HC in the presence of NO<sub>x</sub>. For the hydrocarbon

oxidation, the reaction is first order in HC and oxygen, and inhibited by CO and NO<sub>x</sub>. For the Pd catalyst in an excess of oxygen, the NO<sub>x</sub> concentration remains constant, and if an inhibition effect is present it can be effectively included in the overall rate constant. Furthermore, with a lean, dual fuel exhaust, oxygen was present in excess, so its concentration is essentially constant. Other investigators (see, for example, Cullis and Willatt, 1983) also have proposed a first order reaction rate in terms of hydrocarbon concentration but zero order in oxygen. Furthermore, several investigators (Cullis and Willatt, 1983; Kolaczkowski et al., 1996) have demonstrated that in the region of 750 K the activation energy for the oxidation of methane changes rather sharply. For example, Kolaczkowski et al. (1996) reported an activation energy of 131 kJ/mol below 770 K, and a value of 19 kJ/mol above 770 K. The high temperature value was recorded in the region of strong washcoat diffusion limitation, and therefore the true activation energy in this temperature region would have been about 38 kJ/mol. Cullis and Willatt (1983) reported high temperature activation energies in the range 24 to 45 kJ/mol and low temperature values in the range of 84 to 92 kJ/mol (for Pd on alumina catalysts). In the reverse flow reactor used in this study, the temperature range covered this transition region, and it was found that two activation energies were required to model the experimental results well. The rate equations based on the Voltz et al. (1973) model had the following form:

$$\left(-R_{\text{CH}_4}\right)_s = k_{\text{CH}_4} \frac{Y_{\text{CH}_4,s} Y_{\text{O}_2,s}}{R(\theta)} \quad (5.14)$$

$$\left(-R_{\text{CO}}\right)_s = k_{\text{CO}} \frac{Y_{\text{CO},s} Y_{\text{O}_2,s}}{R(\theta)} \quad (5.15)$$

$$R(\theta) = T_s \left[1 + k_{a1} Y_{\text{CO},s}\right]^2 \quad (5.16)$$



$$k_{\text{CH}_4} = A_1 \exp\left(\frac{-E_1}{R_g T}\right) \quad (5.17)$$

$$k_{\text{CO}} = A_2 \exp\left(\frac{-E_2}{R_g T}\right) \quad (5.18)$$

$$k_{a1} = A_3 \exp\left(\frac{-E_3}{R_g T}\right) \quad (5.19)$$

Note that the explicit NOx inhibition effect shown in equation (4.15) has been removed from equation (5.16). The low and essentially constant concentration of NO made this term relatively unimportant so NOx inhibition has been effectively incorporated into the rate constant.

The kinetic constants in the rate equations are unique to each catalyst formulation. The following values gave a good agreement for the reverse flow converter studied in this investigation:

For CH<sub>4</sub> in low temperature region (less than 780 K):

$$A_1 = 6.572 \times 10^{12} \text{ mol.K}/(\text{m}^2.\text{s}), \quad E_1 = 1.29 \times 10^5 \text{ J/mol}$$

For CH<sub>4</sub> in high temperature region (greater than 780 K):

$$A_1 = 3.853 \times 10^6 \text{ mol.K}/(\text{m}^2.\text{s}), \quad E_1 = 3.5 \times 10^4 \text{ J/mol}$$

For the CO kinetic constants and the adsorption constant at all temperatures:

$$A_2 = 1.553 \times 10^8 \text{ mol.K}/(\text{m}^2.\text{s}), \quad E_2 = 5.5 \times 10^4 \text{ J/mol}$$

$$A_3 = 65.5, \quad E_3 = 7990 \text{ J/mol}$$

The model includes CO homogeneous oxidation (that is, gas phase reaction) and the rate expression proposed by Dryer (1972) was used:

$$(-R_{\text{CO}})_H = 1.26 \times 10^{10} \exp\left(-\frac{20131}{T_b}\right) C_{\text{CO},b} C_{\text{O}_2,b}^{0.25} C_{\text{H}_2\text{O},b}^{0.5} \quad (5.20)$$

The homogeneous reaction of methane was ignored in the model since its reaction is negligible at the catalytic converter.

### 5.3.4 Heat and Mass Transfer Coefficients

The one-dimensional model requires values for the local heat and mass transfer coefficients. These values were obtained from the Nusselt and Sherwood numbers, and included the entry length effects. The entry length is important because of the segmented design used in the converter. In this investigation, it was assumed that the channels could be approximated as cylindrical ducts for the purposes of calculating heat and mass transfer coefficients. Although the channels of the ceramic substrate are square, the application of the washcoat tends to round the corners, so a round channel is a better approximation than a square one (Hayes and Kolaczkowski, 1994). For constant wall temperature, the Nu number for simultaneously developing thermal and hydrodynamic boundary layers for a gas with a Prandtl number of 0.7 is (Tronconi and Forzatti, 1992):

$$Nu_T = 3.657 + 8.827 \left(\frac{1000}{Gz}\right)^{-0.524} \exp\left(-\frac{48.2}{Gz}\right) \quad (5.21)$$

The correlation for simultaneously developing flow at a Prandtl number of 0.7 with constant wall flux is (Hayes and Kolaczkowski, 1997):

$$Nu_H = 4.364 + 13.18 \left( \frac{1000}{Gz} \right)^{-0.524} \exp \left( -\frac{60.2}{Gz} \right) \quad (5.22)$$

The local Nu value in a system with chemical reaction at the wall was approximated by interpolating between  $Nu_T$  and  $Nu_H$  using the interpolation formula of Brauer and Fetting (1966):

$$\frac{Nu - Nu_H}{Nu_T - Nu_H} = \frac{Da Nu}{(Da + Nu) Nu_T} \quad (5.23)$$

The Graetz number,  $Gz$ , and the Damköhler number,  $Da$ , are defined for an arbitrary reaction of component A by:

$$Gz = \frac{D_T Re Pr}{z} \quad (5.24)$$

$$Da = \frac{\eta(-R_A)_S D_H}{4 C_{A,S} D_{AB}} \quad (5.25)$$

The Sherwood number was obtained by substituting the Schmidt number,  $Sc$ , for the Prandtl number in the equation for Graetz number, that is, Equation (5.24).

### 5.3.5 Effectiveness Factor

It has been shown (Hayes and Kolaczkowski, 1994; Leung et al., 1996) that diffusion in the washcoat can be significant at typical reactor operating conditions, and must be included in the reactor model. The effectiveness factor can be used to quantify the effect of the diffusion in the catalyst, and is defined for reactant A as:

$$\eta = \frac{\text{Average Rate for the catalyst washcoat}}{\text{Rate evaluated at the surface conditions}} = \frac{(-R_A)_{\text{Average}}}{(-R_A)_S} \quad (5.26)$$

Both methane and carbon monoxide react in the washcoat. The effectiveness factor for each reaction was determined by approximating the washcoat as an isothermal flat plate and solving the appropriate mole balance equations. The mole balance equations for CO and CH<sub>4</sub> are:

$$(D_{\text{eff}})_{\text{CH}_4} C \frac{dY_{\text{CH}_4}^2}{dx^2} - \frac{(-R_{\text{CH}_4})}{L} = 0 \quad (5.27)$$

$$(D_{\text{eff}})_{\text{CO}} C \frac{dY_{\text{CO}}^2}{dx^2} - \frac{(-R_{\text{CO}})}{L} = 0 \quad (5.28)$$

The boundary condition for Equations (5.27) and (5.28) are:

$$\text{at } x = 0: \frac{dY_{\text{CO}}}{dx} = 0 \quad \text{and} \quad \frac{dY_{\text{CH}_4}}{dx} = 0$$

$$\text{at } x = L \text{ (washcoat surface): } Y_{\text{CO}} = Y_{\text{CO},S} \quad \text{and} \quad Y_{\text{CH}_4} = Y_{\text{CH}_4,S}$$

$(D_{\text{eff}})_{\text{CH}_4}$  and  $(D_{\text{eff}})_{\text{CO}}$  are the effective diffusivities of methane and carbon monoxide in the washcoat based on the entire cross sectional area of the catalyst, both catalyst and pores, and include terms for the catalyst porosity and tortuosity. The diffusion in the pores of a typical monolith reactor washcoat is dominated by Knudsen diffusion, and therefore the effective diffusion coefficient can be written as:

$$D_{\text{eff}} = \frac{\varepsilon}{\tau} 97 a \left( \frac{T}{M} \right)^{1/2} \quad (5.29)$$

The tortuosity factor for the washcoat was taken as 8.0, the washcoat porosity was 0.41 and the mean pore diameter 10 nanometers (Li, 1997).

## 5.4 Reverse Flow Cycling Time Evaluation

### 5.4.1 Model Verification

This model was first evaluated by the simulation of reverse flow operation at a low load engine mode 1500 RPM and 80 N·m. This engine mode had a steady engine exhaust gas composition, which is shown in Table 5-3. In this simulation, six 30 second cycles were simulated. Each cycle consisted of 15 seconds of forward flow and 15 seconds of reverse flow.

Table 5-3 Engine Exhaust Parameters for 1500 rpm, 80 Nm

Engine Mode		Exhaust Composition						Texh. (K)	Mass Flow Rate (g/s)
Speed (rpm)	Torque (Nm)	HC (ppm)	CO (ppm)	NO (ppm)	O <sub>2</sub> (%)	CO <sub>2</sub> (%)	H <sub>2</sub> O (%)		
1500	80	4724	1816	249	13.33	3.46	6.82	535	45.82

Texh.: Engine Exhaust Temperature

N<sub>2</sub>: Balance of Engine Exhaust Composition

The transient simulations required an initial condition to be given. The initial condition used in the model was the experimentally measured reactor temperature profile at the time denoted zero, as shown in Figure 5-9. The inlet gas temperature was the experimentally measured inlet gas temperature, which was a function of time during the reverse flow cycling, as shown in Figure 5-10. It was found that the inlet temperature varied from 585 K to 680 K, with the reverse flow inlet side running hotter than the forward flow side. In other words, the forward flow inlet temperature was not equal to the reverse flow inlet for this “symmetric” reverse flow operation. This effect was a

result of the previous mode of the system. Prior to commencing a reverse flow sequence, the converter was usually run in unidirectional flow mode. This operation increases the exhaust gas temperature, which results in the outlet side ductwork becoming hotter than the inlet ductwork. When the engine load was reduced, which lowered the exhaust temperature, some of the energy stored in the ductwork is transferred to the fluid. With reverse flow operation, the initially higher solid temperature on the reverse flow cycle inlet side causes a higher inlet gas temperature than on the forward flow side.

The conversion of HC and CO at the reactor exit were plotted as a function of time for both experimental and simulated values in Figure 5-11. It was seen that the conversion of the reactor was reasonably well approximated by the model. The development of the reactor temperature in different locations as a function of time during the reverse flow cycling is shown in Figure 5-12. The solid line is the simulation and the dotted line the experimental result. The agreement between the two is good, which indicates that the model gives a reasonable approximation of the reactor performance for the temperature range used.

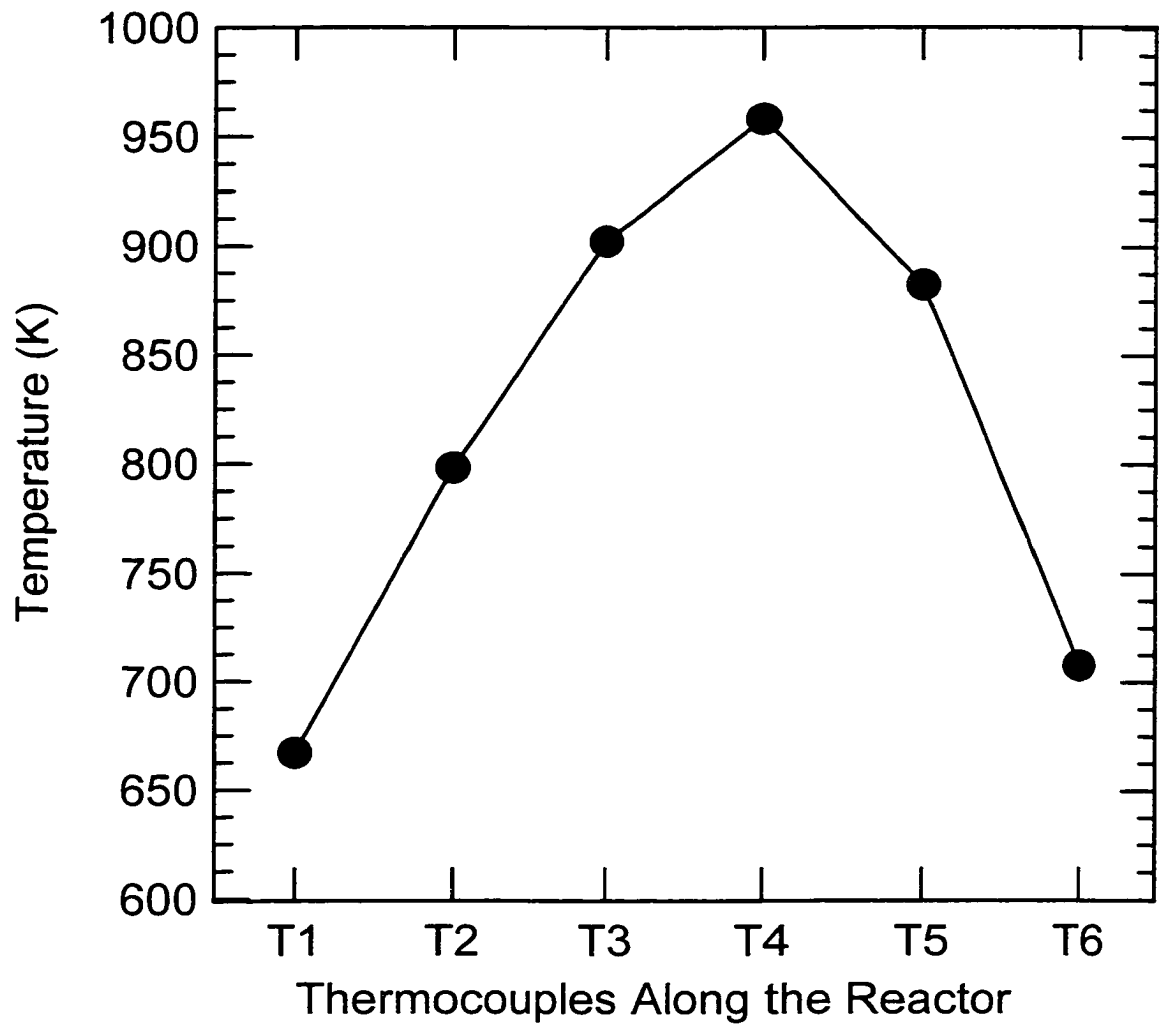


Figure 5-9 The initial reactor temperature profile for starting simulation



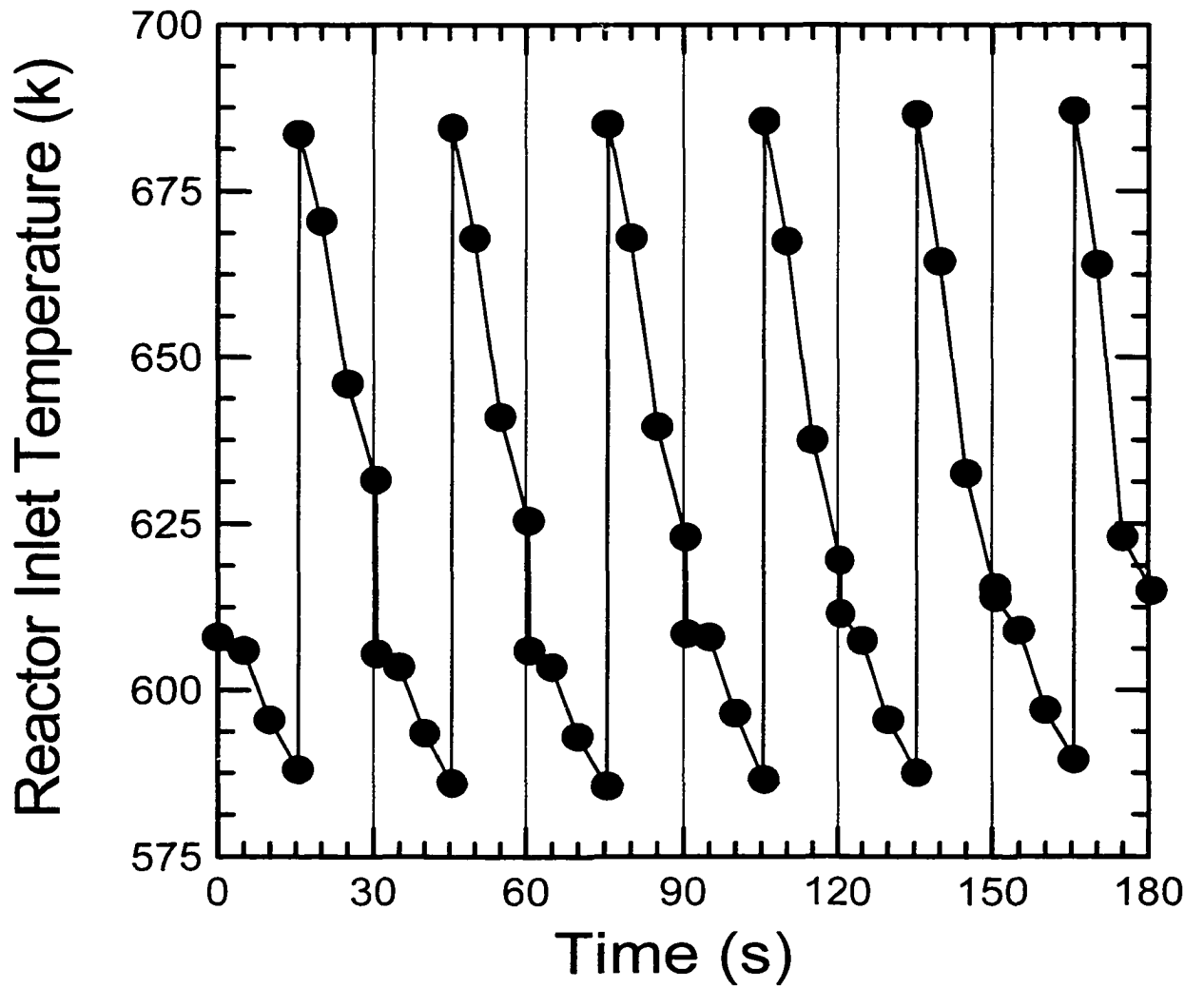


Figure 5-10 The transient converter inlet temperature for the reverse flow simulation

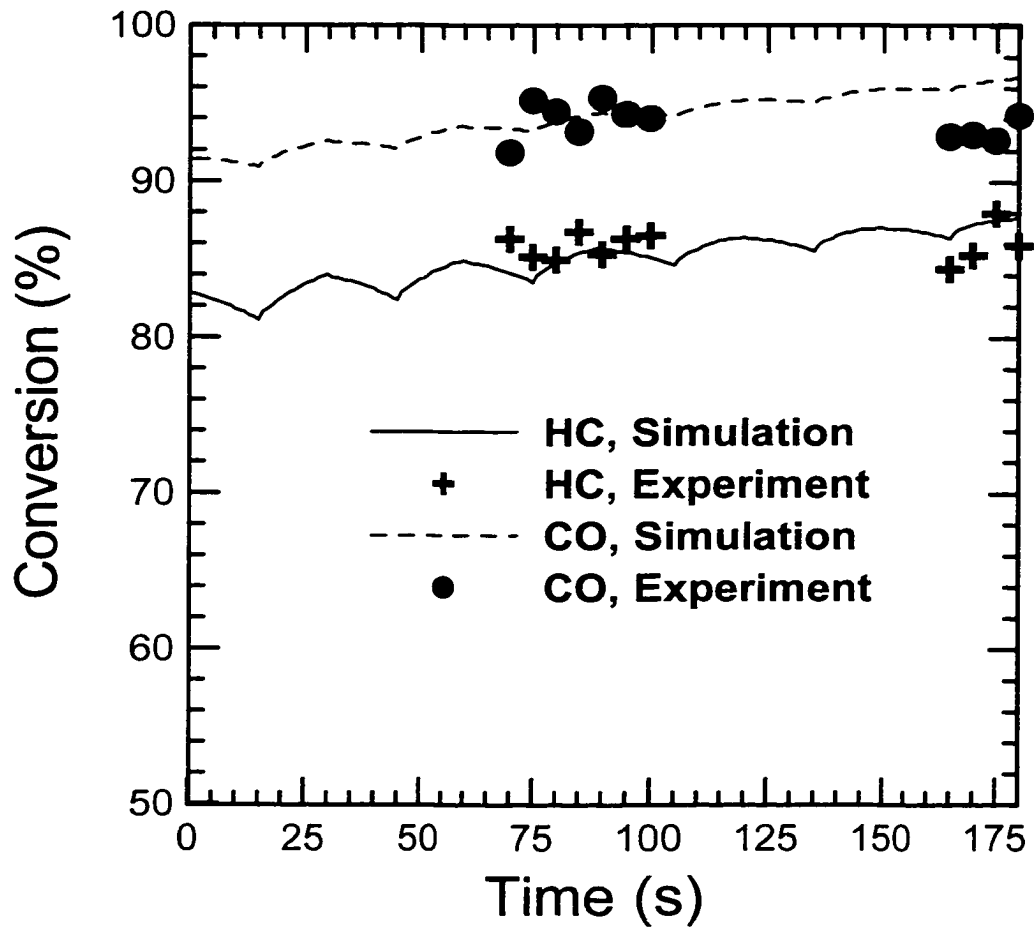


Figure 5-11 Comparison of transient HC and CO conversion between experiment and simulation

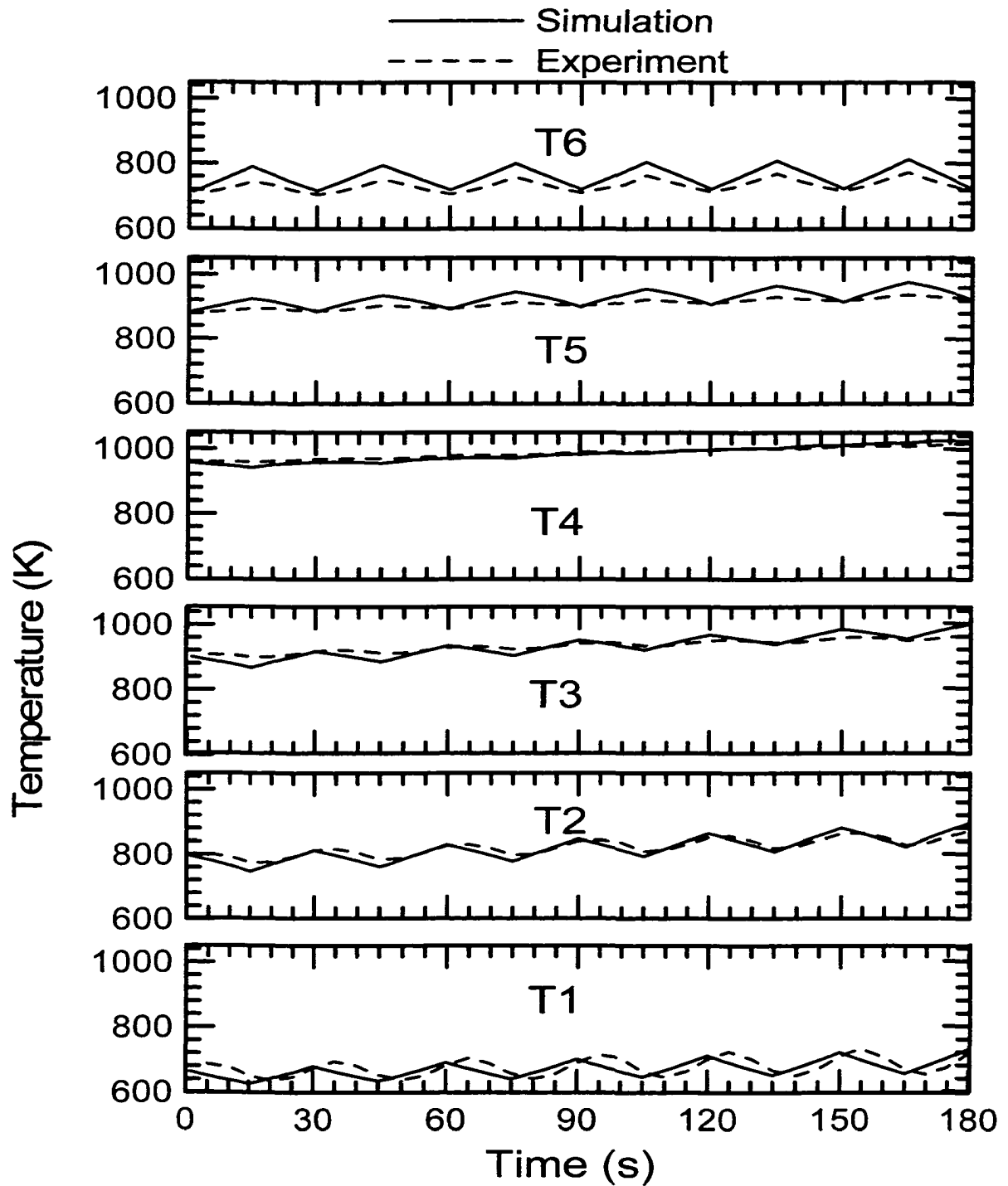


Figure 5-12 Comparison of transient reactor temperature between experiment and simulation

## 5.4.2 Reverse Flow Cycling Time Evaluation

The performance of the catalytic converter was modelled using a series of symmetrical cycles of differing duration, as summarized in Table 5-4.

Table 5-4 Simulation with Variable Cycling Time

Method	Forward Time (s)	Reverse Time (s)	Cycle Duration (s)
1	5	5	10
2	30	30	60
3	60	60	120
4	120	120	240

All simulations used the same initial reactor temperature and the same transient reactor inlet temperature, which are shown in Figure 5-9 and Figure 5-10, and the same steady engine exhaust composition (Table 5-3).

The simulated HC and CO conversion for the different cycle times are compared in Figure 5-13. The reactor temperatures  $T_3$  and  $T_4$ , which were located around the middle of reactor, are compared in Figure 5-14. It can be seen from Figure 5-13 that the shorter cycle time produces the highest time-averaged conversion and, from Figure 5-14, the highest time-averaged reactor temperature. The cycle time of 60 seconds gave the most rapid rise in the peak temperature observed. Longer cycle times produced more extreme variations in the temperatures at the two thermocouple positions.

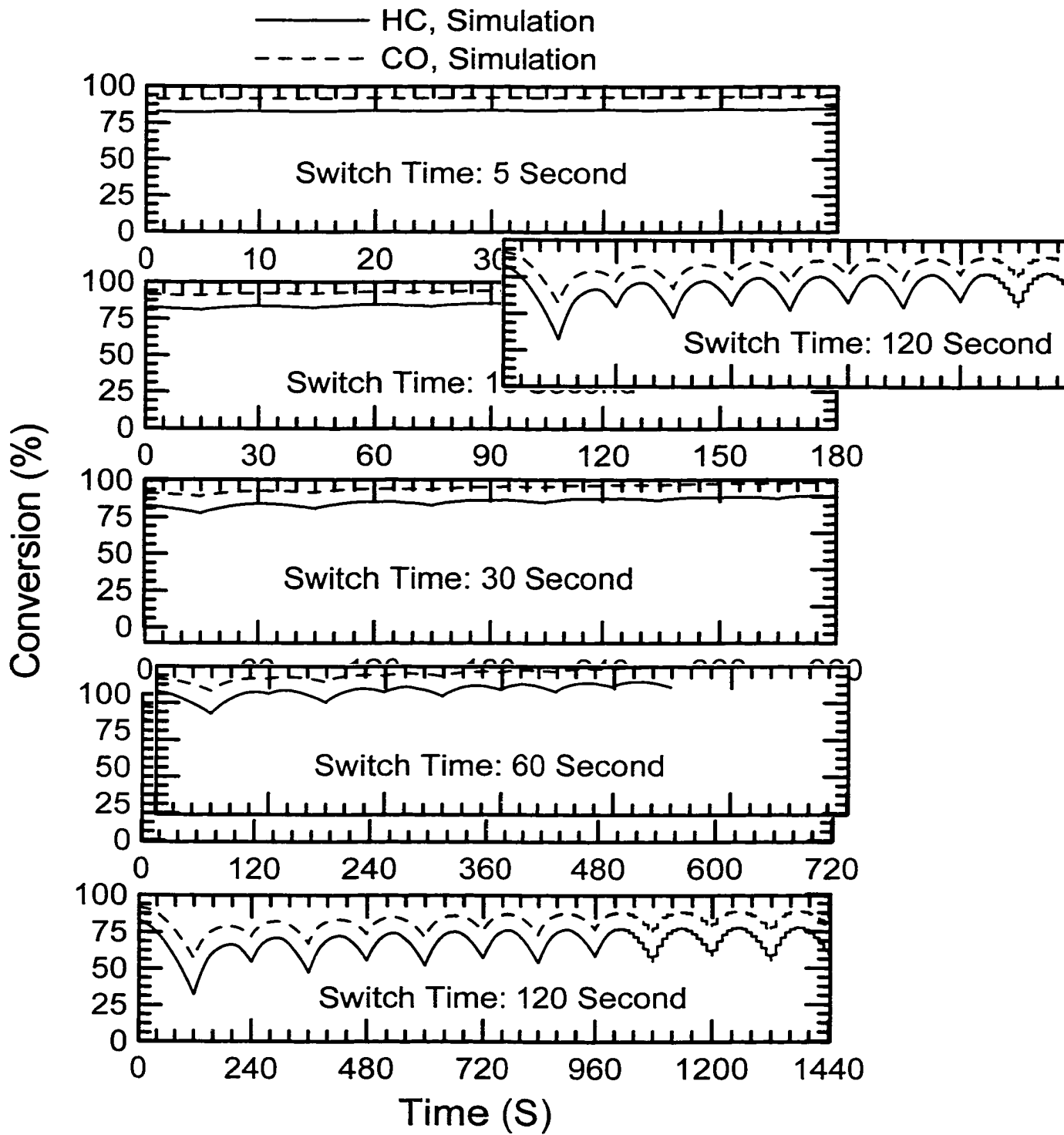


Figure 5-13 Comparison of transient HC and CO conversion with different cycling time

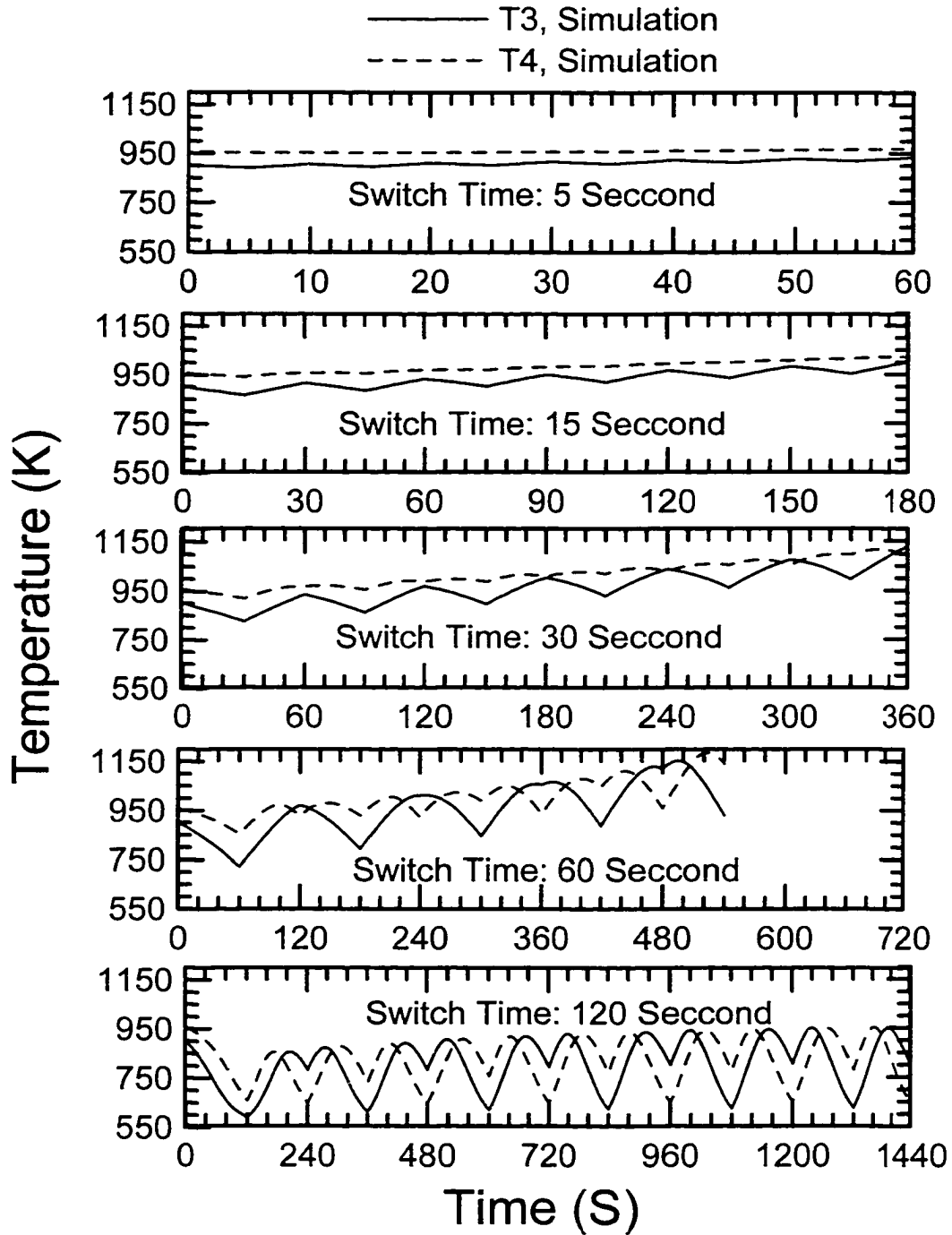


Figure 5-14 Comparison of the maximum reactor temperature  $T_3$  and  $T_4$  with different cycling time

## 5.5 Conclusions

Based on the experimental and modelling study of variable reverse flow cycling time for dual fuel engine operations, the following conclusions were drawn:

1. A short reverse flow cycling time can maintain the reactor at a high temperature level which can give a steady high HC and CO conversion even though the engine exhaust temperature is below the autothermal temperature for unidirectional operation.
2. A longer reverse flow cycling time can lead to a reduction in the reactor temperature level which reduces the HC and CO conversion.
3. A medium reverse flow cycling time can increase the original reactor temperature greatly. Although this increase is good for the HC and CO conversion, there is the possibility that the catalyst could be heated to an excessive temperature and damaged.

## 5.6 Nomenclature

$A_1$ : Pre-exponent factor for CH<sub>4</sub> rate constants, mol · K/(m<sup>2</sup> · s)

$A_2$ : Pre-exponent factor for CO rate constant, mol · K/(m<sup>2</sup> · s)

$A_3$ : Pre-exponent factor for CO inhibition

$A_c$ : Cross-sectional area of channel, m<sup>2</sup>

$A_w$ : Wall cross-sectional area, m<sup>2</sup>

$a$ : Mean pore radius of washcoat, 10 × 10<sup>-9</sup> m

$C_b$ : Total molar concentration, mol/m<sup>3</sup>

$C_i$ : Concentration for species *i* in the bulk, mol/m<sup>3</sup>

$(C_i)_S$ : Concentration for species  $i$  in the surface of washcoat,  $\text{mol/m}^3$   
 $C_p$ : Constant pressure heat capacity,  $\text{J}/(\text{kg} \cdot \text{K})$   
 $C_{pw}$ : Constant pressure heat capacity of the wall,  $\text{J}/(\text{kg} \cdot \text{K})$   
 $[CO]_{in}$ : Reactor inlet CO concentration, ppm  
 $[CO]_{out}$ : Reactor outlet CO concentration, ppm  
 $Da$ : Damkholer number, dimensionless  
 $D_{AB}$ : Binary diffusion coefficient,  $\text{m}^2/\text{s}$   
 $(D_{eff})_i$ : Effective diffusivity in washcoat,  $\text{m}^2/\text{s}$   
 $D_H$ : Hydraulic diameter, m  
 $(D_I)_i$ : Dispersion coefficient for species  $i$ ,  $\text{m}^2/\text{s}$   
 $D_T$ : Channel diameter, m  
 $E_1$ : Activation energy for  $\text{CH}_4$ ,  $\text{J}/\text{mol}$   
 $E_2$ : Activation energy for CO,  $\text{J}/\text{mol}$   
 $E_3$ : Activation energy for CO adsorption,  $\text{J}/\text{mol}$   
 $Gz$ : Gratz number, dimensionless  
 $h$ : Heat transfer coefficient,  $\text{W}/(\text{m}^2\text{K})$   
 $[HC]_{in}$ : Reactor inlet HC concentration, ppm  
 $[HC]_{out}$ : Reactor outlet HC concentration, ppm  
 $(\Delta H_R)_i$ : Heat of species  $i$  reaction,  $\text{kJ}/\text{mol}$   
 $k_f$ : Thermal conductivity of fluid,  $\text{W}/(\text{m} \cdot \text{K})$   
 $k_{m,i}$ : Mass transfer coefficient for species  $i$ ,  $\text{m}/\text{s}$   
 $k_w$ : Thermal conductivity of converter wall,  $\text{W}/(\text{m} \cdot \text{K})$   
 $L$ : Effective washcoat thickness, m



$M$ : Molar mass of a substance, g/mol

$Nu$ : Nusselt number, dimensionless

$Nu_H$ : Nusselt number with constant heat surface flux boundary condition, dimensionless

$Nu_T$ : Nusselt number with constant wall temperature boundary condition, dimensionless

$Pr$ : Prandtl number, dimensionless

$R_g$ : Gas constant

$R$ : Radius of Channel, m

$Re$ : Reynolds number, dimensionless

$(-R_i)$ : Reaction rate of species  $i$ , mol/(m<sup>2</sup>·s)

$(-R_i)_{Average}$ : Average reaction rate of species  $i$  at the washcoat, mol/(m<sup>2</sup>·s)

$(-R_i)_H$ : Rate of species  $i$  homogeneous reaction, mol/(m<sup>3</sup>·s)

$(-R_i)_S$ : Reaction Rate of species  $i$  at the external surface of washcoat, mol/(m<sup>2</sup>·s)

$Sc$ : Schmidt number, dimensionless

$Sh$ : Sherwood number, dimensionless

$T_b$ : Bulk mean temperature, K

$T_s$ : Washcoat surface temperature, K

$v_m$ : Mean axial velocity, m/s

$W_p$ : Wetted wall perimeter, m

$Y_i$ : Mole fraction of species  $i$  in wet basis

$Y_i^*$ : Mole fraction of species  $i$  in dry basis

$Y_{i,b}$ : Molar fraction of species  $i$  in bulk flow

$(Y_{i,b})_o$ : Molar fraction of species  $i$  at the inlet of converter

$Y_{i,s}$ : Molar fraction of species  $i$  in washcoat

## GREEK SYMBOLS

$\alpha$ : Thermal diffusivity, m<sup>2</sup>/s

$\alpha_i$ : Thermal dispersion coefficient, m<sup>2</sup>/s

$\rho$ : Gas mass density, kg/m<sup>3</sup>

$\rho_w$ : Wall density, kg/m<sup>3</sup>

$\eta_i$ : Effectiveness factor for species i,

$\delta_w$ : Converter wall thickness, m

$\varepsilon$ : Porosity of washcoat

$\tau$ : Tortuosity factor of washcoat

$\chi_{HC}$ : HC conversion over the catalytic converter: 
$$\chi_{HC} = \frac{[HC]_{in} - [HC]_{out}}{[HC]_{in}} \times 100\%$$

$\chi_{CO}$ : CO conversion over the catalytic converter: 
$$\chi_{CO} = \frac{[CO]_{in} - [CO]_{out}}{[CO]_{in}} \times 100\%$$

## 5.7 References

Brauner H. W. and F. Fetting, "Stofftransport bei wandreaktion im einlaufgebiet eines strömungsrohres", Chem. ing. Techno. 38, 30-35, 1966.

Checkel M. D., B. Liu, M. Zheng, E. Mirosh, "A Special Catalytic Converter for Dual Fuel Engine Light Load Emissions", 1998 Spring Technical Meeting, Combustion Institute, Canadian Section, 25-27 May, Toronto, Canada.

Corbo P., M. Gambino, S. Iannaccone and A. Unich, "Comparison between lean-burn and stoichiometric technologies for CNG heavy-duty engines", SAE950057, 1995.

Cullis, C.F. and B.M. Willatt, "Oxidation of methane over supported precious metal

- catalysts", *J. Cat.*, 83 267-285, 1983.
- Deluchi M. A., R. A. Johnson and D. Sperling, "Transportation fuels and the greenhouse effect", *Transportation Research Record*, In Press.
- Douville B., "Performance, emissions and combustion characteristics of natural gas fuelled of diesel engines", M. Sc. Thesis, Department of Mechanical Engineering, The University of British Columbia, 1994.
- Dryer F. L., "High temperature oxidation of carbon monoxide and methane in a turbulent flow converter", Ph. D. Thesis, Princeton University, 1972.
- Gambino M., R. Cericola, P. Corbo, S. Iannaccone, " Carbonyl compounds and PAH emissions from CNG heavy-duty engine", *ASME, Journal of Engineering for Gas Turbines and Power*, 115, n. 4, 747-749, 1993
- Hanamura K., R. Echigo and S. A. Zhdanok, " Superadiabatic combustion in a porous medium", *Ind. J. Heat Mass Transfer*, 36, 1993
- Hayes R. E. and S. T. Kolaczkowski, "Introduction to catalytic combustion", Gordon and Breach Science Publishers, Reading 1997.
- Hayes R. E. and S. T. Kolaczkowski, "Mass and heat transfer effects in catalytic monolith converters", *Chem. Eng. Sci.*, 49 3587-3599, 1994.
- Heywood J. B., "Internal combustion engine fundamentals", McGraw-Hill Inc., New York, 1988.
- Kolaczkowski S. T., W. J. Thomas, J. Titiloye and D. J. Worth, "Catalytic combustion of methane in a monolith reactor: heat and mass transfer under laminar flow and pseudo-steady-state reaction conditions", *Combust. Sci. and Tech.*, 118, 79-100, 1996.
- Leung D., R. E. Hayes and S. T. Kolaczkowski, "Diffusion limitation effects in the washcoat of a catalytic monolith reactor", *Can. J. Chem. Eng.* 74, 94-103, 1996.
- Li , P. K. L., "Catalytic Combustion of methane in monoliths", Ph. D. Thesis, University of Bath, 1997.
- Liu B., R. E. Hayes, M. D. Checkel, M. Zheng and E. Mirosh, " Transient simulation of a catalytic converter for a dual fuel engine", *Can. J. Chem. Eng.*, in press, 1999.

- Matros Yu. Sh. and G. A. Bunimovich, " Reverse-flow operation in fixed bed catalytic reactors", Catal. Rev.-Sci. Eng., 38(1), 1-68, 1996.
- Mtui P., "Pilot ignition, natural gas combustion in diesel engines", PhD Thesis, The University of British Columbia, Canada, 1996.
- Oh S. H. and J. C. Cavendish, "Transients of monolithic catalytic converters: response to step changes in feed stream temperature as related to controlling automobile emissions", Ind. Eng. Chem. Prod. Res. Dev. 21, 29-37, 1982.
- Siemund S. and J. P. Leclerc, "Three-Way monolithic converter: simulations versus experiments", Chem. Eng. Sci. 51, 3709-3720, 1996.
- Strots V. O., G. A. Bunimovich, Yu. Sh. Matros, M. Zheng and E. A. Mirosh, "Novel catalytic converter for natural gas powered diesel engines", SAE 980194, 1998.
- Tronconi E. and P. Forzatti, "Adequacy of lumped parameter models for SCR converters with monolith structure", AIChE J. 38, 201-210, 1992.
- Voltz S. E., C. R. Morgan, D. Liederman and S. M. Jacob, "Kinetic study of carbon monoxide and propylene oxidation on platinum catalysts", Ind. Engng. Chem. Prod. Res. Dev. 12, 294-301, 1973.
- Zelenka P., W. Cartellieri, P. Herzog, " Worldwide diesel emissions standards, Current experience and future needs ", Applied Catalysis B: Environmental 10, 3-28,1996.

## Chapter 6

### Chemical Kinetic Study of Reverse Flow Catalytic Converter

*Chapter 6 makes a more detailed kinetic study of palladium catalyst for CH<sub>4</sub> and CO oxidation under reverse flow operations. It is an experimental and modelling study based on the prototype reverse flow design shown in Figure 2-3 c), which is the same catalyst as in Chapter 5. The model used is the same as that shown in Chapter 5. However, it develops a new kinetic approach for both methane and CO oxidation. Both CO and methane oxidation over palladium catalyst in an excess of oxygen and water are well described using apparent first order kinetics with respect to the corresponding CO and methane concentration. It is also found that the catalyst activities undergoes an apparent transition with reactor temperature. The transition temperature is about 874 K, at which point the apparent activation energy decreased dramatically. The kinetic data found are the same as to those found in Chapter 5. However, the transition temperature for methane oxidation is much higher than that from Chapter 5. Since the study in Chapter 6 is based on a wide range of engine and reactor operations, it gives more reliable information.*

---

Note: This chapter has been submitted for publication by “Chemical Engineering Science”, Co-authors: R. E. Hayes, M. D. Checkel, M. Zheng and E. Mirosh. It is advised that some content of Sections 6.1, 6.2 and 6.3 may repeat materials in the previous Chapters.

## 6.1 Introduction

Concern over high levels of pollutants in vehicular exhaust gas, and concomitant government regulations specifying limits on them, has led to much research into methods of reducing such emissions. Research has been directed into novel engine configuration, thermal and catalytic reactors for deep oxidation of pollutants, as well as alternative fuel systems. A promising alternative fuel technology for the reduction of emissions from diesel fuel engines is the conversion of such engines to operate on a mixture of diesel fuel and natural gas, which is mostly composed of methane. In this dual fuel configuration, natural gas acts as the primary fuel and comprises up to 90% of the total fuel used. The remaining amount of fuel is diesel, which is required to ensure effective ignition. A natural gas/diesel dual fuel engine offers an attractive alternative to both diesel and spark ignition engines. Composed primarily of methane, natural gas readily forms homogeneous air-fuel mixtures which can be ignited and burned over a wide flammability range (Weaver, 1989; Sakai, 1991). This pre-mixed combustion produces much lower nitrogen oxide ( $\text{NO}_x$ ) emissions and soot emissions compared to diesel engines. The fuel is chemically inert with low photochemical reactivity and low global toxicity of the exhaust gases compared to that from diesel engines (Gambino et al., 1992). At the same time, the low carbon/hydrogen ratio permits reduced carbon dioxide emissions for a given engine efficiency (Corbo et al., 1995). Natural gas also has excellent knock resistance which, when combined with the lean mixtures inherent in a dual fuel engine, permits diesel like compression ratios for optimum engine efficiencies. There is, however, a significant difficulty associated with this dual fuel combination. At

low to moderate engine loads a lower fuel combustion efficiency has been observed (Karim, 1991), which results in significant amounts of hydrocarbon (HC) and carbon monoxide (CO) in the exhaust gas. Most of the HC in the dual fuel engine exhaust is methane, which, although chemically resistant and toxicologically inert, is a strong "greenhouse" gas (Lampert et al., 1997; Oh et al., 1991). By mass, methane has 12 to 30 times the greenhouse effect as CO<sub>2</sub> (Deluchi et al.). Although the United States diesel engine emission standard only gives limits for the Non-Methane Hydrocarbon (NMHC) exhaust, in the European Community, Japan and Korea, the Total Hydrocarbon (THC) in the exhaust gas is considered (Zelenka et al., 1996; Lampert et al., 1997). An obvious solution to the problem of high HC levels in the exhaust is to use a catalytic converter in the exhaust system to reduce the HC and CO to an acceptable level.

Catalytic converters have been widely used on gasoline engines since about 1979, with the most commonly used catalyst at present being the three-way-catalyst (TWC), which oxidizes CO and HC, and reduces NO<sub>x</sub> (Shelef and Graham, 1994; Miyoshi et al., 1995). Catalytic converters have also been used on diesel engines (Clerc, 1996; Hosoya and Shimoda, 1996; Farrauto and Voss, 1996). Owing to the importance of catalytic converters, it is not surprising to find that many experimental and modelling studies have been reported in the literature. See, for example, the review of Leclerc and Schweich (1993). Most attention has focused on converters for gasoline engines and, to a lesser extent, those for straight diesel applications. Some investigations for methane catalytic oxidation in natural gas fuelled engines were reported by Summers et al. (1991), Sakai et al. (1991), Oh et al. (1991) and Lampert et al. (1997). Bittner and Aboujaoude (1992)

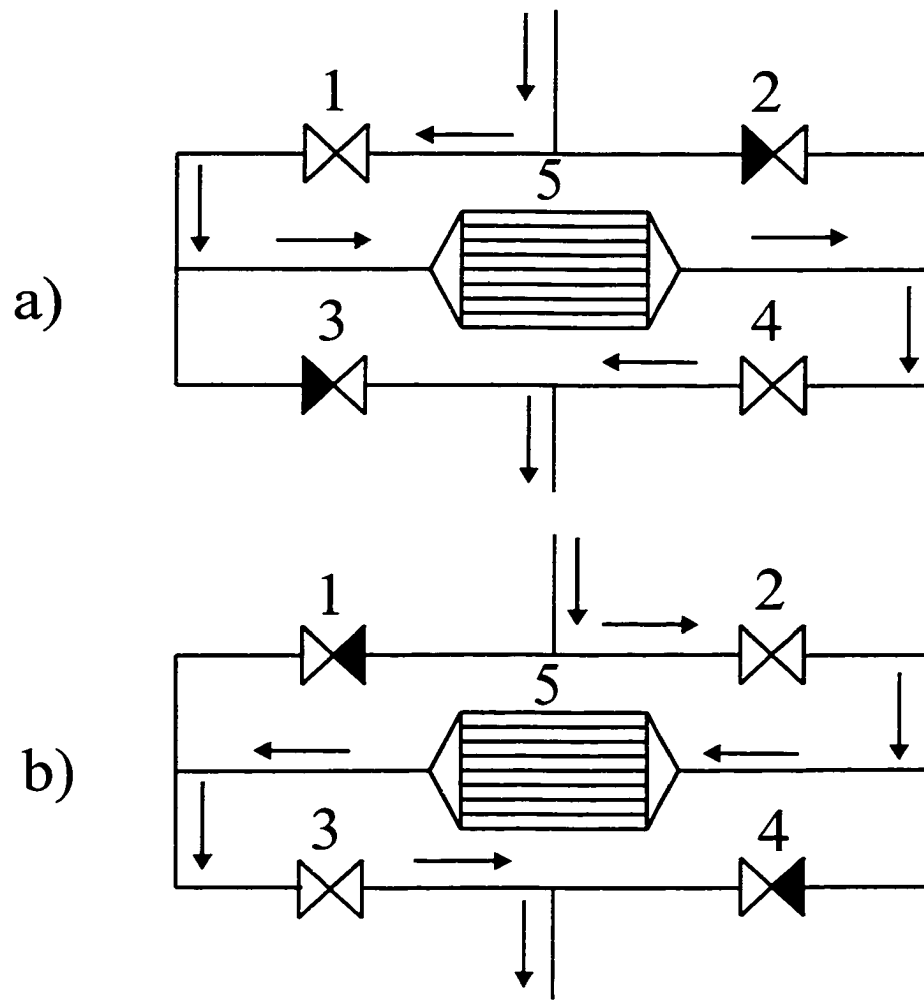
reported an investigation of catalytic control of  $\text{NO}_x$ , CO and NMHC emissions from stationary diesel and dual fuel engines. Liu et al. (2000) presented the results of a relatively low temperature experimental and modelling study for the dual fuel configuration with a uni-directional flow catalytic converter. However, the performance and operating conditions of a catalytic converter for the natural gas/diesel system have not been widely studied. These systems are significantly different from the TWC system. For example, the TWC on a gasoline engine operates at conditions close to stoichiometric, whilst dual fuel engines typically operate in a lean combustion environment, which results in a large excess of oxygen in the exhaust gas. Because of a high compression ratio and the lean mixture, the exhaust gas temperature is also typically much lower than that observed in gasoline engines, which can lead to lower reaction rates.

The development of a catalytic converter for an engine predominantly fueled by methane presents a certain challenge. Of all of the hydrocarbons, methane is the least reactive, and therefore the most difficult to oxidize. A further difficulty is that methane emissions from the engine increase as the engine load decreases. Because the exhaust gas temperature also decreases as the load decreases, there is a tendency for the reaction rate to fall at light engine load. Palladium (Pd) based catalysts are commonly used for methane oxidation in catalytic combustion applications, especially in primary combustion (Hayes and Kolaczkowski, 1997), but usually such applications operate at much higher temperatures than those found in the low load engine exhaust. In the absence of a substantially more active catalyst than the classical palladium based ones, it



is therefore essential to maintain a high reaction temperature in the converter under low load conditions. One possible solution to this problem is to use a reversing flow catalytic converter, which is capable of maintaining temperatures superior to the adiabatic temperature rise. The principles of the reversing flow reactor are briefly elucidated below.

The concept of the reversing flow reactor is simple: the feed is periodically switched between the two ends of the reactor (Matros and Bunimovich, 1996). The operation of the reverse flow catalytic converter is controlled using valves, as shown schematically in Figure 6-1. In Figure 6-1(a) the control valves 1 and 4 are opened and the engine exhaust flows to the catalytic converter from left to right. This mode can be called the forward flow. In Figure 6-1(b) the control valves 2 and 3 are opened and the engine exhaust flows to the catalytic converter from right to left. This mode is called the reverse flow. The total cycle consists of these two operations, and the term switch time is used to denote the time at which the flow is changed from forward flow to reverse flow. If the forward flow time is the same as the reverse flow, the operation is referred to as symmetric reverse flow operation. If the two flow modes have different times, then the operating mode is referred to as unsymmetric operation. The cycle duration is the total time for one cycle, that is the sum of the times for forward and reverse flow.



1, 2, 3, 4: Control Valve  
 5: Catalytic Converter

Figure 6-1 The reverse flow catalytic converter concept.

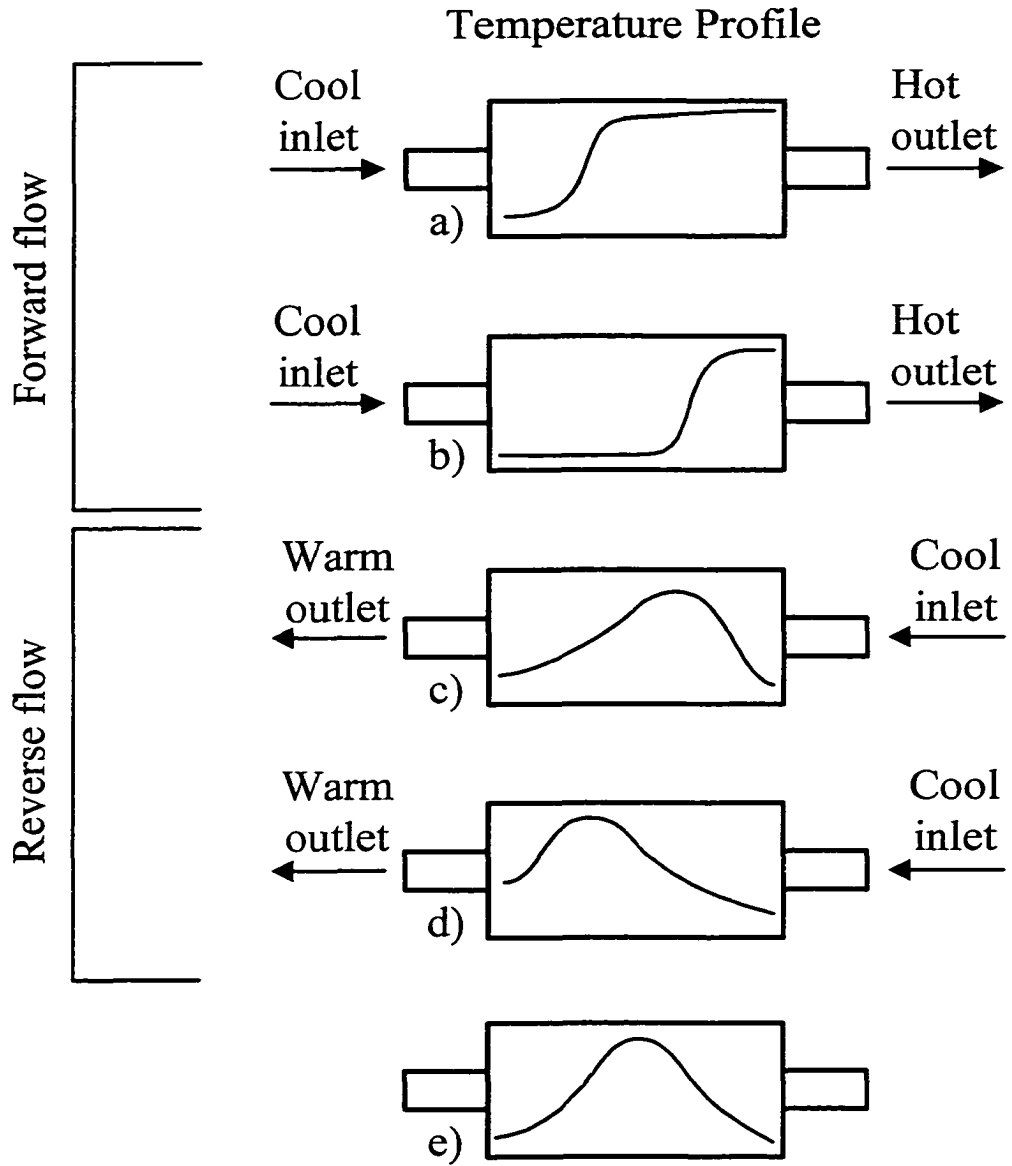


Figure 6-2 The "heat trap" effect for reverse flow operation.

For an exothermic reaction, the reverse flow catalytic reactor exhibits what has been referred to as a “heat trap” effect, and this effect can be used to achieve and maintain an enhanced reactor temperature as compared to a single direction flow mode of operation. The principle of the “heat trap” effect is illustrated in Figure 6-2. Figure 6-2(a) illustrates a reactor temperature profile that might be observed in a standard unidirectional flow operation for a combustion reaction. The temperature initially rises slowly as the reaction commences, and then more sharply as the heat liberated in the reaction accelerates the rate owing to the exponential temperature dependence of the rate constant. The shape of the curve depends on the operating conditions, especially the inlet gas temperature. If the inlet temperature is lowered, the reaction rate will fall, and the temperature peak will tend to migrate towards the reactor exit. At a sufficiently low temperature, the reaction will effectively be extinguished and the converter will lose most of its effectiveness as the leading edge of the “hot spot” (where most reaction occurs) migrates out of the reactor. If a temperature pattern shown in Figure 6-2(a) or (b) is established, the reverse flow operation can then be used to take advantage of the high temperatures near the reactor exit to preheat the reactor feed. When the feed is switched to the “exit”, the energy stored in the reactor during the previous reaction is then effectively used to preheat the feed. Because this stored energy is added to the feed stream, it is possible to achieve temperatures higher than the adiabatic temperature rise, based on the fresh feed inlet temperature. Provided that the reactor is initially at a sufficiently high temperature and the cycle time is carefully chosen, it is possible to achieve autothermal reactor operation at feed temperatures well below those required for

autothermal operation with uni-directional flow. In such a case, a quasi-steady state operation may be achieved in which the reactor temperature profile has a maximum value near the centre of the reactor, which slowly oscillates as the feed is switched between the two ends of the reactor, as shown in Figures 6-2 (c-e). This temperature effect has been referred to as a heat sink (Matros and Bunimovich, 1996) and also a “heat trap” (Strots et al., 1998). Hanamura et al. (1993) demonstrated a reverse flow operation in which the solid phase temperature rise was as high as 13 times the adiabatic temperature rise. Some modelling studies have also been used to investigate reverse flow thermal effects (Purwono et al.; Guit, 1993; Wallace and Viljoen, 1995; Özgülsen and Cinar, 1994). Reverse flow reactors have been used industrially for the oxidation of VOC (Volatile Organic Compounds), oxidation of sulphur dioxide ( $\text{SO}_2$ ), the synthesis of methanol, and others. Typically these applications have very low gas velocity and the reverse flow cycle duration can be as high as 4 hours. Engine exhaust reactors have a much higher gas velocity and consequently a faster switching frequency is expected. The cycling time is the major factor controlling the migration and magnitude of the temperature peak, and as such should be selected with care.

This chapter reports an experimental and numerical investigation of a dual fuel engine catalytic converter operating with reversing flow. The numerical model is used to determine the kinetic parameters for methane and carbon monoxide oxidation reactions. The effects of inlet temperature and cycle time are illustrated.

## 6.2 Equipment

The performance of the reverse flow converter was studied using the exhaust from a dual fuel engine. The engine was a naturally aspirated, four cylinder ISUZU 4BE1 engine of 3.6 litres displacement and was modified to operate with a dual fuel system. The engine was installed in an eddy current dynamometer test bed equipped with a reversing flow catalytic converter. Engine speed and torque were controlled using a digital dynamometer controller and a digital “throttle” controller. The digital dynamometer controller was set in the RPM (engine speed) mode and the digital “throttle” controller was set in the position mode. For a desired engine operating condition, the engine was first set to the desired engine speed using the dynamometer controller, and then adjusted to give the desired engine torque using the “throttle” controller to control engine fueling.

The catalytic converter used a ceramic monolith honeycomb substrate with square channels. The converter contained six segments of monolith honeycomb placed in series, with each segment measuring 0.152 m × 0.152 m and separated by a 2 mm gap. Four segments were coated and an inactive segment was placed at each end of the reactor. Both active and inactive segments were 0.0508 m in length. The segmented design was used to give multiple entry regions in the converter, where the heat and mass transfer coefficients are larger than in the fully developed region. The physical properties of the monolith segments are given in Table 6-1. The washcoated monolith segments were provided by Johnson-Matthey and used as supplied.

Table 6-1 Physical Parameters of the Converter

Wall Density	2500 kg/m <sup>3</sup>
Wall thermal conductivity	2 W/(m.K)
Wall heat capacity	1400 J/(kg. K)
Effective wall thickness	0.25 mm
Thickness of washcoat layer	0.05 mm
Porosity of washcoat	0.41
Channel hydraulic diameter	1.4 mm
Channel open frontal area	1.96 mm <sup>2</sup>
Porosity of monolith	72%
Size of each brick (length × width × height)	50.8mm × 152.4mm × 152.4mm

The exhaust system containing the converter is illustrated in Figure 6-3. The gas flow direction to the converter is determined by the position of the control valve. The gas flow direction shown in Figure 6-3 is reverse flow. When the control valve is switched to the other position, the gas flow direction changes to forward flow. It was possible to operate the valve to give uni-directional flow in either direction, or to give reverse flow operation with any switch and cycle times. The composition of the engine exhaust gas was determined before and after the converter using the analytical facilities summarized by Liu et al. (2000). The components measured were O<sub>2</sub>, CO<sub>2</sub>, CO, NO<sub>x</sub> and HC. HC measurement provided both total hydrocarbon (THC) and CH<sub>4</sub>, and normally more than 95% of THC was CH<sub>4</sub>. The instruments were calibrated with standard gases before each

test. The data were recorded on a dry basis and were converted to a wet basis using the relationship of Heywood (1988).

$$Y_i = (1 - Y_{\text{H}_2\text{O}}) Y_i^* \quad (6.1)$$

For a hydrocarbon  $\text{C}_n\text{H}_m$  the mole fraction of water was calculated using the equation:

$$Y_{\text{H}_2\text{O}} = \left( \frac{m}{2n} \right) \left( \frac{Y_{\text{CO}}^* + Y_{\text{CO}_2}^*}{1 + \frac{Y_{\text{CO}}^*}{K_1 Y_{\text{CO}_2}^*} + \left( \frac{m}{2n} \right) (Y_{\text{CO}}^* + Y_{\text{CO}_2}^*)} \right) \quad (6.2)$$

The formula  $\text{C}_n\text{H}_m$  represents an averaged composition that depends on the flowrate of each fuel.  $K_1$  is an experimental constant with a value between 3.8 and 3.5 (Douville, 1994).

The temperature profile in the catalytic converter was measured by inserting thermocouples ( $T_1$  to  $T_6$ ) into the catalyst segments. A single thermocouple was installed in the centre of each segment. The inlet gas temperature was measured by thermocouple, either  $T_{\text{in},1}$  or  $T_{\text{in},2}$ . For forward flow,  $T_{\text{in},1}$  is inlet gas temperature and  $T_{\text{in},2}$  is outlet gas temperature. For reverse flow,  $T_{\text{in},2}$  is the inlet gas temperature and  $T_{\text{in},1}$  is outlet gas temperature.



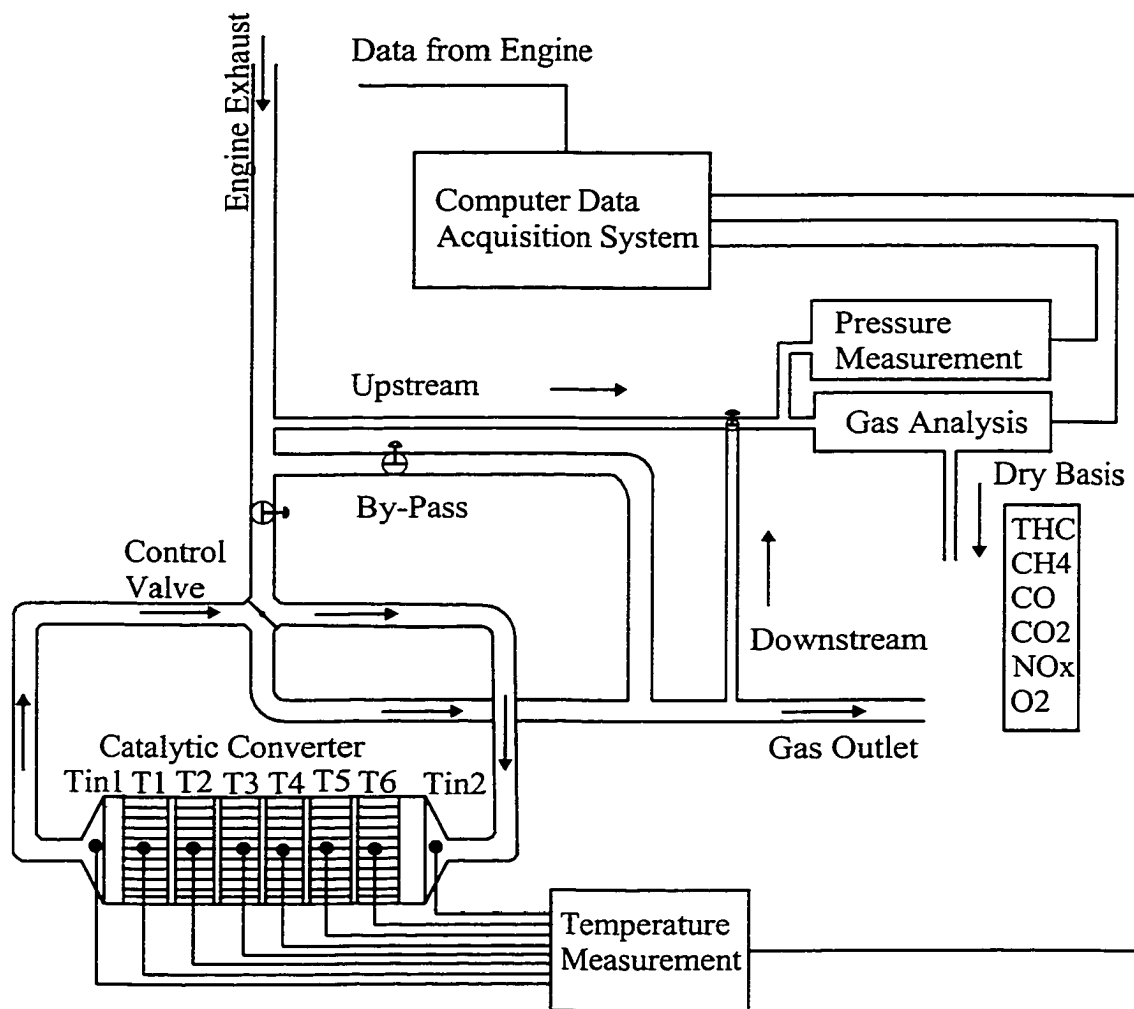


Figure 6-3 Experimental set-up.

### 6.3 Experimental Results

Three reverse flow tests were made under different light engine load operations. Two of the tests used the same engine operation to show the effect of initial conditions. The engine mode, exhaust composition, exhaust temperature and flowrate for these three tests are summarized in Table 6-2, which shows the variation of engine exhaust composition and temperature. The exhaust temperature varied from 535K to 727K. THC concentration varied from 2139 ppm to 4724 ppm. CO concentration varied from 1233 ppm to 1816 ppm. All experiments had excess O<sub>2</sub>, which varied from 9.02% to 13.33%. H<sub>2</sub>O concentration varied from 6.82 % to 11.44%.

Table 6-2 Exhaust Gas Properties for the Three Cases Studied

Test Case	Engine mode		Exhaust composition						Texh. (K)	Mass Flow Rate (g/s)
	Speed (rpm)	Tor. (Nm)	HC (ppm)	CO (ppm)	NO (ppm)	O <sub>2</sub> (%)	CO <sub>2</sub> (%)	H <sub>2</sub> O (%)		
Case 1	1500	150	2139	1233	770	9.10	5.93	11.44	727	43.38
Case 2	1500	150	2759	1264	737	9.02	5.86	11.31	722	42.71
Case 3	1500	80	4724	1816	249	13.33	3.46	6.82	535	45.82

N<sub>2</sub>: Balance of Engine Exhaust Composition

Texh.: Engine Exhaust Temperature

Tor.: Engine Torque

For these three tests, the catalytic converter was initially heated by running the engine at a relatively heavy load which gave a high exhaust temperature. The flow

direction in the catalytic converter was manually controlled to establish a temperature profile with a temperature peak in the middle of the reactor. The temperature profiles in the reactor before the new engine loading was applied, and before automatic reverse flow operation was commenced, are shown in Figure 6-4 for the three tests. Case 1 had the lowest temperature, with Case 2 higher and Case 3 higher again. Once the given profile was achieved, the reverse flow operation was started and the engine operating conditions were changed. These new engine modes had lower exhaust temperatures, but higher HC and CO concentrations compared to the previous heavy load modes.

Details of the cycle duration, switch time and number of cycles run for each of the three cases are given in Table 6-3. Symmetric cycles were used for all cases, with a switch time of 30 s for Cases 1 and 2 and 15 s for Case 3. Experimental reactor temperatures measured during the reverse flow operation are shown in Figures 6-5. Figure 6-5 shows the middle reactor temperatures corresponding to  $T_3$  and  $T_4$  as a function of time. It is seen that the temperatures  $T_3$  and  $T_4$  increase with time under flow cycling for each case, and Case 2 gave the highest rate of increase. The conversion of HC and CO is shown in Figure 6-6. As the temperature increases, HC conversion for Cases 1 and 2 increase gradually. Even though the temperature also increased in Case 3, the HC conversion remained at about 85 % during the reverse flow cycling. CO conversion was observed to remain above 90 % in each case.

Table 6-3 Reverse Flow Cycling Time

Test Case	Forward Flow Time, s	Reverse Flow Time, s	Cycle Duration, s	Number of Cycles	Elapsed Time, s
Case 1	30	30	60	7	420
Case 2	30	30	60	6	360
Case 3	15	15	30	6	180

The difference in catalytic converter performance between the reverse flow and the unidirectional flow modes is shown in Figure 6-7. For this series of experiments, the catalytic converter was first operated in unidirectional mode with the engine running at 1500 rpm, 200 Nm. The resulting steady state temperature profile in the converter is shown as the centre line in Figure 6-7. The engine operating mode was then changed to light load operation at 1500 rpm and 160 Nm, at which point the catalytic converter was changed to operate in a reverse flow manner with the flow switch time 25 second (total cycle time 50 seconds). The exhaust temperature for the new engine mode was 689 K. During the reverse flow operation, the catalytic converter temperature gradually developed to achieve a maximum reactor temperature higher than 850 K, after 5 minutes of reverse flow operation. The temperature profile is shown as the uppermost line in Figure 6-7. The methane conversion for this reactor temperature was about 77%. In the second experiment, the initial engine condition was the same as before, however, after the change in engine operating mode was made, the converter continued to operate in the unidirectional mode. The temperature and conversion dropped, and the final steady state

temperature profile is shown as the bottom curve in Figure 6-7. The methane conversion was only 20%. The performance advantage obtained using reverse flow operation is clear.

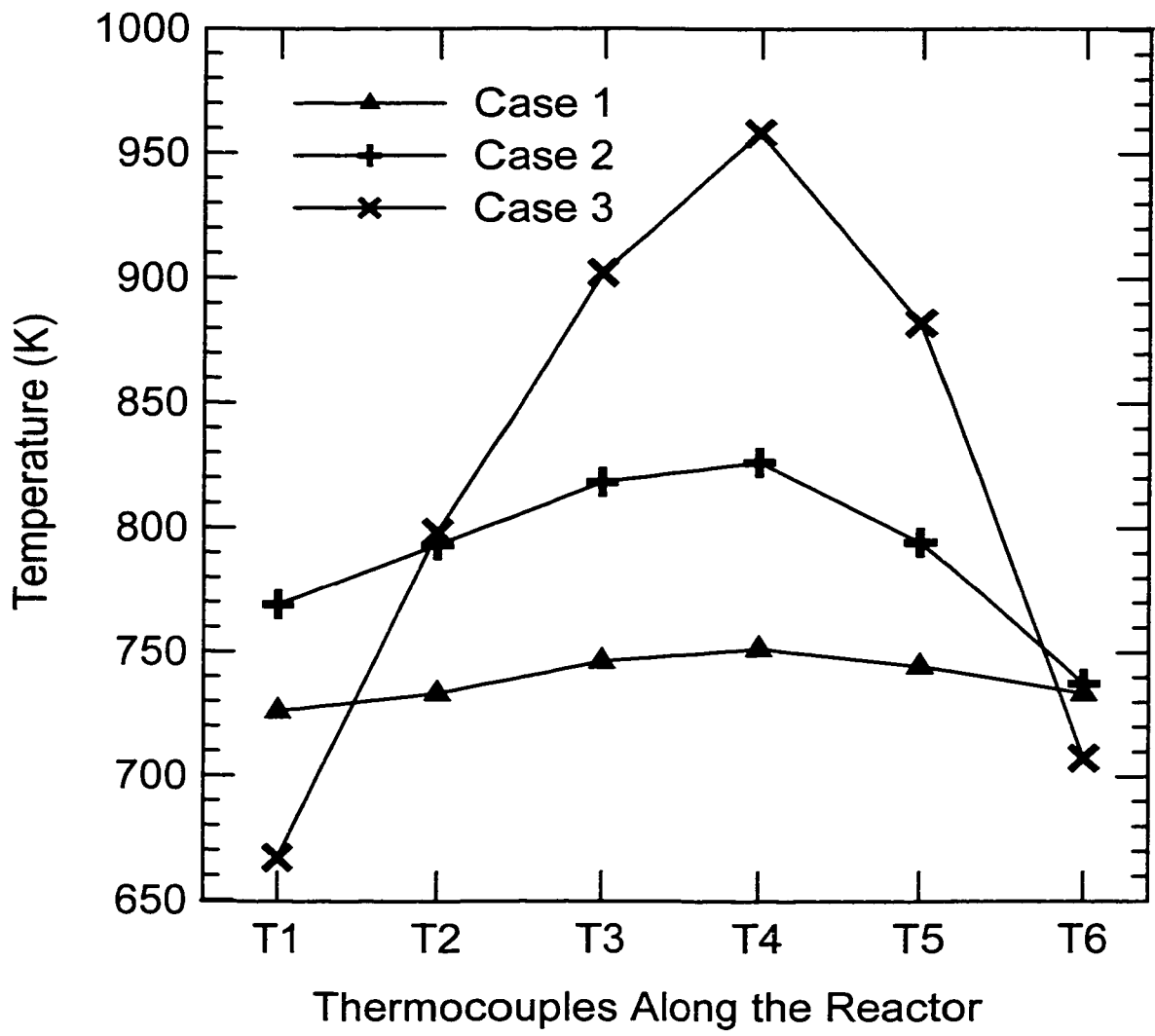


Figure 6-4 Initial Reactor Temperature Profiles

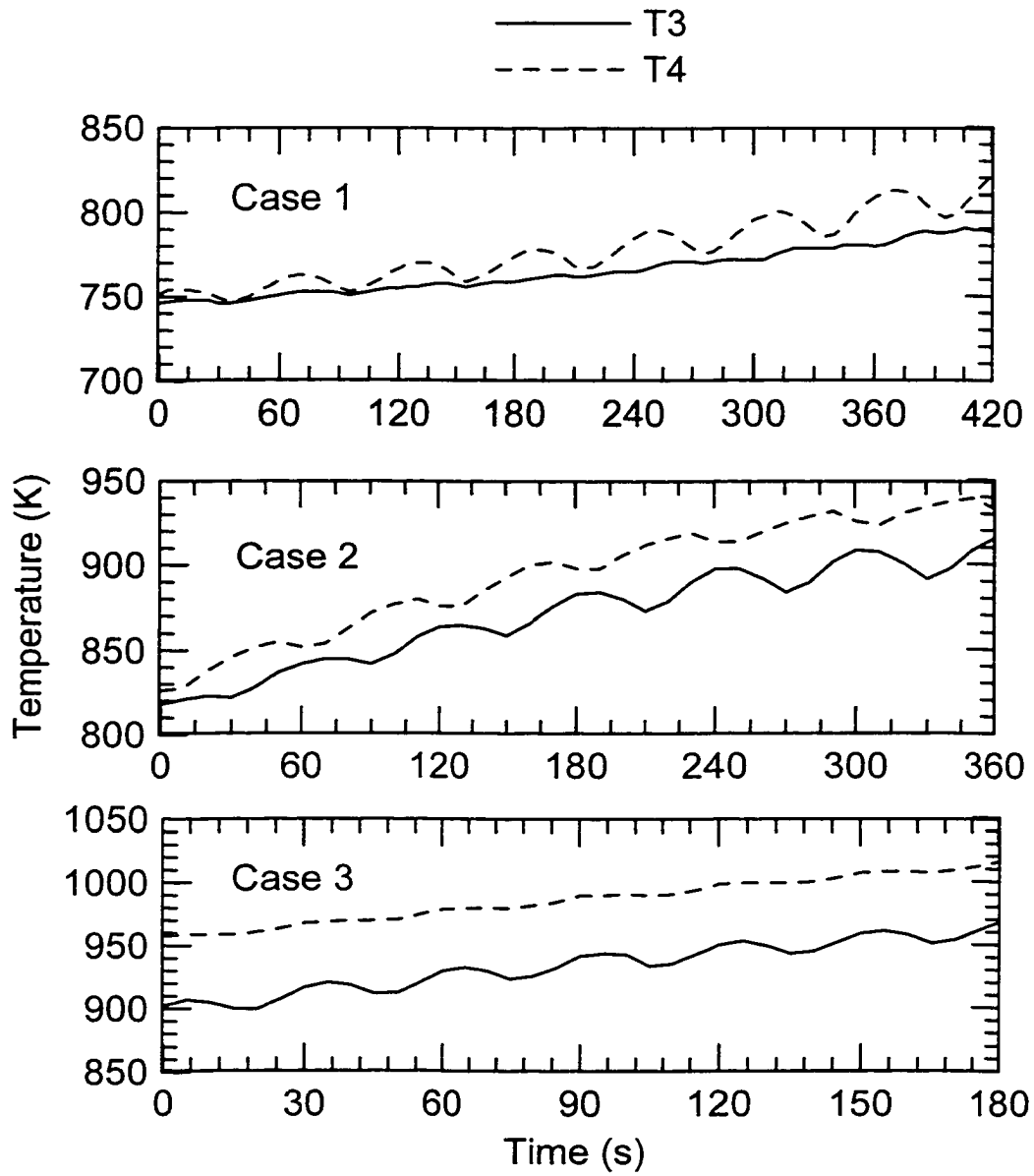


Figure 6-5 The Development of the Middle Reactor Temperature  $T_3$  and  $T_4$  with Reverse Flow Cycling.

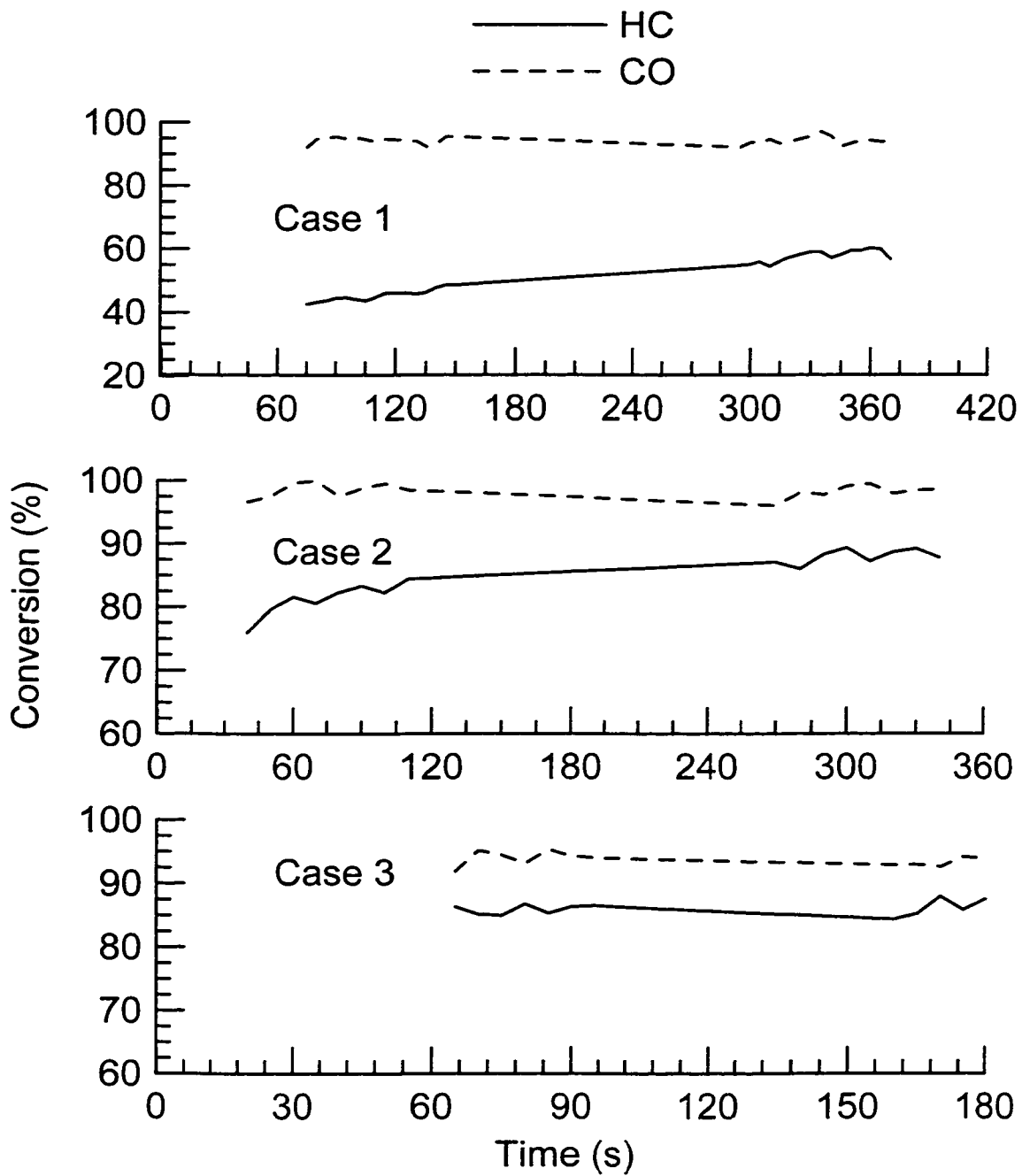


Figure 6-6 HC and CO conversion with reverse flow cycling



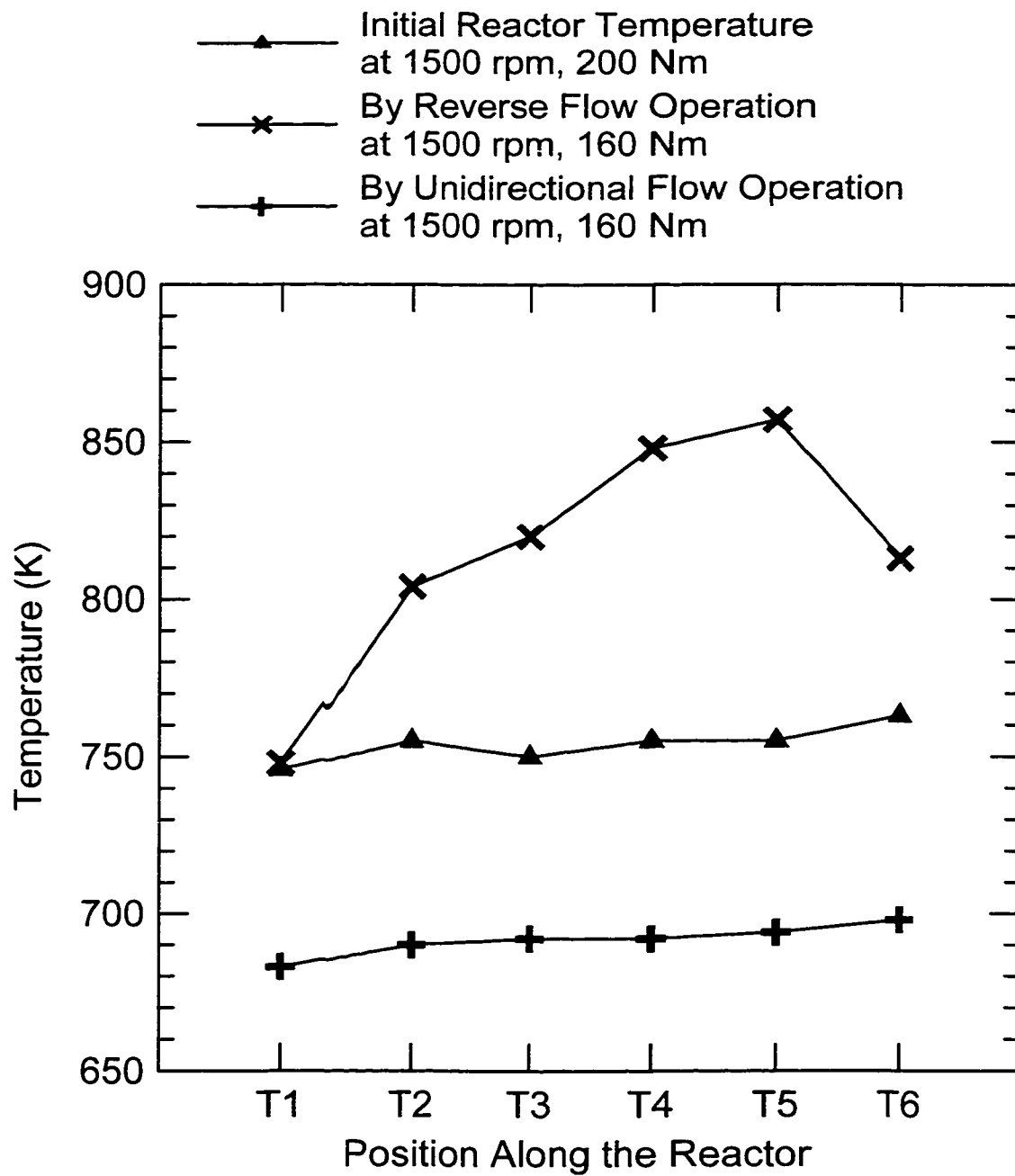


Figure 6-7 Comparison Between the Unidirectional Operation and the Reverse Flow Operation

## 6.4 Mathematical Model

### 6.4.1 Assumptions

In this section, a mathematical model for the reverse flow converter is described. Mathematical models of washcoated monolith reactors of varying complexity have been reported, and are reviewed in Leclerc and Schweich (1993) and Hayes and Kolaczkowski (1997). In this investigation a single channel model was used, which assumes that all of the channels in the reactor experience the same operating conditions. In such a model, the gas phase can be modelled in one, two or three space dimensions. As noted in Hayes and Kolaczkowski (1997), for channels of the order of 1 mm hydraulic diameter under the operating conditions found in this converter, the 1D model provides a very close agreement to the 2D or 3D model, and offers a greatly reduced computational time. It is doubtful whether the added cost of the solution of 2D or 3D models could be justified in this investigation, because the error involved in other assumptions (especially the simplified kinetic model) would have been greater than the error in assuming a 1D model. The 1D model ignores radial temperature and concentration gradients and accounts for the discontinuity at the wall with heat and mass transfer coefficients. Some other major assumptions made are listed below:

- The gas was assumed to be an ideal gas with density changes owing to temperature changes included.
- The pressure drop in the reactor was assumed to be zero and pressure fluctuations resulting from flow pulsation were ignored.
- The gas phase was assumed to be in a pseudo-steady state with the wall. This

assumption is valid because of the widely differently time scales governing the transient terms in the solid and gaseous phases.

- Accumulation of mass in the washcoat is ignored, that is the solid phase mole balance was a steady state one.
- Washcoat diffusion was included. The washcoat was modelled as a one dimensional isothermal flat plate. The validity of this assumption is discussed in more detail shortly.
- The mole average velocity is taken to be equal to the mass average velocity. This assumption is reasonable because the reactants are present in low concentration and the mass transport by advection dominates the mass transport by diffusion. Furthermore, the change in moles on reaction is very small and the reactants are only present in low concentrations.
- The start of each segment corresponds to the beginning of a new development length for the fluid phase. The solid phase is continuous across the segments. This assumption is expanded in the section on model equations.

### **6.4.2 Model Equations**

The one-dimensional model equations which follow are based on those given in Hayes and Kolaczowski (1997) and are similar to those used by Liu et al (2000). Although the combustion products from an internal combustion engine are a complex mixture, the model is expressed in terms of methane and carbon monoxide only. These

components are the primary pollutants in the exhaust gas. The oxidation of CH<sub>4</sub> and CO can be represented by the following overall reactions:



The mole balance equations for the fluid phase are written assuming a steady state, that is, a pseudo steady state in the transient model, see Hayes et al., (1992) or Lee and Aris (1977). The fluid phase mole balance for methane is:

$$\frac{d}{dz} \left( (D_l)_{\text{CH}_4} C_b \frac{dY_{\text{CH}_4,b}}{dz} \right) - \frac{d(C_b v_m Y_{\text{CH}_4,b})}{dz} - \frac{4}{D_H} k_{m,\text{CH}_4} C_b (Y_{\text{CH}_4,b} - Y_{\text{CH}_4,s}) = 0 \quad (6.5)$$

The fluid phase mole balance for CO is:

$$\frac{d}{dz} \left( (D_l)_{\text{CO}} C_b \frac{dY_{\text{CO},b}}{dz} \right) - \frac{d(C_b v_m Y_{\text{CO},b})}{dz} - (-R_{\text{CO}})_H - \frac{4}{D_H} k_{m,\text{CO}} C_b (Y_{\text{CO},b} - Y_{\text{CO},s}) = 0 \quad (6.6)$$

The homogeneous reaction of CO was included in the model, because this reaction can proceed at lower temperatures than hydrocarbon oxidation. The rate expressions for homogeneous CO oxidation proposed by Dryer (1972) was used:

$$(-R_{\text{CO}})_H = 1.26 \times 10^{10} \exp\left(-\frac{20131}{T_b}\right) C_{\text{CO},b} C_{\text{O}_2,b}^{0.25} C_{\text{H}_2\text{O},b}^{0.5} \frac{\text{mol}}{\text{m}^3\text{s}} \quad (6.7)$$

Owing to the relatively low temperatures used in the reactor, the homogeneous combustion of methane was not expected to be significant. The reaction of methane was ignored in the model.

The subscript  $b$  denotes the mean bulk (gas phase) concentration. The bulk fluid energy balance equation is:

$$\frac{d}{dz} \left( \alpha_l \frac{dT_b}{dz} \right) - v_m \frac{dT_b}{dz} - \frac{(\Delta H_R)_{CO}}{\rho C_p} (-R_{CO})_H + \frac{4}{D_H} \frac{h}{\rho C_p} (T_S - T_b) = 0 \quad (6.8)$$

When the reactor inlet was at the coordinate denoted  $z=0$  (forward flow), the mean velocity is positive. When the reactor inlet is at coordinate  $z=L$  (reverse flow), the velocity is negative. The boundary conditions employed for Equations (6.5), (6.6) and (6.8) were Dirichlet conditions at the inlet and Neumann conditions at the outlet. Because the flow direction in the reactor was periodically reversed, the reactor inlet and outlet boundary conditions also had to be periodically changed to reflect the change in operating mode. When the reactor inlet corresponded to a coordinate of  $z=0$ , the boundary conditions were:

$$\text{at } z = 0: \quad Y_{CH_4} = (Y_{CH_4})_0; \quad Y_{CO} = (Y_{CO})_0; \quad T_b = T_{b0}$$

$$\text{at } z = L \quad \frac{dY_{CH_4,b}}{dz} = 0; \quad \frac{dY_{CO,b}}{dz} = 0; \quad \frac{dT_b}{dz} = 0$$

When the flow was switched so that the reactor inlet corresponded to  $z=L$ , the boundary conditions were also reversed. It should be noted that although diffusive boundary conditions (Danckwerts conditions) are more appropriate at the reactor inlet for the dispersed plug flow equation, their use does not lead to a significantly better solution when the advection strongly dominates the flow (Hayes and Kolaczowski, 1997).

When laminar flow is modelled using a one dimensional model, the effective dispersion coefficient for the mole and energy balance equations are (Hayes and Kolaczkowski, 1997):

$$D_I = D_{AB} + \frac{v_m^2 R^2}{48 D_{AB}} \quad \text{and} \quad \alpha_I = \alpha + \frac{v_m^2 R^2}{48 \alpha}$$

The mole balance equations for the solid phase are expressed in terms of the rate of mass transport to the external washcoat surface and the average reaction rate in the catalyst volume. The latter incorporates the effectiveness factor. The two mole balance equations are:

$$k_{m,CH_4} C_b (Y_{CH_4,b} - Y_{CH_4,S}) = \eta_{CH_4} (-R_{CH_4})_S \quad (6.9)$$

$$k_{m,CO} C_b (Y_{CO,b} - Y_{CO,S}) = \eta_{CO} (-R_{CO})_S \quad (6.10)$$

The reaction rates in Equations (6.9) and (6.10) have units of  $\text{mol/m}^2\text{s}$ . They are the reaction rates evaluated at the external surface of the washcoat (washcoat surface/gas interface), hence the use of the effectiveness factor to account for diffusion in the washcoat. The units imply that they are based on the geometric external surface area of the washcoat. This method of defining the rate is common in monolith channels. The units on the mass transfer coefficient are m/s. The energy balance equation for the solid phase includes the enthalpy change of both reactions:

$$\frac{\partial}{\partial z} \left( k_w \delta_w \frac{\partial T_S}{\partial z} \right) - h(T_S - T_b) - \sum_{i=1}^n [\eta_i (\Delta H_R)_i (-R_i)_S] = \delta_w \rho_w C_{pw} \frac{\partial T_S}{\partial t} \quad (6.11)$$

The enthalpy of the two exothermic reactions in kJ/mol can be written as functions of temperature:

$$(\Delta H_R^\circ)_{\text{CH}_4} = -806.9 + 1.586 \times 10^{-2} T - 8.485 \times 10^{-6} T^2 - 3.963 \times 10^{-9} T^3 + 2.16 \times 10^{-12} T^4 \quad (6.12)$$

$$(\Delta H_R^\circ)_{\text{CO}} = -279.581 - 1.861 \times 10^{-2} T + 2.52 \times 10^{-5} T^2 - 1.2247 \times 10^{-8} T^3 + 2.255 \times 10^{-12} T^4 \quad (6.13)$$

The boundary and initial conditions for Equation (6.11) are the same for both forward and reverse flow directions:

$$\text{at } z = 0 \text{ and at } z = L, \quad \frac{dT_s}{dz} = 0$$

$$\text{at } t = 0, \quad T_s = T_{s0}$$

The boundary conditions were applied at the entrance and exit to the reactor only. For the sake of computation, the gap was ignored and the reactor assumed to be continuous. Therefore axial dispersion in the gas phase was assumed to occur across segment boundaries, as well as axial heat conduction in the solid phase. This latter assumption is not expected to cause significant error, because the conduction in the substrate is relatively low. At the beginning of each segment a new combined development length was, however, assumed to start, which resulted in a sudden change in the values of the Nusselt and Sherwood numbers.

### 6.4.3 Heat and Mass Transfer Coefficients

The one-dimensional heterogeneous model requires values for the local heat and mass transfer coefficients, or the Nusselt and Sherwood numbers. For the segmented monolith the entry length should be included. It was assumed that the channels could be approximated as cylindrical ducts for the purposes of calculating heat and mass transfer coefficients. Although the channels of the ceramic substrate are square, the application of the washcoat tends to round the corners, so a round channel is a better approximation than a square one (Hayes and Kolaczkowski, 1994). For constant wall temperature, Tronconi and Forzatti (1992) presented a  $Nu$  correlation for simultaneously developing thermal and hydrodynamic boundary layers for a fluid with a Prandtl number of 0.7:

$$Nu_T = 3.657 + 8.827 \left( \frac{1000}{Gz} \right)^{-0.524} \exp \left( -\frac{48.2}{Gz} \right) \quad (6.14)$$

The Graetz number is defined as:

$$Gz = \frac{D_r}{z} Re Pr \quad (6.15)$$

The correlation for simultaneously developing flow at a Prandtl number of 0.7 with constant wall flux is given by Hayes and Kolaczkowski (1997):

$$Nu_H = 4.364 + 13.18 \left( \frac{1000}{Gz} \right)^{-0.524} \exp \left( -\frac{60.2}{Gz} \right) \quad (6.16)$$

The heat and mass transfer coefficients with reaction boundary conditions at the wall have values that lie between those calculated from Equations (6.14) and (6.16). The local  $Nu$  value in a system with chemical reaction at the wall was approximated by



interpolating between  $Nu_T$  and  $Nu_H$  using the interpolation formula of Brauer and Fetting (1966):

$$\frac{Nu - Nu_H}{Nu_T - Nu_H} = \frac{Da Nu}{(Da + Nu) Nu_T} \quad (6.17)$$

The Damköhler number,  $Da$ , is defined for an arbitrary reaction of component A by:

$$Da = \frac{\eta(-R_A)_S D_H}{4 C_{A,S} D_{AB}} \quad (6.18)$$

The Sherwood number was obtained by substituting the Schmidt number,  $Sc$ , for the Prandtl number in the equation for Graetz number, that is, Equation (6.15).

#### 6.4.4 Effectiveness Factor

The intrinsic rate expressions give values for the reaction rate in the absence of internal heat and mass transfer limitation. It has been shown (Hayes and Kolaczkowski, 1994; Leung et al., 1996) that diffusion resistance in the washcoat can be significant at the operating conditions used in this reactor, and must therefore be included in the reactor model. The effectiveness factor can be used to quantify the effect of the diffusion in the catalyst, and is defined for reactant A as:

$$\eta = \frac{\text{Average rate for the catalyst washcoat}}{\text{Rate at the surface conditions}} = \frac{(-R_A)_{\text{Average}}}{(-R_A)_S} \quad (6.19)$$

Both methane and carbon monoxide react in the washcoat. Because of the low reactant concentration and the thickness of the washcoat it is valid to assume that the washcoat is

isothermal (Leung et al., 1996). The washcoat geometry for the square channel typically consists of a fillet type structure, with the washcoat thicker in the corners than the mid-side (Hayes and Kolaczowski, 1997). This structure would require a two dimensional model to simulate exactly. A one dimensional approximation can be made by approximating the washcoat as a flat plate with the same characteristic length as the non-uniform washcoat. Although this approximation introduces a small error (see Leung, et al. (1996) for details), it results in a substantial saving in execution time. Furthermore, the exact geometry, porosity and tortuosity factor in the washcoat were not known, and therefore the added rigor of the 2D washcoat model was not considered to be justified. Errors associated with modelling the washcoat will be reflected in the values of the rate constants. The mole balance equations for the two reacting species in a one dimensional washcoat are:

$$(D_{\text{eff}})_{\text{CH}_4} C \frac{dY_{\text{CH}_4}^2}{dx^2} - \frac{(-R_{\text{CH}_4})}{L} = 0 \quad (6.20)$$

$$(D_{\text{eff}})_{\text{CO}} C \frac{dY_{\text{CO}}^2}{dx^2} - \frac{(-R_{\text{CO}})}{L} = 0 \quad (6.21)$$

Note that in each case the reaction rate is divided by the characteristic length of the washcoat to give a consistency of units. The characteristic length is the volume of the washcoat divided by the external area at the washcoat/channel interface. The boundary condition for Equations (6.20) and (6.21) are:

$$\text{at } x = 0, \quad \frac{dY_{\text{CO}}}{dx} = 0 \quad \text{and} \quad \frac{dY_{\text{CH}_4}}{dx} = 0$$

at  $x = L$  (washcoat surface)  $Y_{CO} = Y_{CO,S}$  and  $Y_{CH_4} = Y_{CH_4,S}$

$(D_{eff})_{CH_4}$  and  $(D_{eff})_{CO}$  are the effective diffusivities of methane and carbon monoxide in the washcoat based on the entire cross sectional area of the catalyst, both catalyst and pores, and include terms for the catalyst porosity and tortuosity. The diffusion in the pores of a typical monolith reactor washcoat is dominated by Knudsen diffusion. If the parallel pore model is assumed, the effective diffusion coefficient can then be written as:

$$D_{eff} = \frac{\varepsilon}{\tau} 97 a \left( \frac{T}{M} \right)^{0.5} \quad (6.22)$$

The tortuosity factor for the washcoat was taken as 8.0, the washcoat porosity was 0.41 and the mean pore diameter 10 nanometres. These values are the same as those found by Hayes et al., (1999) who analyzed a washcoated monolith similar to the one used in this study, which was also supplied by Johnson-Matthey.

For most kinetic expressions, a numerical solution is required for the mole balance equations in the washcoat. However, for first order kinetics, Equations (20) and (21) can be solved analytically to give:

$$\eta = \frac{\tanh(\Phi)}{\Phi} \quad (6.23)$$

Where the Thiele modulus,  $\Phi$ , is given by:

$$\Phi = \sqrt{\frac{Lk}{D_{eff}}} \quad (6.24)$$

In Equation (6.24)  $k$  is the first order rate constant in m/s.

### **6.4.5 Numerical Solution**

The mole and energy balance equations were solved using the Galerkin finite element method with quadratic shape functions. The discretization of the time differential in the transient solid phase energy balance [Equation (6.11)] was done using a fully implicit Gear scheme. The non-linear algebraic equations [Equations (6.9) and (6.10)] were expressed in the weak form to aid convergence. The systems of non-linear equations arising from the discretization were solved using a quasi-Newton method with an under-relaxation factor applied to the solid phase energy balance equation. Further information on the finite element modelling of monolith reactor channels can be found in Hayes et al. (1992) and Hayes and Kolaczowski (1997). In all of the simulations reported, the reactor was discretized using 120 quadratic finite elements. The step size in all cases was 1 second. Refining the discretization gave no noticeable improvement in the solution.

## **6.5 Kinetics**

A paramount consideration in the development of a usable reactor model is the determination of a reliable kinetic model. The model used will of necessity be a simplification of the true situation prevailing, both for reasons of computational cost and because of the difficulty in determining the mechanism and parameter values. In this investigation it was desired to develop a relatively simple kinetic model that was capable of capturing the principal features of the reversing flow reactor under the range of operating conditions experience with the given dual fuel engine.

The kinetics of the reactions involved in automotive catalytic converters have been widely studied for gasoline engines, although most modelling studies use modified versions of the expressions proposed by Voltz et al. (1973); see, for example, Oh and Cavendish (1982), and Siemund et al. (1996). The expressions of Voltz et al. (1973) are of the LHHW type, and consider the oxidation of CO and HC in the presence of NO<sub>x</sub> and were obtained on a platinum based catalyst. Hydrocarbons are subdivided into "slow" and "fast" burning HC. Considering CH<sub>4</sub> to be a "slow burning" HC, the Voltz et al. (1973) equations adapted for methane and CO oxidation this work have the following form (Liu et al., 2000):

$$(-R_{\text{CH}_4})_s = k_{\text{CH}_4} \frac{Y_{\text{CH}_4,s} Y_{\text{O}_2,s}}{R(\theta)} \quad (6.25)$$

$$(-R_{\text{CO}})_s = k_{\text{CO}} \frac{Y_{\text{CO},s} Y_{\text{O}_2,s}}{R(\theta)} \quad (6.26)$$

$$R(\theta) = T_s [1 + k_{a1} Y_{\text{CO},s}]^2 [1 + k_{a4} Y_{\text{NO},s}^m] \quad (6.27)$$

In a previous investigation, (Liu et al., 2000) showed that modified Voltz type kinetic expression was able satisfactorily to reproduce transient experimental data from a uni-directional flow simulation. In spite of that, the Voltz model was not developed for palladium catalysts, and it is more appropriate to examine the oxidation kinetics reported in the literature for methane combustion over palladium catalysts.

The kinetics of methane oxidation over palladium catalysts has been studied by many researchers; see for example Cullis and Willatt (1983) and the references cited therein. The kinetics of the oxidation reaction are commonly fitted using a power law rate

expression:

$$(-R_{\text{CH}_4})_s = k P_{\text{CH}_4}^n P_{\text{O}_2}^m \quad (6.28)$$

The order of the reaction with respect to methane is generally reported to one or slightly less, whilst the order of reaction with respect to oxygen is zero or close to zero. If one assumes a Mars and van Kreveln type of reaction mechanism (Golodets 1983), then the following rate expression can be derived for the oxidation of methane (in the absence of water inhibition effects):

$$(-R_{\text{CH}_4})_s = \frac{k_1 C_{\text{CH}_4} C_{\text{O}_2}}{k_2 C_{\text{O}_2} + k_3 C_{\text{CH}_4}} = \frac{k_3 C_{\text{CH}_4}}{1 + k_4 \frac{C_{\text{CH}_4}}{C_{\text{O}_2}}} \quad (6.29)$$

If the concentration of oxygen is relatively large, and  $k_2 \gg k_3$ , (that is,  $1 \gg k_4 \frac{C_{\text{CH}_4}}{C_{\text{O}_2}}$ )

then Equation (6.29) can simplify to an expression that is first order in methane and zero order in oxygen, whilst at low oxygen pressure a small oxygen dependence could be observed. Such observations are consistent with experimental findings.

Water is known to inhibit the oxidation of methane over palladium, presumably by occupying reaction sites on the palladium oxide particles. Power law expressions have also been reported with an inhibition effect owing to water. For example, Giezen (1997) developed a methane oxidation kinetic expression after evaluating the effects of  $\text{CH}_4$ ,  $\text{CO}_2$ ,  $\text{O}_2$  and  $\text{H}_2\text{O}$  in the temperature range of 453 to 788 K. The reported expression is:

$$(-R_{\text{CH}_4})_s = k C_{\text{CH}_4} C_{\text{O}_2}^{0.1} C_{\text{CO}_2}^0 C_{\text{H}_2\text{O}}^{-0.8} \quad (6.30)$$

Equation (6.29) can also be extended to include water inhibition. Assuming that the water adsorbs on oxygen sites (Beld et. al, 1994; Golodets, 1983) the resulting rate expression is:

$$(-R_{\text{CH}_4})_s = \frac{k_3 C_{\text{CH}_4}}{1 + K_{\text{H}_2\text{O}} C_{\text{H}_2\text{O}} + k_4 \frac{C_{\text{CH}_4}}{C_{\text{O}_2}}} \quad (6.31)$$

Provided that  $(1 + K_{\text{H}_2\text{O}} C_{\text{H}_2\text{O}}) \gg \left(k_4 \frac{C_{\text{CH}_4}}{C_{\text{O}_2}}\right)$ , then Equation (6.31) reduces to:

$$(-R_{\text{CH}_4})_s = \frac{k_3 C_{\text{CH}_4}}{1 + K_{\text{H}_2\text{O}} C_{\text{H}_2\text{O}}} \quad (6.32)$$

An expression in the form of Equation (6.32) is preferred to one of the form of Equation (6.30) because it can handle the complete range of water concentration, including zero. If a large amount of water is present, such as the case in a secondary combustion application, then the water concentration is constant and  $1 \ll K_{\text{H}_2\text{O}} C_{\text{H}_2\text{O}}$ . In this case, the oxidation rate will have the appearance of a pseudo first order reaction. By analogy, a similar derivation can be made to show that at relatively low concentrations of CO and in a large excess of water, the oxidation of CO can also be approximated by a power law expression that is first order in CO and zero order in oxygen.

It should be pointed out that the modified Voltz equations successfully used by Liu et al. (2000) are in fact equivalent to first order rate expressions in terms of either methane or CO under the conditions used in the reactor: excess oxygen, relative low  $\text{NO}_x$  concentration and low CO concentration.

In conclusion, both methane and CO catalytic reactions could be developed as pseudo first order reactions. This is based on the lean combustion engine exhaust characteristics. It has excess oxygen and water, and low NO<sub>x</sub> and CO concentration. The effect from CO could be ignored and those from oxygen, water and NO<sub>x</sub> could be incorporated into the apparent rate constant. In the following section, the first order kinetics is applied to the modelling study and the kinetic data are given based on the experiment data.

An additional complexity in the oxidation of methane is that there is an apparent shift in the activation energy as the temperature increases. The temperature at which this transition occurs has been reported to be a function of catalyst starting composition. Although it is essential to differentiate changes in apparent activation energy that occur as a result of the onset of heat and mass transfer effects, there appears to be sufficient evidence in the literature that there is indeed a genuine activation energy change in the reaction. Some of the significant papers that have reported this phenomena are cited in the following paragraph.

Cullis and Willatt (1983) studied the methane oxidation over Pd catalysts in the temperature range of 500 to 800 K and observed a change in activation energy of reaction. Depending on the catalyst loading, supporting material and its structure, and the reactant composition, the transition temperature varied from 654 K to 720 K. Below the transition temperature, the activation energy ranged from 75 kJ/mol to 95 kJ/mol. Above the transition temperature, the activation energy decreased to a value in the region 23 to 45 kJ/mol.



Kolaczkowski et al (1996) reported an investigation of the oxidation of methane over palladium in a monolith reactor. They measured global reaction rates. At low temperatures (less than 770 K) they reported an activation energy around 131 kJ/mol. As temperatures exceeded 770 K, the apparent activation energy began to drop sharply, and global rate data were well correlated with an activation energy of around 19 kJ/mol. Kolaczkowski et al (1996) attributed the decline in activation energy to both internal and external mass transfer resistance. Indeed, for the reaction rates reported, it can be shown (Leung et al, 1996) that washcoat diffusion resistance would have been a significant factor. However, the change in activation energy from 131 kJ to 19 kJ cannot be explained solely by internal diffusion resistance. Kolaczkowski et al. (1996) recognized this, and explained the sharp drop in activation in terms of external mass transfer resistance. In a subsequent experimental and modelling study (Hayes et al, 1996), however, the external diffusion resistance was found to be insufficient to account for this effect. In an investigation of the high temperature oxidation of methane over the same catalyst, it was found that a reaction rate expression with an activation energy of 19 kJ/mol was extremely good in modelling the complex transient behavior of the monolith reactor. In that investigation, the external mass and heat transfer effects were included explicitly in a two dimensional axisymmetric model, and the internal diffusion resistance was included as a lumped parameter in the kinetic expression. At the high temperatures employed in that study the reaction was in the asymptotic diffusion resistance region, therefore one would expect that the intrinsic activation energy would have been of the order of 38 kJ/mol (twice the diffusion limited value).

Sakai et al. (1991) studied the catalytic converter for natural gas fuelled engine. They found the Pd catalyst performance also underwent a transition from low temperature to high temperature. The transition temperature was 690 K. Below this temperature, the activation energy was 76.5 kJ/mol. Above this temperature, it dropped to 61 kJ/mol. These observations for the transition of methane catalytic oxidation are summarized in Table 6-4.

Based on the literature, it was concluded that for the operating conditions of the reverse flow converter, first order models for both methane and CO oxidation were appropriate.

Table 6-4 Activation Energy and Transition Temperature for Methane Oxidation over Palladium Based Catalyst

Reference	Activation Energy kJ/mol		Transition Temperature (K)
	Low Temperature Region	High Temperature Region	
Cullis and Willatt (1983)	75-95	23-45	654-720
Kolaczowski et al. (1996)	131	19*	770
Sakai et al. (1991)	76.5	61	690

\* Influenced by Internal Diffusion

## 6.6 Model Results and Analysis

The kinetic constants were evaluated by simulating the three reverse flow experiments described in Section 6.3, the conditions for which were given in Tables 6-2 and 3. The initial condition used in the model was the experimentally measured reactor temperature profile at the time denoted zero, which are shown in Figure 6-4. The measured reactor inlet temperatures were used as the inlet boundary conditions. These temperatures as a function of time are shown in Figure 6-8. Although the outlet temperature from the engine was constant after the step change to operating conditions, the inlet temperature to the reactor changed slowly over the course of the experiment owing to the thermal mass of the ductwork. It was found that the forward flow inlet temperature was not equal to the reverse flow inlet for these “symmetric” reverse flow operations. This effect was a result of the different thermal masses of the inlet and outlet ductwork, as well as different temperatures for each set of ductwork at the commencement of the reverse flow operation.

The temperature range over which the reactor operating during reverse flow operation covered the range for which transitions in activation energy had been reported. The temperatures are also higher than those observed for uni-directional flow for the same mode of engine operation (Liu et al., 2000). To obtain an estimate of the low temperature kinetic parameters, a series of steady state uni-directional flow experiments was conducted. The engine operating modes, inlet compositions, concentrations and exhaust gas temperatures are given in Table 6-5. The average reactor temperature for these tests ranged from 694 to 919 K. To obtain a rough estimate of the activation

energy for these runs, the simulator was run with a constant value of first order rate constant for each of the two reactions. The value of rate constant that gave an agreement between experimental and simulated conversion was then plotted as a function of the reciprocal of the average reactor wall temperature, as shown in Figure 6-9. The estimated kinetic expressions were, for methane oxidation:

$$(-R_{\text{CH}_4})_s = 3.0 \times 10^9 \exp\left(\frac{-1.59 \times 10^5}{R_g T}\right) C_{\text{CH}_4} \quad (6.33)$$

and for CO oxidation:

$$(-R_{\text{CO}})_s = 6.8 \times 10^3 \exp\left(\frac{-5.49 \times 10^4}{R_g T}\right) C_{\text{CO}} \quad (6.34)$$

The temperatures over which this set of experiments was performed includes the temperatures experience by the reactor during the operation of Case 1 and for the first part of Case 2. The latter portion of the Case 2 experiment and all of the Case 3 experiment were both conducted at higher temperatures. It was not possible to obtain steady state uni-directional flow data at these higher temperatures, and therefore the initial estimates of the kinetic parameters for the high temperature region were based on literature values from Cullis and Willatt (1983), Sakai et al. (1991) and Kolaczkowski et al. (1996), as shown in Table 6-4.

Table 6-5 Steady State Results for the Unidirectional Flow Converter at Low Temperature

Engine Mode		Temperature (K)			Exhaust Composition						Gm g/s	Conver.	
Speed rpm	Tor. Nm	T <sub>in</sub>	T <sub>o</sub>	T <sub>a</sub>	HC ppm	CO ppm	NO ppm	O <sub>2</sub> %	CO <sub>2</sub> %	H <sub>2</sub> O %		HC %	CO %
1500	140	675	704	694	3335	1635	1002	9.59	5.28	10.25	41.07	18	94
1500	180	717	737	737	1533	738	1081	6.40	6.93	13.27	40.04	37	93
1500	200	752	768	767	816	578	1539	5.23	7.47	14.27	44.56	60	93
2600	120	801	868	823	3204	1986	126	8.97	5.65	11.00	73.39	71	97
2600	130	831	935	890	4116	2116	356	8.96	5.47	10.68	72.16	88	95
2600	140	844	903	876	2293	1674	273	7.61	6.26	12.11	72.72	85	97
2600	155	877	938	919	2143	1692	572	7.27	6.43	12.44	72.39	95	94
2600	158	884	938	911	1905	1454	599	7.16	6.55	12.65	72.64	93	97

Tor.: Engine Torque

T<sub>in</sub>: Reactor Inlet Temperature

T<sub>o</sub>: Reactor Outlet Temperature

T<sub>a</sub>: Reactor Average Temperature

Gm: Mass Flow Rate

Conver.: Conversion

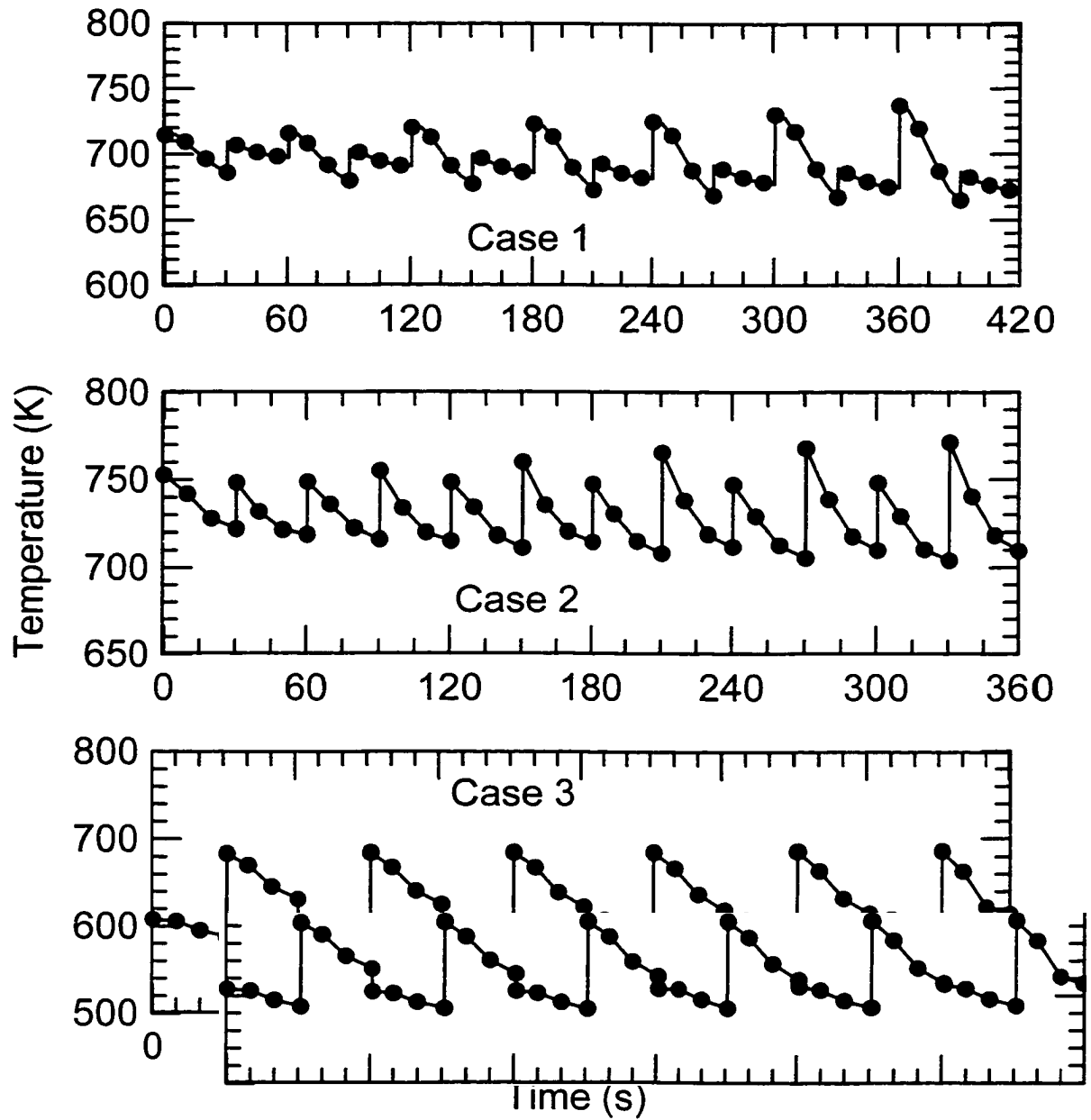


Figure 6-8 The Transient Reactor Inlet Temperature During Reverse Flow Cycling.

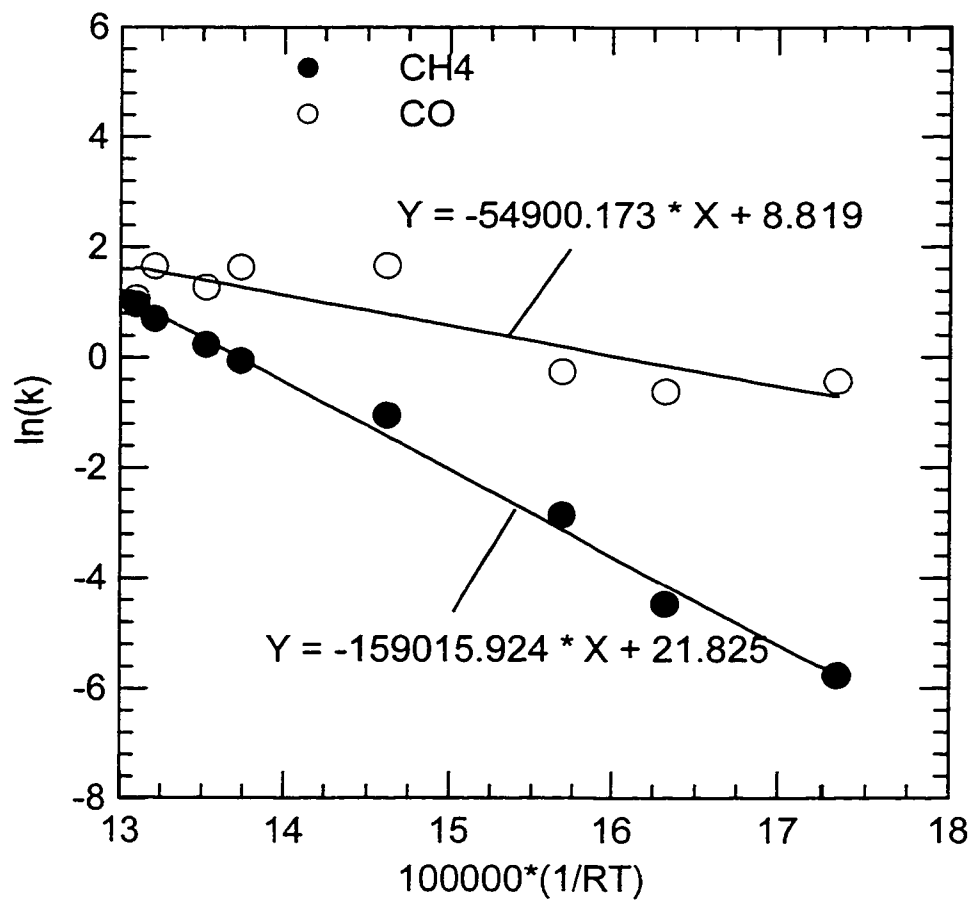


Figure 6-9 Arrhenius Plot for CH4 and CO Oxidation.

Once the initial estimates of the kinetic parameters were obtained, the simulator was run for the three experimental cases. The values of the kinetic constants, and the transition temperature between low and high temperature regions, were adjusted until a good match was obtained between the simulated and measured outlet concentrations, and also the measured and predicted wall temperature. This latter comparison is a very good test for the agreement of the model to the experimental data. It is usually considered easier to match outlet conversion with a model, and wall temperature profile matching is a good validation method (Hayes and Kolaczkowski, 1997). Table 6-6 gives the values of the kinetic parameters that gave the best fit to the data. Note that for Case 1, the entire simulation effectively falls in the low temperature region, and thus the high temperature values have no relevance. They were obtained by taking the high temperature activation energy and the transition temperature, and then calculating the pre-exponential factor that gave the same rate constant at the transition temperature. Similarly, for Case 3 the entire operation is effectively controlled by the high temperature kinetic constants. Only in Case 2 do both temperature regions play a significant role, and it was from this experiment that the value of the transition temperature was determined. The optimal low temperature value for the activation energy of 129 kJ/mol compares favourably with literature values, especially the result of Kolaczkowski et al. (1996), who used a very similar catalyst. The low temperature value also compares favourably with literature values. It is similar to the value of Kolaczkowski et al. (1996) ( after their value is adjusted for intra-phase diffusion resistance), and within the range reported by Cullis and Willatt (1983). The transition temperature, however, is somewhat higher than any of



these investigators has reported, but it agrees very well with further experimental work currently in progress by Hayes et al. (personal communication, May 2000). Furthermore, the agreement among the values of the kinetic constants for each of the three cases suggests that the proposed first order kinetic rate equations for methane are reasonable approximations for the range of operating conditions encountered.

At the temperature ranges considered, CO conversion is uniformly high. This means the kinetic constants are based on a very narrow range of values. However, the values calculated are consistent between cases, and similar to those of other researches. They produce conversion results matching the experimental data.

Table 6-6 Best Fit Kinetic Parameters for Reverse Flow Operation

Case	CH <sub>4</sub> Oxidation				CO Oxidation		Tran. Temp. (K)	Domi. Temp. Region
	Low Temp. Region		High Temp. Region		A	E		
	A	E	A	E				
Case 1	$1.419 \times 10^7$	129	25.25	35	$5.411 \times 10^3$	54.9	854	Low
Case 2	$2.264 \times 10^7$	129	40.29	35	$5.479 \times 10^3$	54.9	854	Both
Case 3	$2.501 \times 10^7$	129	44.5	35	$1.791 \times 10^3$	54.9	854	High

A: Pre-exponent factor, m/s

E: Activation energy, kJ/mol

Low Temp. Region: Low Temperature Region

High Temp. Region: High Temperature Region

Tran. Temp.: Transition Temperature of Catalyst Kinetics

Domi. Temp. Region: Dominant Temperature Region of Methane Catalytic Reaction

The conversion of HC and CO at the reactor exit plotted as a function of time for both experimental and simulated values is shown in Figure 6-10. Good agreement between simulated and experimental values was observed. The development of the reactor temperature in the middle of reactor as a function of time during the reverse flow cycling in these three cases are shown in Figure 6-11 and 6-12. The solid line is the simulation and the dotted line the experimental result. The agreement between the two is also good. Axial temperature profiles in the beginning, middle and final stage of reverse flow cycling for both experimental and simulation are compared in Figures 6-13, 6-14 and 6-15. They show the temperature status and development in the six locations along the reactor. A good match between experiment and simulation could also be found.

To obtain a common kinetic data set, the average values for the pre-exponential factors were calculated. The pre-exponential factor for the low temperature region was obtained by averaging the values for case 1 and case 2. The value for the high temperature region was calculated from the high temperature values for case 2 and case 3. The transition temperature was then obtained by determining the temperature at which the high temperature and low temperature values gave the same value for the rate constant. These data are summarized in Table 6-7. Figure 6-16 shows the simulation results with this common kinetic data set. It compares the HC and CO conversion as a function of time for both experimental and simulated values. Generally, the agreement between experiment and simulation was good, however, as expected, there is more deviation between the experimental values and the predicted values.

Table 6-7 Average Values of Kinetic Parameters for the Three Cases Studied

CH <sub>4</sub> Oxidation				CO Oxidation		Transition Temp. for CH <sub>4</sub> Reaction, K
Low Temp. Region		High Temp. Region		<i>A</i>	<i>E</i>	
<i>A</i>	<i>E</i>	<i>A</i>	<i>E</i>			
$1.750 \times 10^7$	129	42.40	35	$3.804 \times 10^3$	55	874

A: Pre-exponent factor, m/s

E: Activation energy, kJ/mol

Temp.: Temperature

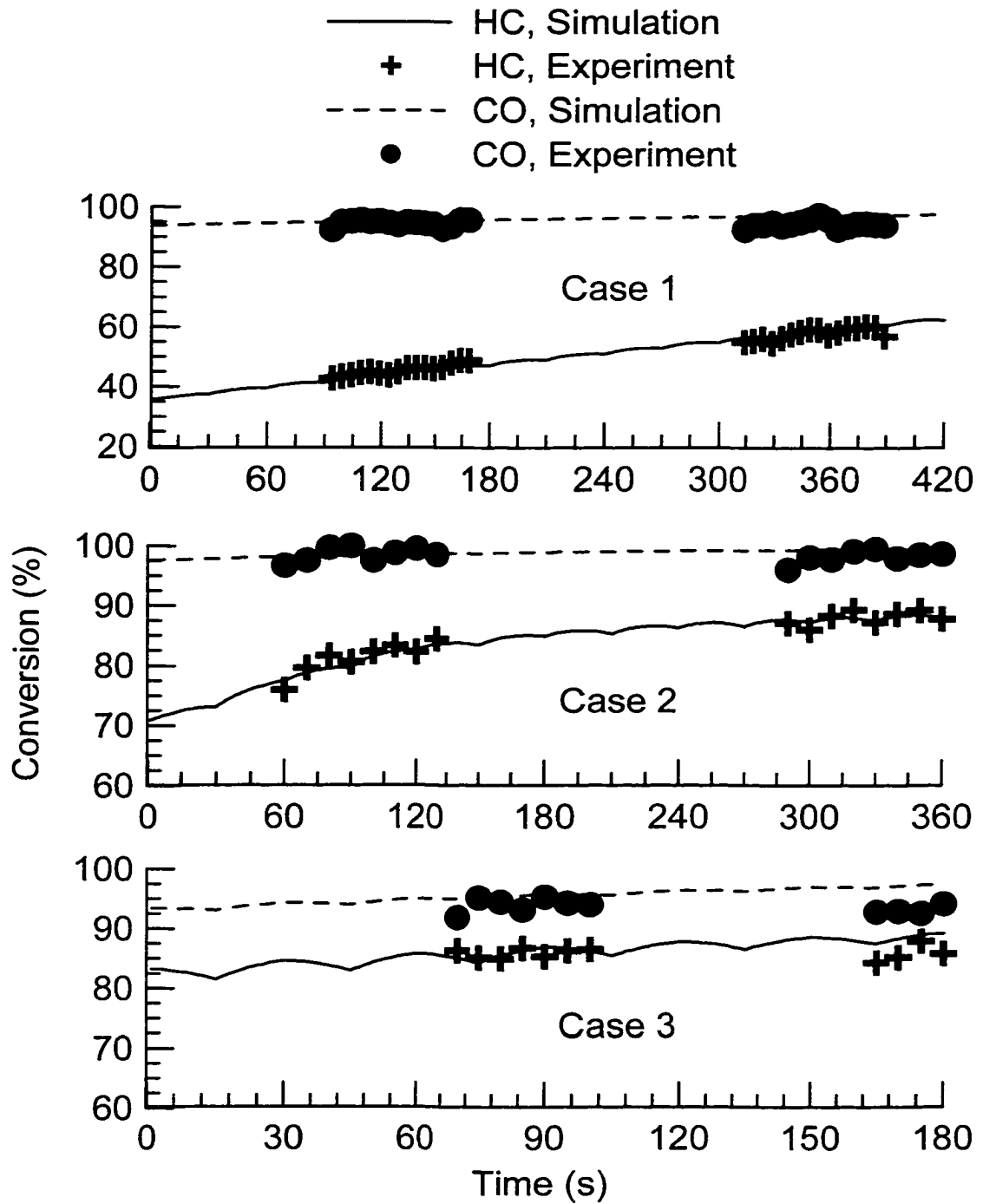


Figure 6-10 Comparison of Transient HC and CO Conversion Between Experiment and Simulation

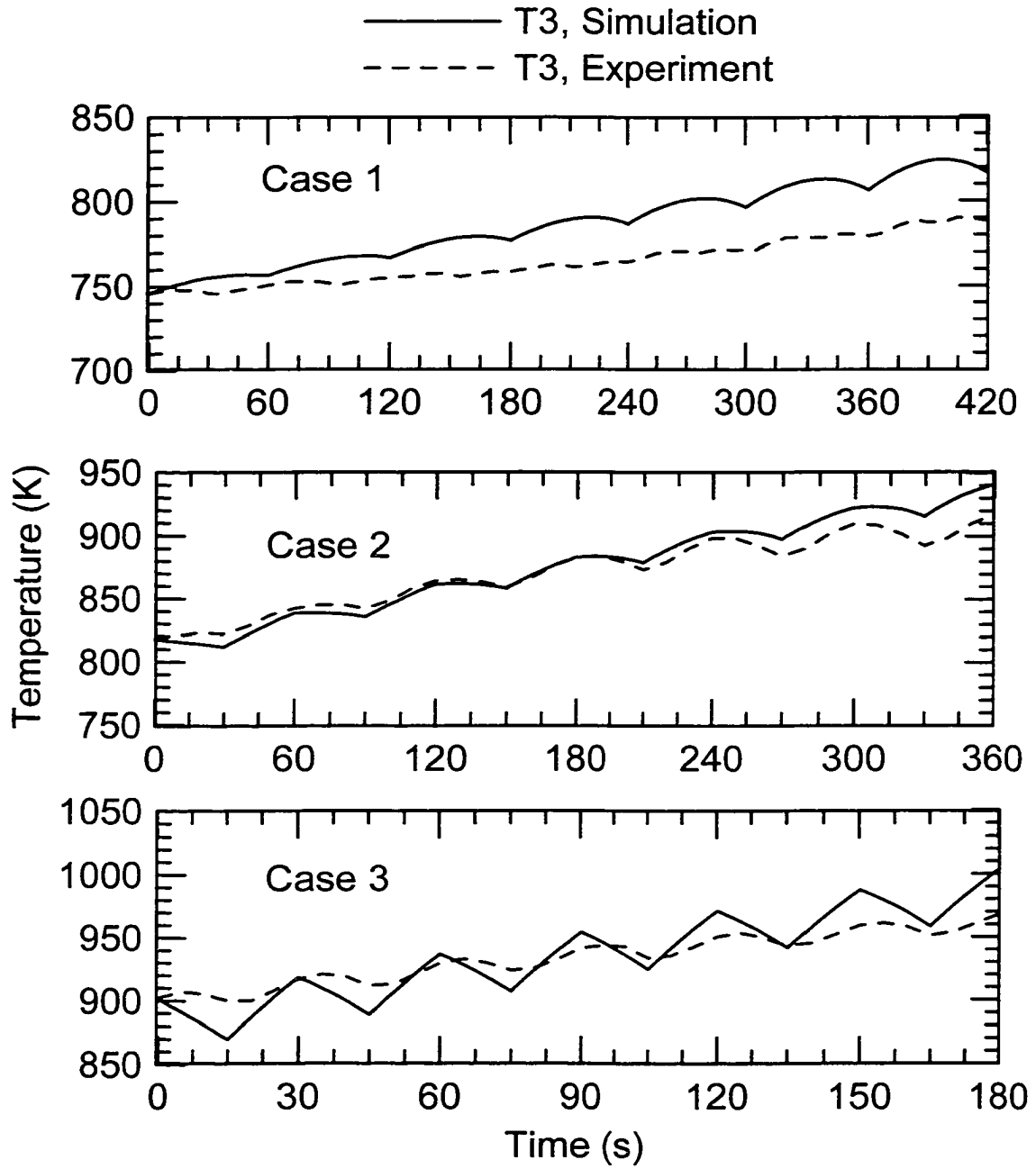


Figure 6-11 Comparison of Middle Reactor Temperature T3 Between Experiment and Simulation

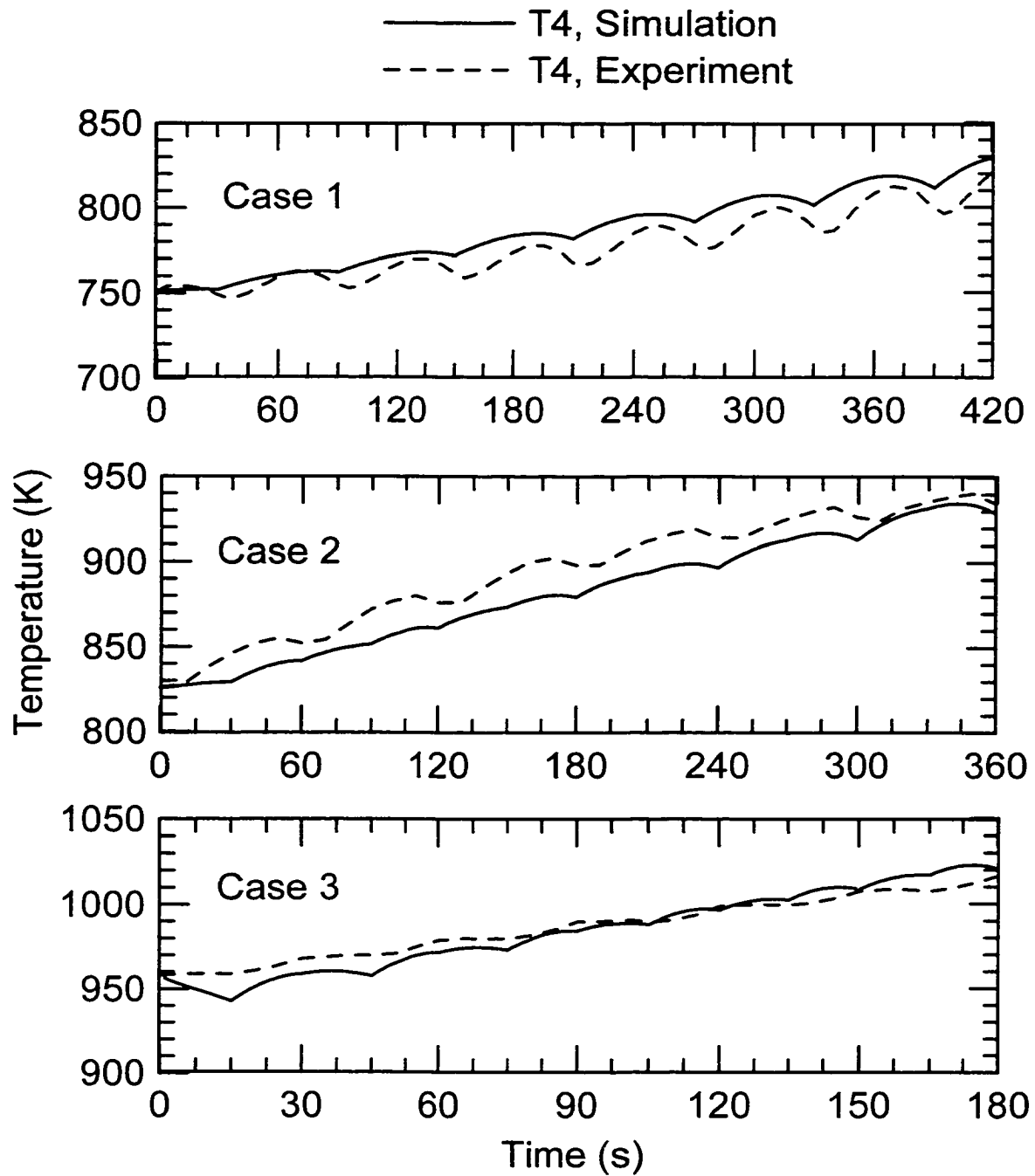


Figure 6-12 Comparison of Middle Reactor Temperature T4 Between Experiment and Simulation

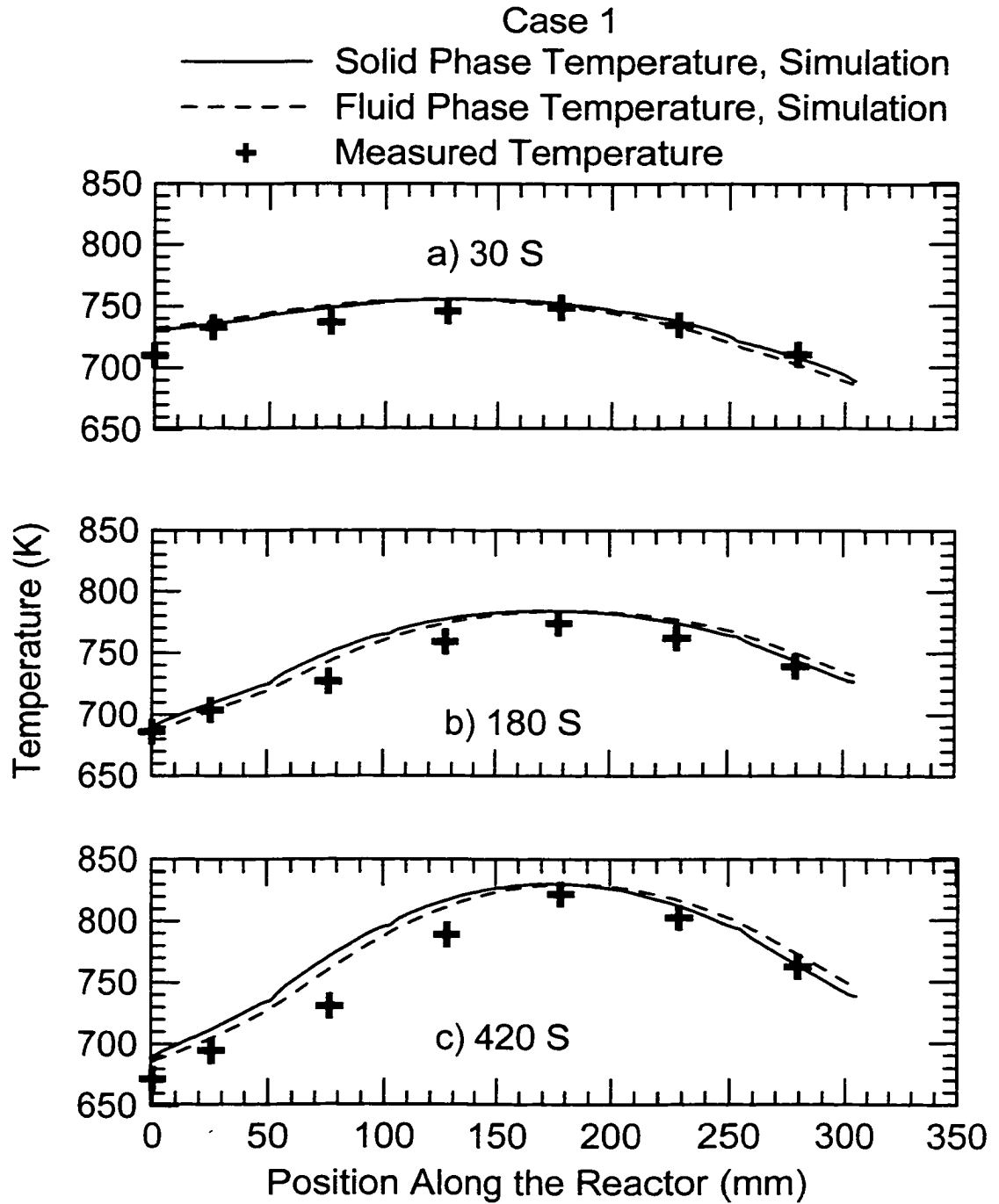


Figure 6-13 Comparison of Simulated and Experimental Reactor Temperature Profiles at Various Elapsed Times for Case 1

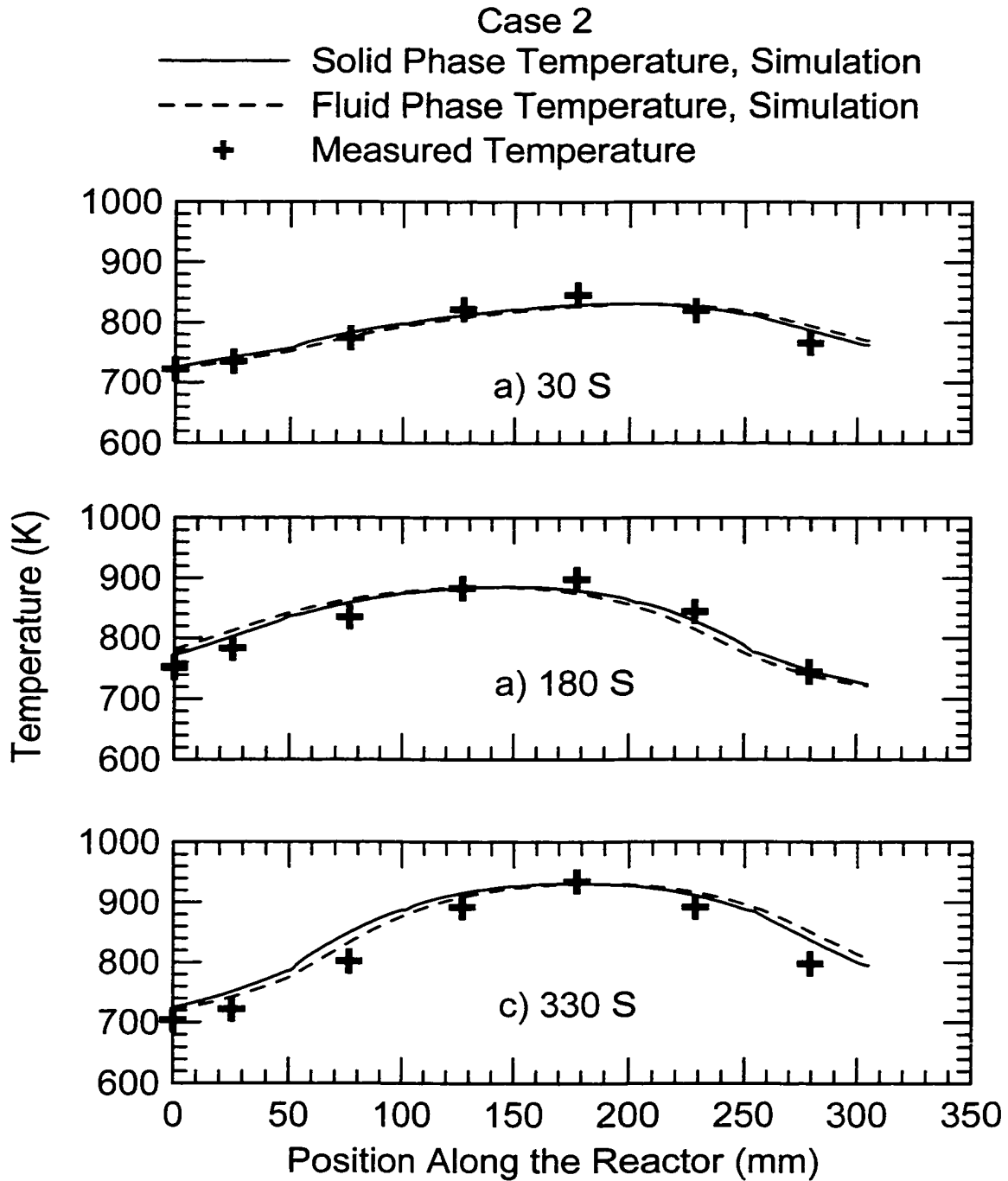


Figure 6-14 Comparison of Simulated and Experimental Reactor Temperature Profiles at Various Elapsed Times for Case 2



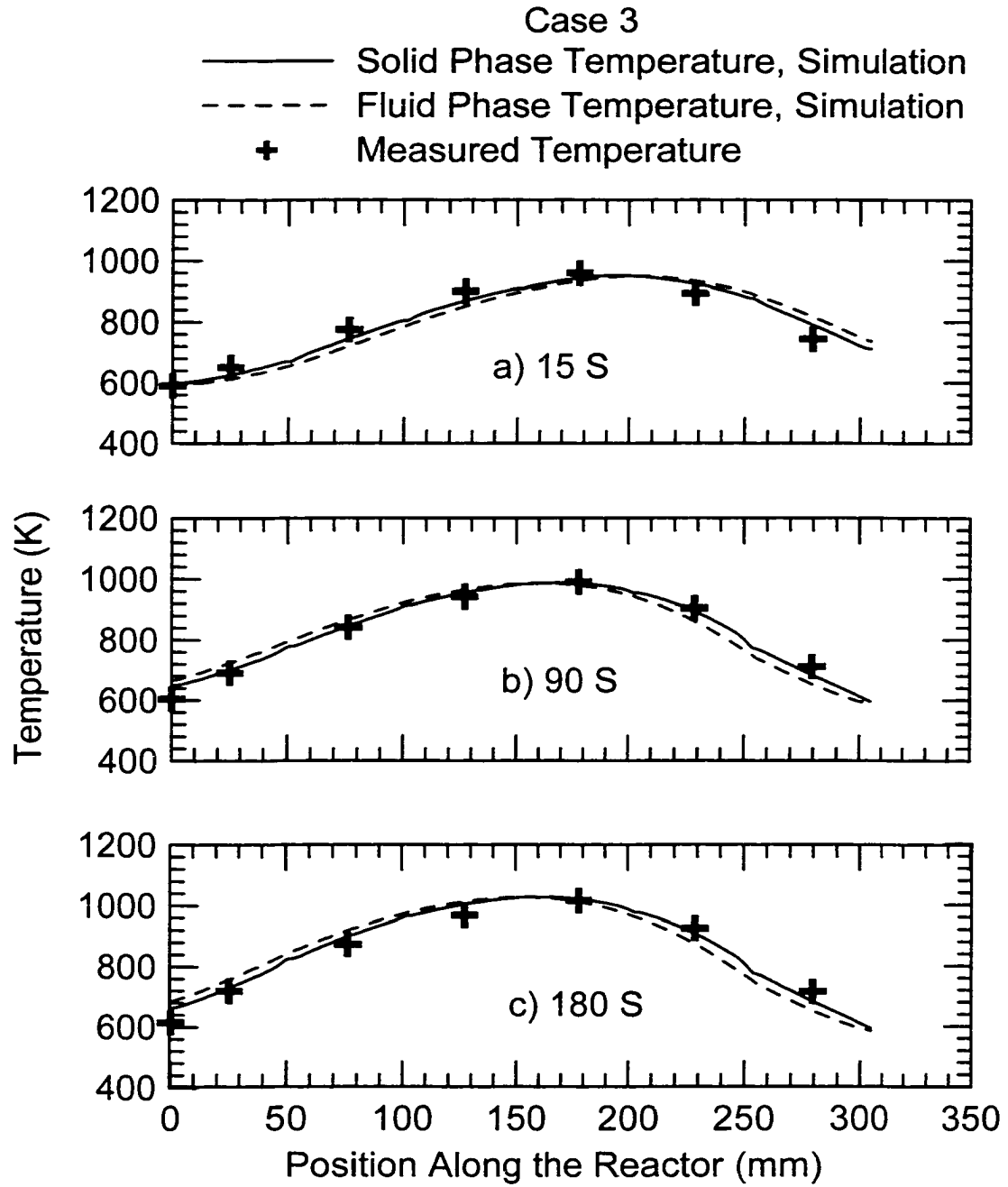


Figure 6-15 Comparison of Simulated and Experimental Reactor Temperature Profiles at Various Elapsed Times for Case 3

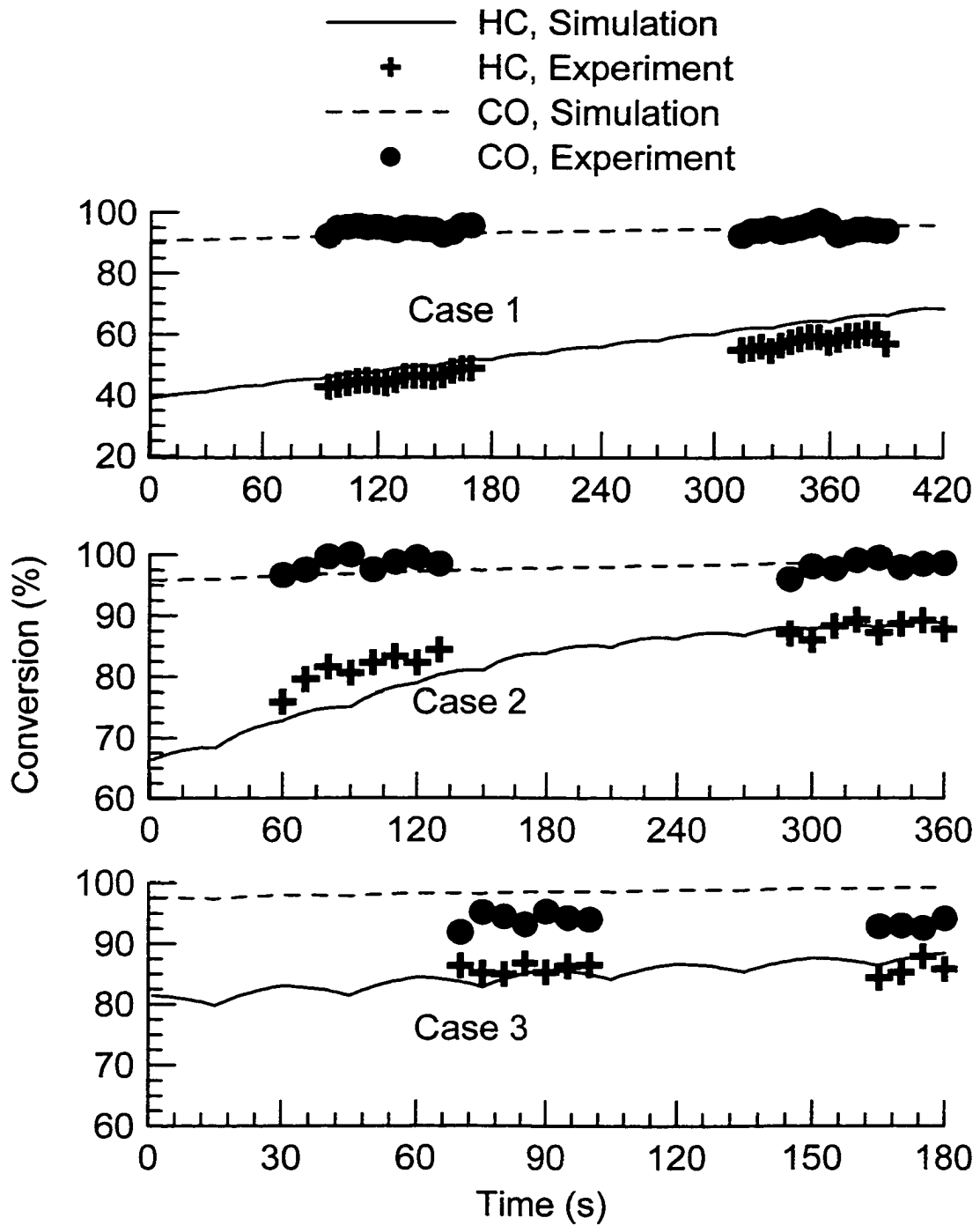


Figure 6-16 Comparison of Transient HC and CO Conversion Between Experiment and Simulation Using Average Values for the Kinetic Parameters

To illustrate the use of the model, it was used to compare the transient performance of the catalytic converter under unidirectional flow and reverse flow modes. Case 3 was selected for illustration. Two simulations were performed, with the same initial and inlet conditions, using the common set of kinetic parameters given in Table 6-7. One simulation used reverse flow operation and the other one unidirectional flow operation. The flow switch time for the reverse flow was 15 seconds with a symmetrical cycle (total cycle time 30 seconds). Figure 6-17 and Figure 6-18 show the difference between the reverse flow and unidirectional flow. Figure 6-17 compares the HC and CO conversion and Figure 6-18 compares the middle reactor temperature  $T_3$  and  $T_4$ . With the reverse flow operation, the reactor temperature gradually increased, as did the HC and CO conversion. However, for the unidirectional flow operation, reactor temperature fell very quickly. Within three minutes, the middle reactor temperature had decreased to about 560 K, the HC conversion dropped to zero and the CO conversion was reduced to only about 50%. This shows the thermal advantage of reverse flow operation, and confirms the experimental observations reported on Figure 6-7.

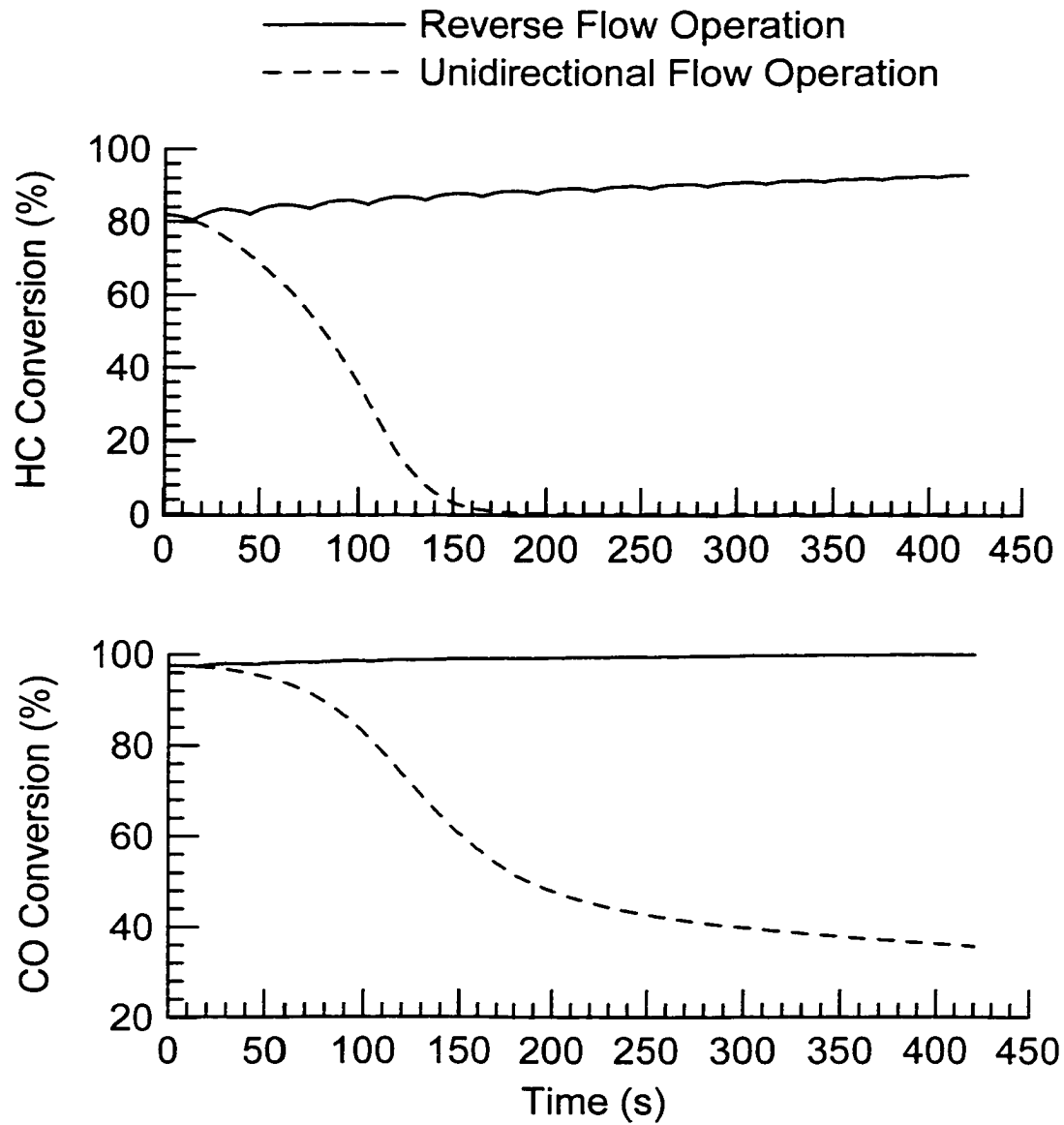


Figure 6-17 Comparison of HC and CO Conversion Between the Reverse Flow Operation and the Unidirectional Flow Operation

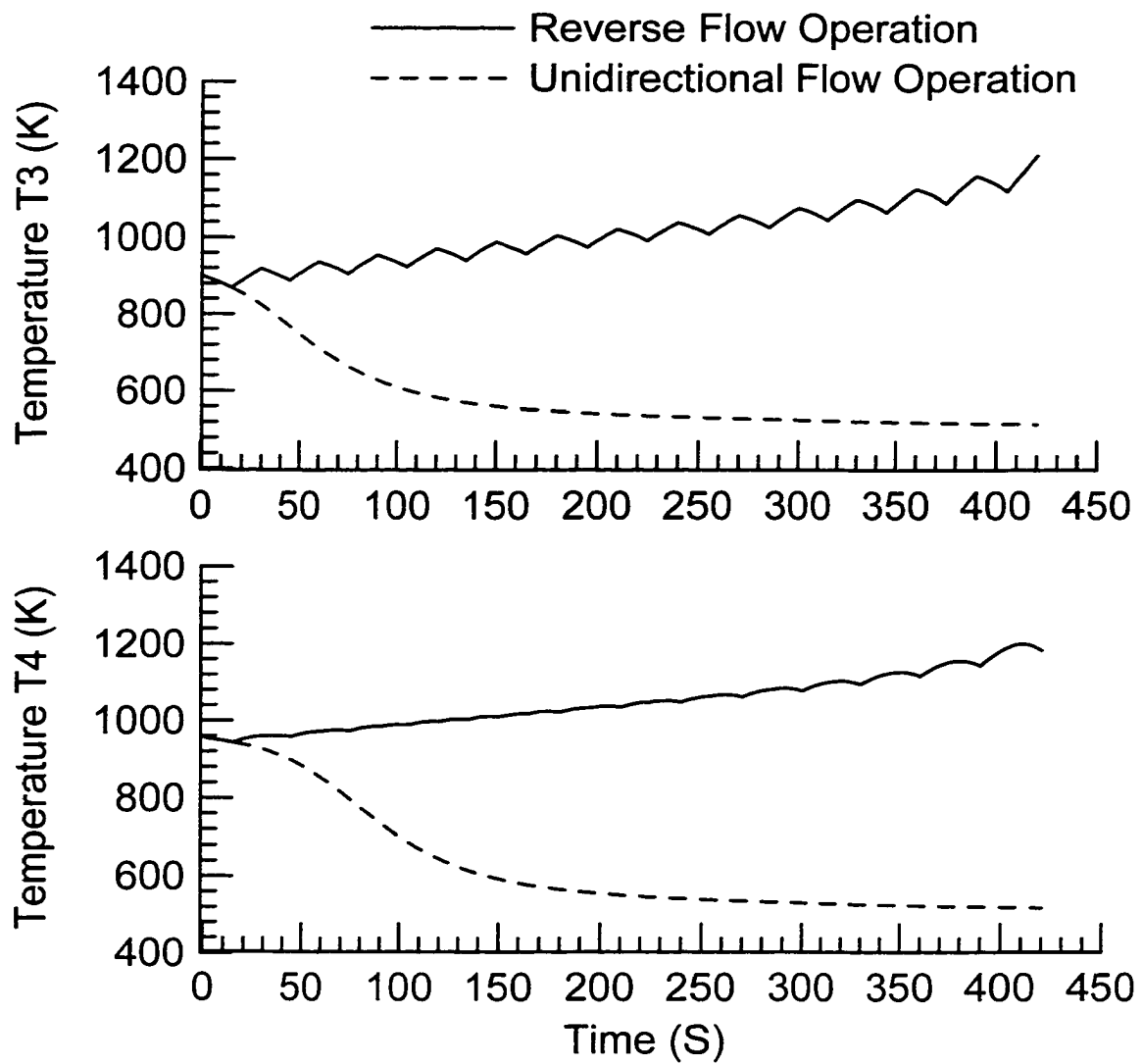


Figure 6-18 Comparison of Middle Reactor Temperatures  $T_3$  and  $T_4$  Between the Reverse Flow Operation and the Unidirectional Flow Operation

## 6.7 Conclusions

Based on the experimental and modelling study of a reverse flow catalytic converter for a natural gas/diesel dual fuel engine, several conclusions were drawn.

The reverse flow catalytic converter is able to achieve a high level of CO and HC conversion at the low inlet temperatures that exist for light load operations, provided that the initial reactor temperature is sufficiently high. The reverse flow catalytic converter can be simulated with reasonable accuracy using a one dimensional single channel model. Both CO and methane oxidation over palladium catalyst in an excess of oxygen and water were well described using apparent first order kinetics. The catalyst underwent an apparent transition at a temperature in the region of 874 K, at which point the apparent activation energy decreased dramatically.

## 6.8 Nomenclature

$A_c$ :	Cross-sectional area of channel, $m^2$
$A_w$ :	Wall cross-sectional area, $m^2$
$a$ :	Mean pore radius of washcoat, m
$C$ :	Molar density (Concentration), $mol/m^3$
$C_b$ :	Total molar concentration, $mol/m^3$
$[CH_4]$ :	$CH_4$ Concentration, $mol/m^3$
$[CO_2]$ :	$CO_2$ Concentration, $mol/m^3$
$[CO]_{in}$ :	Reactor inlet CO concentration, ppm
$[CO]_{out}$ :	Reactor outlet CO concentration, ppm
$C_{i,b}$ :	Concentration for species $i$ in the bulk, $mol/m^3$
$C_{i,s}$ :	Concentration for species $i$ in the surface of washcoat, $mol/m^3$

$C_p$ :	Constant pressure heat capacity, J/(kg · K)
$C_{pw}$ :	Constant pressure heat capacity of the wall, J/(kg · K)
$Da$ :	Damköhler number, dimensionless
$D_{AB}$ :	Binary diffusion coefficient, m <sup>2</sup> /s
$(D_{eff})_i$ :	Effective diffusivity in washcoat, m <sup>2</sup> /s
$D_H$ :	Hydraulic diameter, $D_H = \frac{4A_c}{W_p}$ , m
$(D_l)_i$ :	Dispersion coefficient for species $i$ , m <sup>2</sup> /s
$D_T$ :	Channel diameter, m
$E$ :	Activation energy, J/mol
$E_1$ :	Activation energy for CH <sub>4</sub> kinetics, J/mol
$E_2$ :	Activation energy for CO kinetics, J/mol
$E_3$ :	Activation energy for CO inhibition, J/mol
$E_4$ :	Activation energy for CH <sub>4</sub> kinetics, J/mol
$Gz$ :	Gratz number, dimensionless
$h$ :	Heat transfer coefficient, W/(m <sup>2</sup> K)
$(\Delta H_R)_i$ :	Heat of species $i$ reaction, J/mol
$[HC]_{in}$ :	Reactor inlet HC concentration, ppm
$[HC]_{out}$ :	Reactor outlet HC concentration, ppm
$k_{a1}$ :	Pre-exponent factor for CO inhibition
$k_{a4}$ :	Pre-exponent factor for NO <sub>x</sub> inhibition
$k_f$ :	Thermal conductivity of fluid, W/(m · K)
$k_i$ :	Pre-exponent factor
$k_i'$ :	Modified pre-exponent factor
$k_{m,i}$ :	Mass transfer coefficient for species $i$ , m / s
$k_o$ :	Pre-exponent factor
$k_o'$ :	Modified pre-exponent factor
$k_R$ :	Modified pre-exponent factor
$k_R'$ :	Modified pre-exponent factor
$k_v$ :	Reaction rate constant based on the catalyst volume

$k_w$ :	Thermal conductivity of converter wall, W/(m · K)
$K_i$ :	Adsorption constant
$L$ :	Effective washcoat thickness, m
$M$ :	Molar mass of a substance, g/mol
$m$ :	The power for NO inhibition in the catalytic kinetic equation
$Nu$ :	Nusselt number, dimensionless
$Nu_H$ :	Nusselt number with constant heat surface flux boundary condition, dimensionless
$Nu_T$ :	Nusselt number with constant wall temperature boundary condition, dimensionless
$[O_2]$ :	O <sub>2</sub> Concentration, mol/m <sup>3</sup>
$P_i$ :	Partial Pressure, Pa
$Pr$ :	Prandtl number, dimensionless
$R_g$ :	Gas constant, 8.314 J/(mol · K)
$R$ :	Radius of Channel, m
$Re$ :	Reynolds number, dimensionless
$(-R_i)$ :	Reaction rate of species $i$ , mol/m <sup>2</sup> s
$(-R_i)_{Average}$ :	Average reaction rate of species $i$ at the washcoat, mol/(m <sup>2</sup> s)
$(-R_i)_H$ :	Rate of species $i$ homogeneous reaction, mol/(m <sup>3</sup> s)
$(-R_i)_S$ :	Reaction Rate of species $i$ at the external surface of washcoat, mol/(m <sup>2</sup> s)
$Sc$ :	Schmidt number, dimensionless
$Sh$ :	Sherwood number, dimensionless
$T$ :	Temperature, K
$T_b$ :	Bulk mean temperature, K
$T_{bo}$ :	Reactor inlet gas temperature, K
$T_S$ :	Washcoat surface temperature, K
$T_{So}$ :	Initial washcoat surface temperature, K
$v_m$ :	Mean axial mass average velocity, m/s
$W_p$ :	Wetted wall perimeter, m
$Y_i$ :	Mole fraction of species $i$ in wet basis
$Y_i^*$ :	Mole fraction of species $i$ in dry basis



$Y_{i,b}$ :	Molar fraction of species $i$ in bulk flow
$(Y_{i,b})_o$ :	Molar fraction of species $i$ at the inlet of converter
$Y_{i,s}$ :	Molar fraction of species $i$ in washcoat

### Greek Symbols

$\alpha$ :	Thermal diffusivity, $\text{m}^2/\text{s}$
$\alpha_t$ :	Thermal dispersion coefficient, $\text{m}^2/\text{s}$
$\rho$ :	Gas mass density, $\text{kg}/\text{m}^3$
$\rho_w$ :	Wall density, $\text{kg}/\text{m}^3$
$\eta$ :	Effectiveness factor
$\eta_i$ :	Effectiveness factor for species $i$
$\delta_w$ :	Converter effective wall thickness, $\text{m}$
$\varepsilon$ :	Porosity of washcoat
$\tau$ :	Tortuosity factor of washcoat
$\gamma$ :	Stoichiometric ratio
$\Phi$ :	Thiele modulus
$\chi_{HC}$ :	HC conversion over the catalytic converter: $\chi_{HC} = \frac{[HC]_{in} - [HC]_{out}}{[HC]_{in}} \times 100\%$
$\chi_{CO}$ :	CO conversion over the catalytic converter: $\chi_{CO} = \frac{[CO]_{in} - [CO]_{out}}{[CO]_{in}} \times 100\%$

## 6.9 References

- Beld L. Van De, M. P. J. Bijl, A. Reinders, B. Van Der Werf and K. R. Westerterp, "The catalytic oxidation of organic contaminants in a packed bed reactor", *Chem. Eng. Sci.*, **49**, 4361-4373, 1994
- Bittner R. W., F. W. Aboujaoude, "Catalytic control of NOx, CO and NMHC emissions from stationary diesel and dual-fuel engines", *J. of Engineering for Gas Turbines and Power*, **114**, 597-601, 1992.

- Brauer H. W. and F. Fetting, "Stofftransport bei wandreaktion im einlaufgebiet eines strömungsrohres", Chem. ing. Technol **38**, 30-35, 1966.
- Clerc J. C., "Catalytic diesel exhaust aftertreatment", Applied Catalysis B: Environmental **10**, 99-115, 1996
- Corbo P., M. Gambino, S. Iannaccone and A. Unich, "Comparison between lean-burn and stoichiometric technologies for CNG heavy-duty engines", SAE950057, 1995
- Cullis C. F. and B. M. Willatt, "Oxidation of methane over supported precious metal catalysis", Journal of Catalysis **83**, 267-285, 1983
- Deluchi M. A., R. A. Johnson and D. Sperling, "Transportation fuels and the greenhouse effect", Transportation Research Record, In Press
- Douville, B., "Performance, emission and combustion characteristics of natural gas fuelling of diesel engines", M.Sc. Thesis, University of British Columbia, Vancouver, BC, 1994.
- Dryer F. L., "High temperature oxidation of carbon monoxide and methane in a turbulent flow converter", Ph. D. Thesis, Department of mechanical and aerospace engineering, Princeton university, 1972
- Farrauto R. J., K. E. Voss, "Monolithic diesel oxidation catalysts", Applied Catalysis B: Environmental **10**, 29-51, 1996
- Gambino M., R. Cericola, P. Corbo, S. Iannaccone, " Carbonyl compounds and PAH emissions from CNG heavy-duty engine", ASME, Journal of Engineering for Gas Turbines and Power, Vol. 115, n. 4, pp. 747-749, 1993
- Giezen J. C. van, "The catalytic combustion of methane", PhD thesis, Nederlands, 1997
- Golodets G. I., "Heterogeneous catalytic reactions involving molecular oxygen", Studies in Surface Science and Catalysis, Vol. 15, Elsevier, Amsterdam, 1983
- Guit Ir. R. P. M., "The selective catalytic reduction of NO<sub>x</sub> in a reverse flow reactor: a quick design procedure", Precision Process Technology, 453-461, 1993 Kluwer Academic Publishers, 1993

- Hanamura K., R. Echigo and S. A. Zhdanok, " Superadiabatic combustion in a porous medium", *Ind. J. Heat Mass Transfer*, 36, 1993
- Hayes R. E., S. T. Kolaczkowski and W. J. Thomas, "Finite-element model for a catalytic monolith converter", *Comput. Chem. Eng.* **16**, 645-657, 1992.
- Hayes R. E. and S. T. Kolaczkowski, "Mass and heat transfer effects in catalytic monolith reactors", *Chem. Eng. Sci.*, **49** 3587-3599, 1994.
- Hayes R. E., S. T. Kolaczkowski, W.J. Thomas and J. Titiloye, "Transient experiments and modeling of the catalytic combustion of methane in a monolith reactor", *Ind. Eng. Chem. Res.*, **35** 406-414, 1996.
- Hayes R. E. and S. T. Kolaczkowski, "Introduction to catalytic combustion", Gordon and Breach Science Publishers, Reading, UK, 1997.
- Hayes R. E. and S. T. Kolaczkowski, "A study of Nusselt and Sherwood numbers in a monolith reactor", *Catalysis Today*, **47** 295-303, 1999.
- Heywood J. B., "Internal combustion engine fundamentals", McGraw-Hill Inc., New York, 1988
- Hosoya M. and M. Shimoda, "The application of diesel oxidation catalysis to heavy duty diesel engines in Japan", *Applied Catalysis B: Environmental* **10**, 83-97, 1996
- Karim, G. A., "An examination of Some Measures for Improving the Performance of Gas Fueled Diesel Engines at Light Load", SAE 912366, 1991.
- Kolaczkowski S. T., W. J. Thomas, J. Titiloye and D. J. Worth, "Catalytic combustion of methane in a monolith reactor: heat and mass transfer under laminar flow and pseudo-steady-state reaction conditions", *Combust. Sci. and Tech.*, Vol. 118, pp. 79-100, 1996
- Lampert J. L., M. S. Kazi and R. J. Farrauto, "Palladium catalyst performance for methane emissions abatement from lean burn natural gas vehicles", *Applied Catalysis B: Environmental* **14**, 211-223, 1997
- Leclerc J. P. and D. Schweich, "Modeling catalytic monoliths for automobile emission control", in *Chemical Converter Technology for Environmentally Safe* 288

- Converters and Products (Edited by de Lasa, H. I. et al.), 547-576, Kluwer Academic Press, Dordrecht, 1993.
- Lee S. and R. Aris, "On the effects of radiative heat transfer in monoliths", *Chem. Eng. Sci.* **32**, 827-837, 1977.
- Leung D., R. E. Hayes and S. T. Kolaczkowski, "Diffusion limitation effects in the washcoat of a catalytic monolith reactor", *Can. J. Chem. Eng.* **74**, 94-103, 1996.
- Liu B., M. D. Checkel, R. E. Hayes, M. Zheng and E. Mirosh, "Transient simulation of a catalytic converter for a dual fuel engine", *Can. J. Chem. Eng.*, in press., 2000
- Liu B., M. D. Checkel, R. E. Hayes, M. Zheng and E. Mirosh, "Experimental and modelling study of viable cycle time for a reversing flow catalytic converter for natural gas/diesel dual fuel engines", SAE 2000-01-0213, Proceedings of SAE 2000 World Congress, Detroit, March 2000.
- Matros Yu. Sh. and G. A. Bunimovich, "Reverse-flow operation in fixed bed catalytic reactors", *Catal. Rev.-Sci. Eng.*, **38**(1), 1-68, 1996.
- Miyoshi N., S. Matsumoto, K. Katoh, T. Tanaka, J. Harada, N. Takahashi, K. Yokota, M. Sugiura and K. Kasahara, "Development of new concept Three-Way Catalyst for automotive lean-burn engines", SAE 950809, 1995.
- Oh S. H., P. J. Mitchell and R. M. Siewert, "Methane oxidation over alumina-supported noble metal catalysts with and without cerium additives", *J. of Catalysis* **132**, 287-301, 1991.
- Oh S. H. and J. C. Cavendish, "Transients of monolithic catalytic converters: response to step changes in feed stream temperature as related to controlling automobile emissions", *Ind. Eng. Chem. Prod. Res. Dev.* **21**, 29-37, 1982.
- ÖZGÜLSEN F. and A. Cinar, "Forced periodic operation of tabular reactors", *Chem. Eng. Sci.*, **49**, 3409-3419, 1994.
- Purwono S., Yu. Sh. Matros, R. R. Hudgins and P. L. Silveston, "Modelling of catalytic combustion of low-heating-value gases using non-adiabatic flow reversal", Department of chemical engineering, University of Waterloo.

- Sakai T., B. C. Chol, R. Osuga and Y. Ko, "Purification characteristics of catalytic converters for natural gas fuelled automotive engine", SAE 912599, 1991
- Shelef M. and G. W. Graham, "Why rhodium in automotive three-way catalysts?", *Catal. Rev.-Sci. Eng.*, 36(3), 433-457, 1994
- Siemund S., J. P. Leclerc, D. Schweich, M. Prigent and F. Castagna, "Three-Way monolithic converter: simulations versus experiments", *Chem. Eng. Sci.* **51**, 3709-3720, 1996.
- Strots V. O., G. A. Bunimovich, Yu. Sh. Matros, M. Zheng and E. A. Mirosh, "Novel catalytic converter for natural gas powered diesel engines", SAE 980194, 1998
- Summers J. C., A. C. Frost, W. B. Williamson and I. M. Freidel, "Control of NO<sub>x</sub>/CO/HC emissions from natural gas fuelled stationary engines with three-way catalysts", 84<sup>th</sup> annual meeting and exhibition, Vancouver, British Columbia, June 16-21, 1991
- Tronconi E. and P. Forzatti, "Adequacy of lumped parameter models for SCR converters with monolith structure", *AIChE J.* **38**, 201-210, 1992.
- Tronconi E. and P. Forzatti, "Adequacy of lumped parameter models for SCR converters with monolith structure", *AIChE J.* **38**, 201-210, 1992
- Voltz S. E., C. R. Morgan, D. Liederman and S. M. Jacob, "Kinetic study of carbon monoxide and propylene oxidation on platinum catalysts", *Ind. Eng. Chem. Prod. Res. Dev.* **12**, 294-301, 1973.
- Wallace K. and H. J. Viljoen, "Modelling of a monolithic catalyst with reciprocating flow", *AIChE Journal*, **41**, No. 5, 1229-1234, 1995
- Weaver C. S., "Natural gas vehicles-A review of the State of the art", SAE 892133, 1989.
- Zelenka P., W. Cartellieri, P. Herzog, "Worldwide diesel emissions standards, Current experience and future needs ", *Applied Catalysis B: Environmental* **10**, 3-28, 1996.

## **Chapter 7**

### **Summary and Recommendations**

*Chapter 7 summarizes the studies from previous chapters. The general conclusions about reverse flow catalytic converter for natural gas/diesel dual fuel engine are drawn. Recommendations for future work are given.*

## **7.1 Introduction**

This chapter summarizes the studies from previous chapters. The general conclusions about reverse flow catalytic converter for natural gas/diesel dual fuel engine are drawn. The recommendations of future work are also given

The main objective of this study was to study the use of a reverse flow catalytic converter for reducing the emission levels of HC and CO from natural gas/diesel engines at light loads. There are two main challenges to control natural gas/diesel dual fuel engine light load emissions. First, most of HC in the engine exhaust is methane and methane is the most stable HC. Second, engine exhaust temperature is too low to keep chemical activity of catalyst at light loads. Reverse flow techniques are introduced to deal these problems.

The design of reverse flow catalytic converter has been developed from prototype to production version through the study. The production version is much more compact design than the prototype. A detailed experimental and modelling study has been conducted for the prototype reverse flow design. These studies are given in Chapters 3, 4, 5 and 6.

A step-wise approach has been used in this study. First, the reverse flow catalytic converter performance is determined experimentally. Then a numerical simulation model for both unidirectional flow mode and reverse flow mode is established. The model is validated against experiment data. The model evaluated by the experiment data is used to determine the best operating parameters of reverse flow catalytic converter for variable engine operations. The model is a tool for both reactor control and reactor design.

## 7.2 Summary of Studies

This thesis is organized in a “paper-format” and it has four main chapters, which is Chapters 3, 4, 5 and 6. Each main chapter is a mile stone of the study. Chapter 3 presents the experimental results of reverse flow catalytic converter under both steady and transient engine operations. It is a detail experimental study based on the production type reverse flow design. Four main conclusions have been given in this chapter:

1. Reverse flow could develop reactor temperature and increase HC and CO conversion greatly under some engine light load operations. The reactor temperature rise by reverse flow could be about two times higher than the adiabatic temperature rise. However, this depends on the proper engine exhaust and reactor temperature status. In some engine light loads, reverse flow fails to develop reactor temperature and increase HC and CO conversion. This occurs because either reactor temperature is too low or HC and CO concentration in engine exhaust is too low.
2. Reverse flow switch time was evaluated from 5 to 240 seconds. It was shown that short switch time was better than long switch time. In order to reduce reverse flow operations and the thermal stress resulted from reverse flow switch for the similar reactor performance, switch times of the order of 15 and 30 second was recommended.
3. During the engine mode transition, reverse flow either performed a “heat trap” or a “cold trap” effect. When initial reactor temperature was high and engine was switched to engine mode with low exhaust temperature, reverse flow has a “heat trap” effect. Depending on the HC and CO concentration, reverse flow could develop



reactor temperature, maintain reactor temperature, or slow down reactor temperature drop. When initial reactor temperature was low and engine was switched to engine mode with high exhaust temperature, reverse flow has a “cold trap” effect. It slows down reactor temperature development with engine exhaust temperature in the early stage of transition. However, in the later stage, reverse flow shows the advantage to develop reactor temperature. The control strategy of reverse flow operation is to use its “heat trap” effect and avoid its “cold trap” effect. When initial reactor temperature was high and engine was changed to engine mode with low exhaust temperature, reverse flow should start for developing reactor temperature, maintaining reactor temperature, or slowing down reactor temperature drop. When initial reactor temperature was low and engine was changed to engine mode with high exhaust temperature, reverse flow should be stopped to avoid slowing down reactor temperature development with engine exhaust temperature in the early stage of engine operation transition (about 10 minutes). However, in the later stage (after 10 minutes), reverse flow could start to develop reactor temperature further.

4. Reverse flow was a good strategy for the Japanese 6-Mode test. It was superior to unidirectional flow. Reverse flow could maintain reactor temperature over 800 K and HC conversion about 80% during 6-Mode test. The switch time of 15 seconds was recommended for reverse flow switch during 6-Mode test.

Chapter 4 establishes a numerical simulation model for the catalytic converter which is operated in the conventional unidirectional flow manner. It is an experimental and modelling study based on the prototype reverse flow design shown in Figure 2-3 b).

The model established is an one dimensional single channel model, which uses locally correct values for the heat and mass transfer coefficients and incorporating washcoat diffusion. The catalytic kinetic approach used is the modified Voltz kinetics. It includes the NO<sub>x</sub> inhibition effect. The activation energy found for methane and CO catalytic reaction is 132.1 and 55 kJ/mol respectively. This model is able to predict the transient operation of the converter to a level sufficient to identify the important trends of reactor response, which includes the reactor thermal response, HC and CO conversion. It provides an acceptable model for the engine operated in the low temperature region. This is a basic modelling exercise and the model is developed to simulate the reverse flow catalytic converter in Chapters 5 and 6.

Chapter 5 builds up a numerical simulation model for the reverse flow catalytic converter. It is a experimental and modeling study based on the prototype reverse flow design shown in Figure 2-3 c). The catalyst is the same as that in Chapter 4, but two inactive bricks are set at each end of the reactor. The model established is a one dimensional single channel model, which uses locally correct values for the heat and mass transfer coefficients and incorporating washcoat diffusion. The model boundary condition changes with the flow direction switch. It uses the same kinetic approach as Chapter 4. However, the NO<sub>x</sub> inhibition effect was incorporated into the apparent rate constant because of its constant low concentration. The activation energy of methane catalytic reaction was found to vary with reactor temperature region for Palladium based catalyst. The transition temperature between low and high reactor temperature region is about 780 K. The methane activation energy is 129 kJ/mol in low temperature region, in which the reactor temperature is lower than 780 K. It drops to 35 kJ/mol if the reactor

temperature is higher than 780 K. The activation energy of CO oxidation is 55 kJ/mol in all temperature range tested. It is obvious the kinetic data found in the low temperature are close to those found in Chapter 4. Based on the proven model, Chapter 5 evaluates the proper reverse flow switch time of reverse flow operation. The chapter concludes:

1. A short reverse flow cycling time can maintain the reactor at a high temperature level which can give a steady high HC and CO conversion even though the engine exhaust temperature is below the autothermal temperature for unidirectional operation.
2. A longer reverse flow cycling time can lead to a reduction in the reactor temperature level which reduces the HC and CO conversion.
3. A medium reverse flow cycling time can increase the original reactor temperature greatly. Although this increase is good for the HC and CO conversion, there is the possibility that the catalyst could be heated to an excessive temperature and damaged.

Chapter 6 makes a more detailed kinetic study of Palladium catalyst for CH<sub>4</sub> and CO oxidation under reverse flow operations. It is a experimental and modelling study based on the prototype reverse flow design shown in Figure 2-3 c), which is the same catalyst as in Chapter 5. The model used is the same as that shown in Chapter 5. However, it develops a new kinetic approach for both methane and CO oxidation. Both CO and methane oxidation over palladium catalyst in an excess of oxygen and water are well described using apparent first order kinetics with respect to the corresponding CO and methane concentration. It is also found that the catalyst undergoes an apparent transition with reactor temperature. The transition temperature is about 874 K, at which point the apparent activation energy decreased dramatically. The methane activation

energy is 129 kJ/mol in low temperature region and it drops to 35 kJ/mol in high temperature region. The activation energy of CO oxidation is 55 kJ/mol in all temperature range tested. It is obvious the kinetic data found are the same as to those found in Chapter 5. However, the transition temperature for methane oxidation is much higher than that from Chapter 5. Since the study in Chapter 6 is based on a more engine and reactor operations, it gives more reliable information.

### **7.3 Recommendations and Future Work**

There are some recommendations about future work of reverse flow catalytic converter, including: control of reverse flow catalytic converter, safety and durability of reverse flow catalytic converter, optimum design of reverse flow catalytic converter, modelling of reverse flow catalytic converter, study of chemical kinetics of Palladium based catalyst.

#### **7.3.1 Control of Reverse Flow Catalytic Converter**

The control strategy of reverse flow operation is trying to use its advantages and avoiding its disadvantages. This includes: Using its “heat trap” effect and avoiding its “cold trap” effect, Choosing proper reverse flow switch time.

Chapter 3 demonstrates the reverse flow catalytic converter performance under the transient engine operations. Reverse flow either has a “heat trap” or a “cold trap” effect during the engine mode transition. When initial reactor temperature is high and engine was switched to a mode with low exhaust temperature, reverse flow has a “heat trap” effect. Depending on the HC and CO concentration, reverse flow could develop

reactor temperature, maintain reactor temperature, or slow down reactor temperature drop. When initial reactor temperature is low and engine is switched to engine mode with high exhaust temperature, reverse flow has a “cold trap” effect. It slows down reactor temperature development with engine exhaust temperature in the early stage of transition. However, in the later stage, reverse flow shows the advantage to develop reactor temperature. When initial reactor temperature is high and engine is changed to engine mode with low exhaust temperature, reverse flow should start for developing reactor temperature, maintaining reactor temperature, or slowing down reactor temperature drop. When initial reactor temperature is low and engine is changed to engine mode with high exhaust temperature, reverse flow should be stopped to avoid slowing down reactor temperature development with engine exhaust temperature in the early stage of engine operation transition (about 10 minutes). However, in the later stage (after 10 minutes), reverse flow could start to develop reactor temperature further. These results are shown by the transitions among three engine modes: Heavy load at 2000 rpm, 170 Nm; Light load at 2000 rpm, 50 Nm and Idle. It might be worth to extend this study to more engine modes.

Chapter 3 and Chapter 5 make some investigations about reverse flow switch time. They shows that the reverse flow with short switch time like 5, 15 and 30 second can build up a very high reactor temperature and give very high HC and CO conversion. The reverse flow with medium switch time 60 second could maintain most of the reactor in the high temperature region and give high HC and CO conversion, however, it produces steep temperature gradient along the reactor and results in the big thermal stress, which can reduce the lifetime of the reactor. The reverse flow with a switch time

of 120 seconds still kept a small part of reactor in the high temperature region, however the HC conversion drops significantly in some engine operations. The reverse flow with a switch time of 240 seconds works like unidirectional flow operation. Reverse flow loses its special “heat trap” effect for such long switch time. For the cases studied, the observed critical switch time for the reactor heat extinction was about 180 second. In order to maintain the reverse flow special “heat trap” effect, the reverse flow switch time should be less than 180 second. To maintain the best HC and CO conversion and reduce the thermal stress along the reactor, the switch time should be as short as possible. However, for the similar reactor chemical activity, in order to reduce the flow switches and extend the life time and durability of reverse flow control facilities, the switch time should be chosen as long as possible. Considering these competing principles, the switch time between 15 second and 30 second is recommended. These studies are all about symmetric reverse flow operation. Some experiments have been done for the unsymmetric reverse flow operation and this helps to keep the temperature peak setting in the middle of reactor. Although this adds the complexity of reverse flow control, it might be worth to explore more about its advantages comparing to symmetric reverse flow operation.

### **7.3.2 Safety and Durability of Reverse Flow Catalytic Converter**

Safety and durability is a very important issue of reverse flow catalytic converter research. During some engine mode transition, the reactor temperature with reverse flow may rise to such a high value that the catalyst is overheated and damaged. This happens especially when reactor temperature is high in one engine mode, and then engine is operated to a light load with very high HC and CO concentration. The chemical reactions

in the reactor become so strong with conditions: high reactor temperature, high HC and CO concentration, and the “heat trap” effect of reverse flow. This could be avoided by: stopping reverse flow right away, operating engine in diesel only, by-pass the engine exhaust to the catalytic converter. This is an area which is worthwhile to make a detailed exploration, especially for the product development of reverse flow catalytic converter.

It is well known that fresh catalyst is very active and ages very quickly. After its steady performance is obtained, there is a question how long it will last. It is expected that the life time of the catalytic converter is depended on how to use it and how to maintain it properly. This is also an interesting area to worth to explore.

### **7.3.3 Optimum Design of Reverse Flow Catalytic Converter**

Both designs of the prototype and the production version of reverse flow have been tested. They all can work properly for the function of reverse flow switch. However, the production version is more compact and easy to be installed in the vehicle. There are some questions about current designs. One is the flexibility of catalytic converter. For different engine, the catalytic converter is supposed to be different. For each individual engine, what is the best reactor configuration? what is minimum catalyst required? how much money we could save for the best reactor performance compared current design? It is worth to make this exploration since the catalyst is very expensive. This becomes an important issue about the optimum reactor design. Reactor modelling will become very important tool to aid to make these decisions. The difference in different designs can be easily compared with modelling data. Currently, the reverse flow model has been validated against the experimental data. It shows it can simulate the reactor performance

properly. However, these studies are limited for the prototype design. It is worth to develop the model for the production version of reverse flow design. Based on the previous experience, this should be done very quickly.

### **7.3.4 Modelling of Reverse Flow Catalytic Converter**

In this dissertation, an one dimensional single channel model is established for the simulation of reverse flow catalytic performance. It assumes that all of the channels in the reactor experience the same operating conditions. In such a model, the gas phase can be modelled in one, two or three space dimensions. As noted in Hayes and Kolaczkowski (1997), for channels of the order of 1 mm hydraulic diameter under the operating conditions found in this converter, the 1D model provides a very close agreement to the 2D or 3D model, and offers a greatly reduced computational time. The 1D model ignores radial temperature and concentration gradients and accounts for the discontinuity at the wall with heat and mass transfer coefficients. Some other major assumptions made are listed below:

- The gas was assumed to be an ideal gas with density changes owing to temperature changes included.
- The pressure drop in the reactor was assumed to be zero and pressure fluctuations resulting from flow pulsation were ignored.
- The gas phase was assumed to be in a pseudo-steady state with the wall.
- Accumulation of mass in the washcoat is ignored, that is the solid phase mole balance was a steady state one.



- Washcoat diffusion was included. The washcoat was modelled as a one dimensional isothermal flat plate.
- The mole average velocity is taken to be equal to the mass average velocity.
- The start of each segment corresponds to the beginning of a new development length for the fluid phase. The solid phase is continuous across the segments.

Currently, the reverse flow model has been validated against the experimental data for the prototype design of reverse flow. It shows it can simulate the reactor performance properly for most of engine and reactor operations. It is worth to develop the model for the production version of reverse flow design.

The catalytic converter is well protected from the heat loss. The thermal insulation material is used to wrap system. However, it is unavoidable that some reactor energy still releases to the environment. It might be worth while to use a two dimensional model to account for this thermal effect.

### **7.3.5 Study of Chemical Kinetics of Palladium Based Catalyst**

The modified Voltz equations are successfully used in simulation for both unidirectional and reverse flow catalytic converters, shown in Chapter 4 and 5. It should be pointed out that the modified Voltz kinetics are in fact equivalent to first order rate expressions in terms of either methane or CO under the conditions used in the reactor: excess oxygen and water, relative low NO<sub>x</sub> and CO concentration. It is not surprise that Chapter 6 uses the first order kinetic expression and it results in the same kinetic data for both methane and CO oxidation.

Water is known to inhibit the oxidation of methane by occupying the reaction sites on the palladium oxide particles. Power law expressions have also been reported with an inhibition effect owing to water. The approach used in Chapter 6 assumes that a relatively large amount of water is present and the oxidation rate has the appearance of a pseudo first order reaction. By analogy, a similar derivation is made to show that at relatively low concentrations of CO and in a large excess of water, the oxidation of CO can also be approximated by a power law expression that is first order in CO and zero order in oxygen. It will be worth while to conduct more study about water inhibition effect for both methane and CO catalytic reactions.

An additional complexity in the oxidation of methane is that there is an apparent shift in the activation energy as the temperature increases. The temperature at which this transition occurs has been reported to be a function of catalyst starting composition. Although it is essential to differentiate changes in apparent activation energy that occur as a result of the onset of heat and mass transfer effects, there appears to be sufficient evidence in the literature that there is indeed a genuine activation energy change in the reaction. The transition temperature is found to be 780 K in Chapter 5. Chapter 6 gives more detailed study about this and it is found to be a higher value 874 K. This is higher compared the observations from Cullis and Willatt (1983), Kolaczkowski et al. (1996) and Sakai et al. (1991). It might be important to conduct more study to see if the transition is in a specific temperature or in a temperature range.

## 7.4 References

- Hayes R. E. and S. T. Kolaczkowski, "Introduction to catalytic combustion", Gordon and Breach Science Publishers, Reading, UK, 1997.
- Cullis C. F. and B. M. Willatt, "Oxidation of methane over supported precious metal catalysis", *Journal of Catalysis* 83, 267-285, 1983
- Kolaczkowski S. T., W. J. Thomas, J. Titiloye and D. J. Worth, "Catalytic combustion of methane in a monolith reactor: heat and mass transfer under laminar flow and pseudo-steady-state reaction conditions", *Combust. Sci. and Tech.*, Vol. 118, pp. 79-100, 1996
- Sakai T., B. C. Chol, R. Osuga and Y. Ko, "Purification characteristics of catalytic converters for natural gas fuelled automotive engine", SAE 912599, 1991

## Appendix A

### Methods to Use Modelling Programs

#### 1. Create the Input Data File

The modelling program is derived from the 1D monolith simulator “monold” written by Dr. Robert E. Hayes. Two programs are used: called “monold” and “prepld”. They are Fortran programs. In order to run “monold”, some control data and initial condition should be given. They are given by a data file, which is created by running the program “prepld”. The data file has an extension of “.par”. Its file name looks like “filename.par”. You can assign the filename according to your interest. The following is an example of “filename.par”:

```
=====
Parameters for monolith simulation
=====

Parameters to specify the problem type
-----
Problem type ..... 5
Number of elements in the problem ..... 120
Homogeneous reaction? (0=no, 1=yes) ..... 1
Catalytic reaction? (0=no, 1=yes) ..... 1
Internal radiation? (0=no, 1=yes) ..... 0
Effectiveness of washcoat (0=no, 1=yes) ..... 1
Kinetic model type (1=power law, 2=lhw type ..... 7
Reaction (1=propane, 2=CO, 3=methane, 4=other) ..... 5
Reading of initial solution ..... 2

Parameters related to numerical method
-----
Number of iterations in time ..... 30
Number of iterations for coupling ..... 500
Number of iterations in temperature ..... 1
Number of iterations in concentration ..... 1

Size of the time step ..... 1.000E+00
Tolerance for stopping criterion ..... 1.000E-06
Sensitivity for stopping criterion ..... 1.000E-06
```

Physical parameters for problem

-----		
Average inlet velocity of gas .....		3.115E+00
Thermal conductivity of gas, $k=a+bT$ a coeff .....		1.679E-02
	b coeff .....	5.073E-05
Pre-exponential factor for the homo reaction .....		1.260E+10
Activation energy for the homo reaction .....		1.674E+05
Pre-exponential factor CH <sub>4</sub> , low temperature .....		2.264E+07
Activation energy CH <sub>4</sub> , low temperature .....		1.290E+05
Pre-exponential CH <sub>4</sub> high temperature .....		4.029E+01
Activation energy CH <sub>4</sub> high temperature .....		3.500E+04
Cross over temperature between two models .....		8.540E+02
Pre-exponential factor CO oxidation .....		5.479E+03
Activation energy CO oxidation .....		5.490E+04
Pre-exponential factor, first adsorption term .....		0.0
Activation energy, first adsorption term .....		0.0
Total system pressure at the reactor exit .....		9.484E+04
Inlet temperature of the gas .....		7.770E+02

Properties of the wall

-----		
Density of the wall material .....		2.500E+03
Thermal conductivity of wall, $k_w = a + bT$ a term .....		2.0
	b term .....	0.0
Heat capacity of the wall, $C_p = a + bT$ a term .....		1.400E+03
	b term .....	0.0
Effective wall thickness of reactor .....		2.500E-04

Properties of the washcoat

-----		
Number of elements in the washcoat .....		20
Coordinate system (0=cartesian 1=radial) .....		0
Number of iterations in concentration .....		200
Thickness of the washcoat layer .....		5.000E-05
Tortuosity factor in washcoat .....		8.000E+00
Porosity of the washcoat .....		4.100E-01
Mean pore diameter in the washcoat .....		1.000E-08

Inlet gas composition

-----		
Mole fraction of methane (THC) .....		2.759E-03
Mole fraction of carbon monoxide .....		1.263E-03
Mole fraction of nitric oxide .....		7.370E-04
Mole fraction of oxygen .....		9.020E-02
Mole fraction of nitrogen .....		7.333E-01
Mole fraction of carbon dioxide .....		5.860E-02
Mole fraction of water vapour .....		1.131E-01

Properties of the reactor channels

-----		
Number of segments in the reactor .....		6
Number of inactive segments in the reactor .....		2
Number of the inactive segment .....		1
Number of the inactive segment .....		6
Reactor diameter in metres .....		1.400E-03

```

Reactor length in metres ..... 3.048E-01
Maximum wall temperature rise per iteration ..... 1.000E+01

Coordinates for the wall temperature profile
-----
Number of locations for the wall temperature ..... 6
Coordinate for temperature on the wall ..... 2.540E-02
Coordinate for temperature on the wall ..... 7.620E-02
Coordinate for temperature on the wall ..... 1.270E-01
Coordinate for temperature on the wall ..... 1.778E-01
Coordinate for temperature on the wall ..... 2.286E-01
Coordinate for temperature on the wall ..... 2.794E-01

```

## 2. Comments about "filename.par"

Parameters to specify the problem type  
-----

Problem type ..... 5

- 1, Concentration only, steady state
- 2, Coupled temperature and concentration, steady state
- 3, Reserved for other use
- 4, Coupled temperature and concentration, fixed reactor inlet temperature,transient
- 5, Coupled temperature and concentration, transient reactor inlet temperature,transient

In my study, "2" is chosen for steady calculation and "5" is chosen for transient calculation

Number of elements in the problem ..... 120

Specify the element number for your calculation, in my case, 20 elements are used for each catalyst brick with a length 50.8 mm along the gas flow direction. 120 is the total of 6 catalyst bricks

Homogeneous reaction? (0=no, 1=yes) ..... 1

If no homogeneous reactions involved, choose "0", other choose "1". In my study, CO homogeneous reaction is involved, so "1" is specified.

Catalytic reaction? (0=no, 1=yes) ..... 1

If no catalytic reactions involved, choose "0", other choose "1". In my study, both CO and methane catalytic reactions are involved, so "1" is specified.







Pre-exponential factor CH4, low temperature ..... 2.264E+07  
Specify the pre-exponent factor of CH4 catalytic reaction in low temperature region. For my study, CH4 kinetics transits from low temperature region to high temperature region.

Activation energy CH4, low temperature ..... 1.290E+05  
Specify the activation energy of CH4 catalytic reaction in low temperature region. For my study, CH4 kinetics transits from low temperature region to high temperature region.

Pre-exponential CH4 high temperature ..... 4.029E+01  
Specify the pre-exponent factor of CH4 catalytic reaction in high temperature region. For my study, CH4 kinetics transits from low temperature region to high temperature region.

Activation energy CH4 high temperature ..... 3.500E+04  
Specify the activation energy of CH4 catalytic reaction in high temperature region. For my study, CH4 kinetics transits from low temperature region to high temperature region.

Cross over temperature between two models ..... 8.540E+02  
Specify the transition temperature from low temperature region to high temperature region for CH4 catalytic reaction.

Pre-exponential factor CO oxidation ..... 5.479E+03  
Specify the pre-exponent factor of CO catalytic reaction

Activation energy CO oxidation ..... 5.490E+04  
Specify the activation energy of CO catalytic reaction

Pre-exponential factor, first adsorption term ..... 0.0  
Specify the pre-exponent factor of adsorption term, this term is depended the kinetic model used. It could be NOx, CO or H2O

Activation energy, first adsorption term ..... 0.0  
Specify the activation energy of adsorption term, this term is depended the kinetic model used. It could be NOx, CO or H2O

Total system pressure at the reactor exit ..... 9.484E+04  
Specify the reactor pressure

Inlet temperature of the gas ..... 7.770E+02  
Specify the inlet gas temperature

For the transient process, the inlet gas temperature may vary with time. The inlet gas temperature is specified in a data file "filename.tin". The "filename.tin" looks like:

0	745
10	750
20	760
30	770

The first column is time and the second column is the inlet gas temperature corresponding to the specific time.

Properties of the wall

-----

Density of the wall material ..... 2.500E+03  
Specify the material density of catalyst wall

Thermal conductivity of wall,  $k_w = a + bT$  a term ..... 2.0  
b term ..... 0.0  
Specify the thermal conductivity of catalyst wall

Heat capacity of the wall,  $C_p = a + bT$  a term ..... 1.400E+03  
b term ..... 0.0  
Specify the heat capacity of catalyst wall

Effective wall thickness of reactor ..... 2.500E-04  
Specify the effective wall thickness of catalyst wall

Properties of the washcoat

-----

Number of elements in the washcoat ..... 20  
Specify the number of elements along washcoat, for my study  
"20" is chosen for the washcoat layer with a thickness 0.05 mm.

Coordinate system (0=cartesian 1=radial) ..... 0  
Specify coordinate system

Number of iterations in concentration ..... 200  
Specify iteration number for concentration calculation along  
washcoat

Thickness of the washcoat layer ..... 5.000E-05  
Specify the thickness of the washcoat layer

Tortuosity factor in washcoat ..... 8.000E+00  
Specify the tortuosity factor of washcoat

Porosity of the washcoat ..... 4.100E-01  
Specify the porosity of washcoat

Mean pore diameter in the washcoat ..... 1.000E-08  
Specify the pore diameter of washcoat

Inlet gas composition

-----

Mole fraction of methane (THC) ..... 2.759E-03  
Specify mole fraction of CH<sub>4</sub> in reactor inlet gas

Mole fraction of carbon monoxide ..... 1.263E-03  
Specify mole fraction of CO in reactor inlet gas

Mole fraction of nitric oxide ..... 7.370E-04  
Specify mole fraction of NO<sub>x</sub> in reactor inlet gas

Mole fraction of oxygen ..... 9.020E-02  
Specify mole fraction of O2 in reactor inlet gas

Mole fraction of nitrogen ..... 7.333E-01  
Specify mole fraction of N2 in reactor inlet gas

Mole fraction of carbon dioxide ..... 5.860E-02  
Specify mole fraction of CO2 in reactor inlet gas

Mole fraction of water vapour ..... 1.131E-01  
Specify mole fraction of H2O in reactor inlet gas

Properties of the reactor channels  
-----

Number of segments in the reactor ..... 6  
Specify segment number of reactor. In my study, 6 catalyst bricks  
are used in one of the prototype design.

Number of inactive segments in the reactor ..... 2  
Specify inactive segment number of reactor. In my study, 2  
inactive bricks are used in one of the prototype design.

Number of the inactive segment ..... 1  
Specify the first inactive segment.

Number of the inactive segment ..... 6  
Specify the second inactive segment.

Reactor diameter in metres ..... 1.400E-03  
Specify the channel diameter of catalyst, calculated with  
hydraulic diameter

Reactor length in metres ..... 3.048E-01  
Specify the reactor length

Maximum wall temperature rise per iteration ..... 1.000E+01  
Specify the maximum wall temperature rise per iteration

Coordinates for the wall temperature profile  
-----

Number of locations for the wall temperature ..... 6  
Specify number of locations to save reactor temperature. For my study, "6" is chosen since 6 thermocouples are set along the reactor.

Coordinate for temperature on the wall ..... 2.540E-02  
Specify the first location to save reactor temperature

Coordinate for temperature on the wall ..... 7.620E-02  
Specify the second location to save reactor temperature

Coordinate for temperature on the wall ..... 1.270E-01  
Specify the third location to save reactor temperature

Coordinate for temperature on the wall ..... 1.778E-01  
Specify the fourth location to save reactor temperature

Coordinate for temperature on the wall ..... 2.286E-01  
Specify the fifth location to save reactor temperature

Coordinate for temperature on the wall ..... 2.794E-01  
Specify the sixth location to save reactor temperature

### 3. Data Output Format

The output data are organized in eight data files. They are:

filename.tor  
filename.ini  
filename.tpf  
filename.hh  
filename.eta  
filename.tem  
filename.con  
filename.xor  
filename.log

In my study, these data file has the following data format:

filename.tor:

0.1000E+01	607.60	719.00	0.3441E-02	0.2717E+02	0.2460E-03	0.8645E+02
0.2000E+01	607.20	719.01	0.3433E-02	0.2732E+02	0.2452E-03	0.8650E+02
0.3000E+01	606.80	719.01	0.3427E-02	0.2746E+02	0.2443E-03	0.8655E+02

Column#1: Reactor inlet gas temperature, K  
 Column#2: Reactor outlet gas temperature, K  
 Column#3: Reactor outlet CH<sub>4</sub> concentration, mole fraction  
 Column#4: Reactor CH<sub>4</sub> conversion, %  
 Column#5: Reactor outlet CO concentration, mole fraction  
 Column#6: Reactor CO conversion, %

filename.ini

1	0.00E+00	5.89E+02	4.72E-03	1.82E-03	5.97E+02	4.72E-03	1.82E-03
2	1.27E-03	5.91E+02	4.72E-03	1.82E-03	6.00E+02	4.72E-03	1.82E-03
3	2.54E-03	5.93E+02	4.72E-03	1.82E-03	6.05E+02	4.72E-03	1.82E-03

Column#1: Order number  
 Column#2: Distance from inlet, m  
 Column#3: Fluid phase temperature, K  
 Column#4: CH<sub>4</sub> mole fraction in fluid phase  
 Column#5: CO mole fraction in fluid phase  
 Column#6: Solid phase temperature, K  
 Column#7: CH<sub>4</sub> mole fraction in solid phase  
 Column#8: CO mole fraction in solid phase

filename.tpf

1	717.2249	719.4792	719.3995	719.3291	719.2796	719.0039
2	715.1876	719.9471	719.802	719.6603	719.5607	719.0107
3	712.8301	720.3958	720.2085	719.9943	719.8437	719.0218

Column#1: Time, s  
 Column#2: Temperature at 25.4 mm from reactor inlet, T<sub>1</sub>, K  
 Column#3: Temperature at 76.2 mm from reactor inlet, T<sub>2</sub>, K  
 Column#4: Temperature at 127 mm from reactor inlet, T<sub>3</sub>, K  
 Column#5: Temperature at 177.8 mm from reactor inlet, T<sub>4</sub>, K  
 Column#6: Temperature at 228.6 mm from reactor inlet, T<sub>5</sub>, K  
 Column#7: Temperature at 279.4 mm from reactor inlet, T<sub>6</sub>, K

filename.hh

1.27E-03	1.64E+02	3.17E-01
2.54E-03	1.64E+02	3.20E-01
3.81E-03	1.65E+02	3.23E-01

Column#1: Distance from reactor inlet, m  
 Column#2: Heat transfer coefficient between fluid and solid phase,  $h$ , W/m<sup>2</sup>K  
 Column#3: Mass transfer coefficient between fluid and solid phase,  $k_m$ , m/s

filename.eta

1	0.83694	0.105937
2	0.833173	0.105316
3	0.823075	0.103719

Column#1: Node number of element

Column#2: Effectiveness factor for CH<sub>4</sub> diffusion in washcoat

Column#3: Effectiveness factor for CO diffusion in washcoat

filename.tem

zone		
0.00E+00	6.77E+02	
1.27E-03	6.78E+02	
2.54E-03	6.80E+02	

It is divided into two zones

Zone 1

Column#1: Distance from reactor inlet, m

Column#2: Solid phase temperature

Zone 2

Column#1: Distance from reactor inlet

Column#2: Fluid phase temperature

filename.con

zone		
0.00E+00	5.25E-04	
1.27E-03	5.25E-04	
2.54E-03	5.25E-04	

It is divided into four zones

Zone 1

Column#1: Distance from reactor inlet, m

Column#2: CH<sub>4</sub> mole fraction in solid phase

Zone 2

Column#1: Distance from reactor inlet

Column#2: CH<sub>4</sub> mole fraction in fluid phase

Zone 3

Column#1: Distance from reactor inlet, m

Column#2: CO mole fraction in solid phase

Zone 4

Column#1: Distance from reactor inlet

Column#2: CO mole fraction in fluid phase

filename.xor

zone

5.92E+02      88.637      99.3269

5.99E+02      88.9106      99.371

Column#1: Average reactor temperature

Column#2: CH4 conversion, %

Column#3 CO conversion, %

filename.log

A diary file of program process, it save information for convergence, iteration number, etc.

## Appendix B

### Programs for Reverse Flow Operation

#### 1. Command File for Reverse Flow Operation

For reverse flow simulation, “monold” is run by a unix command file. The command file “filename” looks like:

```
#
cp ./rtran18/8015_0.par ./rtran18/8015.par
./bin_jan00/monold_sun ./rtran18/8015

cp ./rtran18/8015.tor ./rtran18/801515.tor
cp ./rtran18/8015.ini ./rtran18/801515.ini
cp ./rtran18/8015.tpf ./rtran18/801515.tpf

#
cp ./rtran18/8015_1.par ./rtran18/8015.par
./bin_jan00/monold_sun ./rtran18/8015

cp ./rtran18/8015.tor ./rtran18/801530.tor
cp ./rtran18/8015.ini ./rtran18/801530.ini
cp ./rtran18/8015.tpf ./rtran18/801530.tpf

#
cp ./rtran18/8015_2.par ./rtran18/8015.par
./bin_jan00/monold_sun ./rtran18/8015

cp ./rtran18/8015.tor ./rtran18/801545.tor
cp ./rtran18/8015.ini ./rtran18/801545.ini
cp ./rtran18/8015.tpf ./rtran18/801545.tpf

#
cp ./rtran18/8015_1.par ./rtran18/8015.par
./bin_jan00/monold_sun ./rtran18/8015

cp ./rtran18/8015.tor ./rtran18/801560.tor
cp ./rtran18/8015.ini ./rtran18/801560.ini
cp ./rtran18/8015.tpf ./rtran18/801560.tpf

#
cp ./rtran18/8015_2.par ./rtran18/8015.par
```



```

./bin_jan00/monold_sun ./rtran18/8015

cp ./rtran18/8015.tor ./rtran18/801575.tor
cp ./rtran18/8015.ini ./rtran18/801575.ini
cp ./rtran18/8015.tpf ./rtran18/801575.tpf

#
cp ./rtran18/8015_1.par ./rtran18/8015.par

./bin_jan00/monold_sun ./rtran18/8015

cp ./rtran18/8015.tor ./rtran18/801590.tor
cp ./rtran18/8015.ini ./rtran18/801590.ini
cp ./rtran18/8015.tpf ./rtran18/801590.tpf

```

## 2. Comments about Command File

```

cp ./rtran18/8015_0.par ./rtran18/8015.par

./bin_jan00/monold_sun ./rtran18/8015

cp ./rtran18/8015.tor ./rtran18/801515.tor
cp ./rtran18/8015.ini ./rtran18/801515.ini
cp ./rtran18/8015.tpf ./rtran18/801515.tpf

```

Line#1: Copy “8015\_0.par” as “8015.par”. “8015\_0.par” gives the reactor initial conditions and the forward flow direction.

Line#2: Run “monold\_sun” use information in files “8015”, use “8015\_0.par”, “8015.tso” and “8015.tin”

Line#3 to Line #5: Save information from 0 to 15 second for forward flow. Only information in “.tor”, “.ini” and “.tpf” is saved. You can save other information as well, add data file you need.

```

cp ./rtran18/8015_1.par ./rtran18/8015.par

./bin_jan00/monold_sun ./rtran18/8015

cp ./rtran18/8015.tor ./rtran18/801530.tor
cp ./rtran18/8015.ini ./rtran18/801530.ini
cp ./rtran18/8015.tpf ./rtran18/801530.tpf

```

Line#1: Copy “8015\_1.par” as “8015.par”. “8015\_1.par” gives the reactor conditions from previous process, and the reverse flow direction.

Line#2: Run “monold\_sun” use information in files “8015”, use “8015\_1.par”, “8015.tin” and other information from previous process.

Line#3 to Line #5: Save information from 16 to 30 second for reverse flow.

```
cp ./rtran18/8015_2.par ./rtran18/8015.par
./bin_jan00/monold_sun ./rtran18/8015
cp ./rtran18/8015.tor ./rtran18/801545.tor
cp ./rtran18/8015.ini ./rtran18/801545.ini
cp ./rtran18/8015.tpf ./rtran18/801545.tpf
```

Line#1: Copy “8015\_2.par” as “8015.par”. “8015\_2.par” gives the reactor conditions from previous process, and the forward flow direction.  
Line#2: Run “monold\_sun” use information in files “8015”, use “8015\_2.par”, “8015.tin” and other information from previous process.  
Line#3 to Line #5: Save information from 31 to 45 second for forward flow.

```
cp ./rtran18/8015_1.par ./rtran18/8015.par
./bin_jan00/monold_sun ./rtran18/8015
cp ./rtran18/8015.tor ./rtran18/801560.tor
cp ./rtran18/8015.ini ./rtran18/801560.ini
cp ./rtran18/8015.tpf ./rtran18/801560.tpf
```

Line#1: Copy “8015\_1.par” as “8015.par”. “8015\_1.par” gives the reactor conditions from previous process, and the reverse flow direction.  
Line#2: Run “monold\_sun” use information in files “8015”, use “8015\_1.par”, “8015.tin” and other information from previous process.  
Line#3 to Line #5: Save information from 46 to 60 second for reverse flow.

```
cp ./rtran18/8015_2.par ./rtran18/8015.par
./bin_jan00/monold_sun ./rtran18/8015
cp ./rtran18/8015.tor ./rtran18/801575.tor
cp ./rtran18/8015.ini ./rtran18/801575.ini
cp ./rtran18/8015.tpf ./rtran18/801575.tpf
```

Line#1: Copy “8015\_2.par” as “8015.par”. “8015\_2.par” gives the reactor conditions from previous process, and the forward flow direction.  
Line#2: Run “monold\_sun” use information in files “8015”, use “8015\_2.par”, “8015.tin” and other information from previous process.  
Line#3 to Line #5: Save information from 61 to 75 second for forward flow.

```
cp ./rtran18/8015_1.par ./rtran18/8015.par
./bin_jan00/monold_sun ./rtran18/8015
cp ./rtran18/8015.tor ./rtran18/801590.tor
cp ./rtran18/8015.ini ./rtran18/801590.ini
cp ./rtran18/8015.tpf ./rtran18/801590.tpf
```

Line#1: Copy "8015\_1.par" as "8015.par". "8015\_1.par" gives the reactor conditions from previous process, and the reverse flow direction.

Line#2: Run "monold\_sun" use information in files "8015", use "8015\_1.par", "8015.tin" and other information from previous process.

Line#3 to Line #5: Save information from 76 to 90 second for reverse flow.

So far, process has three reverse flow cycles. Each cycle is consisted of 15 second forward flow and 15 second reverse flow. All information is saved. Process will continue if you feed it the proper conditions.

### 3. Program for Data Organization

The output data files like "filename.tor" and "filename.tpf" save the information in individual data files. To put all information continuously, a QuickBasic program is written to speed this process. It looks like:

```
COMMON SHARED dataPATH$, dfile$
DECLARE SUB readfile (dataPATH$, dfile$)

'#####
' Tor_Read.BAS /for Modeling Data File ".tor" reading
' B Liu      1-August-98
'#####
outputPATH$ =
"d:\BenE\Modelnew\Reverse\Sept2\8015\transi12\TimeTor\qbdata\"
dataPATH$ = "d:\BenE\Modelnew\Reverse\Sept2\8015\transi12\TimeTor\"
INPUT "outfile$ = ", outfile$
PRINT
PRINT

'open and print title of output data files
OPEN outputPATH$ + outfile$ FOR OUTPUT AS #2
PRINT #2,
PRINT #2, "Time, Tin, Tout, YCH4, XCH4, YCO, XCO"
PRINT #2, "S, K, K, PPM, %, PPM, %"
READ dfile$
DO UNTIL dfile$ = "final"
    CALL readfile(dataPATH$, dfile$)
    READ dfile$
LOOP
CLOSE #2

COLOR 14, 4
PRINT STRING$(80, "2"), SPACE$(80), SPACE$(80), SPACE$(80), STRING$(80,
"2")
PRINT "Done"

END
```

```

SUB readfile (dataPATH$, dfile$)
'open the file and read the first line

      OPEN dataPATH$ + dfile$ FOR INPUT AS #1
      PRINT
      PRINT "This is the header information from the file"
      COLOR IFC%, IBC%: PRINT " "; dfile$: COLOR NFC%, NBC%
      DO UNTIL EOF(1)
            LINE INPUT #1, junk$
            PRINT #2, junk$
      LOOP
      CLOSE #1

END SUB

```

```

'##### 1500RPM, 80NM, RFS, Sept.2, 97
DATA 801515.tor,801530.tor,801545.tor,801560.tor
DATA 801575.tor,801590.tor,8015105.tor,8015120.tor
DATA 8015135.tor,8015150.tor,8015165.tor,8015180.tor
DATA 8015195.tor,8015210.tor,8015225.tor,8015240.tor
DATA 8015255.tor,8015270.tor,8015285.tor,8015300.tor
DATA 8015315.tor,8015330.tor,8015345.tor,8015360.tor
DATA 8015375.tor,8015390.tor,8015405.tor,8015420.tor
DATA 8015435.tor,8015450.tor,8015465.tor,8015480.tor
DATA 8015495.tor,8015510.tor,8015525.tor,8015540.tor
DATA 8015555.tor,8015570.tor,8015585.tor,8015600.tor
DATA final

```

This program organize all “.tor” files in one data file according to time. Then it is easy to plot data and show information. Similarly, other data file like “.tpf” can also be organized with similar program.

## Appendix C

### Programs for Data Analysis

#### 1. Program for Adiabatic Temperature Rise Calculation

The following is a matlab program. It calculates the adiabatic temperature rise for specific reactor inlet gas.

```
#####
% Calculate Adiabatic Temperature Rise
% Ben Liu Feb. 18, 2000
#####
format long
clear

m1=input('Mair, g/s, m1= ');
m2=input('Mfuel1, g/s, m2= ');
m3=input('Mfuel2, g/s, m3= ');
M_T=m1+m2+m3;
n1=m1/28.96;
n2=m2/16;
n3=m3/226;
n_T=n1+n2+n3;

y1=input('O2, %, y1= ');
y2=input('CO2, %, y2= ');
y3=input('CO, ppm, y3= ');
y4=input('THC, ppm, y4= ');
y5=input('NOx, ppm, y5= ');

% Dry Composition, Balance N2
y1=y1*1e-2;
y2=y2*1e-2;
y3=y3*1e-6;
y4=y4*1e-6;
y5=y5*1e-6;
y6=1-(y1+y2+y3+y4+y5);

% Wet Composition
m_n=input('CnHm, Ratio of m/n, Diesel: 1.8-2, NG: 3.8, m/n= ?');
m_n=3.8;
K1=3.65;

y77=(0.5*m_n)*(y2+y3)/(1+y3/(K1*y2)+(0.5*m_n)*(y2+y3));
y11=(1-y77)*y1;
y22=(1-y77)*y2;
y33=(1-y77)*y3;
y44=(1-y77)*y4;
y55=(1-y77)*y5;
y66=(1-y77)*y6;

M_W=32*y11+44*y22+28*y33+16*y44+30*y55+28*y66+18*y77;
```

```

N_T=M_T/M_W;

Ydry=[100*y1 100*y2 1000000*y3 1000000*y4 1000000*y5 100*y6];
Ywet=[100*y11 100*y22 1000000*y33 1000000*y44 1000000*y55 100*y66
100*y77];

%Mole In Reactor Inlet#####

N_O2_in=y11*N_T
N_CO2_in=y22*N_T
N_CO_in=y33*N_T
N_CH4_in=y44*N_T
N_NO_in=y55*N_T
N_N2_in=y66*N_T
N_H2O_in=y77*N_T

%Energy from Reaction#####

T=input('Input Reactor Inlet Temperature (K): Tin=? ')
Q_CH4=-806.9+1.586e-2*T-8.485e-6*T^2-3.963e-9*T^3+2.16e-12*T^4 %kJ/mol
Q_CH4=Q_CH4*N_CH4_in*1e3 %J

Q_CO=-279.581-1.861e-2*T+2.52e-5*T^2-1.2247e-8*T^3+2.255e-12*T^4
Q_CO=Q_CO*N_CO_in*1e3 %J

Q_T=Q_CH4+Q_CO %J
Q_T=-Q_T %Change to a positive number
%Mole After Complete Reaction#####

N_O2_out=N_O2_in-N_CH4_in-0.5*N_CO_in
N_CO2_out=N_CO2_in+N_CH4_in+N_CO_in
N_NO_out=N_NO_in
N_N2_out=N_N2_in
N_H2O_out=N_H2O_in+2*N_CH4_in

N_T_out=N_O2_out+N_CO2_out+N_NO_out+N_N2_out+N_H2O_out

%Mole Fraction After Complete Reaction#####

YO2=N_O2_out/N_T_out
YCO2=N_CO2_out/N_T_out
YNO=N_NO_out/N_T_out
YN2=N_N2_out/N_T_out
YH2O=N_H2O_out/N_T_out

%CP from Reactor outlet Gas Mixture#####

%for O2
a=25.44;
b=1.518e-2;
c=-0.7144e-5;
d=1.31e-9;
CP_O2=a+b*T+c*T^2+d*T^3 %J/mol.K

%for CO2
a=22.22;
b=5.9711e-2;

```

```

c=-3.495e-5;
d=7.457e-9;
CP_CO2=a+b*T+c*T^2+d*T^3 %J/mol.K

%for NO
a=29.29;
b=-0.0938e-2;
c=0.9731e-5;
d=-4.18e-9;
CP_NO=a+b*T+c*T^2+d*T^3 %J/mol.K

%for N2
a=28.85;
b=-0.1569e-2;
c=0.8067e-5;
d=-2.868e-9;
CP_N2=a+b*T+c*T^2+d*T^3 %J/mol.K

%for H2O
a=32.19;
b=0.192e-2;
c=1.054e-5;
d=-3.589e-9;
CP_H2O=a+b*T+c*T^2+d*T^3 %J/mol.K

CP_Mixture=Y_O2*CP_O2+Y_CO2*CP_CO2+Y_NO*CP_NO+Y_N2*CP_N2+Y_H2O*CP_H2O

%Adiabatic Temperature Rise#####

dT=Q_T/(CP_Mixture*N_T_out)

```

## 2. Program for Transformation From Dry Basis to Wet Basis

The following is a matlab program. It calculates the gas composition in wet basis.

```

#####
%This is a matlab file to calculate the wet composition
%March 29, 1999, B Liu
#####

clear

path='c:\BenE\Thesis\Chapt2\'
indata=input('Dry Data File Name= ? ')
fid1=fopen([path indata], 'r');
A=fscanf(fid1, '%f %f %f %f %f %f', [6 inf]); %6 is the column number of
input data file
A=A';
status1=fclose(fid1);

m1=input('Mair, g/s, m1= ');

```

```

m2=input('Mfuel1, g/s, m2= ');
m3=input('Mfuel2, g/s, m3= ');
M_T=m1+m2+m3;
n1=m1/28.96;
n2=m2/16;
n3=m3/226;
n_T=n1+n2+n3;
% m_n=input('CnHm, Ratio of m/n, Diesel: C16.4H29.2, NG: CH3.8, m/n=
?');
x=n2+16.4*n3;
y=3.8*n2+29.2*n3;
m_n=y/x;
K1=3.65;

outdata=input('Wet Data File Name= ? ')
fid2=fopen([path outdata], 'w')
[m,n]=size(A);

for i=1:m

    %initial concentration
    y1=A(i,2);
    y2=A(i,3);
    y3=A(i,4);
    y4=A(i,5);
    y5=A(i,6);

    % Dry Composition, Balance N2
    y1=y1*1e-2;
    y2=y2*1e-2;
    y3=y3*1e-6;
    y4=y4*1e-6;
    y5=y5*1e-6;
    y6=1-(y1+y2+y3+y4+y5);

    % Wet Composition

    y77=(0.5*m_n)*(y2+y3)/(1+y3/(K1*y2)+(0.5*m_n)*(y2+y3));
    y11=(1-y77)*y1;
    y22=(1-y77)*y2;
    y33=(1-y77)*y3;
    y44=(1-y77)*y4;
    y55=(1-y77)*y5;
    y66=(1-y77)*y6;

    y11=100*y11;
    y22=100*y22;
    y33=1e6*y33;
    y44=1e6*y44;
    y55=1e6*y55;
    y66=100*y66;
    y77=100*y77;

    ywet=[A(i,1) y11 y22 y33 y44 y55 y66 y77];

```



```

        %Save data
        fprintf(fid2,'%6.0f %6.3f %6.3f %6.0f %6.0f %6.0f %5.3f
%6.3f\n',ywet);

end

status2=fclose(fid2);

disp('Job is Done')

```

### 3. Program for Inlet Gas Temperature Correction

The following is a matlab program. It corrects the measured inlet gas temperature

```

#####
% This is the program I use for Tin correction
% Ben Liu      August, 1998
#####

#####, Heat By Conduction
Tg_indi=input('Measured Reactor Inlet Temperature, Tg_indi= k ');
Ts=input('Guessed Reactor Wall Temperature, Ts= k ');
k_Ther=15; % Heat Conductivity of Thermocouple
A_Cross=7.9133E-6; %Cross Section Area, m^2
A_Surf=759.6759E-6;% Surface Area
L_Ther=76.2E-3; % Length
Q_cond=(Tg_indi-Ts)*k_Ther*A_Cross/L_Ther % Heat from Conduction

#####, Heat By Radiation

Q_rad=(Tg_indi^4-Ts^4)*5.67E-8*0.3*A_Surf % Heat from Conduction

#####, Re at Reactor inlet
M_Rate=input('Total Mass Flow Rate, M_Rate= kg/s ');
v_Visco=input('Air Kinetic Viscosity at Inlet Temperature, V_visco=
m^2/s ');
P_Press=input('Reactor Pressure, P_Press=, kpa '); % , kpa
P_Press=P_Press*1000; % pa
MW=input('Molecular Weight, MW=, kg/kmol '); % Molecular Weight
R=8314; % J/kmol.K
p_desity=P_Press*MW/(R*Tg_indi) %kg/m^3
V_Rate=M_Rate/p_desity;
L_Rea=152.4E-3; % Reactor Width
Ac=L_Rea^2; % Reactor Area, M^2
V_Velo=V_Rate/Ac
D=3.175E-3
Re=V_Velo*D/v_Visco

#####, Heat Transfer Coefficient, h

```

```

Pr=0.7;          % Prantal Number
Nu=0.3+0.62*Re^0.5*Pr^(1/3)/(1+(0.4/Pr)^(2/3))^0.25 % Nu Number,
Cylinder
%Nu=2+(0.4*Re^0.5+0.06*Re^(2/3))*Pr^0.4 % Sphere

k_Air=input ('Air Heat Conductivity at Inlet Temperature, k= w/m*k ');
h=Nu*(k_Air/D)   % Heat Convection Coefficient

#####, Gas Temperature , k

Tg_Cor=Tg_indi+(Q_cond+Q_rad)/(h*A_Surf) % Gas Temperature Wanted

```

#### 4. Program for Reactor Calculation

The following is a matlab program. This is a program to do the general calculation for the prototype catalytic converter. Calculation includes: Reactor inlet gas information, Channel gas flow information, etc.

```

#####
%This is a program to do the general calculation for the prototype
%catalytic converter, Calculation includes: Reactor inlet gas
%information, Channel gas flow information, etc.
%      Ben Liu          Feb. 22, 1998
#####

format long
clear

m1=input('Mair, g/s, m1= ');
m2=input('Mfuel1, g/s, m2= ');
m3=input('Mfuel2, g/s, m3= ');
M_T=m1+m2+m3;
n1=m1/28.96;
n2=m2/16;
n3=m3/226;
n_T=n1+n2+n3;

y1=input('O2, %, y1= ');
y2=input('CO2, %, y2= ');
y3=input('CO, ppm, y3= ');
y4=input('THC, ppm, y4= ');
y5=input('NOx, ppm, y5= ');

% Dry Composition, Balance N2
y1=y1*1e-2;
y2=y2*1e-2;
y3=y3*1e-6;
y4=y4*1e-6;
y5=y5*1e-6;
y6=1-(y1+y2+y3+y4+y5);

% Wet Composition

```

```

% m_n=input('CnHm, Ratio of m/n, Diesel: 1.8-2, NG: 3.8, m/n= ?');
m_n=3.8;
K1=3.65;

y77=(0.5*m_n)*(y2+y3)/(1+y3/(K1*y2)+(0.5*m_n)*(y2+y3));
y11=(1-y77)*y1;
y22=(1-y77)*y2;
y33=(1-y77)*y3;
y44=(1-y77)*y4;
y55=(1-y77)*y5;
y66=(1-y77)*y6;

M_W=32*y11+44*y22+28*y33+16*y44+30*y55+28*y66+18*y77;
N_T=M_T/M_W;

Ydry=[100*y1 100*y2 1000000*y3 1000000*y4 1000000*y5 100*y6];
Ywet=[100*y11 100*y22 1000000*y33 1000000*y44 1000000*y55 100*y66
100*y77];

N_exh=[y11*N_T y22*N_T y33*N_T y44*N_T y55*N_T y66*N_T y77*N_T];

#####, 1st Output
TFR_Mass_Engine=M_T
TFR_Molar_Engine=n_T
MW_Reactor_In=M_W
TFR_Molar_Reactor_In=N_T
Comp_Dry=Ydry
Comp_Wet=Ywet
FR_Comp=N_exh

#####
% Flow Rate and Flow Velocity Calculation

#####, basic Parameter
p_Hg=13579.04; % KG/M^3
p_H2O=1000; %KG/M^3
R=8.314; %J/mol.k
g=9.8; % m/s^2

#####, pressure
H_Hg=700;
H_H2O=input('Inlet Pressure Difference Compared Air, H_H2O= cmH2O ');
%CM H2O
P_u_d=input('Pressure Difference, P_u_d= pa ');

P_air=p_Hg*g*H_Hg*1e-3; %pa
dP_up=p_H2O*g*H_H2O*1e-2; % pa

P_up=P_air+dP_up;
P_down=P_up-P_u_d;
P_ave=(P_up+P_down)/2;

#####, temperature
T1=input('T1= °C ');
T2=input('T2= °C ');
T3=input('T3= °C ');

```

```

T4=input('T4= °C ');
T5=input('T5= °C ');
T6=input('T6= °C ');

T_ave=(T1+T2+T3+T4+T5+T6)/6;    %°C
T_ave=T_ave+273;                %k

#####, Open Channel Number

Tnum_CH=6400;

W_Brick=152.4;                   % Wide of Brick,mm
A_Brick=W_Brick^2;              % Area of Brick,mm^2

D_Cell=Tnum_CH/A_Brick; % Density of Cell, cell/mm^2

W_Blocked=10;                   % Wide of Blocked, mm
A_Blocked=W_Blocked^2; % Area of Blocked, mm
CH_Blocked=D_Cell*A_Blocked; % Channel Blocked

num_CH=Tnum_CH-CH_Blocked;

#####, Channel Velocity

TFR_Mass=M_T;
M_W=M_W;
T=298;

MFR_CH=TFR_Mass/num_CH; % Mass Flow Rate Per Channel, g/s
D_Exh=(P_ave*M_W)/(R*T); % Exhaust Density, g/m^3
D_Exh=D_Exh*1e-3; % Exhaust Density, kg/m^3

VFR_CH=MFR_CH*1e-3/D_Exh; % Channel Volume Flow Rate, m^3/s

W_CH=1.4; % For a Brick, Channel Wide, mm
Len_CH=50.8; % For a Brick, Channel Length, mm

Area_CH=W_CH^2; % Channel Area, mm^2

Vel_CH=VFR_CH/(Area_CH*1e-6); % Channel Velocity, m/s

#####, Hydraulic_Diameter, mm

Peri_CH=4*W_CH; % Perimeter of Channel
DH_CH=4*Area_CH/Peri_CH; % Hydraulic Diameter of Channel
u=18.348E-6; % Viscosity of Air at 298k,kg/m.s
Re_CH=MFR_CH*1e-3/(u*DH_CH*1e-3);

#####, 2nd Data Output
T_ave

P_up
P_down
P_ave

```

```
D_Exh
%num_CH
MFR_CH
VFR_CH
Vel_CH
Re_CH
```

## 5. Program for Data calculation from Japanese 6 Mode Test

The following is a matlab program. It calculate the gas composition from Japanese 6-Mode test.

```
#####
% This is for concentration calculation of
% Japanese 6 Mode Test
% Ben Liu March 15, 2000
#####

format long
clear

w1=0.355;
w2=0.071;
w3=0.059;
w4=0.107;
w5=0.122;
w6=0.286;

Y_HC=0;
Y_CO=0;
Y_NO=0;

for i=1:6

    if i==1
        w=w1;
    elseif i==2
        w=w2;
    elseif i==3
        w=w3;
    elseif i==4
        w=w4;
    elseif i==5
        w=w5;
    elseif i==6
        w=w6;
    end
```

```

disp('#####')
disp('#')
fprintf('#Please Enter Data from Mode: %2.0f\n',i)
disp('#')
disp('#####')

m1=input('Mair, g/s, m1= ');
m2=input('Mfuel1, g/s, m2= ');
m3=input('Mfuel2, g/s, m3= ');
M_T=m1+m2+m3;
n1=m1/28.96;
n2=m2/16;
n3=m3/226;
n_T=n1+n2+n3;

%Find CxHy for dual fuel
x=n2+16.4*n3;
y=4*n2+29.2*n3;

a=y/x
pause
k=1-a*(m2+m3)/m1;

y_COnew=input('CO, ppm, y_CO= ');
y_CO=y_CO+k*w*y_COnew;

y_HCnew=input('HC, ppm, y_HC= ');
y_HC=y_HC+w*y_HCnew;

y_NOnew=input('NO, ppm, y_NO= ');
y_NO=y_NO+k*w*y_NOnew;

end
y_HC
y_CO
y_NO

```